Proteomic Analysis of the Unfolded Protein Response in Melanoma

Erin K. Sykes

Faculty of Science
The University of Sydney

A thesis submitted in fulfillment of the requirements for the degree of Doctor of Philosophy

2023

Abstract

Melanoma is the third most common cancer in Australia, with an estimated 17,756 new cases diagnosed in Australia in 2022. Melanoma is one of the most aggressive neoplasms with the 5-year survival of 61% and 26%, for stage III and stage IV disease, respectively. Despite enormous advancements made in the last decade in the treatment of metastatic melanoma, due to drug resistance and high drug toxicities, improvements in treatment strategies and new therapies are needed. Additionally, there are no known biomarkers able to predict patients with metastatic disease that are likely to have poor outcome and therefore inform clinician of which patients may benefit from aggressive treatment strategies. Thirty-two potential biomarkers were analysed by selected reaction monitoring (SRM) in lymph node metastases from 30 stage III melanoma patients. From this, a 14-protein panel was discovered, able to predict patients likely to have poor outcome and therefore those who may potentially benefit from more aggressive therapeutic strategies.

From the above study in melanoma patients, the Unfolded Protein Response (UPR) was revealed to be a major cellular pathway up-regulated in patients with poor outcome. The UPR is a cellular stress response, which is initiated by a build-up of unfolded protein in the endoplasmic reticulum (ER) and activates a cascade of signalling pathways to return the cell to homeostasis. Increased activation of the UPR is also associated with more aggressive phenotypes and increased metastasis in several cancers including melanoma. However, the UPR mechanisms that promote tumour progression and metastases are not well understood.

To characterise this stress response in melanoma, the UPR was activated in melanoma cell line models and analysed by quantitative mass spectrometry. Using iTRAQ labelling on subcellular fractions from two melanoma cell lines, 64 proteins were identified as differentially abundant with increased UPR activation. The 64 proteins are involved in pathways that would contribute to melanoma progression including altered metabolism, modulation of the cell cycle, proliferation, survival and apoptosis, cellular adhesion and modulation of global RNA and proteins synthesis. Among them, eight UPR-associated proteins were validated by SRM in whole cell lysates from a broader cell line panel, identifying these proteins as core modulators of the UPR across melanoma's heterogenous disease phenotypes. Using public pan-cancer databases, an i*n silico* analysis of the eight UPR-associated proteins was performed in patient data from 16 solid tumour categories. This analysis revealed the eight UPR-associated proteins were markers of poor survival across several cancer types including melanoma. The combined data demonstrates the UPR is a major contributor to cancer progression and metastasis.

The study contributes to our knowledge of melanoma biology by elucidating the broad impact of the UPR on several cellular pathways and mechanisms that would promote tumour growth and increase the metastatic potential of melanoma. Furthermore, novel UPR drug targets were identified, including cooperative pathways that could be targeted in combinatorial therapies.

Authorship attribution statement

Chapter 1 of this thesis contains the complete published journal article:

Erin K. Sykes, Swetlana Mactier and Richard I. Christopherson. **Melanoma and the Unfolded Protein Response**. *Cancers*, March 2016. DOI: 10.3390/cancers8030030 [1]

I designed the content of the review, conducted all research and wrote the manuscript with edits from the co-authors.

Chapter 3 of this thesis contains the complete published journal article:

Erin K. Sykes, Cassandra E. McDonald, Shila Ghazanfar, Swetlana Mactier, John F. Thompson, Richard A. Scolyer, Jean Y. Yang, Graham J. Mann and Richard I. Christopherson. **A 14-protein signature for rapid identification of poor prognosis stage III metastatic melanoma.** *Proteomics – Clinical Applications*, January 2018. DOI: 10.1002/prca.201700094 [2]

I designed the experimental study with the co-authors, supervised C.M. on the sample preparation, designed and carried out all mass spectrometry experiments, interpreted the statistical analysis done by S.G. and wrote the manuscript with edits from the co-authors.

In addition to the statements above, in cases where I am not the corresponding author of a published item, permission to include the published material has been granted by the corresponding author.

Erin K. Sykes

27th June 2023

As supervisor for the candidature upon which this thesis is based, I can confirm that the authorship attribution statements above are correct.

Prof. Phillip Robinson

28th June 2023

Statement of originality

This is to certify that to the best of my knowledge the content of this thesis is my own work. This thesis has not been submitted for any degree or other purposes. I certify that the intellectual content of this thesis is the product of my own work and that all the assistance received in preparing this thesis and sources have been acknowledged.

Erin K. Sykes

24th June 2023

Table of contents

List of tables and figures

List of abbreviations

2D-DIGE	Two-dimensional fluorescence difference in-gel electrophoresis
α-MSH	α-melanocyte stimulating hormone
AJCC	American Joint Committee on Cancer
APCs	Antigen presenting cells
ATF6	Activating transcription factor 6
Bax	Apoptosis regulator BAX
Bcl-2	Apoptosis regulator Bcl-2
BRAF	Serine/threonine-protein kinase B-raf
BRAFi	BRAF inhibitor
BSA	Bovine serum albumin
CHAPS	3-[(3-cholamidopropyl)dimethylammonio]-1-propanesulfonate
CHOP	C/EBP homologous protein
COT	Mitogen-activated protein kinase kinase kinase 8
CTLA-4	Cytotoxic T-lymphocyte-associated protein 4
DAPI	4',6-diamidino-2-phenylindole
DHA	Docosahexaenoic acid
DLDA	Diagonal Linear Discriminant Analysis
DMEM	Dulbecco's Modified Eagle's Medium
DMSO	Dimethyl sulfoxide
DTT	Dithiothreitol
ECM	Extracellular matrix
EDTA	Ethylenediaminetetraacetic acid
eIF2α	Eukaryotic initiation factor 2α subunit
EMT	Epithelial-to-mesenchymal transition
ER	Endoplasmic reticulum
ERAD	ER-associated degradation
ERSE	ER stress response element
FAK	Focal adhesion kinase
FDR	False discovery rate
FGF	Fibroblast growth factor
GEF	Guanidine Exchange Factor
G-proteins	GTP-binding proteins
GRP78	Glucose-regulated protein78 kDa
HDAC	Histone deacetylase
HEPES	(4-(2-hydroxyethyl)-1-piperazineethanesulfonic acid)
HLB	Hydrophilic-lipophilic balanced
HSP70	Heat shock 70 protein
HUVEC	Human umbilical vein endothelial cells
IGF-1	Insulin-like growth factor
IRE1	Serine/threonine-protein kinase/endoribonuclease IRE1
iTRAQ	Isobaric tags for relative and absolute quantification
KCl	Potassium chloride

KM	Kaplan–Meier
LDH	Lactate dehydrogenase
MAPK	Mitogen-Activated Protein Kinase
MCR1	Melanocortin receptor
MEKi	MEK inhibitor
Met-tRNA	Methionine-transfer RNA
$MgCl_2$	Magnesium chloride
MITF	Microphthalmia-associated transcription factor
MMPs	Matrix metalloproteinases
MMP-2	Matrix-metalloprotease-2
MMP-9	Matrix-metalloprotease-9
NaF	Sodium fluoride
$NaVO_3$	Sodium metavanadate
NIST	National Institute of Standards and Technology
NF1	Neurofibromatosis 1
NF-κB	Nuclear factor kappa-light-chain-enhancer of activated B cells
NIPALS	Nonlinear Iterative Partial Least Squares
NP-40	Nonyl phenoxypolyethoxylethanol
OS	Overall survival
PBS	Phosphate-buffered saline
PCA	Principal component analysis
PD-1	Programmed cell death protein 1
PDI	Protein disulfide isomerase
PD-L1	Programmed cell death ligand-1
PERK	Eukaryotic translation initiation factor 2-alpha kinase 3
PFS	Progression free survival
PI	Propidium iodide
PMSF	Phenylmethylsulfonyl fluoride
PP1	Protein phosphatase 1
PRM	Parallel Reaction Monitoring
PTEN	Phosphatidylinositol 3,4,5-trisphosphate 3-phosphatase and dual-specificity protein phosphatase
PVDF	Polyvinylidene difluoride
Rb	Retinoblastoma protein
RIDD	Regulated IRE1-dependent decay
RNAse	Ribonuclease
RUV	Remove Unwanted Variation
SCX	Strong cation exchange
SDS	Sodium dodecyl sulfate
SMAC	Second mitochondria-derived activator of caspase
SNVs	Single-nucleotide variants
SRM	Selected reaction monitoring
TCEP	Tris-(2-carboxyethyl)-phosphine
TME	Tumour microenvironment

TRAF2	TNF-associated receptor factor 2
TRAIL	TNF-related apoptosis-including ligand
Tris-HCl	Tris hydrochloride
TYRP1	Tyrosinase-related protein 1
UPR	Unfolded protein response
UV	Ultra-violet
VEGF	Vascular endothelial growth factor
XBP1	X-box binding protein 1
XBP1s	XBP1 spliced

Chapter 1: Introduction

The following chapter details a previously published works in full:

Erin K. Sykes, Swetlana Mactier and Richard I. Christopherson. **Melanoma and the Unfolded Protein Response**. *Cancers*, March 2016. DOI: 10.3390/cancers8030030

Section 1.1 contains original material produced for the coursework requirements for the award of Doctorate of Philosophy.

Section 1.2 contains the above published article, produced in full as part of the required coursework for the award of Doctorate of Philosophy. I designed the content of the review, conducted all literature research and wrote the manuscript. Original updates were made herein to Table 1 of the review in section 1.2.3.2 to better reflect current knowledge and therapeutic advancements since 2016.

1.1 Melanoma

Melanoma arises from malignancies in melanocytes, specialised pigment producing cells found in the basal layer of the epidermis. Melanocytes occur in the skin, eyes and hair follicles where they produce the pigment melanin. The different melanocytes give rise to different melanoma types; uveal, mucosal and cutaneous melanoma which arise in the eyes, mucosal membrane and skin, respectively. The focus of this study is cutaneous melanoma, the most common of the three melanocyte derived cancers (Section 1.1) and the role of a cellular stress response, the unfolded protein response (UPR), in melanoma (Section 1.2).

Epidermal melanin acts as a photoprotective agent, absorbing ultra-violet (UV) radiation. Melanocytes produce and package melanin into lysosome-related organelles, called melanosomes, through the process of melanogenesis [3]. Melanocyte cell progression and the production of mature melanosomes are controlled by factors, such as hormones and growth factors, released by nearby keratinocytes, fibroblasts, endocrine, inflammatory and neuronal cells [4]. Mature melanosomes are then secreted into neighbouring keratinocytes through dendritic processes. The melanosomes are distributed around the keratinocyte nuclei, forming supranuclear caps, which act to protect from UV-induced DNA damage. However, melanocytes themselves are also susceptible to UV-induced DNA damage that can lead to the accumulation of mutations and neoplastic transformation. Although rarer than other skin cancers, melanoma is a far more aggressive and lethal neoplasm. This is seen in the mortality rate of skin cancers, while contributing to just 1% of all skin cancer cases, melanoma accounts for 80% of skin cancer deaths [5].

The highly aggressive nature of melanoma is in part due to the inherent properties of melanocytes that are required to carry out their normal functioning. In order to exert their protective role, melanocyte cells have enhanced DNA damage repair pathways, skewed survival/apoptotic balance and enhanced stress responses [6-9]. This is evident in melanocytes by the resistance of these cells to both TNF-related apoptosis-including ligand (TRAIL) and Fas ligand-induced apoptosis [10]. These inherent characteristics of melanocyte are hallmarks of cancer, resulting in an enhanced rate of malignant progression and producing a more aggressive tumour type.

1.1.1 Melanoma incidence and epidemiology

Melanoma is the 17th most common cancer worldwide with an estimated 324,635 new cases diagnosed in 2020 resulting in 57,043 deaths [11]. Large geographic variation exists for the prevalence of melanoma incidences, with Australia and New Zealand having the highest incidence rates in the world. In Australia, melanoma is the third most common cancer with an estimated 17,756 new cases in 2022. Additionally, melanoma is one of the few remaining cancers with an increasing incidence rate. If current trends continue, it is estimated the worldwide number of cases of melanoma will double by 2040 [12].

1.1.2 Melanoma staging

The classification system set out by the American Joint Committee on Cancer (AJCC), is the mostly widely accepted system for staging and classification of cutaneous melanoma [13]. The AJCC staging system standardises cancer staging and assists in patient risk stratification. The current AJCC 8th edition staging system for cutaneous melanoma categorises melanoma in five main stages (0-IV) with subgroups in each stage to refine predictions of patient prognosis and treatment selection (**Figure 1-1**) [14]. Stage 0 is defined as melanoma *in situ* in which the malignant cells are confined to the upper epidermal layers. Both stage I and II include the primary tumour but make a crucial distinction in the staging based on tumour depth. This is due to the major increase in risk posed to patients as the primary tumour invades into the dermis by just millimetres. The thickness of the primary tumour, termed Breslow thickness, is a key criterion in assessing patient prognosis for both probability of metastasis from the primary site and the probable outcome of resulting metastatic disease. AJCC stage III melanomas are defined as local metastases, in which melanoma cells that have migrated past the dermis and subcutaneous tissue can metastasise into local lymph nodes and spread within the epidermis. Stage IV melanomas are characterised as having distant metastases to other organs and distant lymph nodes. Melanoma most commonly metastasise to lymph nodes, lungs, brain, liver and bones [15]. This is due to a common lineage shared by these organs, which all arise from the ectoderm during developmental progression. As a result, the microenvironment and growth factors at these sites are similar to the epidermis, constituting a niche environment where melanoma cells are already well adapted for metastases.

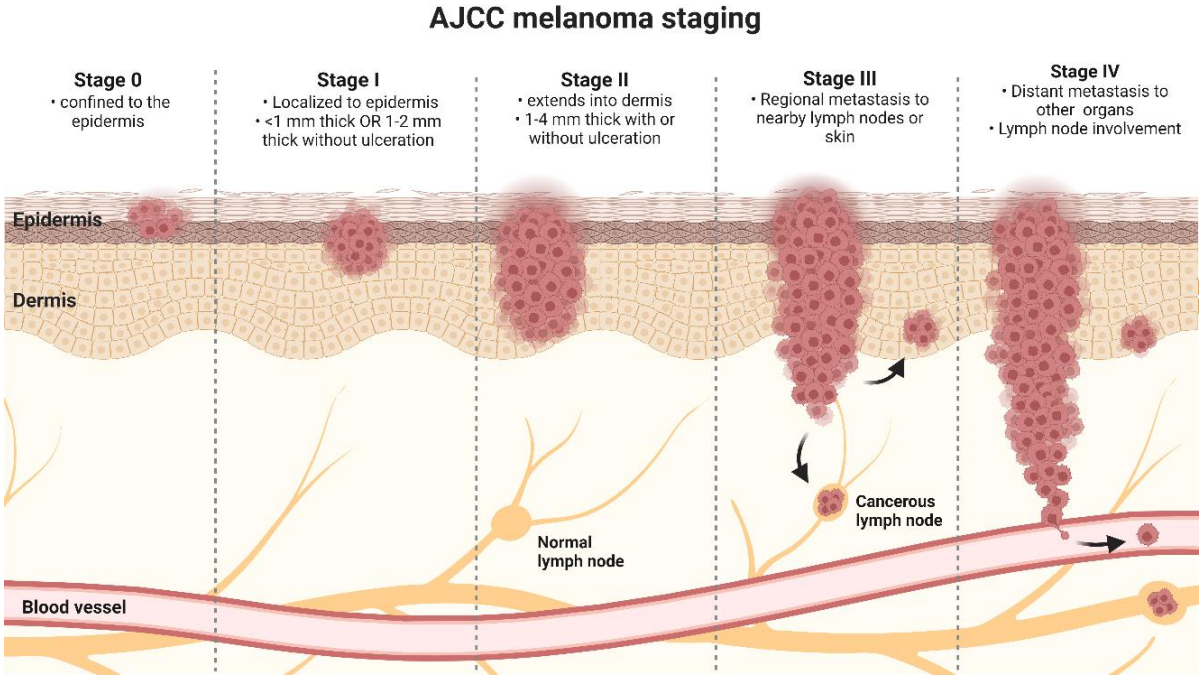

Figure 1-1. AJCC cutaneous melanoma staging. Summary of the AJCC 8th edition for cutaneous melanoma staging, illustrating the five major stages of melanoma progression from primary disease (stages 0, I and II) to local (stage III) and distant (stage IV) metastases.

1.1.3 Melanoma risk factors and aetiology

Genetic and environmental factors have been identified that are correlated with the risk of developing melanoma and the severity of disease, including gender, age, geographical region and ethnicity. The major environmental influence for increased risk of melanoma, is exposure to UV radiation. A strong association exists between the number of sunburns in an individual's lifetime and risk for melanoma, with greater risk posed for sunburns that occur during childhood [16, 17]. The association of UV exposure as a main driver of oncogenic potential has been established for decades but was made apparent by a large cohort genomic analysis of 333 melanoma patients in which 80% of patients had over 65% of the mutational burden arising specifically from UV-induced DNA damage [18]. Australia and New Zealand have the highest incidence rates worldwide, with 36.6 and 31.6, respectively, per 100,00 individuals compared with 3.4 per 100,000 as the worldwide average [19]. The increased regional risk is multifaced; associated with both UV factors such as climate, the artic ozone hole, pollution levels and lifestyle but also genetic factors associated with population ethnicity.

Another major risk factor for melanoma is the presence and number of nevi, a benign growth or pigmentation on the skin that can be congenital or acquired [20]. The number of nevi present on an individual is mostly associated with genetic factors but acquired nevi also have an association with exposure to sunlight. While most nevi remain stable and do not acquire a malignant phenotype, nevi are precursor lesions to an estimated 20-40% of cutaneous melanomas [21-24]. Additionally, the risk of developing melanoma increases with the number of nevi present even after adjusting for other environmental and familial risk factors [20, 25]. Furthermore, an inherited genetic link exists, associating the development of nevi and melanoma susceptibility genes.

There is a significant increase in the risk of melanoma with gender, with males having greater incidence rates as well as poorer prognosis than females, with males account for 58% of new cases and 64% of deaths from melanoma [26]. However, the risk for developing melanoma is higher for females before the age of 24, after which age males have higher incidence rates. The increased risk for males is multifactorial, including sex hormones, lifestyle and immune response. The association between sex hormones and melanoma has been well established but is still not well understood [27]. There is a correlation with pregnancy and higher risk of developing melanoma, termed pregnancy-associated melanoma [28, 29]. Whilst pregnant women display rapid rates of disease progression [30, 31]. This increased risk is again multifactorial involving increased lymphangiogensis, the presence of growth factors, increased hormonal levels and altered immune tolerance [29, 31-33].

There are several genetic and inheritable risk factors for melanoma, with 2% of all cases and 10% of malignant metastatic cases having a family history of the disease [34, 35]. The amount of melanin produced by individuals is a key risk factor with light skin colour, poor tanning ability and light eye colours predisposing to increased melanoma risk [36]. Red hair and freckling confer an increased risk of melanoma as this group has other underlying genetic links beyond pigmentation [36, 37]. Two inheritable gene mutations in *CDK4* and *CDNK2A* have been identified in familial melanoma cases [38]. Both genes are involved in regulation of cell cycle progression and senescence and are therefore essential in controlling aberrant proliferation. *CDK4* encodes the cyclin-dependent kinase, CDK4, which phosphorylates retinoblastoma protein (Rb), allowing for cell cycle progression. While *CDNK2A* encodes $p16^{INK4a}$ an inhibitor of CDK4, which prevents hyperphosphorylation of Rb resulting in cell cycle arrest. Inherited CDK4 mutants, although rare, cause overexpression of the gene product or prevent its inhibition resulting in unregulated cell cycle progression. Mutations in *CDNK2A*,

found in 39% of familial cases, prevent binding and inhibition of CDK4, again resulting in unchecked cell progression [38]. Furthermore, genetic variants of melanocortin receptor (MCR1) are associated with melanoma susceptibility [37, 39]. In familial melanoma cases, MCR1 variants increase the penetrance of *CDNK2A* mutants, especially for variants associated with red hair phenotype [39]. The MCR1 variant also confers a pigment independent risk factor, as evidenced by individuals with MCR1 variants and dark complexions who exhibit increased melanoma prevalence [40]. Over 400 single-nucleotide variants (SNVs) have been identified that impart increased melanoma risk, including a cumulative effect whereby individuals carrying more than 15 risk associated SNVs have a greater risk than those with less than six SNVs [18, 41, 42].

1.1.4 Oncogenic signalling in melanoma

Melanoma is a complex heterogenous disease and an in depth understanding of the biology underpinning this neoplasm is crucial for designing effective therapies. The disruption of key signalling cascades, Ras/Raf/MEK/ERK, Ras/PI3-K/PTEN/Akt and the microphthalmia-associated transcription factor (MITF) pathway have a crucial role in melanoma oncogenesis.

The most frequently mutated pathway in melanoma is the Mitogen-Activated Protein Kinase (MAPK) pathway consisting of a series of serine/threonine protein kinases, Ras/Raf/MEK/ERK, that mediate a phosphorylation cascade regulating cell survival and proliferation through various transcription factors (**Figure 1-2**). BRAF mutations are present in 50% of cutaneous melanomas, while NRAS mutations are found in 25% [18]. Melanocytes themselves require constant but transient ERK activation from neighbouring keratinocytes to not only maintain their proliferative potential but to regulate differentiation, senescence and the apoptotic/survival balance [43, 44].

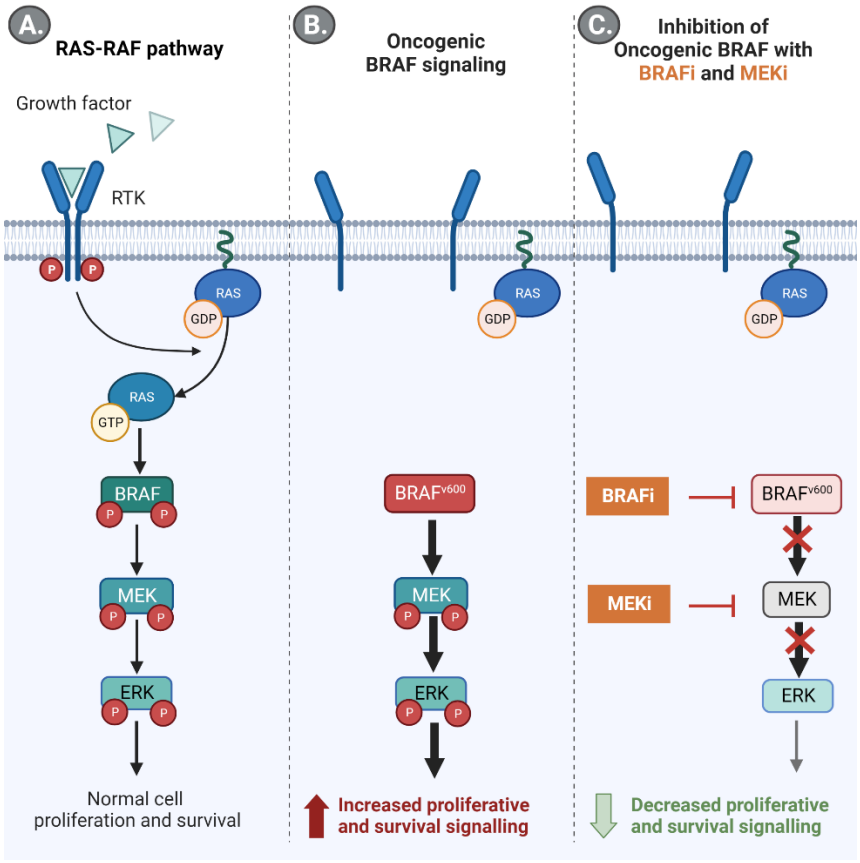

Figure 1-2. Ras/Raf/MEK/ERK signalling in melanoma. Signalling via the Ras/Raf/MEK/ERK with **A)** the normal phosphorylation cascade induced by extracellular growth factor binding to membrane receptor tyrosine kinases (RTKs), **B)** increased proliferative capacity from aberrant oncogenic signalling resulting from mutation in BRAF, resulting on downstream activation of MEK and ERK in the absence of extracellular growth factors and **C)** decreased proliferative signalling due to BRAF inhibitor and MEK inhibitor obstructing the kinase cascade and blocking the activation of ERK.

The three Ras proteins are small GTP-binding proteins (G-proteins) with GTPase activity, that typically reside on the inner surface of the cell membrane. Ras is activated in response to growth factors, hormones and cytokines, allowing Guanidine Exchange Factor (GEF) to exchange bound GDP for GTP [45]. Active GTP-Ras then recruits and binds to downstream effectors including Raf, which is in turn activated via phosphorylation [46]. Humans encode three *Ras* genes (HRAS, KRAS and NRAS) generated by alternate splicing, of which NRAS is the most predominant in melanocytes [47]. Of the 25% of melanomas in which NRAS is mutated, the most common is an amino acid substitution of leucine to glutamine at position 61 [48, 49]. Although Ras activation is generally associated with proliferation, excessive activation leads to senescence, which would explain why Ras mutations are less common in melanoma than downstream Raf activating mutations [50]. Furthermore, one of the downstream targets of Ras is Phosphatidylinositol 3,4,5-trisphosphate 3-phosphatase and dual-specificity protein phosphatase (PTEN), an inhibitor of the MAPK cascade [51]. Explaining

why mutual mutation in BRAF and PTEN are found in 20% of melanomas, as inactivating mutations in PTEN are required to prevent inhibition of the constitutively active MAPK pathway [52].

Of the three Raf proteins, ARAF, BRAF and CRAF, are initiators of the MAPK pathways phosphorylation cascade. After Ras activation, Raf proteins are recruited to the inner surface of the plasma membrane, where Ras in complex with other effector proteins phosphorylates and activates Raf kinase activity [53]. Of the 50% of melanoma bearing a mutant BRAF, 90% are a single amino acid substitution from valine to glutamate at position 600, the BRAFV600E mutant [18]. Substitution to a negatively charged amino acid at this glycine-rich loop, mimics the normal post-translational modification in this region of a negatively charge phosphorylation which disrupts the loop conformation [54, 55]. As this loop acts to constraint wildtype BRAF in an inactive conformation, the single substitution results in constitutive activation of the kinase [55]. Unlike, ARAF and CRAF isoforms, BRAF only requires a single amino acid substitution to become constitutively active, conferring an increase in kinase activity between 1.3 up to 700-fold [56]. Mutant BRAF promotes survival and anti-apoptotic signalling in melanoma, through constitutive activation of downstream targets, such as ERK which itself has over 160 client proteins involved in regulating cytoskeletal proteins, metabolic enzymes, other signalling cascades and transcription factors [57-60]. For example, Nuclear factor kappa-light-chain-enhancer of activated B cells (NF-κB), is an anti-apoptotic factor, that is activated by BRAF and protects against Fas-induced apoptosis [61, 62]. Also, BRAF increases MDM-2 levels via p53 resulting in inhibition of apoptosis and promoting the epithelial-to-mesenchymal transition [63, 64]. Mutant BRAF promotes cell growth and proliferation through a number of mechanisms, including induction of cyclin D1 and microphthalmia-associated transcription factor (MITF), a major regulator of melanogenesis [65, 66]. MITF is the major regulator of melanocyte differentiation and maturation, controlling many proliferative and survival pathways. Oncogenic BRAF also increases cAMP levels, resulting in expression of MITF at levels that promote growth but low enough to avoid inducing apoptosis [65, 67, 68].

Oncogenic BRAF also promotes metastasis and invasion in melanomas, with mutant BRAF bearing melanomas more likely to metastasise to the liver, lungs and brain [69]. Metastasis is promoted by mutant BRAF via increased expression of migratory proteins, mainly matrix metalloproteinase's (MMP's) and β-integrins [70]. Key to gaining a metastatic potential, melanoma must establish keratinocyte-independent growth and the ability to induce autocrine growth factors. These factors, including fibroblast growth factor (FGF), insulin-like growth

factor (IGF-1), vascular endothelial growth factor (VEGF) and α-melanocyte stimulating hormone (α-MSH) signalling, are upregulated via the constitutively active ERK pathway, which in turn has a positive feedback to increase ERK activity [71-73].

Despite their high frequency in melanoma, BRAF mutations are not themselves an initial oncogenic event that allows for malignant transformation. Rather they are an early event in melanoma progression conferring pro-survival and proliferative signalling [74]. This is evidenced in 82% of nevi possessing mutant BRAF yet are benign in nature, although they are more susceptible to malignant transformation [75]. BRAF mutations are also not prognostic markers for early stage I and II melanomas. Furthermore, BRAF mutational status does not correlate with Breslow thickness, the most reliable indicator of clinical outcome in early disease [76, 77].

Due to importance of the Ras/Raf/MEK/ERK pathway in melanoma oncogenesis, the pathway became a major pharmacological target for the treatment of melanoma. Targeting this pathway for inhibition with BRAF inhibitors (BRAFi) and MEK inhibitors (MEKi) was one of two major breakthroughs made in the treatment of metastatic melanoma, (**Figure 1-2**) as discussed below.

1.1.5 Melanoma treatments and survival

Primary (stage I and II) melanomas are highly curable with surgical resection, with a 95% survival rate even without adjuvant treatment. The high mortality rates due to melanoma occurs with metastatic disease, stage III and IV. As of a decade ago, there was no effective treatment for metastatic melanoma. Melanoma is notoriously resistant to generic chemotherapies, such dacarbazine, having a partial response of 12-24% and a complete response rate of only 1-5% [78]. The last decade however has seen two major breakthroughs in the treatment of metastatic melanoma, with the introduction of targeted therapies and immunotherapies.

As discussed above, constitutive activation of BRAF and downstream MEK/ERK plays a major role in melanoma biology and was therefore a promising drug target. Inhibitors against BRAF (BRAFi's) were introduced for metastatic melanoma patients bearing activating BRAF mutations in 2011. Of the 60% of patients that exhibit an initial response to the BRAFi dabrafenib, marginal increases in overall patient survival of 13.1 and 12.9 months were seen for BRAF (V600E) and BRAF (V600K) patients, respectively [79]. However, drug resistance was a major issue in the single agent clinical trials. After initially demonstrating a marked

reduction in overall tumour burden patients would exhibit a relatively rapid recurrence of disease, with a median progression free survival (PFS) of 5.8 months [80, 81]. Additionally, the recurrent tumours would often display a more aggressive phenotype and patients had accelerated progression of their disease, resulting in death [82]. This recurrence and acquisition of a more aggressive tumour can occur through a number of resistance mechanisms. The mechanisms driving this resistance can be broadly ascribed to two categories, MAPK-dependent (including point mutations in downstream MEK1, amplification of mutant BRAF, BRAF splice variants, activating upstream NRAS mutations and overexpression of COT kinase) and MAPK-independent (activation of parallel PI3K/PTEN/AKT pathways, overexpression of growth factor and activation of MET kinase) (**Figure 1-3**) [83-88]. In addition to drug resistance, 20% of patients receiving BRAFi developed cutaneous squamous cell carcinomas [89]. Further details on BRAFi resistance mechanisms can be found in the recent review by Zhong *et al*. [90].

To overcome resistance to BRAFi, combinatorial therapies with BRAFi and MEKi, which target the downstream activation of this MAPK pathway, are now one of the standard treatments for metastatic melanoma, **Figure 1-3**. Inhibiting downstream MEK negates several of the BRAFi resistance mechanisms above including mutations in NRAS and MEK, aberrant BRAF splicing and activation of PI3K/PTEN/AKT pathway of which MEK is a downstream target [84, 91]. Combinatorial BRAFi/MEKi exhibits increased efficacy over BRAFi alone in responding metastatic melanoma patients, with PFS increased from 5.8 to 9.4 months with BRAFi/MEKi compared to BRAFi [79]. Patients exhibiting a complete or partial response to therapy also increased from 54% to 76%. However, even with dual therapies, innate and acquired drug resistance is still an issue, with many of the same resistance mechanism for BRAFi contributing to BRAFi/MEKi resistance (**Figure 1-3**) [91]. Therefore, alternate therapeutic strategies are currently being trialled such as intermittent dosing with BRAFi/MEKi and triplet therapies which are discussed below [92].

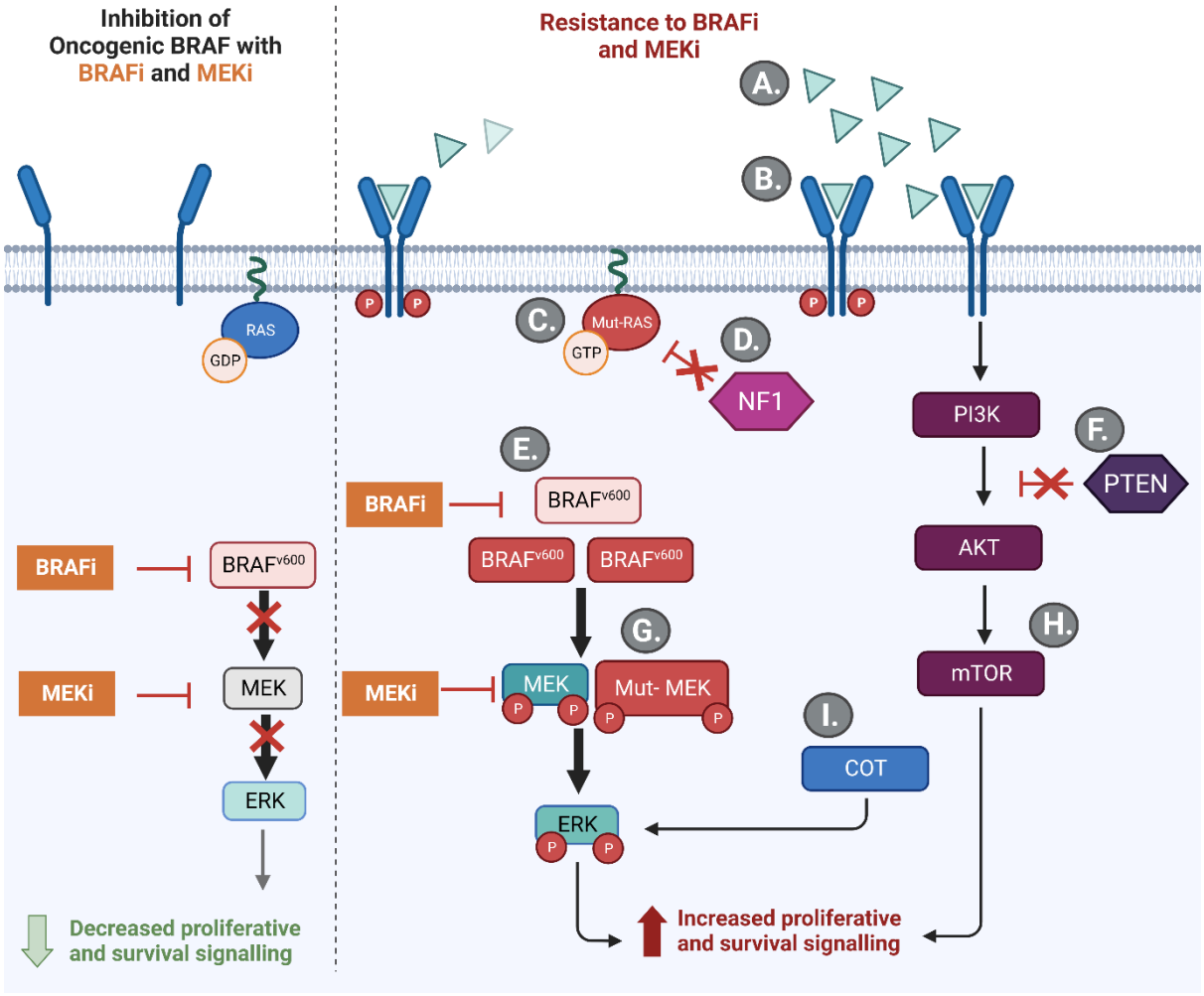

Figure 1-3. Mechanisms of resistance to BRAF inhibitor and MEK inhibitor targeted therapies. Innate and acquired mechanisms that impart resistance to BRAFi and MEKi targeted therapies. BRAFi and MEKi inhibit Ras/RAF/MEK/ERK signalling leading to decreased proliferation and cancer cell death, shown in the left panel. Resistance to MAPK-inhibitors can occur through mechanisms independent of the MAPK cascade, shown in the right panel. **A**) Melanoma can increase the levels of growth factors and **B**) the abundance of growth factor receptor on the cell surface to perpetuate growth and survival signalling via alternate pathways such as the **H**) PI3K/ PTEN/AKT pathway. Activation of the parallel signalling pathway PI3K/ PTEN/AKT is upregulated via **F**) inactivating mutations in PTEN, an inhibitor of the pathway. The MAPK kinase pathway can also be reactivated via mutations in the **C**) upstream NRAS and **G**) downstream MEK, **D**), loss of function mutations in tumour suppressor Neurofibromatosis 1 (NF1) that inhibits Ras, **E**) increased abundance of mutant BRAF to outcompete inhibitor concentrations, **E**) prevent BRAFi binding via alternate splicing of BRAF, **G**) prevent MEKi binding via MEK mutations and **I**) upregulation of mitogen-activated protein kinase kinase kinase 8 (COT) to activate downstream ERK.

The other major advancement in the treatment of metastatic melanoma was the introduction of immunotherapies targeting immune checkpoint inhibitors; cytotoxic T-lymphocyte-associated protein 4 (CTLA-4) and Programmed cell death protein 1 (PD-1), gaining FDA approval in 2011 and 2014, respectively. The inflammatory immune response possesses a series of stimulatory and inhibitor checkpoint pathways that allow for fast, dynamic modulation of immune activation, thereby ensuring a swift response against pathogens or cancers while

also protecting healthy tissue from auto-immune responses. In gaining a malignant potential, tumours acquire mechanisms to either dampen the immune response in order to evade tumour-specific immunity or to exploit the immune system to increase oncogenic capacity. Anti-CTLA-4 and anti-PD-1 immunotherapies work to counteract the mechanisms utilised by cancers to evade unfavourable immune responses (**Figure 1-4**). These checkpoint inhibitors have the advantage of having efficacy in both mutant and wildtype BRAF melanomas [93].

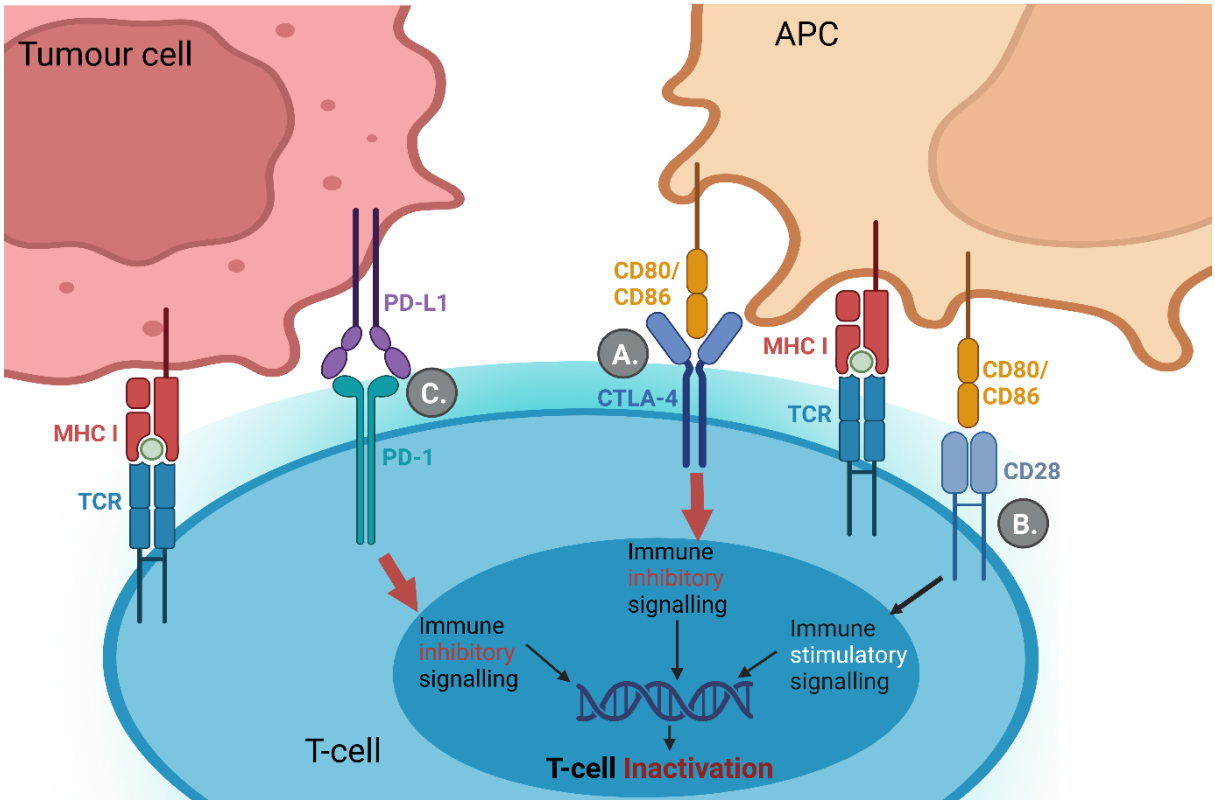

Figure 1-4. Inhibition of T-cell activation by CTLA-4 and PD-1 cell surface receptors. Major histocompatibility complex I (MHC I) proteins on the surface of tumour cells present fragmented tumour peptides to the T-cell receptor (TCR) on the immune cell to initiate an immune response. **A**) CTLA-4 on the surface of immune cells acts to control the immune response at primary immune sites via binding of CD80/86 on immune stimulatory cell (APC) with CTLA-4 receptors on T-cells perpetuating T-cell inactivation. **B**) T-cell activation is balanced by opposing signalling from CD28 binding with CD80/86, although with lower affinity, resulting in activation of T-cells. **C**) T-cells are inactivated within the tumour microenvironment (TME) by binding of PD-L1 on tumour cells with PD-1 on active T-cells.

CTLA-4 is an immunoglobin found on the surface of T-cells and along with CD28 is one of the major mediators of T-cell activation. CTLA-4 binds to B7 ligands, CD80 and CD86, that are produced by nearby dendritic cells in response to inflammatory signalling. Upon ligand binding, CTLA-4 produces an inhibitory cascade in T-cells thereby inhibiting their activation. The negative stimulatory effects of CTLA-4 are attenuated by positive stimulation from CD28, a competitive binder of CD80 and CD86, allowing for dynamic modulation of the activity of

antigen presenting cells (APCs). The objective of CTLA-4 targeted immunotherapies is activation of T-cells upstream in the immune cascade at primary sites, such as lymph nodes and spleen, via activation of conventional adaptive T-cells and/or T-regulatory cells. Anti-CTLA-4 monoclonal antibodies bind to the CTLA-4 receptor, preventing binding of ligand CD80 and CD86 thereby inhibiting the negative stimulation of T-cells (**Figure 1-5**). CD80 and CD86 are now free to bind CD28, producing a positive stimulatory effect of the T-cells, allowing proliferation and migration to the tumour site. The response rate of anti-CTLA-4 monotherapies in metastatic melanoma patients is 24% with median overall survival of 10 months [94-96]. Importantly, long term response was seen in 25% of responders and a small subset of patients continued to have disease free survival even after discontinuation of therapy [97-99]. However, as the overall number of patients who responded to anti-CTLA-4 immunotherapies alone was low and there were associated side effects, particularly adverse immune events and liver toxicity, further refinement of immune checkpoint inhibitor therapy was required.

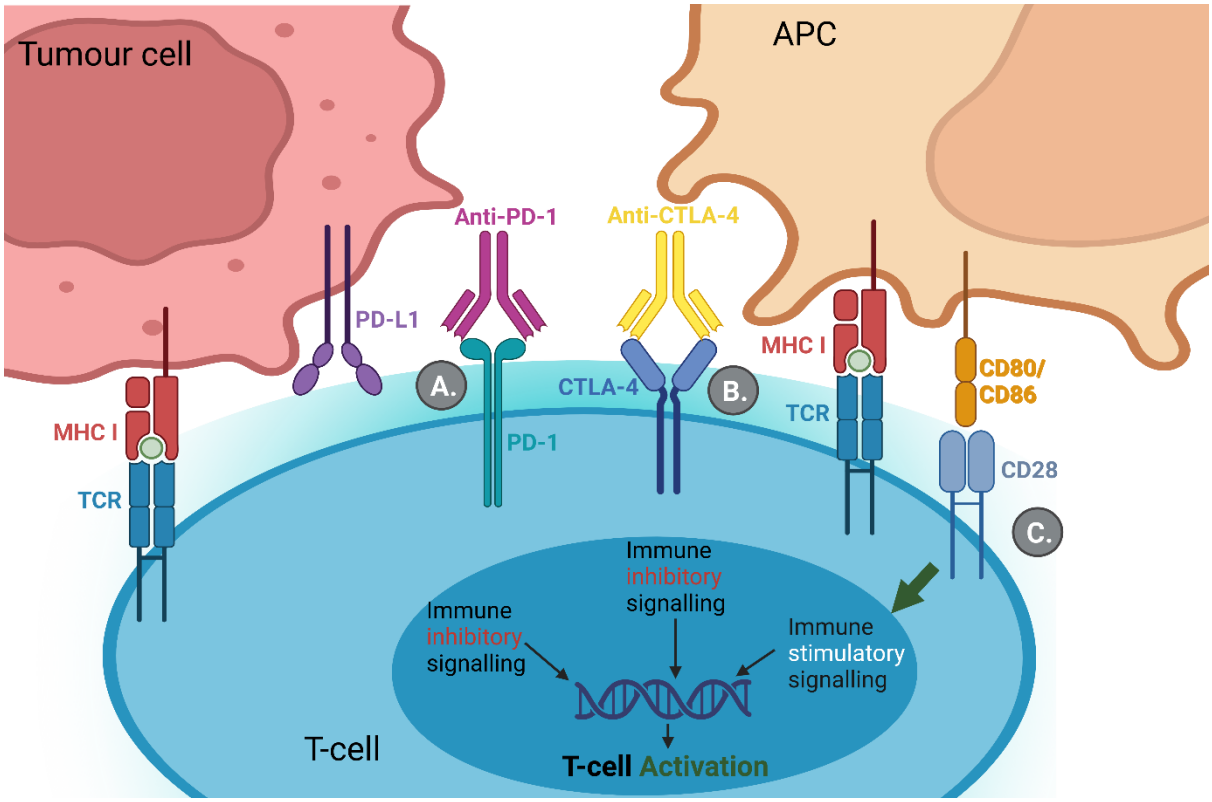

Figure 1-5. Activation of T-cell with Anti-CTLA-1 and Anti-PD-1 immunotherapies. A) Anti-PD1 antibodies bind PD-1 on the T-cell surface, inhibiting the interaction of PD-1 and PD-L1 and preventing T-cell inactivation. **B**) Anti-CTLA-4 binds CTLA-4 on active T-cells preventing binding of ligand CD80 and CD86 inhibiting T-cell inhibitory signalling. **C**) In the presence of immunotherapies ligands CD80 and CD86 are now free to bind CD28 on T-cells allowing for activation of the immune cell against the tumour cells.

While anti-CTLA-4 immunotherapies activate the immune response early in the immune cascade, anti-PD-1 immunotherapies activate the immune response against tumours within the tumour microenvironment (TME). Persistent antigen exposure, such as that observed in tumours or with long term infection, results in the cell surface expression of PD-1 on activated T-cells. The ligand of PD-1, programmed cell death ligand-1 (PD-L1), is similarly expressed in response to inflammatory cytokines on tumour and other cells which are targets of the immune system. Binding of PD-L1 on tumour cells with PD-1 on active T-cells, results in an inhibitory cascade to inactivate the T-cells, thereby allowing the tumour to escape the antitumour immune response (**Figure 1-4**). Persistent inactivation of T-cells by PD-L1 leads to T-cell exhaustion and immune evasion. Anti-PD-1 immunotherapies such as, nivolumab, pembrolizumab and pidilizumab, are monoclonal antibodies that bind PD-L1, thereby preventing PD-1/PD-L1 binding that would result in T-cell inactivation (**Figure 1-5**). Not only does anti-PD-1 immunotherapy result in an increased T-cell populations at the tumour site and pro-inflammatory signalling, but can also reverse T-cell exhaustion of immune cells already present within the TME [100]. Response rates for metastatic melanoma patients to anti-PD-1 immunotherapies as a single agent are relatively low, with 30-40% exhibiting complete or partial responses [101, 102]. However, responders had a significant increase in survival, with an overall survival (OS) probability of 82.7% at 3-years [102]. Anti-PD-1 immunotherapies have fewer side effects compared to anti-CTLA-4 targeted therapies but still cause serious side effects such as hepatic toxicity [102]. Importantly, long term stable responses to therapy are seen in 37% of responding patients [103].

Due to the complementary roles of CLTA-1 and PD-1 checkpoint inhibitors in activating the immune response upstream at primary immune sites and downstream within the TME, there exists a rationale for a cooperative combinatorial treatment strategy to increase the proportion of patients that respond and to prevent acquired resistance. Combined immune checkpoint inhibition with CTLA-4 and PD-1 exhibits increased overall response rates in patients from 20% with anti-CTLA-4, compared to 40-60% with combined checkpoint inhibition [104]. However, the combined checkpoint inhibitors demonstrate a marked increase in adverse events, 54-59% up from 21-28% with a single agent [105]. Overall long term survival was increased with combinatorial therapies, even for patients who discontinued therapy due to side effects with a 3-year survival rate of 68% [104].

Acquired resistance is also an issue for immune checkpoint inhibitors, with approximately 20% of responders gaining a resistant phenotype [106]. Mechanisms underpinning both primary and acquired resistance include T-cell exhaustion, loss of PTEN, low mutational burden, activation of WNT signalling, decrease in antigen presentation and absence of T-regulatory cells in the TME [107-110]. Due to the influence of MAPK-activation on presentation to the immune system a rationale exists to combine BRAFi/MEKi targeted therapies with immunotherapies to treat metastatic melanoma. MAPK activation has been shown to decrease antigen presentation, immune infiltration and increase immune-suppressive cytokines [111, 112]. This is seen in melanoma patients in which BRAF inhibition is associated with changes in the TME that promote an immune response. Several clinical trials are currently underway to test the efficacy of this triplet treatment strategy [113-117]. In a 2022 update from a combined triplet therapy trial (BRAFi/MEKi with anti-PD-1) in late stage melanoma, patients with triplet therapies were reported to have lower response rate than doublet therapies however those that did respond exhibited higher complete response rates for triplet therapies [118]. Further details about resistance mechanisms to immunotherapies in melanoma can be found in recent review by Ziogas *et al.* [90].

Significant advancements in the treatment of metastatic melanoma have occurred in the last decade, with significant improvements to patient survival both with targeted therapies and immunotherapies. However, as with most cancer therapies, innate and acquired resistance remains a major impediment for initial and long-term patient response. As such, studies to identify new therapeutic targets and treatment strategies are a priority for the treatment of melanoma. A major cellular mechanism, the unfolded protein response (UPR), was identified to be upregulated in several cancer types including melanoma. The components of the UPR have garnered interest as potential drug targets against melanoma and to define how this stress response contributes to melanoma progression. The following section 1.2 contains the full published review article, in accordance with the University of Sydney thesis guidelines, on the UPR with a focus on its role in melanoma [1].

1.2 Unfolded Protein Response and Melanoma

Membrane and secretory proteins, that account for 30% of human proteins [119], are folded and mature within the endoplasmic reticulum (ER) before export to the cell surface via the trans-Golgi network. Due to the frequent bulk of protein processing occurring within this organelle, the ER has an exquisitely fine-tuned stress response to cope with the protein load. The UPR is activated by the accumulation of unfolded protein within the ER that initiates a widespread but refined signalling cascade (**Figure 1-6**).

1.2.1 Activation of the UPR

The UPR signalling cascade is mediated by three key ER trans-membrane proteins, eukaryotic translation initiation factor 2-alpha kinase 3 (PERK), serine/threonine-protein kinase/endoribonuclease IRE1 (IRE1) and activating transcription factor 6 (ATF6). These proteins reside within the ER bound via their luminal domains to a regulatory protein glucose-regulated protein 78 kDa (GRP78), which is considered the master regulator of the UPR [120]. GRP78 is a member of the heat shock 70 protein (HSP70) family of chaperones. During stress when unfolded proteins accumulate in the ER, GRP78 binds the unfolded proteins, releasing the three UPR mediators. Each induces a distinct signal transduction pathway mediating a particular arm of the UPR. The three arms of the UPR cumulatively result in up-regulation of ER resident chaperones, the suppression of global protein synthesis and the degradation of existing proteins via ER-associated degradation (ERAD) and degradation of organelles through autophagy.

The release of IRE1 from GRP78 allows it to dimerise and undergo auto-phosphorylation resulting in activation of its ribonuclease (RNAse) activity [121, 122]. The activated IRE1 RNAse domain then cleaves the mRNA transcript of X-box binding protein 1 (XBP1) [123]. The now mature XBP1 mRNA is translated into a functional transcriptional factor, XBP1 spliced (XBP1s) (**Figure 1-6**).

PERK acts similarly to IRE1 upon GRP78 release, allowing it to dimerise and phosphorylate eukaryotic initiation factor 2α subunit (eIF2α) to suppress global protein translation [122]. Phosphorylated eIF2α also activates ATF4 to facilitate transcription of UPR responsive genes (**Figure 1-6**) [124]. Additionally, ATF4 initiates negative feedback on eIF2α, by promoting expression of another transcription factor C/EBP homologous protein (CHOP) that de-

phosphorylates eIF2α via Growth arrest and DNA damage-inducible protein (GADD34) and Protein phosphatase 1 (PP1) [125, 126].

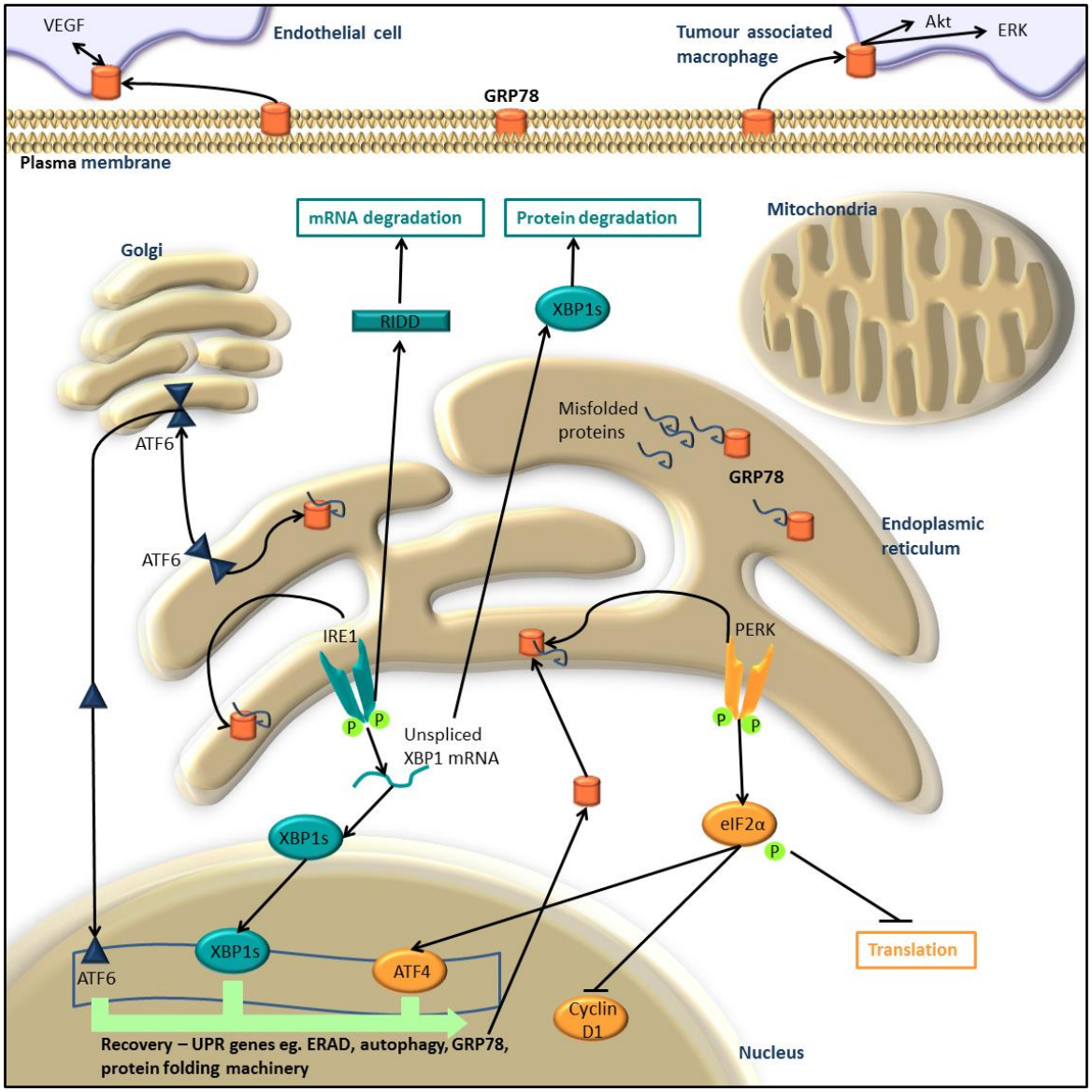

Figure 1-6. Cellular recovery modulated by the UPR signalling cascade. Misfolded proteins within the ER are bound by the ER chaperone GRP78, resulting in its displacement from three ER transmembrane proteins. The three proteins PERK, IRE1 and ATF6, initiate the UPR signalling cascades. PERK dimerises, trans-autophosphorylates then phosphorylates eIF2α. Active eIF2α then inhibits cyclin D1 to halt the cell cycle, preventing Met-tRNA recruitment to the 40S ribosomal subunit for global suppression of protein synthesis, eIF2α also activates the transcription factor ATF4. IRE1 dimerises and trans-autophosphorylates to become active, cleaving unspliced XBP1 mRNA through its ribonuclease activity to form an active transcription factor, XBP1s. XBP1 splicing also results in protein degradation via activation of ERAD and autophagy. ATF6 freed from GRP78, translocates to the Golgi where its cytosolic-transcription factor domain is cleaved by SiP1 and SiP2, then localises to the nucleus. The three transcription factors ATF4, XBP1s and ATF6 increase the expression of UPR responsive genes to maintain homeostasis, including ER-chaperones, ERAD and autophagic proteins. The chaperone GRP78 is also upregulated, moving to the cell surface and into circulation. Circulating GRP78 propagates growth in tumour associated macrophages and endothelial cells by activating signalling cascades within these cells.

ATF6 exists in two isoforms ATF6α and ATF6β, that upon GRP78 release, translocate to the Golgi compartment where they are cleaved by the proteases SiP1 and SiP2, releasing the ATF6 cytosolic domain [127, 128]. The ATF6 domain translocates to the nucleus where it acts via cis-acting ER stress response element (ERSE) on the promoters of several ER chaperone genes, up-regulating their transcription [129].

1.2.1.1 Return to homeostasis

In order to repeal stress, the UPR reduces the influx of proteins into the ER. IRE1 phosphorylation of eIF2α prevents methionine-transfer RNA (Met-tRNA) recruitment and results in global suppression of protein synthesis, reducing the protein folding burden of the ER [130]. eIF2α mediates the recruitment of Met-tRNA to the 40S ribosomal subunit and is the rate-limiting step in protein translation [131]. Selected UPR genes are preferentially translated via cap-independent translation of internal ribosome-entry sites [132]. Additionally, active IRE1 selectively degrades mRNA bound for the ER in a process called regulated IRE1-dependent decay (RIDD). In mammals, mRNA with a conserved sequence similar to that found in the transcription factor XBP1, are targeted by IRE1 for degradation, thereby relieving the protein processing load in the ER [123]. All three mediators of the UPR; ATF6 directly, IRE1 via XBP1s and PERK via ATF4, act to increase the expression of several chaperones, including GRP78, to assist in protein folding within the ER [129, 133-135]. Other non-stress specific responses are also perturbed by these transcription factors such as amino acid metabolism, redox state and mitochondrial metabolism [136-139].

The overlap that exists between the signalling cascades is potentially a means by which increased control of the UPR response, and its outcome can be exerted. In lower eukaryotes such as yeast, the entire UPR is mediated by IRE1, however higher eukaryotes have adapted to include two additional UPR cascades, allowing for more precise control of this stress response [140]. During ER stress, these three arms of the UPR act in concert to return the cell to homeostasis [141]. There is considerable overlap between the three initial signalling cascades presumably to enable fine-tuning of the UPR to adapt to different levels of stress within the cell and control the result of the UPR.

The UPR also controls two protein and organelle degradative pathways, ER associated degradation (ERAD) and autophagy (**Figure 1-6**) that are responsible for the clearance of aberrant proteins from the cell. The induction of ERAD mainly occurs through IRE1-XBP1s signalling [122]. ERAD is another way in which the ER controls homeostasis through selective

degradation via the destruction of misfolded proteins present in the ER. During ER stress, the induction of the UPR expands the capacity of ERAD to eliminate unfolded proteins. Several ERAD components are up-regulated through UPR transcription factors (**Figure 1-6**), while ER chaperones up-regulated through the UPR selectively target misfolded proteins to the cytoplasm for poly-ubiquitination and degradation by the 26S proteasome [24]. ERAD and the UPR exhibit reciprocal activation, acting in concert to clear misfolded proteins from the ER [24]. Disruption of ERAD via proteasome inhibition has been shown to induce cell death in cells with ER-stress, as such it is concluded that ERAD is crucial in adaption to chronic UPR and the avoidance of melanoma to UPR-induced apoptosis [142-144]. Activation of the UPR in turn activates a co-operative mechanism within the cell known as autophagy. Autophagy is the process of degrading and recycling whole organelles via autophagosomes, a membrane vesicle that targets its package to lysosomes. The UPR co-activates the autophagy program via both PERK-eIF2-ATF4 and JNK signalling [124, 145]. Similar to the UPR, autophagy promotes cellular recovery by degrading proteins in cancerous cells, while resulting in cell death in un-transformed cells [145, 146]. For the cell to process the misfolded proteins, the UPR prompts ER expansion. Autophagy is instrumental therefore in the resolution of the UPR by degrading excess organelles whose protein folding capacity is no longer required. When autophagy is inhibited in cells under acute ER stress, the cells are unable to recover and undergo apoptosis [147], suggesting that autophagy is an essential aspect of the UPR program, enabling avoidance of UPR-induced apoptosis in cancers. Patients with metastatic melanoma with high levels of autophagy had shorter survival and exhibited less response to temozolomide, a DNA damaging agent, and sorafenib, a RAF inhibitor [148]. The implications of autophagy in cancer progression are extensive and are well reviewed by Mathew *et al*. and White [149, 150].

Collectively the UPR relieves ER stress and returns cells to homeostasis through a cooperative, highly co-ordinated response involving inhibition of global protein synthesis, up-regulation of UPR-responsive genes involved in ER protein folding and through the selective degradation of ER-targeted mRNA by RIDD, misfolded proteins via ERAD and whole organelles or proteins by autophagy.

1.2.1.2 UPR-induced apoptosis

In the case of acute or prolonged ER stress when the cell fails to return to homeostasis, the UPR can induce apoptosis. UPR-induced apoptosis is initiated through the same signalling mechanisms that are triggered to restore the cell to homeostasis and, as such, the UPR engages in a fine balancing act between cellular recovery and death. This is achieved through complex

regulation in which the three UPR arms modulate one another to promote either survival or death, and in the case of cancer the UPR encourages cellular recovery as the outcome.

On failing to resolve ER-stress, UPR-induced apoptosis is activated by both PERK and IRE1 cascades and the direct activation of caspase-12. Prolonged ER stress leads to PERK phosphorylating eIF2α and inducing ATF4 expression that in turn results in the up-regulation of CHOP, a transcription factor that stimulates the expression of several pro-apoptotic genes (**Figure 1-7**) [151, 152]. Increased expression of CHOP by the UPR results in decreased apoptosis regulator Bcl-2 (Bcl-2) levels and translocation of Bcl-2 antagonist of cell death (Bax) to the mitochondria to induce apoptosis [153]. In this way, the UPR is able to mediate apoptosis through well characterised apoptotic signalling pathways that result in mitochondrial membrane disruption. Acute ER-stress and activation of IRE1 signalling can relocalise Bak and Bax (Bcl-2 antagonist of cell death) to the mitochondria to propagate apoptosis [154]. Activation of IRE1 in response to prolonged ER-stress will induce apoptosis via recruitment and phosphorylation of TNF-associated receptor factor 2 (TRAF2) that activates JNK through the ASK1 signalling cascade (**Figure 1-7**) [155]. Protein kinase JNK, then promotes mitochondrial-dependent apoptosis involving unknown downstream targets. Caspase-12 (human ortholog caspase-4) is itself a critical effector in UPR apoptosis, indeed null caspase-12 mutants have reduced sensitivity to ER-stress induced apoptosis [156]. Pro-caspase-12 resides in the ER-membrane and when prolonged, acute ER-stress is present, phosphorylated IRE1 cleaves caspase-12 initiating the caspase cascade cleaving caspase-9 then caspase-3, eventuating in apoptosis [157]. The ability to bypass classical apoptotic cascades is of particular interest for cancer research. Oncogenic mutations render the cells resistant to apoptotic mechanisms, therefore this particular UPR-induced apoptosis could provide a valuable form of therapy.

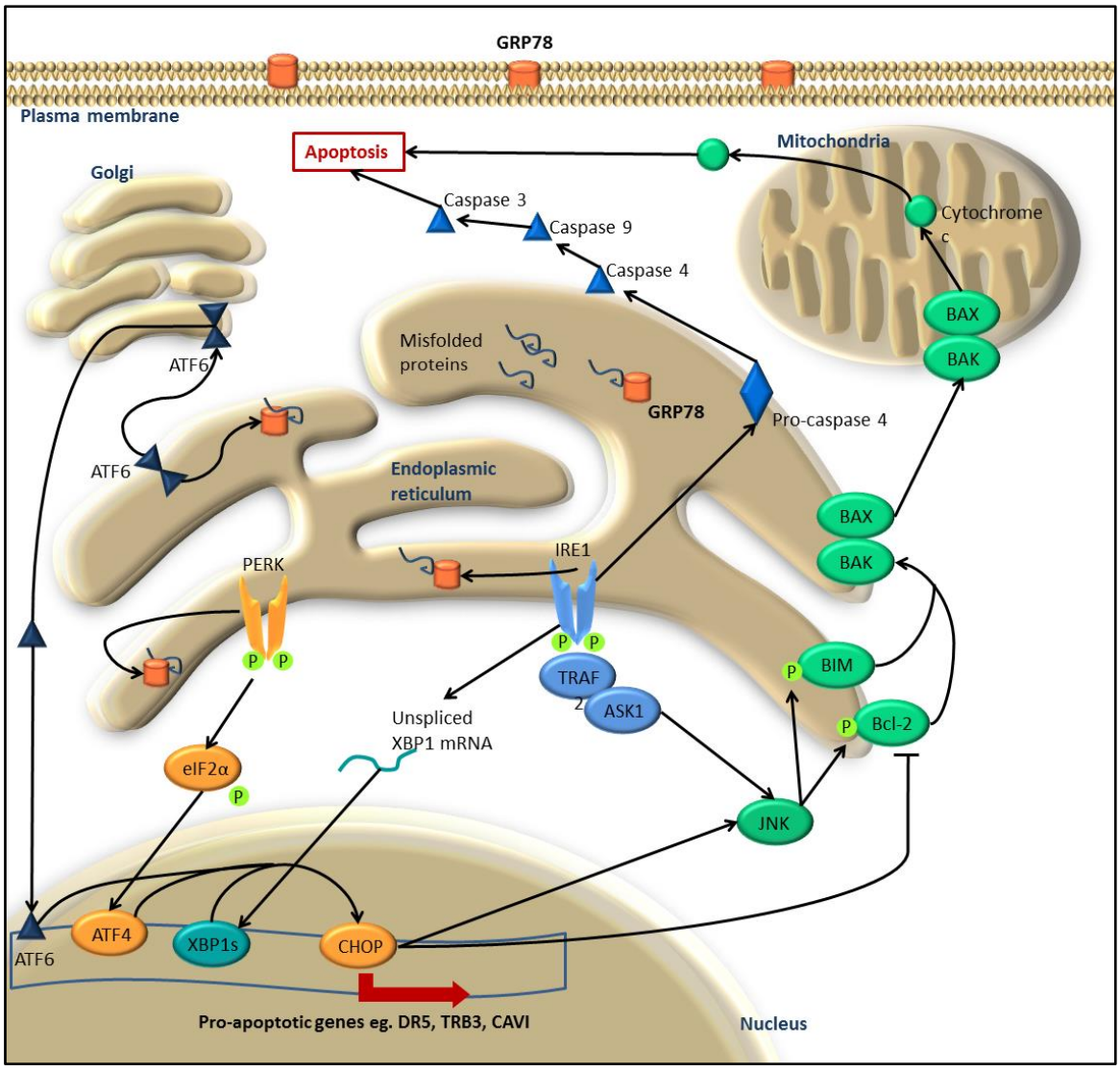

Figure 1-7. Apoptosis modulated by the UPR signalling cascade. In the case of acute, prolonged ER-stress, the UPR stimulates apoptosis modulated by the same three proteins that initiate UPR cellular recovery. Activated PERK, IRE1 and ATF6 increase the expression of the transcription factor CHOP. CHOP up-regulates several pro-apoptotic genes including DR5 (death receptor 5), TRB3 (tribbles homolog 3) and CAVI (carbonic anhydrase VI). Additionally, CHOP activates JNK (c-JUN N-terminal kinase) that propagates apoptosis by phosphorylating Bcl-2 (B-Cell CLL/Lymphoma 2) and BIM (Bcl2-like protein 11) to initiate Bcl-2 apoptotic signalling and release of cytochrome C. JNK is also activated by dimerised IRE1 through TRAF2-ASK1 signalling. Additionally, IRE1 directly cleaves procaspase-4 to initiate the apoptotic caspase cascade.

1.2.2 UPR in Melanoma and other cancers

The UPR plays an important role in the function of cells and is routinely activated to deal with the high flux of proteins processed through the ER at certain times within the cell cycle. Cancers are subject to many forms of stress due to poor vascularisation and high proliferation. Therefore, it is not surprising that the UPR is highly activated in cancer cells that are subject to hypoxia, nutrient deprivation and altered pH and require more proteins for neoplastic growth, in particular secretory proteins, to exploit their microenvironment. The UPR may assist in

several aspects of tumour biology, ranging from tumourigenesis, apoptotic evasion, metastasis, angiogenesis and chemotherapy resistance.

Numerous studies have found a link between activation of the UPR and cancer progression. One of the best studied proteins of the UPR is GRP78, levels of which are highly elevated in several cancers including prostate [158], colorectal [159, 160], breast [161, 162], ovarian and lung cancers [163]. In human melanoma samples, increased levels of GRP78 positively correlate with increased progression, tumour size and poor outcome for patients [164]. As such, elevated GRP78 has been identified as a potential biomarker for early diagnosis of melanoma [165]. Additionally, increased and sustained activation of other UPR mediators, IRE1 and ATF6 are critical for melanoma survival [166].

The UPR has been proposed as a critical early event in neoplastic transformation. In mouse models for breast and prostate cancer, GRP78 knock-out protects against cancer growth [167], proliferation and angiogenesis [168]. In human melanoma cells, knockdown of GRP78 results in decreased proliferation [169]. Similarly, decreases of other UPR mediators; XBP1, IRE1 and PERK, through knock-downs, knock-outs and null mutations in a range of cancer models result in decreased tumour size and reduced angiogenesis [170-174]. Paradoxically, auto-antibodies against GRP78 promote tumour growth and inhibit apoptosis by activating the UPR, resulting in growth and survival of melanoma, prostate and ovarian cancers [175-177].

Furthermore, the role of the UPR in cancer metastasis is becoming more evident, with research conducted into the contribution of ER stress and the UPR in cancer migration and invasion. Studies have focused in particular on dissecting the role of GRP78 in numerous human cancers. Elevated levels of GRP78 correlated with increased metastasis in prostate, gastric, colon, lung, oesophageal and breast cancers; and hepatocellular and non-small cell lung carcinomas *in vitro* and *in vivo* [164, 178-184]. In prostate, colorectal, gastric and breast cancer and oesophageal squamous cell carcinoma, increased levels of GRP78 correlated with an increase in metastatic potential [181, 182, 184-187]. Comparison of primary cutaneous melanomas to their matched lymph node metastasis showed significant increases in GRP78 levels in disseminated melanoma. In primary cutaneous melanoma, Papalas *et al*. found a decrease in GRP78 with invasive depth but with a rapid increase of GRP78 levels at the invasive front of the tumour [188]. Studies in various cancer cell lines demonstrate the same positive correlation between increased levels of GRP78 with cell invasion and migration [179, 181, 182, 189, 190], with knockdowns of GRP78 *in vitro* resulting in decreased cell migration

and invasion [179, 181, 189]. In addition to a decrease in metastatic potential, knockdown of GRP78 also resulted in the decrease of several proteins associated with metastasis, including vimentin, E-cadherin, matrix-metalloprotease-2 (MMP-2) and matrix-metalloprotease-9 (MMP-9) [181, 189, 190].

The increased metastatic potential with the UPR may in part be explained by its link to the epithelial-to-mesenchymal transition (EMT). Increased UPR, in particular the chaperone GRP78, has been found to promote EMT in various cell types including melanocytes and thereby promote tumourigenesis and dissemination. In breast cancer, the UPR mediator XBP1 was found to facilitate EMT promoting tumour invasion [191]. EMT drives both neoplastic transformation and promotes a metastatic phenotype in melanoma with increased levels of EMT genes and EMT-inducing transcription factors conferring more adhesive, invasive and migratory properties [192, 193].

In addition to the increased production of membrane and secretory proteins made possible by ER expansion and up-regulation of chaperones by the UPR, there are several other mechanisms that are of benefit to cancers. The UPR has been implicated in adapting the microenvironment to the tumour's needs, in other ways besides increasing secretory protein output. For example, the UPR can promote angiogenesis, essential for maintaining nutrient supply and growth for metastasis. GRP78 is found on the cell surface and secreted into the circulation by various solid tumours including melanoma [175, 194, 195]. Cell surface and circulating GRP78 has been found to act as a signalling hub and promotes cell proliferation and angiogenesis. One of the signalling responses induced by cell surface GRP78, that has strong implications in melanoma biology, is the upregulation of vascular endothelial growth factor (VEGF). VEGF stimulates the growth of solid tumours and angiogenesis in the TME. In melanoma patient samples, levels of VEGF correlate with cancer progression [196]. Karali et al., found that VEGF activated IRE1 and ATF6 through mTOR, contributing to the survival effect of VEGF on endothelial cells through activation of the Akt pathway [197]. Furthermore, inhibition of several UPR mediators decreased VEGF-induced vascularisation in mouse Matrigel plug angiogenesis assay, comprising extracellular matrix proteins [197]. Cell surface GRP78 has also been shown to assist in invasion via its interaction with focal adhesion kinase (FAK), a major signalling protein in cell migration, adhesion and spreading. In hepatocellular carcinoma cell lines, over-expression of GRP78 caused an increase in FAK expression and tumour invasiveness [186]. Additionally, in colorectal cancer GRP78 increased cell migration

and invasion into the extracellular matrix (ECM) through its interaction with β1-integrin and FAK [184].

Circulating GRP78 is capable of binding to endothelial cells and activating ERK and Akt signalling, protecting these cells from anti-angiogenic drugs (**Figure 1-6**) [198]. IRE1, PERK and ATF6 also directly regulate levels of VEGF mRNA [199]. The relationship between GRP78 and VEGF may be through reciprocal regulation, with Katanasaka *et al*. reporting increased GRP78 cell surface expression in VEGF-activated human umbilical vein endothelial cells (HUVEC) [200, 201].

It is evident that the role of the UPR is more widespread than previously thought, exemplified by research on GRP78. The influence of GRP78 on the EMT, its ability to stimulate angiogenesis via VEGF and to induce signalling cascades in neighbouring cells, suggests that the UPR repeals stress on a systemic level and has previously been oversimplified as a single cellular response. This widespread functionality may explain the paradoxical nature of GRP78, such as the ability of GRP78 auto-antibodies to perpetuate the UPR. Understanding how components of the UPR such as GRP78 promote tumour growth and metastasis through interaction with other cells and components of the TME is worthy of investigation. Additionally, therapies that target these specific interactions of the UPR with the TME may provide increased cancer specificity.

Another benefit of the UPR is its protein and organelle degradation mechanisms, ERAD and autophagy, respectively, the activations of which are coupled to the UPR. It has been proposed that these mechanisms play a key role during metastasis by recycling and supplying essential building blocks while the cell adapts to its new environment [202, 203]. Recent evidence has implicated cellular dormancy in melanoma metastasis especially for uveal melanoma [204-206]. That has led to the proposal of prolonging melanoma dormancy as a possible treatment, with Ossowski and Aguirre-Ghiso proposing that therapies should focus on expanding long term dormancy [204]. A strong link has been established between tumour dormancy and the UPR, with ERAD proposed as an important stimulus in the growth of dormant metastases [202]. While mentioned briefly within this review, the roles of ERAD and autophagy in cancer are extensive and have been reviewed in detail elsewhere [142, 202, 207].

Research continues to unravel the effect of this complex stress response on cancer and to define the specific outcomes resulting from the UPR. For example, the effect of increased

MEK/ERK signalling on tumourigenesis, the EMT switch promoting tumour dissemination and the effect of increased angiogenesis via VEGF for metastatic growth.

1.2.2.1 UPR and MEK/ERK

One of the key oncogenic signalling pathways in melanoma is MEK/ERK [208], with BRAF, the upstream regulator, constitutively activated in 66% of malignant melanomas [209]. Oncogenic signalling from MEK/ERK increases cellular protein production thereby increasing the ER-burden and activating the UPR [169, 210]. Indeed, it has been shown that MEK activation is essential for survival of melanoma under acute ER-stress [211]. Sustained induction of IRE1 and ATF6 is linked to increased MEK/ERK activation that protects melanoma from UPR-induced apoptosis, while inhibition of MEK/ERK partially blocks IRE1 and ATF6 [166]. It has also been reported that inhibition of BRAF or MEK prevents IRE1 and ATF6 activation, that in turn increases UPR-induced apoptosis [169]. Recent research suggests a reciprocal activation event between the UPR and MEK/ERK signalling that goes beyond a simple increase in cellular protein load, as stated above. Conversely, Beck *et al.* reported that melanomas treated with the RAF inhibitor vemurafenib had increased ER stress [212]. These contradictory findings may in part explain how melanoma adapts to chronic ER-stress. Constitutively active MEK may modulate particular arms of the UPR, such as IRE1, thereby preventing UPR-induced apoptosis while maintaining, or even increasing, its cytoprotective functions.

1.2.3 UPR and Chemotherapy

1.2.3.1 Drug resistance

The greatest challenge in the treatment of metastatic melanoma is its resistance to chemotherapy. Melanoma relatively quickly acquires resistance to drugs that are initially effective. Various studies have reported a correlation between increased levels of UPR markers and drug resistance [213]. Furthermore, the ER is a site for drug detoxification and the mere presence of anti-cancer drugs elicits an increased UPR response. In human melanoma cells, knockdown of GRP78 sensitised the cells to UPR-induced apoptosis under acute ER-stress, highlighting the potential of the UPR as a therapeutic target [169]. GRP78 has also been shown to protect against anti-angiogenic drugs in xenograft models of human breast cancers [198, 214]. The UPR was found to be responsible for resistance of melanomas to vinca alkaloids, a class of anti-mitotic drugs that bind microtubules, used in combined therapies against metastatic melanoma [215]. Hypoxia is known to contribute to chemotherapeutic resistance

through numerous mechanisms such as downregulation of DNA repair enzymes, poor drug delivery and chemical modification of drugs [216, 217]. Under hypoxic conditions, the UPR is activated and initiates its cellular recovery program, allowing the cell to survive and adapt to the treatment. The hypoxia-sensitive protein Galectin-1 that is upregulated in melanoma, offers a cytoprotective effect to various anti-cancer drugs via modulation of the UPR in melanoma cells [218]. Histone deacetylase (HDAC) is commonly up-regulated in cancer resulting in oncogenic activation by influencing both gene expression and direct modification of proteins. HDAC inhibitors directly influence aberrant gene expression via epigenetic regulation resulting in growth arrest and apoptosis in cancers. Despite showing promise as an anti-cancer therapy, either intrinsic or acquired resistance to HDAC inhibitors is commonly observed in sub-populations of cancer cells, with acquired cross-resistance to other anti-cancer drugs a major problem in this therapeutic strategy [219-221]. Numerous combinatorial therapies with HDAC inhibitors are currently under investigation in various cancers including melanoma. Inhibiting HDAC in melanoma cells improved the response to BRAF inhibitors, resulting in growth arrest and increased apoptosis [222, 223]. HDAC inhibitors in combination with Ipilimumab, a monoclonal antibody against the immune suppressor CTLA-4, are currently in Phase I trials for melanoma. HDAC1 is a repressor for GRP78 expression, inhibition therefore leads to increased UPR activation and resistance to HDAC inhibitors, while over-expression attenuates this resistance [224]. UPR inhibitors may overcome HDAC inhibitor resistance and are a potential avenue for combination treatment of metastatic melanoma.

1.2.3.2 The UPR as a drug target

The UPR is an attractive therapeutic target due to its link with apoptosis and role in drug resistance. Harnessing apoptosis mechanisms and inhibiting pathways that evoke resistance is a current focus for anti-cancer drug development (**Table 1-1**). The UPR is upregulated in cancers, providing a means by which drugs can be targeted specifically to cancer cells through targeting UPR mediators. One of the main difficulties in finding effective treatments for cancer is establishing a therapy that is effective given the heterogeneity of malignancies, among sub-clone metastases from a single tumour. The UPR is not inherently an oncogenic pathway; rather, it is a normal cellular process that may be corrupted for the benefit of the cancer. Therefore, targeting the UPR could be effective against a wide range of cancers despite their individual mutational status. The UPR, specifically GRP78, assists in angiogenesis, therefore inhibiting the UPR may block both UPR associated angiogenesis and cytoprotection. Additionally, the UPR upregulates numerous pro-apoptotic proteins that initiate several

apoptotic cascades. Of particular interest for the treatment of melanoma, which is notoriously resistant to apoptosis, is the direct activation of caspase-3 via JNK.

A number of drugs directly targeting the UPR are currently in clinical trial, including several GRP78 inhibitors (**Table 1-1**). PAT-SM6, in phase I clinical trials against melanoma and phase I/IIa in multiple myeloma, is a monoclonal antibody reported to bind a cancer specific GRP78 cell surface isoform, thereby inducing apoptosis in cancer cells [225, 226]. Another GRP78 targeting drug is docosahexaenoic acid (DHA), an omega-3 fatty acid, that inhibits total and cell surface GRP78 expression and increases apoptosis in cancer cells [227-229]. In melanoma cell lines, DHA induces cell cycle arrest and increased apoptosis [230]. As DHA is not only non-toxic but carries health benefits, its positive effects have been widely tested on numerous cancers, showing decreased growth and metastasis [229, 231-233]. Under the stress of nutrient-deprivation, Arctigenin, a plant lignin, specifically blocked the expression of GRP78 with activation of XBP1 and ATF4, resulting in ROS/MAPK-mediated apoptosis [234-236]. The UPR mediator PERK is another major target for drug development. PERK suppresses global protein synthesis, controls ATF4 transcriptional regulation of UPR responsive genes and CHOP-mediated apoptosis. Small molecule drug screening has identified several PERK inhibitors, including GSK2656157 and GSK2606414, that exhibit anti-tumoural effects but with severe side-effects against pancreatic tissue [237, 238]. Indeed, cells that have a functionally high secretory protein burden and therefore constant induction of the UPR, such as pancreatic β-cells, have been identified as a major obstacle to targeting the UPR. As such, the rationality of targeting major UPR components, such as GRP78, must be questioned and the implications of therapeutics directed at the source of this widespread and uncharacterised response examined, especially given the contradictory role exhibited by GRP78. Greater therapeutic benefit may be gained by targeting multiple downstream effectors and UPR-tumour specific interactions. Such as, characterising how the UPR contributes to cancer progression and the pathways involved may identify new potential drug targets.

Table 1-1. Drug therapies targeting the UPR for the treatment of cancer. Superscript denotes combinatorial therapeutic trials.

Drug/s	Target	Effects	Study /clinical trial
Versipelostatin	GRP78 and GRP94	• Inhibits transcription of GRP78/94 target genes • Initiates UPR-induced apoptosis under glucose deprivation	Preclinical [239, 240]
Docosahexaenoic acid	GRP78	• Decreased levels of GRP78 • Induced apoptosis • Increased expression of UPR proteins ERdj5 and PERK	Preclinical **melanoma** [230] Phase II/ III **melanoma** [241, 242] Phase II/III/IV solid tumours
PAT-SM6	GRP78	• Monoclonal antibody binds cell surface GRP78 to induce apoptosis	Phase I **melanoma** [225] Phase I/ II multiple myeloma
Arctigenin	GRP78	• Induces apoptosis via ROS/MAPK	Preclinical [234-236]
Honokiol	GRP78	• Inhibits angiogenesis • Decreases MAPK signalling	Preclinical
Resveratrol	XBP1	• Promotes ER-stress induced apoptosis	Phase I multiple myeloma, colorectal cancer Phase I/II prostate cancer
Bortezomib *in combination with* [1]*azacytidine,* [2]*decitabine*	26S proteosome	• Inhibits ERAD • Increases ER-stress from accumulated misfolded proteins • Induces UPR-mediated apoptosis	FDA-approved multiple myeloma, acute myeloid leukemia, Phase II metastatic melanoma [1,2]Phase I multiple myeloma
Carfilzomib	26S proteosome	• Inhibits ERAD • Increases ER-stress from accumulated misfolded proteins • Induces UPR-mediated apoptosis	Phase III multiple myeloma Phase II lymphoma
GSK2656157	PERK	• Inhibits PERK kinase • Decrease blood vessel density	Preclinical [237, 238]
ISRIB	ATF4	• Inhibits ATF4 expression • Reverses eIF2α effects	Preclinical
MKC-3946	IRE1	• Inhibits XBP1 splicing	Preclinical [243]

Numerous studies have reported increased efficacy of existing chemotherapies when combined with both UPR inhibitors and activators, to prevent cytoprotective effects or induce apoptosis. Furthermore, the co-activation of MEK/ERK and the UPR provides an interesting opportunity for combination therapies in melanoma targeting this key oncogenic pathway. Patients with late stage BRAF mutant melanomas administered vemurafenib, a BRAF inhibitor, show significant tumour regression and increased survival. However, relatively rapid resistance is acquired, with most patients relapsing with a lethal drug resistant phenotype. Interestingly, induction of ER-stress and the UPR in vemurafenib-resistance melanoma results in increased apoptosis [212]. In a melanoma mouse model, Thakur *et al*. showed that

proliferation of vemurafenib-resistant cells was dependent on the presence of the drug [244]. A combination therapy alternating vemurafenib and UPR inducers may prevent the emergence of drug resistance. The GRP78 suppressor, Arctigenin, sensitises cancer cells to cisplatin-induced apoptosis via STAT3 inhibition [245]. DHA, an omega-3 fatty acid, sensitises cancers to various chemotherapies [246-248]. Phase III clinical trials for metastatic melanoma have been conducted with DHA conjugated to paclitaxel, a microtubule disrupting agent. Despite limited patient benefit, the drug was well-tolerated leading to speculation that further combined therapies with DHA-paclitaxel may have increased efficacy [241, 242]. In melanoma cell lines DHA has exhibited synergy with cyclooxygenase inhibitors and decreased melanoma growth with type 1 transforming growth factor beta [249, 250]. The chelating agent, D-penicillamine, currently used to treat rheumatoid arthritis, was found to induce caspase-dependent apoptosis in cultured metastatic melanoma cells with activation of the UPR [251]. Inhibition of the UPR also increased the efficacy of DNA-damaging agents, such as cisplatin and adriamycin in human melanoma cells. Both cisplatin and adriamycin increased the UPR, and silencing GRP78 sensitised melanoma to apoptosis induced by these agents [252]. Bortezomib, an inhibitor of the 26S proteosome, that induces the accumulation of unfolded proteins, is effective against a range of cancers by increasing cellular stress and initiating UPR-induced apoptosis. In melanoma, bortezomib was found to induce ER stress and increase apoptosis [253, 254]. Bortezomib was also found to inhibit nuclear factor κB-mediated gene expression in melanomas in vitro. The combination of bortezomib with temozolomide in melanoma mouse models induced long-term remission [255]. Melanoma progression correlates with decreased expression of tumour necrosis factor-related apoptosis-inducing ligand (TRAIL) receptors, with most cancers resistant to TRAIL-induced apoptosis [187]. The UPR has been found to increase TRAIL-induced apoptosis in melanoma cells via up-regulation of the TRAIL receptor [256]. Drug synergy between bortezomib and TRAIL has been demonstrated in melanoma cells by increasing TRAIL-induced apoptosis [257, 258]. When used in combination with other drugs the effects were even more potent, as seen in melanoma treated with bortezomib, TRAIL and a second mitochondria-derived activator of caspase (SMAC) mimetic [259]. Fenretinide, a retinoic acid derivative that produces reactive oxygen species and increases levels of unfolded proteins, also induced the UPR in melanoma. Furthermore, inhibition of GRP78 and protein disulfide isomerase (PDI), another UPR mediator, sensitised melanoma to apoptosis in combination with bortezomib and fenretinide [260-262]. Additionally, of importance in the treatment of metastatic melanoma is the contribution of the UPR to vemurafenib-resistance. Patients with late-stage BRAF mutant melanomas administered vemurafenib, the BRAF

inhibitor mentioned above, show significant tumour regression and increased survival [263, 264]. However, relatively rapid resistance is acquired with most patients relapsing with a lethal drug resistant phenotype [265]. Induction of ER-stress and the UPR in vemurafenib-resistance results in increased apoptosis [212, 266]. This provides a potential therapeutic combination.

The reliance of cancer on the UPR and the increased levels of UPR mediators provides a target for development of anti-cancer drugs. Prasad *et al*. reported that activation of the UPR in melanoma, specifically IRE1 and XBP1, prior to the introduction of oncolytic viruses enhanced adenovirus levels specifically in cancerous cells and resulted in increased tumour cell killing [267]. In addition, up-regulated GRP78 on the surface of cells is a target for peptidic ligands to melanoma [268], a potential avenue for specific peptide-conjugated drug delivery to cancers.

1.2.4 Conclusion

The known role of the UPR in cancer progression and metastasis, particular for melanoma, continues to evolve. The link between melanoma progression and the UPR is well established, what is less clear is how cancers adapt to chronic UPR induction while being resistant to its apoptotic mechanisms. Understanding the factors that influence the balance between the survival and death responses of the UPR is essential for targeting this stress response. Given that cancers constantly activate the UPR to respond to environmental stress, it is likely that they develop mechanisms to evade UPR-induced apoptosis. Therefore, combinatorial drug treatments that target the UPR are promising with dual treatments expected to be most effective in combating melanoma. Further research into the role of the UPR in malignancy will help in development of drugs that modulate drug resistance and apoptosis. The dependence of melanomas on the UPR for survival has prompted focused interest on this pathway for development of effective treatments for metastatic melanoma.

1.3 Aims

Melanoma patients with metastatic disease have variable outcomes, with some patients having more aggressive disease phenotypes and only select patients responding to current therapies. The aim of this study was to utilise proteomics to identify proteins, pathways and mechanisms that would contribute to melanoma progression. The outcome of these findings would contribute to our understanding of melanoma biology and contribute to the future diagnosis or prognosis of patients. Additionally, may identify novel drug targets and potentially identify novel combinatorial treatment strategies to improve patient drug responses.

A previous study conducted in our laboratory by Mactier *et al*. [269], using isobaric tag for relative and absolute quantitation (iTRAQ) labelled mass spectrometry (MS) and 2-D Fluorescence Difference Gel Electrophoresis (DIGE) identified 84 proteins that were differential in good and poor prognosis stage III melanoma patients. Based off this discovery study the first aim of this project was to validate the differential abundance of the proteins associated with poor patient outcome utilising an orthogonal technique. Then using the validated proteins define a prognostic panel with the ability to predict stage III melanoma patients likely to have poor outcome after surgical intervention and to deliver the prognosis panel as a Selected Reaction Monitoring (SRM) assay, due to the clinical utility of this technique.

From both the above study [2] and the work carried out by Mactier *et al*. [269], the Unfolded Protein Response (UPR) was identified to be upregulated in melanoma patients with poor outcome, therefore this stress response was selected for further study in melanoma cell line models. The aim was to identify proteins that are differentially abundant in cell lines with increased UPR activation utilising quantitative discovery proteomic techniques. The differentially abundant proteins were then validated using an orthogonal mass spectrometry technique, SRM. The observed changes in the melanoma proteome could contribute to our understanding of how this cellular stress response contributes to melanoma progression.

The proteins identified to be differentially abundant with increased UPR activation in melanoma cell lines were then studied with bioinformatic analysis of publicly available proteomic and transcriptomic cell line and patient dataset. The differentially abundant UPR-associated proteins were examined for their association with patient survival in melanoma and pan-cancer cohorts.

1. Validate 34 of the 84 proteins identified to be differentially abundant in poor prognosis stage III melanoma patients from the previous study by Mactier *et al.* utilising an orthogonal mass spectrometry technique, Selected Reaction Monitoring (SRM).
2. Identify a prognostic protein panel utilising SRM in stage III cutaneous melanoma able to identify patients likely to have poor outcome and therefore require aggressive therapeutic interventions.
3. Establish a melanoma cell line model for *in vitro* study of the Unfolded Protein Response (UPR).
4. Characterise changes in the melanoma proteome that occur with increased UPR activation utilising cell line models and quantitative discovery proteomics to identify how this stress response contributes to melanoma progression.
5. Orthogonally validate proteins differentially expressed with increased UPR induction using SRM in a broader melanoma cell line panel to identify key proteins of the UPR across heterogenous disease phenotypes.
6. Validate through *in silico* analysis the contribution of the differentially abundant UPR-associated proteins to melanoma progression and their association with UPR activation.
7. Compare with *in silico* analysis the abundance of the differentially abundant UPR-associated proteins in cell line models with MEK inhibitor sensitivity/resistance.
8. Determine the prognostic significance of the differentially abundant UPR proteins in melanoma and pan-cancer publicly available transcriptomic and proteomic datasets.

Chapter 2: Materials and Methods

2.1 Materials, kits and reagents

All materials, kits and reagents were purchased from Sigma-Aldrich (St Louis, Mo, USA) unless otherwise stated.

2.2 Preparation of melanoma patient samples for selected reaction monitoring mass spectrometry

2.2.1 Clinical Samples

Melanoma lymph node metastases were obtained from the Melanoma Institute Australia (BioSpecimen Bank) with ethical approval from the Sydney Southwest Area Health Service Institutional Ethics Review Committee (RPAH Zone), protocol numbers: X08-0155/HREC, 08/RPAH/262, X11-0023/HREC, 11/RPAH/32 and X07-0202/HREC/07/RPAH/30. Lymph node samples were obtained with informed consent from AJCC stage IIIc patients undergoing surgery at the Melanoma Institute Australia (Sydney, NSW, Australia). Patient samples (n=30) were classified into Good prognosis (> 4 years survival, 8.1 years median survival, n=16) and Poor prognosis (< 2 years survival, 0.5 years median survival, n=14) cohorts based on patient survival post-resection. Clinico-pathologic characteristics of the melanoma patients and their tumours are summarised in **Table 3-1**, **Supplementary Table S3-1** and **Supplementary Table S3-2**. Details on specimen collection and clinic-pathological characterisation are as previously described by Mann et al. [12].

2.2.2 Protein isolation and digestion

For preparation of protein extracts from melanoma lymph node resections, methods were taken from Mactier *et al.* [269] frozen samples were ground to a powder with liquid nitrogen and solubilised in dissolution buffer (7 M urea, 2 M thiourea, 4% (w/v) CHAPS, 65 mM DTT, 2 mM tributylphosphine (TBP) and 40 mM Tris base) with sonication (Ultrasonics Model W-225R, Ultrasonics, Inc., Plainview, NY, USA). Protein lysates were desalted and nucleic acids removed using the BioRad 2D clean up kit according to the manufacturer's instructions. Protein extracts in 0.5 M triethylammonium bicarbonate (TEAB), pH 8.0 and 0.1% (w/v) SDS were reduced with 10 mM tris (2-carboxyethyl)phosphine (TCEP) for 1 hr at 60ºC and alkylated with 50 mM iodoacetamide for 45 min at room temperature in the dark. Proteins were digested

with sequencing grade trypsin (Promega, Madison, WI, USA) overnight (37ºC, pH 8.0) at a protease to substrate ratio of 1:25. The resulting peptides were purified and concentrated using cation exchange chromatography (SCX, AB-SCIEX, Framingham, MA, USA) and reverse phase chromatography with hydrophilic-lipophilic balanced (HLB) Oasis C18 nano-columns (Waters, Milford. MA, USA) according to the manufacturer's instructions. Peptides were resuspended in 0.1% (v/v) formic acid and quantified using the Qubit Protein Assay kit (Thermo Fisher Scientific, Waltham, MA, USA).

2.2.3 SRM analysis - acquisition and LC methods

Proteotypic peptides of target proteins and their corresponding SRM assays were predicted using the National Institute of Standards and Technology (NIST) NIST_human_IT consensus library, Skyline software 2.0 with collision energy optimisation [270] and SRMAtlas [271]. Collision energies for all transitions were optimised using Skyline [272]. Peptide samples were spiked with the corresponding ^{13}C- and ^{15}N-labelled synthetic peptides (JPT Peptide Technologies, Berlin, Germany, see **Supplementary Table S3-3**). Samples were analysed in duplicate using an AB-SCIEX 5500 QTRAP MS equipped with a nano-electrospray ion source. Liquid chromatography separations of peptides were performed on an Eksigent nanoLC system (Dublin, CA, USA) coupled to a 75 µm id x 190 mm fused silica emitter (New Objective, Woburn, MA, USA), packed with a Magic C18AQ resin (5 µm, 200 Å). Peptide mixtures (5 µL), containing 0.5 µg of endogenous peptides and 10-50 fmol of heavy-labelled synthetic peptides, were first loaded onto a ZORBAX 300SB C18 Nanoflow HPLC column (300 µm x 5 mm x 5 µm; Agilent Technologies, Santa Clara, CA, USA) and then passed onto the fused silica emitter. Peptides were separated with a 25 min linear gradient from 3% to 40% acetonitrile with 0.1% formic acid at 300 nL/min. The MS was operated in positive ion, scheduled SRM mode (detection time window: 240 s; target scan time: 1.5 s). QTRAP performance was monitored with a calibration curve of increasing light:heavy peptide ratio and bovine serum albumin standard.

2.2.4 Data analysis

Data files (.wiff) were imported into Skyline and manually inspected for correctness. Skyline criteria were set to a mass tolerance of 0.5 on monoisotopic *y*- and *b*-ions generated by tryptic digestion with zero missed cleavages. Peaks were searched against (NIST) Human mass

spectral database. Total peak area ratios (ratios of the sum of 3 areas corresponding to 3 transitions) of light (L: endogenous peptides) to heavy (H: isotopically-labelled peptides) were log-transformed for analysis. These data represent the relative abundances of peptides in Good and Poor prognosis melanoma patients.

Statistical analyses were performed on combined SRM data from the current study and previous work by Mactier *et al* [269]. Peptide abundance was quantified by obtaining the light isotope abundance for each peptide and patient from the above output. Missing data were imputed using the k-Nearest Neighbours approach with parameter k set as 5. The peptide data were then normalised using the Remove Unwanted Variation (RUV) procedure [273]. Differentially abundant proteins were identified by fitting linear fixed effects models on the peptides belonging to the protein, or in the case of a single peptide, a two-sided *t*-test. The ten new proteins were found to be differentially abundant based upon a criterion of unadjusted *p*-value < 0.05, no fold-change cut-off was employed.

Next, classification of proteins was performed to determine the cross-validation error rates on predicting prognosis status of patients using the protein data, with various sets of proteins as input into this data. The Diagonal Linear Discriminant Analysis (DLDA) method was used to perform classification, and 5-fold cross validation was repeated 100 times to obtain error rates, each incorporating a feature selection step based on resubstitution error rate. Classification and cross-validation were implemented using the ClassifyR R package [274].

The Kaplan-Meier (KM) survival curves stratified samples based on their classification prediction result using the DLDA classifier trained on all other samples, leave one out method. The Cox proportional hazards model was fit with the top classifiers and the log rank test was used to calculate the *p*-value for separation of the two survival curves. Unadjusted *p*-values are reported in the top-right corner of each plot. The overall workflow is summarised in **Figure 3-1**.

2.2.5 *In silico* validation

The top classifier proteins from the DLDA and Cox proportional hazard model were input into SurvExpress, an online biomarker validation tool [275] using the Cancer Genome Atlas data on 335 cutaneous melanoma patient with genomic, transcriptomic and proteomic profiles [276]. Cox survival analysis was performed as described by Aguirre-Gamboa *et al.* [275] censoring by survival and risk with maximised risk group feature selected.

2.3 Cell culture of melanoma cell lines

Melanoma cell lines (**Table 2-1**) were supplied by Dr John Allen (The Centenary Institute, The University of Sydney). Cells were cultured as an adherent monolayer in Dulbecco's Modified Eagle's Medium (DMEM) supplemented with 10% (v/v) foetal calf serum (FCS), 44 mM sodium hydrogen carbonate and 0.1% (v/v) PenStep (100 Units penicillin and 100 μg Strepamycin) and grown in vented-capped culture flasks in a humidified incubator at 37°C with 5% carbon dioxide. Cells were grown to 80-90% confluency then detached with 0.05% (w/v) Trypsin, 0.02% (w/v) EDTA and passaged 1:10 to maintain optimum growth.

To maintain stock and limit mutational changes cell lines were cryopreserved in liquid nitrogen. Cells were washed with PBS and centrifuged at 400 x g, 5min, 20°C (Hettich, Universal 32R), before resuspending in heat-inactivated FCS. An equal volume of heat-inactivated FCS containing 20% (v/v) dimethyl sulfoxide (DMSO) was then added drop wise to the suspension to a final density of 2-5 x 10^6 cells/ mL. Cells were aliquoted into cyrovials and gradually frozen to -80°C prior to long-term storage in liquid nitrogen. To revive cells, cryovials were rapidly thawed in a 37°C water bath then washed twice with growth medium and pelleted at 400 x g, 5 min, 20°C (Hettich, Universal 32R). Cell pellets were resuspended in growth medium and cultured as described above.

Cell viability and density was determined using the trypan blue exclusion method. Cell suspensions were mixed with an equal volume of 0.4% (w/v) Trypan blue solution and loaded onto a Neubauer haemocytometer. Trypan blue permeates and stains only dead cells, therefore the number of stained (dead) and unstained (viable) cell can be counted under an inverted light microscope (Nikon TMS, Kanagawa, Japan) and cell density and viability determined by the following equations. A cell viability cut-off of >95% was employed for the use of cell line samples in any of the following experimental protocols.

Cell Viability = [(# unstained cells) / (# stained + unstained cells)] x 100

Cell Density = (# unstained cells / # squares counted) x 10^4 x dilution factor

Table 2-1. Melanoma cell lines used in Chapter 4 and 5. Cell lines used in iTRAQ (Chapter 4) and SRM (Chapter 5) experiments to model the unfolded protein response with information on melanomas from which the cell line was derived and the known mutations of biological importance.

Cell line	Stage	Site	Known mutations of relevance [277]
WMM1175	Primary	Dermis	$BRAF^{V600E}$, NRAS, CDKN2A
Mel-RM	Metastasis	Lymph node	NRAS, HGNC
SK-Mel-28	Primary	Dermis	$BRAF^{V600E}$, CDK4, EGFR, PTEN, TP53
WMM1215	Unknown	Unknown	$BRAF^{V600E}$, PDGFRA

2.3.1 Cell culture thapsigargin treatment

2.3.1.1 SRB assay

The sulforhoamine B (SRB) assay was performed according to the manufacturer's instructions (Invitrogen). Cells were seeded at 30% confluence in a 96 well plate. At 48 hrs after the initial seeding cells were at 60% confluence in log growth phase and treated with varying concentrations of thapsigargin (0.1 – 10 µM), or a 0.1 % (v/v) DMSO control. Empty wells containing media alone served as a control for background staining. Treatment and cell growth was halted in 24 h intervals by 10% (v/v) trichloroacetic acid fixation for 1 h at 4°C. Plates were washed five times with MilliQ water then dried. Proteins were stained with 0.4% (w/v) SRB dye in 1% (v/v) acetic acid for 25 min at room temperature, followed by the removal of excess dye with five times 1% (v/v) acetic acid. The SRB dye was solubilised in 10 mM Tris base (pH 10.0) for 5 min with agitation and the absorbance at 492 nm measured on a 96-well plate reader (Multiskan EX, Thermo Electron Corporation, Shanghai, China). A background reading was measured at 690 nm to subtract for plastic interference. The background plate and proteins from the media determined by the media alone wells were subtracted from the plate readings. The final protein content of each cell was calculated as a percentage of the untreated control cells.

2.3.1.2 Sub-G1 DNA assay

The Sub-G1 DNA assay uses the nucleic acid stain propidium iodide (PI) to assess cell viability. MEL-RM and WMMM1175 melanoma cell lines were seeded into 175 cm^2 flasks at 30% confluence. Cells were treated with thapsigargin 48 h after seeding at 1 µM for 48 h as determined by the SRB assay described above. Cells were harvested by tryptic digestion as described in Chapter 2.3. Any apoptotic cells detached from the plate surface during incubation

were also collected for the assay. Cells were centrifuged at 350 x g, the supernatant was centrifuged at 1,000 x g to ensure the collection of any buoyant apoptotic cells. Cells were resuspended in PBS, then fixed with nine times volume of fixed in 70% (v/v) ethanol for 1 h at 4°C. Cells were washed three times with PBS before resuspending in 0.2 M $NaHPO_4$ with 0.1% (v/v) Triton-X 100 for 5 min. Cells were centrifuged and resuspending in 0.002% (w/v) PI with 0.02% (w/v) RNase for 1 h at room temperature in the dark. Cells were then analysed for DNA content by flow cytometry, 488 nm in-line laser excitation and absorbance at 600 nm with forward side scatter, collecting 50,000 events. Gating was imposed for the cell population to remove cell debris and DNA aggregates. Flow cytometry data was analysed with FlowJo, overlaying DNA sub-populations.

2.3.2 Subcellular fractionation of melanoma cell lines

2.3.2.1 Cell lysis

Approximately 5 x 10^8 cells were harvested by trypsinisation, washed once with PBS, then with ice cold PBS and centrifuged (400 x g, 5 min, 4℃). Cells were washed again with lysis wash buffer (10 mM HEPES, 10 mM KCl, 1.5 mM $MgCl_2$, 0.5 mM PMSF**,** 10 mM NaF, 1 mM $NaVO_3$, pH 7.9, 4℃), pelleted then resuspended in lysis death buffer (10 mM HEPES, 10 mM KCl, 1.5 mM $MgCl_2$, 0.5 mM PMSF, 10 mM NaF, 1 mM $NaVO_3$, 0.05% (v/v) NP-40, 0.1% (w/v) okadaic acid, pH 7.9, 4℃), and incubated on ice for 10 min to induce hypotonic swelling. Cells were homogenised with seven strokes of a Dounce-homogeniser, and lysis checked microscopically. The whole cell lysate was then centrifuged (800 x g, 10 min, 4℃) to pellet the crude nuclear fraction from the supernatant containing the mitochondrial, cytoplasmic and membrane fractions.

2.3.2.2 Nuclei isolation and purification

The crude nuclear pellet was resuspended in 10 mL of nuclear isolation buffer (0.25 M sucrose, 20 mM Tris-HCl, 10 mM $MgCl_2$, 1 mM EDTA, pH 7.4, 4°C) and layered onto a two-step sucrose gradient consisting of 10 mL 1.28 M sucrose buffer (1.28 M sucrose, 20 mM Tris-HCl, 10 mM $MgCl_2$, pH 7.4, 4°C) over 15 mL of 1.89 M sucrose barrier (1.89 M sucrose, 20 mM Tris-HCl, 10 mM $MgCl_2$, pH 7.4, 4°C). Purified nuclei collected from the sucrose interface were pelleted by centrifugation at 5,400 x g for 45 min at 4°C (Beckman Optima™ L-100 XP ultracentrifuge, SW32Ti swinging bucket rotor). The nuclei were washed with lysis buffer (10

mM HEPES, 10 mM KCl, 1.5 mM $MgCl_2$, pH 7.9, 4℃), pelleted at 1,000 x g, 5 min, 4℃ (Hettich, Universal 32R), and stored at -80℃.

2.3.2.3 Mitochondria isolation and purification

The supernatant isolated above was diluted 1:10 with 10X cytoplasmic extraction buffer (0.3 M HEPES, 1.4 M KCl, 30 mM $MgCl_2$, pH 7.9, 4℃) and centrifuged at 15,000 x g for 25 min at 4℃ (Sorvall, Evolution RC). The pellet was resuspended in isotonic buffer (0.25 M sucrose, 10 mM Tris-HCl, 1 mM EDTA, pH 7.4, 4℃). Then layered over a discontinuous sucrose gradient consisting of 13 mL of 1.0 M sucrose buffer (1 M sucrose, 10 mM Tris-HCl, 10 mM $MgCl_2$, 1 mM EDTA, pH 7.4, 4℃) over 18 mL of 1.5 M sucrose barrier (1.5 M sucrose, 10 mM Tris-HCl, 2.5 mM $MgCl_2$, 1 mM EDTA, pH 7.4, 4℃) and centrifuged 87,000 x g for 90 min at 4℃ (Beckman Optima™ L-100 XP ultracentrifuge, SW32Ti swinging bucket rotor). Whole mitochondria were collected from the sucrose interface and diluted 1:2 with Tris buffer (50 mM Tris-HCl, 150 mM NaCl, 1 mM EDTA, 0.5 mM PMSF, pH 7.5, 4℃) then pelleted at 15, 000 x g for 20 min at 4℃ (Hettich, Universal 32R) and stored at -80℃.

2.3.2.4 Isolation of cytosolic and membrane fractions

The combined cytoplasmic and membrane fractions isolated above were centrifuged at 100,000 x g for 60 min at 4°C (Beckman Optima™ L-100 XP ultracentrifuge, SW32Ti swinging bucket rotor). The supernatant containing the cytoplasmic fraction was snap frozen in liquid N_2 and both fractions were stored at -80°C.

2.4 Proteome preparation of melanoma cell line samples for iTRAQ and selected reaction monitoring mass spectrometry

2.4.1 Lysis of cells and subcellular fractions

Melanoma cells were harvested by tryptic digestion and washed with PBS as described above. Cells were then lysed with the addition of 0.1% SDS with 0.1% Benzonase and incubated on ice for 20min to allow for DNase digestion. Cells were then sonicated on ice for 30sec with 1 min pause between each cycle.

2.4.2 Chloroform/ methanol protein clean

Due to the high lipid content present in cell lines cell lysates were cleaned with the chloroform/methanol precipitation method. Sample: methanol: chloroform: water ratio was

1:3:0.75:2.25. The entire procedure was carried out on ice with vortexing after each addition. Protein samples lysed as above were aliquoted, 200 µL, into polypropylene tubes. Ice cold methanol, 600 µL was added, followed by 150 µL ice cold chloroform and then 450 µL ice cold MilliQ water. Protein lysates were centrifuged for 10min at 10000 x g to form the protein interphase. The top chloroform layer was removed with care taken not to disturb the precipitated protein interface. Methanol, 500µL, was added, then the protein precipitate pelleted by centrifugation 10min, 10,000 x g. The protein precipitate was washed twice with 1 mL of methanol and centrifuged at 10,000 x g for 10min before allowing the pellet to air dry.

2.4.3 Protein and peptide quantitation

Proteins were solubilised in buffer appropriate for the downstream procedures and quantified by Qubit fluorometric protein assay kit according to the manufacturer's instructions (Thermo Scientific, USA). Briefly, Qubit working solution was prepared by mixing the Qubit buffer with Qubit reagent (1:200). Assay were carried out in thin-walled PCR tubes, with 1-10 µL of protein lysate diluted in working solution to a total volume of 200 µL. Proteins were incubated with the fluorophore for 15 min in the dark before absorbance reading taken on the Qubit fluorometer 2.0 in Protein mode. Proteins concentrations were determined using the absorbance of standards provided in the Qubit kit.

2.4.4 Tryptic digestion

Protein samples were solubilised in 0.5 M in TEAB, pH 8.0 with 0.1% (w/v) SDS. Disulphide bonds were then reduced with 4.4 mM tris-(2-carboxyethyl)-phosphine (TCEP) for 1 h at 60℃. Cysteine residues were blocked with 10 mM iodoacetamide in 100 mM TEAB and incubated for 45 min at room temperature in the dark. Tryptic digestion was performed by the addition of sequence grade modified trypsin (Promega, Madison, WI, USA) at a ratio of 1:25, trypsin: protein and incubated at 37℃ overnight. Samples were dried in a vacuum centrifuge concentrator 5301 (Eppendorf, Hamburg, Germany).

2.4.5 Peptide labelling with iTRAQ tags

Tryptically digested peptides were chemically derivatised for quantitative MS using isobaric tags for relative and absolute quantification (iTRAQ). Peptide labelling with 8-plex iTRAQ tags was performed as per the manufacturer's instructions (AB-SCIEX, Foster city, CA, USA). Peptide samples were dried in a vacuum centrifuge concentrator 5301 (Eppendorf, Hamburg, Germany) and reconstituted in 1 M TEAB. iTRAQ labels were prepared with the addition of 50 µL of isopropanol to each iTRAQ label tube at room temperature, then 20 µL of the iTRAQ label solution was added to each peptide sample. The pH of the samples was adjusted to >7.5 and the peptide mixtures incubated for 2 h at room temperature. The labelled peptides from each iTRAQ set i.e. 113-119, 121, were combined in LowBind Eppendorf tubes (Eppendorf, Hamburg, Germany).

2.4.6 Peptide purification and desalting

Contaminants and salt in peptide preparations was removed with strong cation exchange (SCX) and hydrophilic-lipophilic balanced (HLB) LC columns.

2.4.6.1 Cation exchange cartridge

Peptides were cleaned using a cation-exchange cartridge (Applied Biosystems, Foster city, CA, USA) according to the manufacturer's instructions. Briefly, samples were diluted with 10 times volume of Cation-Exchange buffer - Load (10 mM potassium phosphate, 25% (v/v) acetonitrile, pH 3.0). The samples pH was adjusted between pH 2.5 and 3.3 with phosphoric acid. The Cation-exchange cartridge was conditioned with Cation-Exchange buffer- Clean (10 mM potassium phosphate, 25% (v/v) acetonitrile, 1 M potassium chloride, pH 3.0), then Cation-Exchange buffer – Load (10 mM potassium phosphate, 25% (v/v) acetonitrile, pH 3.0). The sample was then loaded onto the cartridge (1 drop/ 5 sec). The cartridge was washed with Cation-Exchange buffer – Load (10 mM potassium phosphate, 25% (v/v) acetonitrile, pH 3.0) and the peptides eluted with Cation-Exchange buffer – Elute (10 mM potassium phosphate, 25% (v/v) acetonitrile, 350 mM potassium chloride pH 3.0) into a LoBind eppendorf tube (Eppendorf, Hamburg, Germany).

Protocols which yielded small proteins and peptide preparations were cleaned with SCX stage tips. SCX stage tips, 200 µL capacity, were conditioned prior to loading samples**. S**amples were resuspended in 20% (v/v) acetonitrile, 0.4% (v/v) formic acid. Samples were loaded onto the column and impurities washed from the solid phase with wash buffer (20% (v/v)

acetonitrile, 0.4% (v/v) formic acid), before eluting peptides with elution buffer (500 mM ammonium acetate, 20% (v/v) acetonitrile).

2.4.6.2 HLB desalting

Peptides were desalted and concentrated by reverse phase chromatography on Oasis® hydrophilic-lipophilic-balanced (HLB) cartridges (Water, Massachusetts, USA) according to the manufacturer's instructions. Briefly the cartridge was conditioned with methanol, followed by acetonitrile then load buffer (5% (v/v) acetonitrile, 0.1 % (v/v) formic acid). The peptide samples were diluted in 0.1% (v/v) formic acid to a final concentration of 5% (v/v) acetonitrile. The peptide samples were then loaded onto the cartridge and washed with load buffer. The peptides were eluted with Elution buffer (50% (v/v) acetonitrile, 0.1% (v/v) formic acid), then with acetonitrile containing 0.1% (v/v) formic acid). The eluent was collected in LowBind eppendorf tubes (Eppendorf, Hamburg, Germany) and concentrated using vacuum centrifuge concentrator 5301 (Eppendorf, Hamburg, Germany). Finally, peptide samples were diluted to 1 μg/μL in 0.1% (v/v) formic acid.

Protocols which yielded small proteins and peptide preparations were cleaned with C18 ziptips according to the manufacturer's instructions. SCX stage tips, 200 μL capacity, were conditioned prior to loading samples**.** Samples were resuspended in 20% (v/v) acetonitrile, 0.4% (v/v) formic acid. Samples were loaded onto the column and impurities washed from the solid phase with wash buffer (20% (v/v) acetonitrile, 0.4% (v/v) formic acid), before eluting peptides with elution buffer (500 mM ammonium acetate, 20% (v/v) acetonitrile.

2.4.7 Quantitative MS analysis of iTRAQ labelled samples

2.4.7.1 SCX off-line fractionation

Prior to MS analysis each set of iTRAQ labelled peptide mixtures was fractionated by strong cation exchange (SCX) chromatography using a column (ZORBAX, Bio-SCX series II, 3.5 mm, 50 x 0.8 mm, Agilent, Palo Alto, CA, USA) attached to an Agilent 1100 HPLC system (Agilent, Palo Alto, CA, USA) in offline mode. The peptide mixtures were diluted in SCX buffer A (25% [v/v] acetonitrile, 0.05% [v/v] formic acid, pH 2.5) and injected onto the SCX column. After washing isocratically for 4 min at 18 μL/min, the peptides were eluted with the gradient from 0% SCX buffer B (25% [v/v] acetonitrile, 0.5 M ammonium formate, 2% [v/v] formic acid, pH 2.5) to 20% SCX buffer B in 42 min and then from 20% B to 100% B in 14 min, 100% B was maintained for 5 min. Fractions were collected at 2 min intervals into a

LowBind Eppendorf 96-well plate (Eppendorf, Hamburg, Germany) using a Probot microfraction collector (Dionex/LC Packings, Lane Cove, NSW, Australia), giving a total of 30 SCX fractions per sample set. Fractions 1-5, 6-7 and 28-30 were pooled to give a total of 23 fractions for MS analysis.

2.4.7.2 Reverse-phase (RP) – Nano-LC electrospray ionisation (ESI) tandem mass spectrometry (MS/MS)

The SCX fractions were analysed by LC-MS/MS. Samples were fractionated by reverse phase liquid chromatography using an Agilent 1100 HPLC system interfaced to a QSTAR Elite ESI mass spectrometer (AB-SCIEX, Foster City, CA, USA). SCX fractions were diluted 1:2 with solvent A (0.1% (v/v) formic acid) and loaded onto a C_{18} trap column (ZORBAX, 300SB-C18, 300 μm x 5 mm, 5 μm, Agilent, Palo Alto, CA, USA) at 10 μL/min and the column washed for 7 min with solvent A. Peptides were eluted from the trap column onto the C_{18} separation column (ZORBAX, 300SB-C18, 150 μm x 150 mm, 3.5 μm, Agilent, Palo Alto, CA, USA). The peptides were then eluted at 0.6 μL/min directly into the ionisation source with an increasing gradient of solvent B; 0 min, 5% solvent B (0.1% (v/v) formic acid in acetonitrile); 8 min, 5% B; 10 min, 15% B; 90 min, 30% B; 105 min, 60% B; 115 min, 5% B; 120 min, 5% B. Flow through samples from the SCX and HLB clean up columns were analysed by 1D-HPLC LC-MS/MS by reverse-phase (RP) fractionation onto the QSTAR Elite ESI mass spectrometer (AB-SCIEX, Foster City, CA, USA) as described above with the exception of a gradually increasing solvent B gradient; 0 min, 5% B (0.1% (v/v) formic acid in acetonitrile); 7 min, 5% B; 9 min, 15% B; 23 min, 60% B; 30 min, 5% B.

Data acquisition was performed on the QSTAR Elite MS in an information-dependent acquisition mode (IDA) using Analyst QS 2.0 software (Applied Biosystems Inc., Foster City, USA). In IDA mode, a TOF-MS survey scan was acquired (*m/z* 350-1750, 0.5 s), with the three most abundant multiply charged ions (2+ to 4+, counts >30) in the survey scan sequentially subjected to product ion analysis. Product ion spectra were accumulated for 2 sec in the mass range *m/z* 100-1800 with a modified Enhance All mode Q2 transition setting favouring low mass ions so that the iTRAQ reporter ions (113-121) intensities were enhanced for quantification. Automatic collision energy and automatic MS/MS accumulation modes were used in the advanced IDA settings. Data acquisition was performed with an exclusion of 30 sec for previous target ions. The performance and dynamic range of the QSTAR Elite ESI MS was assessed with a peptide standard consisting of 0.1 μM BSA, 20 nM fetuin, 0.1 μM Glu-1-

fibrinopeptide B peptide (GluFib) and 10 nM renin in 0.5% (v/v) acetonitrile with 0.01% (v/v) formic acid.

2.4.7.3 Data analysis of iTRAQ samples

The data acquired from the MS/MS of each iTRAQ set was analysed using ProteinPilot™ v4.0 software (AB-SCIEX, Foster City, CA, USA) utilising the Paragon™ algorithm for protein identification and the Pro Group™ algorithm to perform a statistical analysis on the peptides found to determine the minimal set of confident protein identifications [278]. MS/MS spectra were searched against the SwissProt protein database (human consensus database, 2014-05-29). The user defined parameters were set to i) sample type: iTRAQ 8-plex; ii) cysteine alkylation: iodoacetamide; iii) digestion: trypsin allowing for 1 missed cleavage; iv) species: *Homo sapiens*; v) instrument: QSTAR Elite ESI. The program was also set to perform bias correction, background correction and iTRAQ reporter ion quantitation with a thorough identification search including biological modifications and oxidation of methionine. To estimate the rate of false positives a concatenated target-decoy database was also searched.

A protein identification threshold of 95% confidence or greater for peptide matches, an unused ProtScore of >1.3 was imposed and a global false discovery rate (FDR) of 1%. The intensity ratios of isobaric tag reporter ion peaks were used to quantify relative peptide abundance and therefore the corresponding protein in samples.

2.4.8 Statistical analysis of iTRAQ data

2.4.8.1 Differentially abundant protein analysis

ProteinPilot results were exported to Microsoft Excel and analysed to identify those proteins whose changes in abundance were statistically significant. A Student's paired *t*-test was performed with equal variance to compare control to treated samples in both Mel-RM and SK-MEL-28 cell lines. Only those proteins whose change in abundance had a fold change of 1.5 or greater with an unadjusted p-value < 0.05 were taken as statistically significant.

2.4.8.2 Hierarchical clustering and principal component analysis

Hierarchical clustering was performed with the python package Seaborn clustermap using Euclidean distance metrics and Pearson's correlation [279]. Missing values were excluded from the correlation analysis so as not to introduce unwanted variance from technical missing

values although values missing biologically, that may be of significance are ignored as a consequence.

Principal component analysis (PCA) was carried out with the python package sklearn [280]. Data was not transformed, unit variance scaling was employed on iTRAQ ratios with Nonlinear Iterative Partial Least Squares (NIPALS) PCA method without imputation.

2.5 Western Blotting

2.5.1 1D gel electrophoresis

Proteins samples were solubilised in SDS-PAGE loading buffer (62.5 mM Tris-HCl (pH6.8), 10% (v/v) glycerol, 5% (v/v) 2-mercaptoethanol, 2% (w/v) SDS and 0.02% (w/v) Bromophenol Blue), heated 95ºC for 5 min and cooled on ice. Protein (10 µg) was loaded onto polyacrylamide gels separated using a 5% polyacrylamide stacking gel (5% (w/v) acrylamide/bis, 125 mM Tris-HCl (pH 6.8), 0.1% (w/v) SDS, 0.05% (w/v) ammonium persulfate and 0.1% (v/v) TEMED) and a 12% polyacrylamide separating gel (12% (w/v) acrylamide/bis, 375 mM Tris-HCl (pH 8.8), 0.1% (w/v) SDS, 0.05% (w/v) APS and 0.1% (v/v) TEMED). Pre-stained molecular weight markers were loaded into a well on each gel. Electrophoresis was carried out in a Bio-Rad mini Protean III gel electrophoresis cell at 120 V in running buffer (192 mM glycine, 0.1% (w/v) SDS, 24.8 mM Tris-HCl (pH 8.3) for approximately 90 min until the dye front had run off the gel.

2.5.2 Western blotting

Western blotting methods were adapted from the original protocol by Towbin *et al.* [281]. Following separation on a 5%/12% SDS-PAGE gel as above, proteins were transferred electrophoretically to a polyvinylidene difluoride (PVDF) membrane at 300 mA for 90 min in a Criterion™ Blotter (BioRad Hercules, CA, USA) with Towbin buffer (25 mM Tris, 192 mM Glycine, 20% (v/v) methanol, 0.1% (w/v) SDS). The membrane was washed three times for 10 min in TBS-T (25 mM Tris, 150 mM sodium chloride, 0.1% (v/v) Tween-20), then blocked in TBS-T containing 5% (w/v) skim milk for 1 hr at room temperature. For antibody specific concentration, buffers and incubation times see **Supplementary Table S2-1**. Membranes were incubated in primary antibodies in TBS-T then washed three times for 10 min in TBS-T. The membrane was then incubated in the corresponding secondary antibody, then washed three

times for 10 min in TBS-T. Secondary antibodies were then detected by incubating membranes for 5 min at room temperature in ECL reagent (SuperSignal® West Pico Chemiluminescent Substrate, Pierce Biotechnology, Il, USA) containing 1:1 Stable Peroxide solution:Luminol/ Enhancer solution. The bands were visualised with X-ray film (Amersham Hyperfilm™ ECL, GE Healthcare, Pistcataway, NJ, USA) and quantified by ImageQuant. The primary and secondary antibodies were stripped from the gel with 1% (v/v) hydrochloric acid for 10 min. Sypro Ruby was used to assess even total protein load for each sample and even transfer onto the membrane. PVDF membranes were incubated in Sypro Ruby protein blot staining (Thermo Fisher Scientific, Waltham, MA, USA) at room temperature with agitation for 15min after activating membranes in 7% (v/v) acetic acid and 10% (v/v) methanol. Membranes were washed with MilliQ water three times for 1 min with agitation. Membranes were air-dried before visualisation on a fluorescence laser image scanner at 532 nm (Fuji, Akasaka Minato-ku, Tokyo, Japan).

2.6 Florescence microscopy

Glass slides were coated with 0.01% (w/v) sterile poly-L-lysine for 5 min at room temperature, the solution was removed and slides dried at room temperature. Cell lines were cultured on the poly-L-lysine cover slides as described above, section 2.3. Cells were fixed with 4% (w/v) paraformaldehyde and washed three times with PBS. Slides were incubated with a blocking buffer (0.3 M glycine, 0.1% (w/v) BSA in PBS) for 1 h at room temperature. Fixed slides were incubated with the primary antibodies diluted in blocking buffer with antibody specific conditions ranging from 1 h to overnight and either room temperature or 4ºC (**Supplementary Table S2-1**). The slides were washed three times with PBS before incubating with the fluorophore conjugated secondary antibodies in 0.05% tween-20 in PBS for 1 h in the dark, followed by three times PBS wash. Fixed cells were then incubated with 1.43 µM 4',6-diamidino-2-phenylindole (DAPI) in 0.05% tween-20 in PBS for 5 min at room temperature and washed three times with PBS. Slides were then covered with mounting buffer (6 mM glycine, 0.1% BSA and 0.0025% (v/v) tween-20 and sealed with a cover slip. Slides were imaged on an Olympus BX51 fluorescent microscope at 10 x and 100 x magnification using set lens with specific fluorescent wavelength for the individual fluorophore conjugated antibody or stain. Image analysis was performed with Image J (National institute of Health, USA).

2.7 Bioinformatic analysis

2.7.1 Pathway analysis

Proteins found to be differentially abundant with increased UPR activation were input in the STRING protein interaction data repository [282]. The STRING repository contains curated data on protein interactions from Biocarta, BioCyc, GO, KEGG, and Reactome. Parameters were set for Species; *Homo sapiens*, evidence; experimental only, confidence score; 900, background proteome; All MS protein identifications uploaded. The Protein-Protein interaction score, interaction strength and interaction false discovery rate were calculated as described by [283].

2.7.2 *In silico* correlation of the UPR associated protein with MEK inhibitor resistance

Proteomic data acquired with SWATH-MS by the Molloy group [284] was mined for an associated between the UPR and the RAS/RAF/MEK/ERK pathway via correlation with MEKi sensitivity in a panel of melanoma cell lines. The sensitivity of ten melanoma cell lines were determined by the Molloy group through cell viability on cells treated with MEK inhibitor, selumetinib. Proteins were calculated to correlated with MEKi sensitivity by comparing the topmost sensitive lines with the most resistance line. UPR proteins were determined to contribute to MEKi resistance if they exhibited a Pearson's correlation >0.5 with the resistance score. Unsupervised hierarchical clustering was performed with the python package fastcluster implemented through Seaborn for visualisation.

2.7.3 Validation in melanoma patient proteomic data

Proteomic SWATH-MS data of 32 stage III melanoma patients generated by the Molloy group [284] was examined to validate the association of identified UPR-associated proteins in an *in vivo* context with patient clinical data. Quantitative proteomic data of 52 proteins and the corresponding patient clinical data, including patient overall survival (OS) was analysed. Pearson's correlations were calculated using the Python package fastcluster [285]. To determine if the UPR associated proteins were associated with patient survival, the cohort was

split into good (>4-year OS) and poor prognostic (<1 year OS) groups and log rank *p*-values calculated with two-tailed *t*-test.

2.7.4 Prognostic validation in melanoma patient transcriptomic data – cSurvival data portal

Publicly available RNA-Seq data from 460 melanoma patients from the TCGA-SKCM dataset with corresponding clinical data was downloaded from the cSurvival data repository [286] which maintains curated and quality-controlled patient data from the TCGA which removes problematic samples (e.g. Prior treatment, failed QC, withdrawn patient consent) [287]. The TCGA data represents fragments per kilobase of transcript per million mapped reads (FPKM) and has undergone upper-quartile normalization. Survival analysis with Kaplan–Meier (KM) survival curves, Hazard ratio and 95% confidence interval were calculated by univariate Cox regression on each of the 8-UPR associated proteins as a predictor of overall survival using the python package lifelines [288]. Pearson's correlation and unsupervised hierarchical clustering were performed using the python package fastcluster implemented through Seaborn for visualisation using Euclidean algorithm was then used to determine the association of UPR activation clusters in melanoma patients [279, 285].

2.7.5 Prognostic validation in a pan-cancer RNA-Seq dataset

Publicly available RNA-Seq data from the TCGA was downloaded from the cSurvival data repository listed above [286, 287]. The TCGA data represents fragments per kilobase of transcript per million mapped reads (FPKM) and has undergone upper-quartile normalization. Sixteen solid tumour cohort were selected for analysis; Bladder carcinoma (n=404), Breast cancers (n=725), Cervical carcinomas (n=304), Oesophageal adenocarcinomas (n=80), Head and Neck squamous cell carcinomas (n=499), Renal clear cell carcinomas (n=530), Hepatocellular carcinomas (n=370), Lung adenocarcinomas (n=504), Lung squamous cell carcinomas (n=495), Ovarian carcinomas (n=373), Pancreatic adenocarcinomas (n=177), Rectal adenocarcinomas (n=165), Sarcomas (n=259), Stomach adenocarcinomas (n=247), Thyroid cancers (n=502) and Uterine endometrial carcinomas (n=542). Survival analysis with Kaplan–Meier (KM) survival curves, Hazard ratio and 95% confidence interval were calculated by univariate Cox regression on each of the eight UPR-associated proteins as a predictor of overall survival using the python package lifelines [288]. Cancer cohorts were first

analysed by cancer type, then tumour types grouped for the final analysis when individually predictive of survival.

Chapter 3: A 14-protein panel for the prognostication of AJCC stage III melanoma patients

The following chapter contained the following published works produced in full including published supplementary material*:*

Erin K. Sykes, Cassandra E. McDonald, Shila Ghazanfar, Swetlana Mactier, John F. Thompson, Richard A. Scolyer, Jean Y. Yang, Graham J. Mann and Richard I. Christopherson. **A 14-protein signature for rapid identification of poor prognosis Stage III metastatic melanoma.** *Proteomics – Clinical Applications*, January 2018. DOI: 10.1002/prca.201700094

I designed the experimental study with the co-authors, supervised C.M. on the sample preparation, designed and carried out all mass spectrometry experiments, interpreted the statistical analysis done by S.G., wrote the manuscript with edits from the co-authors.

3.1 Introduction

The incidence of melanoma is the most rapidly increasing of all cancers in the USA where it has increased 15-fold over the past 40 years [289]. Australia and New Zealand have the highest incidence of melanoma in the world with 17,756 cases in 2022, accounting for 10.4% of all new cancers, resulting in 1,281 deaths [290, 291]. The highly aggressive nature of melanoma is reflected in the high mortality rates; accounting for just 4% of all skin cancers, melanoma is responsible for 80% of skin cancer-related deaths [292]. With early detection, accurate diagnosis and appropriate treatment, mainly via surgical resection, primary localised melanoma (stages I and II) is highly curable with a 95% 5-year survival rate [293]. However, melanoma has the potential to metastasise early and the prognosis for patients with lymph node or distant metastases (AJCC stage IV) is poor [294]. For patients with lymph node metastatic disease (AJCC stage III), the most effective treatments are lymph node resection, with or without adjuvant therapies like radiation [295] and interferon α-2b [296]. Advances in mutation-targeted and immune-checkpoint targeted therapies have extended AJCC stage IV patient survival [297]. Adjuvant therapy with immune-checkpoint inhibition in resected stage III disease have improved the overall survival of patients, however the toxicity and expense of these treatments mean that they would be better restricted to patients at high risk of relapse [99, 298].

The life expectancy of patients with AJCC stage IIIc melanoma varies greatly; according to the 7th Edition AJCC staging system, 30-40% will survive beyond five years, while a similar proportion will die within 1 year [299]. Histological and pathological factors (e.g., tumour thickness, pigmentation, ulceration, mitotic rate, invasion of blood vessels or lymphatics and immune cell response) are the predominant attributes used to determine prognosis of melanoma patients, with Breslow thickness of the primary lesion being the most reliable predictor of disease progression [13, 300, 301]. The AJCC uses these parameters to define 4 stages of melanoma. However, current diagnostic methods are limited in their ability to predict individual risk of disease progression, especially in bifurcating stage III patients. The inability to accurately classify melanoma sub-groups and rationally select treatments is reflected in the high mortality rates of late-stage melanoma patients, even with new therapies.

Molecular biomarkers could provide additional prognostic information and insight into the mechanisms of melanoma progression, and guide treatment selection, especially in the adjuvant setting. Several studies have identified biomarkers that correlate with clinical outcomes in melanoma patients. Gene expression profiling of lymph node metastases has been used to

classify stage IV melanomas into four sub-types associated with biological parameters such as pigmentation and immune response that correlate with clinical outcomes [302]. For stage III melanoma patients, mRNA profiling has been utilised to attempt to categorise high risk patients [303]. Levels of tyrosinase-related protein 1 (TYRP1) mRNA, a melanocyte-specific gene, in skin and lymph node metastases, are associated with metastasis-free survival and overall survival in patients with stage III melanoma [304]. Whole-genome mRNA profiling of primary tumours identified a nine gene signature capable of predicting clinical outcomes across all AJCC stages of melanoma [305]. Expression levels of p27 have been identified as a stage specific marker of poor prognosis in stage III and IV melanoma patients [306]. Additionally, gene expression signatures in stage III melanoma patients have been identified that predict response to immunotherapy [307]. Mann *et al.*, 2013 combined data on gene mutations and mRNA expression with clinical pathological parameters to predict survival outcomes in stage III melanoma [299]. The presence of BRAF and NRAS mutations, and the absence of an immune-related (leukocyte) transcriptome profile, were associated with poor survival of stage III melanoma patients [303]. Despite research in this area, clinicians lack a reliable prognostic test for stratification of high-risk stage III melanoma patients. In addition, a reliable method to predict patient response to specific treatments is not currently available.

Several studies have sought to identify differentially abundant proteins in melanoma, such as S100α and lactate dehydrogenase (LDH) in patient serum. In the seventh and eighth editions of the AJCC staging system, LDH was included as a prognostic marker for stage III and IV melanomas [300], increased levels were observed in patients, particularly those with distant metastases (stage IV) [308-310]. However, single protein biomarker screens are unreliable, elevated levels of LDH are associated with several other disease states making false positives common [311-314]. In addition, single protein screens fail to account for the heterogeneity of cancers, not all patients will exhibit altered levels of a particular protein. The use of a panel of biomarkers overcomes these limitations with increased reliability for broad diagnosis. Additionally, biomarker panels could predict drug response for individual tailored treatments.

Our group has previously profiled fresh frozen clinical samples from stage III melanoma patients with Poor outcomes (n=14, <2 year survival post lymph node resection) and Good outcomes (n=16, >4 year survival) using mass spectrometry (MS) with isobaric tags for relative and absolute quantitation (iTRAQ), and two-dimensional fluorescence difference in-gel electrophoresis (2D-DIGE) followed by quantification of selected proteins by Selected Reaction Monitoring (SRM). Twenty-two proteins were validated as potential prognostic

markers [269]. Here we have used SRM to identify ten proteins that are differentially abundant in tumours from patients with Good and Poor outcomes. The SRM data were combined with our previous SRM dataset on AJCC stage III melanoma patients and the combined protein quantitation subjected to Diagonal Linear Discriminant Analysis (DLDA) to generate an improved prognostic signature comprising 14 proteins. The new signature is better able to separate the two prognostic cohorts compared to the previous signature, (*p*-value=0.00019 and *p*-value=0.00036, respectively). The new 14-protein panel can more reliably predict patients likely to have poor outcomes and who would benefit from aggressive therapy. The results obtained here show that MS, in particular SRM, provides a rapid, reproducible method for the stratification of stage III melanoma patients using a panel of biomarkers.

3.2 Methods

Detailed protocols are described below or can be found in Chapter 2: Materials and Methods. Briefly, patient lymph node metastases were examined using selected reaction monitoring (SRM) mass spectrometry (MS) to identify proteins with differential abundance between Poor and Good prognostic cohorts. The differentially abundant proteins from this study were then combined with a study previously conducted in our laboratory, detailing differential protein abundances in the same patient cohort discovered by iTRAQ MS analysis and 2D-DIGE. The combined protein list was then subjected to Diagonal Linear Discriminant Analysis (DLDA) to generate a refined prognostic signature comprising 14-proteins. An overview of the workflow is outlined in **Figure 3-1**.

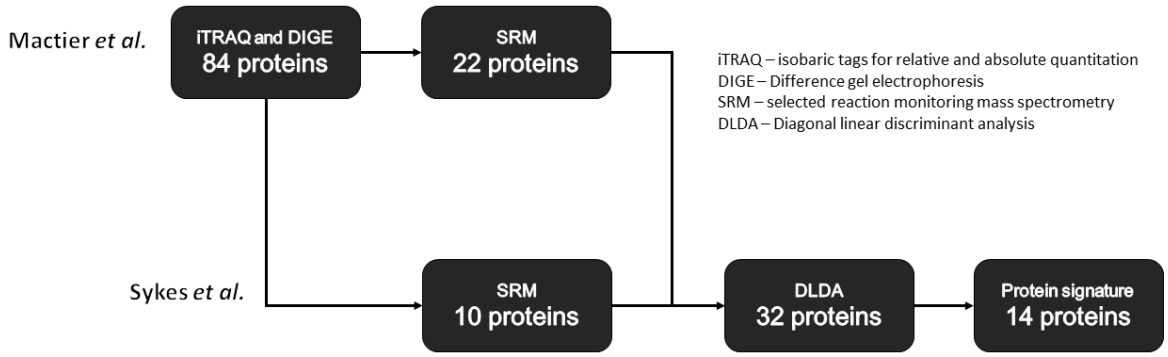

Figure 3-1. Workflow of differential protein analysis of Good and Poor prognosis stage III melanoma patients. Our group has previously identified 84 proteins differentially abundant between whole tissue extracts from Good (n=19, > 4 years survival) and Poor (n=14, < 2 years survival) stage III melanoma patients using iTRAQ and DIGE analysis. Mactier *et al.* validated 22 of these differentially abundant proteins by SRM. In the current study, 34 of the 84 differentially abundant proteins were selected for further validation by SRM. Ten of the 34 selected proteins were validated to be differentially abundant between Good (n=16, >4 years survival post-resection) and Poor (n=14, <2 years survival) stage III melanoma patients. The proteins validated by SRM in both studies, 22 from Mactier *et al*. and 10 from the current study, were combined and subjected to DLDA. A final 14-protein panel was refined for prognostication of stage III melanoma patients.

3.2.1 Clinical Samples

Melanoma lymph node metastases were obtained from the Melanoma Institute Australia (BioSpecimen Bank) with ethical approval from the Sydney Southwest Area Health Service and with patient consent, as detailed in Chapter 2.1.1. Patient samples (n=30) were classified into Good prognosis (> 4 years survival, 8.1 years median survival, n=16) and Poor prognosis (< 2 years survival, 0.5 years median survival, n=14) cohorts based on patient survival post-resection. Clinico-pathologic characteristics of the melanoma patients and their tumours are summarised in **Table 3-1**, **Supplementary Table S3-1** and **Supplementary Table S3-2**.

Details on specimen collection and clinic-pathological characterisation are as previously described by Mann *et al.* [299].

Table 3-1. Clinico-pathologic characteristics of 36 AJCC stage III melanoma patients and their tumours.

Variable	Poor prognosis (n=16)	Good prognosis (n=14)	Good vs Poor (*p*-value)[a]
Age (years, median)	61.6	60.2	0.38
Sex (% Female)	42.9%	42.1%	1.00
Survival (days, median)	189.5	2,939	n/a
Survival (days, range)	27-344	1,499-4,357	n/a
Previous primary melanoma			
Body site (% severe sun damage)	28.6%	42.1%	0.43
Stage at diagnosis (% stage I or II)	71.4%	73.7%	0.18
Breslow thickness (median, mm) [b]	2.6	2.9	0.74
Mitotic rate (median, mm^2) [b]	6.3	5.1	0.66
Melanoma sub-type (% with a nodular component)	21.4%	21.1%	0.33
Presence of regression	57.1%	36.8%	0.26
Ulceration	30.8%	6.7%	0.13
Nodal tumour analysed			
Metastasis size (median, mm)[b]	37.5	35	0.45
Extranodal spread	50%	21.1%	0.14
Number of invasive nodes (median)[c]	10	2	0.05
Cell size (large)	57.1%	68.4%	0.21
Pigmentation (present)	42.9%	15.8%	0.07
Mutational status			
BRAF	42.9%	47.4%	1.00
NRAS	28.6%	36.8%	0.72
PIK3CA	7.1%	0%	0.42
cKIT, MET, EGFR	0%	0%	n/a
FLT3	0%	5.3%	1.00
PDGFRA	7.1%	0%	0.42

[a] *p*-value was calculated by Fisher's exact test (R statistical environment), except for: [b] age, Breslow thickness, mitosis and metastasis size (Mann-Whitney, R statistical environment); n/a, not applicable [c] number of invasive nodes (Student's *t*-test, Excel).

3.2.2 Protein isolation and digestion

Sample preparation in Chapter 3 was performed by Cassandra MacDonald as part of the requirement for the completion of the degree B.Sc (Hons) at the University of Sydney

Detailed methods for the preparation of protein extracts from melanoma lymph node resections for mass spectrometry can be found Chapter 2.1.2. Briefly, cleaned protein extracts were reduced and alkylated with TCEP and iodoacetamide, respectively. Tryptic digestion was performed with a protease to substrate ratio of 1:25 overnight at 37ºC, pH 8.0. The resulting peptides were purified and concentrated using strong cation exchange chromatography (SCX) followed by reverse phase chromatography with hydrophilic-lipophilic balanced (HLB) C18 nano-columns. Peptides were resuspended in 0.1% (v/v) formic acid and quantified using the Qubit Protein Assay kit.

3.2.3 SRM analysis

Detailed methods for the SRM acquisition methods and LC conditions can be found in Chapter 2.2.3. Target proteins (34) were selected for SRM validation from the 84 differentially abundant proteins identified previously by iTRAQ LC-MS/MS and DIGE analyses of stage III melanoma [269]. The 34 proteins were removed from validation in the previous study as the lower fold-changes were deemed to be too low to be of statistical or biological significance. Proteins were selected for further validation in the current study based on fold-change values, *p*-values, biological significance, and the presence of proteotypic peptides conforming to the requirements of SRM analysis. Collision energies for all transitions were optimised using Skyline [272] and peptide samples spiked with the corresponding ^{13}C- and ^{15}N-labelled synthetic peptides (JPT Peptide Technologies, Berlin, Germany, see **Supplementary Table S3-3**). Samples were analysed in duplicate using an AB-SCIEX 5500 QTRAP MS equipped with a nano-electrospray ion source. Liquid chromatography separations of peptide samples were performed in nanoflow with 0.5 µg of endogenous peptides and 10-50 fmol of heavy-labelled synthetic peptides. Peptides were separated with a 25 min linear gradient from 3% to 40% acetonitrile with 0.1% formic acid at 300 nL/min. The MS was operated in positive ion, scheduled SRM mode (detection time window: 240 s; target scan time: 1.5 s).

3.2.4 Data analysis

Statistical analysis in Chapter 3 was performed by Shila Ghazanfar as part of the requirement for the completion of the degree Doctorate of Philosophy at the University of Sydney

Detailed methodology on the data and statistical analysis carried out on the melanoma patient SRM data can be found in Chapter 2.2.4. Briefly, SRM data files were processed in Skyline and manually inspected for correct peak picking. Total peak area ratios of all transitions (ratios of the sum of 3 areas corresponding to 3 transitions) of light (L: endogenous peptides) to heavy (H: isotopically-labelled peptides) were log-transformed for analysis. These data represent the relative abundances of peptides in Good and Poor prognosis melanoma patients.

Statistical analyses were performed on combined SRM data from the current study and previous SRM data from Mactier *et al* [269]. Peptide abundance was quantified by obtaining the light isotope abundance for each peptide, missing data was imputed using the k-Nearest Neighbours approach then normalised using the RUV procedure [273]. Differential proteins were identified by fitting linear fixed effects models. Ten new proteins were found to be differentially abundant based upon a criterion of unadjusted p-value < 0.05, no fold-change cut-off was employed.

Next, to identify a minimal panel of proteins able to predict the prognosis status of patients Diagonal Linear Discriminant Analysis (DLDA) method was used to perform classification, and 5-fold cross validation was repeated 100 times to obtain error rates of the patient classification. Cox proportional hazards model was fit with the top classifiers, i.e., differentially abundant proteins with the greatest contribution to predicting patient outcome and KM survival curves used to stratified patients based on the predictive performance of the protein panel. The overall workflow is summarised in **Figure 3-1**.

3.2.5 *In silico* validation

The performance of the 14-protein panel was tested in a larger patient cohort with a variety of mutations using transcriptomic data. The top classifier proteins from the DLDA and Cox proportional hazard model were input into SurvExpress, an online biomarker validation tool [275] using the Cancer Genome Atlas data on 335 cutaneous melanoma patients with genomic, transcriptomic and proteomic profiles [276]. Cox survival analysis was performed as described

by Aguirre-Gamboa *et al.* [275] censoring by survival and risk with maximised risk group feature selected.

3.3 Results

SRM analyses of lymph node resections from 30 AJCC stage III melanoma patients identified proteins with differential abundance between Good (n=16, > 4 years survival post-resection) and Poor (n=14, < 2 years survival) prognostic groups (**Table 3-1** and **Supplementary Table S3-1**). Of the 34 proteins surveyed by SRM (**Supplementary Table S3-3**), 10 showed significant differential abundance between Good and Poor prognosis groups (**Table 3-2**).

3.3.1 Selected Reaction Monitoring

A total of 10 proteins from the 34 screened were identified by SRM as differentially abundant between Good and Poor prognosis groups (**Figure 3-2** and **Table 3-2**). Seven of these proteins were present at lower levels in Poor prognosis patients; Myosin regulatory light chain 12A (MYL12A), Thioredoxin-dependent peroxide reductase mitochondrial (PRDX3), Glucosidase 2 subunit beta (GLU2B), Alpha-actinin-4 (ACTN4), Phosphoglycerate kinase 1(PGK1), Tryptophan-tRNA ligase (WARS) and Tenascin (TNC). Additionally, three of the ten proteins were at higher levels in Poor prognosis patients Glutathione S-transferase (GSTP1), Tumour rejection antigen (Gp96) 1 (Q59FC6) and T-complex protein 1 subunit eta (CCT7). Proteins were quantified using three peptides each with three transitions for each protein, in some cases transition intensities were too low for analysis and proteins were quantified using one or two peptides (**Supplementary Table S3-3**).

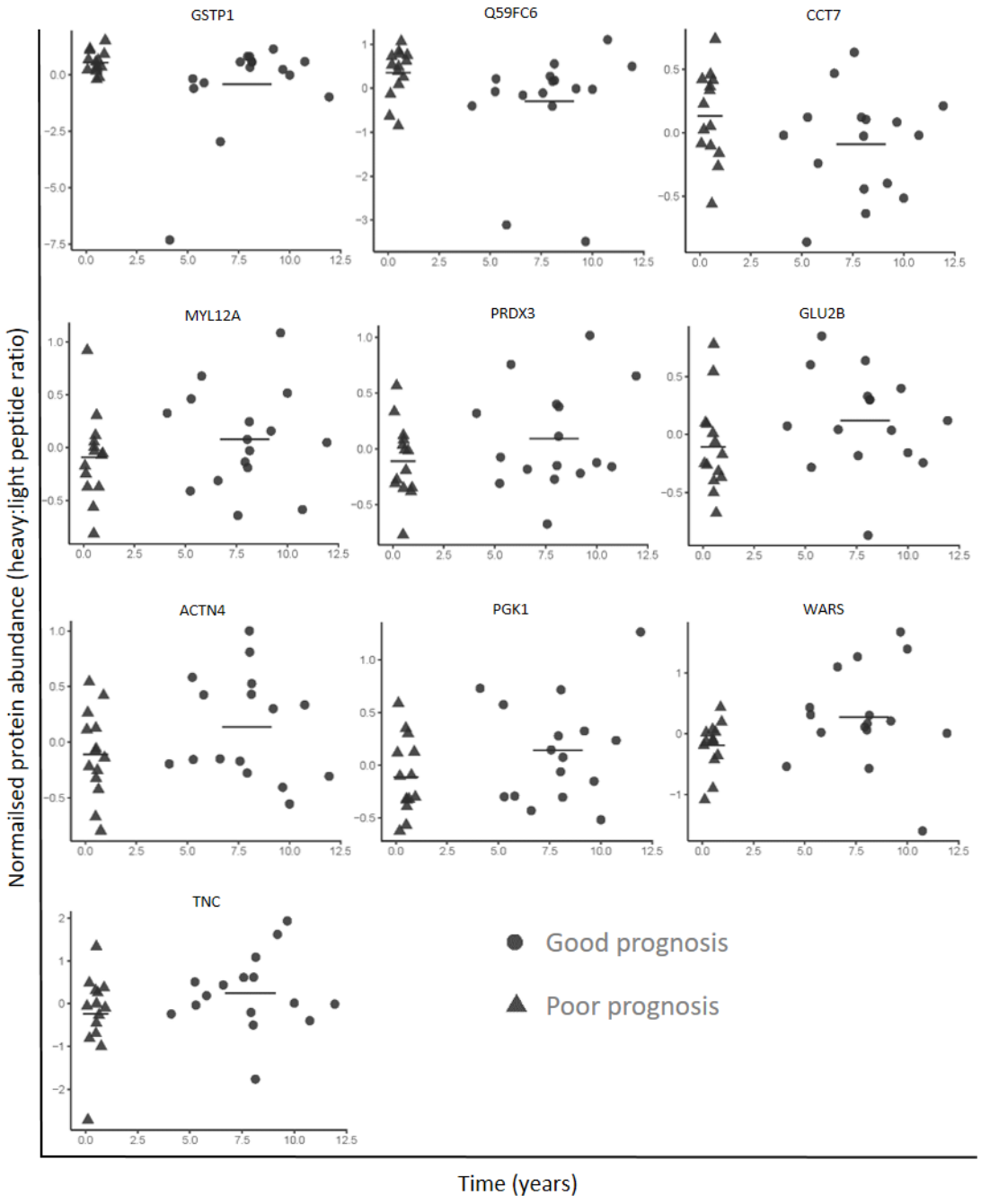

Figure 3-2. Individual patient levels of the ten differentially abundant proteins between Good and Poor prognosis stage III melanoma. Lymph node resections from Good (n=16, >4 years survival post-resection, circles) and Poor (n=14, <2 years survival, triangles) prognostic groups were analysed by SRM. Dot points represent the mean intensities of three transitions of proteotypic peptides assayed for each protein. Peptide intensities were normalised by the RUV procedure. Horizontal bars represent the median protein abundance for the Good and Poor prognostic groups. Significance was determined as *p*-value <0.05, see **Table 2** for *p*-values.

Table 3-2. Differentially abundant proteins between Good and Poor prognosis patient groups with AJCC stage III melanoma. Lymph node samples from Good (n=16, >4 years survival post-resection) and Poor (n=14, <2 years survival) prognosis patients were analysed by SRM. Protein significance was determined as *p*-value <0.05 and *p*-values were adjusted (denoted Adj. *p*-value) by false discovery rate (FDR) correction. The fold-change was determined by a ratio of Poor over Good outcome (P/G).

Accession number	Gene name	Protein name	Major cancer function	Average fold-change (P/G)	*p*-value	Adj. *p*-value
P09211	GSTP1	Glutathione S-transferase	Metabolic	1.86	0.020	0.061
Q59FC6	Q59FC6	Tumour rejection antigen (Gp96)	Stress response	1.52	0.021	0.064
Q99832	CCT7	T-complex protein 1 subunit eta	Stress response	1.10	0.029	0.079
P19105	MYL12A	Myosin regulatory light chain 12A	Unknown	-1.12	0.050	0.134
P30048	PRDX3	Thioredoxin-dependent peroxide reductase, mitochondrial	Stress response	-1.14	0.015	0.052
P14314	GLU2B	Glucosidase 2 subunit beta	Metabolic	-1.16	0.007	0.032
O43707	ACTN4	Alpha-actinin-4	Invasion	-1.17	0.006	0.029
P00558	PGK1	Phosphoglycerate kinase 1	Metabolic	-1.18	0.009	0.042
P23381	WARS	Tryptophan-tRNA ligase	Angiogenesis	-1.34	0.015	0.052
P24821	TNC	Tenascin	Invasion	-1.36	0.012	0.047

All ten-differentially abundant proteins apart from MYL12A, have known roles in cancer development and growth. Ingenuity Pathway Analysis clustered all ten differentially abundant proteins to the functional category of "cancer growth and metastasis" (*p*-value $4.84e^{-2}$ to $1.29e^{-5}$). The proteins functions corresponded to altered metabolism, increase in invasive potential, angiogenesis, modified molecular chaperones and a decrease in tumoural immunogenicity (**Table 3-2**). Glutathione S-transferase [315-317], Tumour rejection antigen (Gp96) 1 [318-321], Tryptophan-tRNA ligase [322-324], Phosphoglycerate kinase 1 [325], Alpha-actinin-4 [326-328], Tenascin [329-331] and Glucosidase 2 [332, 333] have previously been identified as potential cancer biomarkers (**Table 3-3**). The protein Myosin regulatory light chain 12A is a possible novel biomarker when used in a marker panel. None of the ten differentially abundant proteins above are in clinical use for melanoma diagnosis or prognosis.

Table 3-3. Incidence of the ten protein biomarkers in human cancers. Published studies on the ten differentially abundant proteins listed in Table 3-2.

Gene name	Cancer	Biomarker/function	References
GSTP1	**Melanoma,** prostate	Increase - poor outcome and drug resistance DNA hypermethylation - risk	[315, 316, 334]
Q59FC6	Multiple myeloma, lung, nasopharyngeal, liver	Increase - poor outcome and radioresistance	[318-321, 335]
CCT7	Colorectal, breast	Increase - cancer phenotype	[336, 337]
MYL12A	Cancer cell lines	Decrease - cancer phenotype	[338]
PRDX3	Ovarian, breast	Increase - cancer phenotype, tumourigenesis	[339, 340]
GLU2B	Breast	Increase - tumour progression, angiogenesis	[341]
ACTN4	**Melanoma**, ovarian, gliomas	Increase - metastasis	[327, 328, 342]
PGK1	Colon, breast, astrocytoma	Increase - metastasis and chemoresistance	[343-345]
WARS	**Melanoma**, colorectal	Decrease - angiogenesis	[322]
TNC	**Melanoma**	Increase - metastasis	[330, 346]

Statistical analysis of the data from Mactier *et al.* using RUV normalisation and a fixed effect model gave good correlation to the analysis from our previous work. The consistency in normalisation is seen when comparing the overall density of normalised peptide abundance values (**Figure 3-3**). In addition, linear regression analysis on the normalised peptide values of the Mactier *et al.* SRM data from the current and former statistical analysis show similar correlation scores to the iTRAQ data (**Figure 3-4** and **Table 3-4**). Additionally, the combined SRM data from both studies under the new method of normalisation and statistical analysis were compared to the iTRAQ protein fold-change values from Mactier *et al.* (**Table 3-4**). These findings demonstrate the validity of using the new statistical methodologies when validating findings from the previous paper.

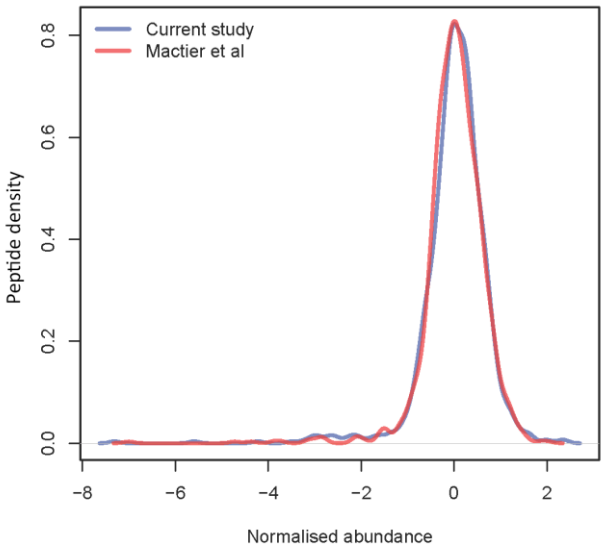

Figure 3-3. Normalisation comparison of SRM data in the previous and current study. Normalisation of the SRM dataset from the previous study shows good correlation to the RUV normalisation in the current study when combining the SRM data with the Mactier *et al.* data.

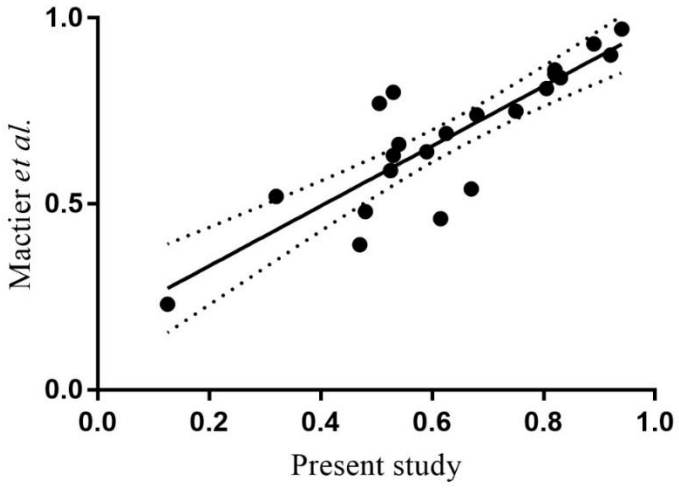

Figure 3-4. Correlation of normalisation and statistical analysis of SRM data with iTRAQ values. The normalisation and data analysis preformed on the SRM data from our previous and current studies were compared for the correlation to iTRAQ quantitation values (Supplementary Table S3-3). Linear regression analysis of the SRM datasets gave a R^2=0.7438, *p*-value=<0.001 with the confidence band of 95% denoted by the dotted lines.

Table 3-4. Concordance of SRM statistical analysis. SRM data on the 22 proteins in Mactier *et al.* analysed by fixed effect model with RUV normalisation [269] compared to the current study using DLDA showing the correlation with iTRAQ data. Adjusted *p*-values (denoted Adj. *p*-value) were calculated by FDR correction.

Accession number	Gene name	**DLDA** (current analysis)				**Fixed Effect Model** (Mactier *et al.* analysis)			
		Average fold-change (P/G)	*p*-value	Adj. *p*-value	Correlation	Average fold-change (P/G)	*p*-value	Adj. *p*-value	Correlation
Q15063	POSTN	1.67	0.0002	0.0018	0.82	1.68	<0.0001	0.001	0.85
P09874	PARP1	1.44	<0.0001	<0.0001	0.805	1.36	<0.0001	0.002	0.81
P08238	HSP90AB1	1.43	<0.0001	<0.0001	0.525	1.37	<0.0001	<0.0001	0.59
P11142	HSPA8	1.29	0.0019	0.0134	0.32	1.27	0.003	0.009	0.52
P17844	DDX5	1.29	<0.0001	<0.0001	0.48	1.22	<0.0001	0.001	0.48
P23526	AHCY	1.28	0.0006	0.0051	0.75	1.19	0.001	0.003	0.75
P12956	XRCC6	1.23	0.0169	0.0552	0.615	1.18	<0.0001	<0.0001	0.46
P00338	LDHA	1.2	0.0024	0.0158	0.83	1.13	0.055	0.098	0.84
P13010	XRCC5	1.19	0.0054	0.0294	0.47	1.15	0.022	0.051	0.39
P60842	EIF4A1	1.18	0.0113	0.047	0.54	1.21	0.002	0.007	0.66
P40227	CCT6A	1.15	0.0123	0.047	0.59	1.12	0.043	0.083	0.64
Q08211	DHX9	1.11	0.1719	0.3173	0.53	1.13	0.034	0.073	0.63
Q99798	ACO2	1.05	0.6146	0.7902	0.67	1.12	0.04	0.083	0.54
P06576	ATP5B	-1.13	0.1811	0.3261	0.89	-1.17	0.013	0.035	0.93
P04179	SOD2	-1.24	0.0639	0.1587	0.83	-1.33	0.022	0.051	0.84
P27797	CALR	-1.25	0.0281	0.0792	0.625	-1.26	0.003	0.008	0.69
Q06323	PSME1	-1.27	0.0057	0.0294	0.82	-1.37	<0.0001	0.001	0.86
P35527	KRT9	-1.34	0.1308	0.2545	0.125	-1.22	0.098	0.158	0.23
Q9UL46	PSME2	-1.38	0.0763	0.1771	0.505	-1.26	0.048	0.09	0.77
P10909	CLU	-1.4	0.0002	0.0018	0.94	-1.36	0.001	0.003	0.97
P13796	LCP1	-1.45	<0.0001	<0.0001	0.92	-1.56	<0.0001	<0.0001	0.9

Accession number	Gene name	**DLDA** (current analysis)				**Fixed Effect Model** (Mactier *et al.* analysis)			
		Average fold-change (P/G)	*p*-value	Adj. *p*-value	Correlation	Average fold-change (P/G)	*p*-value	Adj. *p*-value	Correlation
O75367	H2AFY	-1.5	0.0013	0.0106	0.68	-1.41	0.001	0.003	0.74
Q9ULZ3	PYCARD	-1.78	<0.0001	0.0002	0.53	-1.7	<0.0001	<0.0001	0.8

3.3.2 Survival analysis

The SRM dataset was combined with our previous proteomic analysis on AJCC stage III melanoma patients involving iTRAQ and DIGE analyses [269]. The combined dataset was subjected to Classification Feature Selection, in which proteins that did not contribute to the prognostic signatures were removed. DLDA was used to perform cross-validation and features were selected repeatedly over each fold of cross-validation. Proteins that had an inclusion frequency of 0.3 or higher were selected for the final protein panel, that is, the protein was included in the classifier over 30% of the time. This resulted in identification of the set of 14 proteins shown in **Figure 3-5** and **Figure 3-6.**

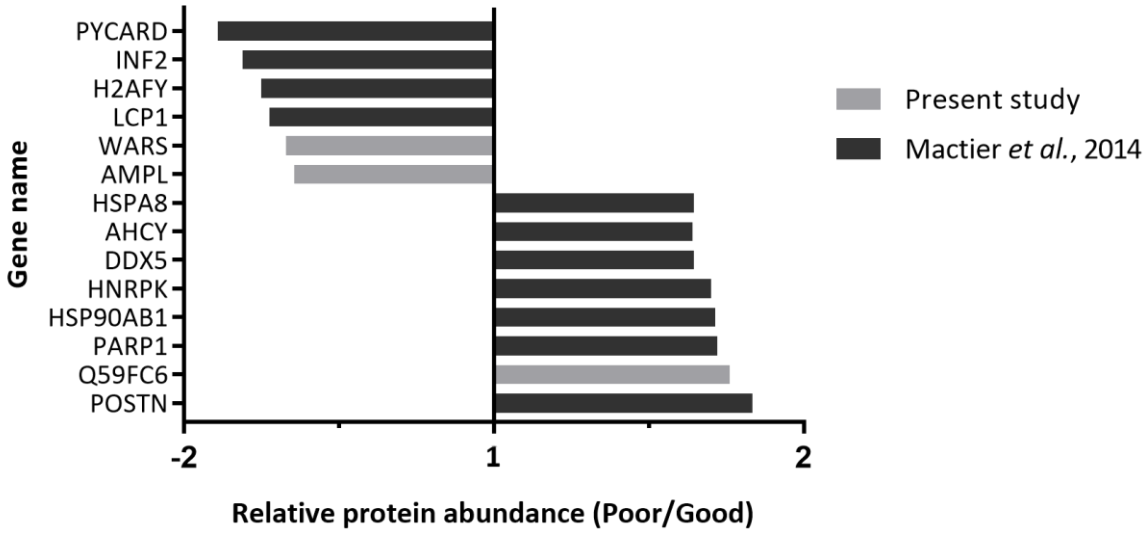

Figure 3-5. A 14-protein panel identifying AJCC stage III melanoma patients with Poor prognosis. Protein SRM data from the current study were combined with proteins datasets from the previous study [269] and subjected to DLDA. Fourteen proteins were derived from an inclusion frequency of repeated 5-fold cross validation of at least 0.3. Protein levels correlate with poor outcome, *p*-value=0.00019.

The new composite 14-protein signature provides improved separation of the Good prognosis patients from the Poor with increased statistical significance, *p*-value=0.00019 compared to *p*-value=0.00036 for our previous signature (**Figure 3-5** and **Figure 3-6**). Fewer Poor prognosis patients are misclassified as good prognosis compared with the Mactier *et al.* panel [269]. The 21-protein signature from Mactier *et al.* misclassified 2 Good and 5 Poor prognosis patients, while the 14-protein panel misclassified 4 Good and 1 Poor prognosis patient (**Table 3-5**).

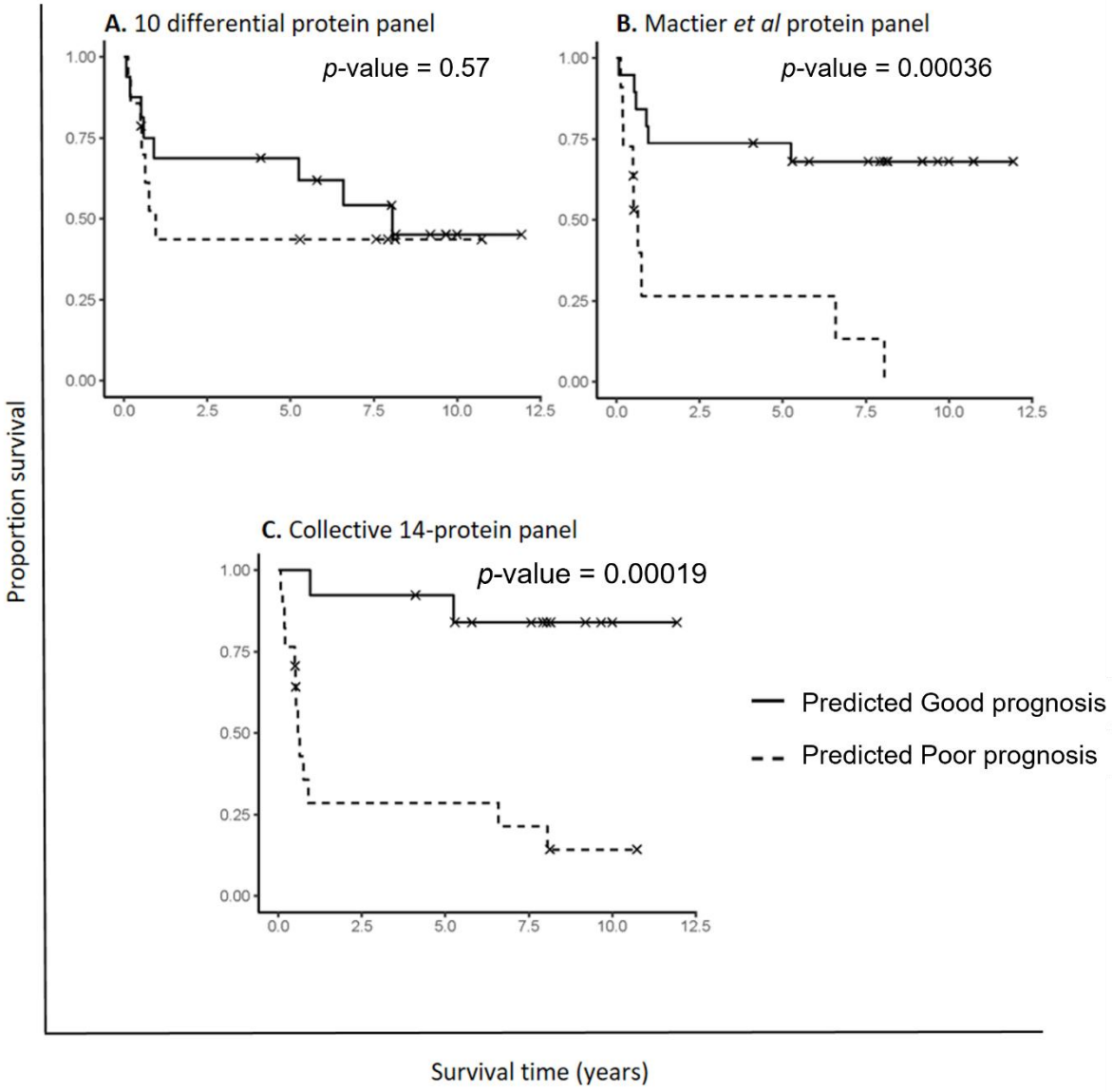

Figure 3-6. Kaplan-Meier curves of overall survival in Good and Poor prognosis patient groups with AJCC stage III melanoma. A cohort of 30 AJCC stage III melanoma patients separated into Good (n=16, >4 years survival post-resection) and Poor (n=14, <2 years survival) prognostic groups were analysed. **A)** Predicted survival outcome utilising 10 differentially abundant proteins identified in this study. **B)** Prognostic signature previously defined by Mactier *et al.* [269] using 21 proteins. **C)** Improved 14-protein prognostic signature comprising 11 proteins from Mactier *et al.* and 3 proteins from the current study to differentiate Good and Poor prognosis AJCC III melanoma patients. (x) denotes censored patients with continued survival, *p*-values were calculated by two-sided *t*-test.

Table 3-5. Comparison of SRM protein signatures ability to predict patient outcome. The ability to correctly predict patient outcome was compared between the Mactier *et al.* 21-protein signature and the 14-protein panel from the current study (Figure 3-5). Good (n=16, >4 years survival post-resection) and Poor (n=14, <2 years survival) patients were fit to the signatures. Mactier *et al.* 21-protein signature misclassified 7 patients (2 Good patients, 5 Poor patients) while the 14-protein panel misclassified 5 patients (4 Good patients, 1 Poor patient).

Patient number	Survival (days)	Patient prognostic classification	
		Mactier *et al.* 21-protein signature	Current study 14-protein signature
PP1	27	Misclassified	Correct
PP2	43	Correct	Correct
PP3	67	Correct	Correct
PP4	70	Correct	Correct
PP5	176	Correct	Correct
PP6	183	Correct	Correct
PP7	189	Correct	Correct
PP8	190	Correct	Correct
PP9	193	Misclassified	Correct
PP10	215	Misclassified	Correct
PP11	235	Correct	Correct
PP12	275	Correct	Correct
PP13	326	Misclassified	Correct
PP14	344	Misclassified	Misclassified
GP5	1499	Correct	Correct
GP7	1913	Correct	Correct
GP8	1929	Correct	Correct
GP9	2115	Correct	Correct
GP10	2408	Misclassified	Misclassified
GP11	2764	Correct	Correct
PP21	2893	Correct	Correct
PP22	2932	Correct	Correct
GP12	2939	Misclassified	Misclassified
GP13	2969	Correct	Misclassified
GP14	2974	Correct	Correct
GP15	3357	Correct	Correct
GP17	3528	Correct	Correct
GP18	3650	Correct	Correct
GP19	3921	Correct	Misclassified
GP20	4357	Correct	Correct

To test the new signature's ability to handle cancer heterogeneity, patients were split into 2 further cohorts based on BRAF mutational status (**Table 3-1** and **S5-2**) and DLDA was repeated. The 14-protein signature was able to classify patients into Good or Poor prognosis groups irrespective of BRAF mutation, with *p*-value=0.022 and *p*-value=0.000029, for wild type, and BRAF mutants, respectively (**Figure 3-7**). The ability of the protein panel to correctly stratify patients irrespective of sex, was also assessed (**Figure 3-8**). The biomarker panel correctly predicted patient's prognosis in the male cohort (*p*-value=0.0078), however, was

unable to correctly classify female patients by prognostic risk, as indicated by a *p*-value of 0.16 despite separation of the prognostic groups.

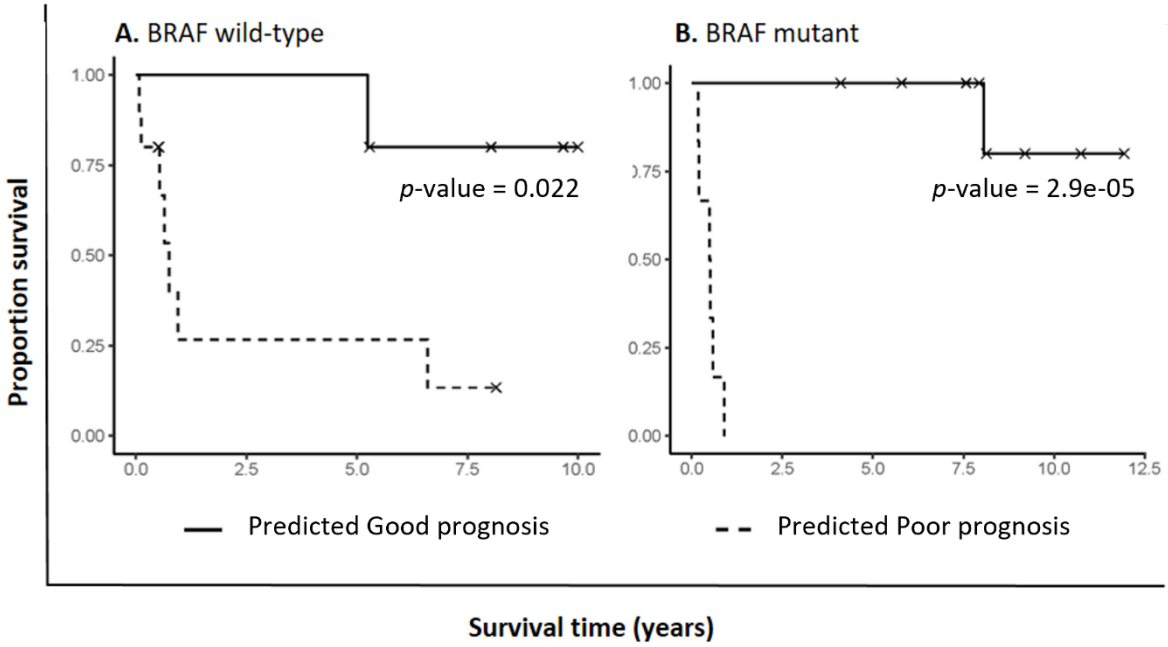

Figure 3-7. Kaplan-Meier curves modelling the 14-protein signature with overall survival of Good and Poor prognosis stage III melanoma patients with wild type or mutant BRAF. **A)** Predicted survival outcomes of AJCC stage III melanoma with wild-type BRAF of Good (n=7, >4 years survival post-resection) and Poor (n=8, <2 years survival) prognosis. **B)** Predicted survival outcomes of AJCC stage III melanoma patients with oncogenic BRAF mutation of Good (n=9, >4 years survival post-resection) and Poor (n=6, <2 years survival) prognosis. (x) denotes censored patients with continued survival, *p*-values were calculated by two-sided *t*-test.

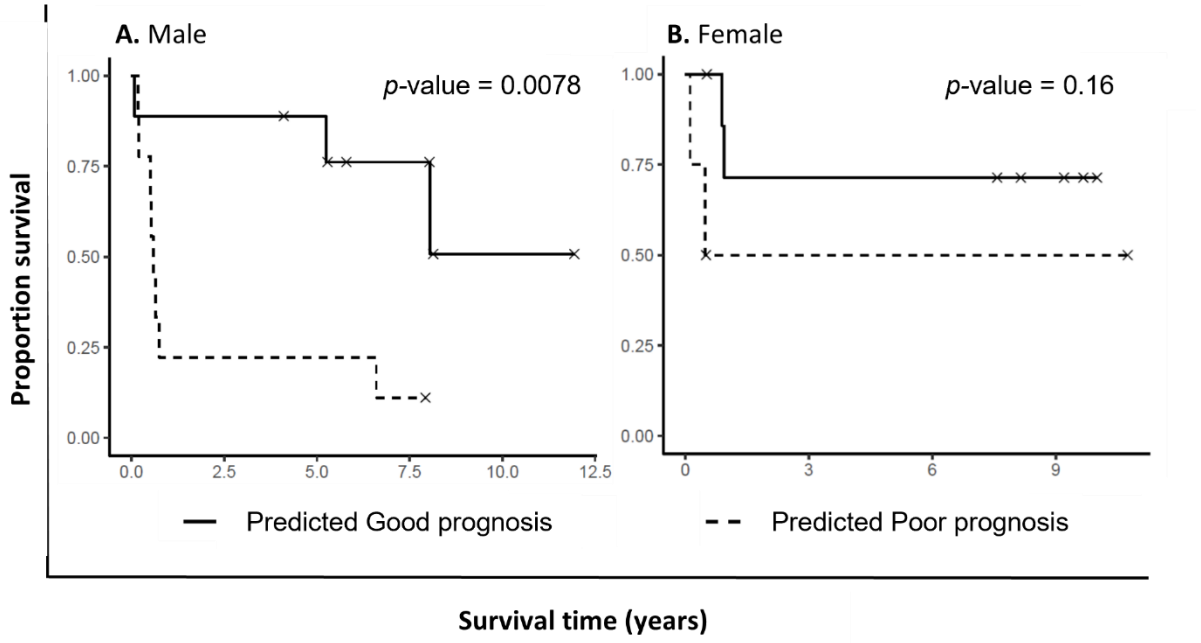

Figure 3-8. Kaplan-Meier curves modelling the 14-protein signature with overall survival of Good and Poor prognosis stage III melanoma patients in Male and Female cohorts. **A)** Predicted survival outcomes of Male AJCC stage III melanoma patients with Good (n=10, >4 years survival post-resection) and Poor (n=8, <2 years survival) prognosis. **B)** Predicted survival outcomes of Female AJCC stage III melanoma patients with Good (n=6, >4 years survival post-resection) and Poor (n=6, <2 years survival) prognosis. (x) denotes censored patients with continued survival, *p*-values were calculated by two-sided *t*-test.

3.3.3 *In silico* validation of the protein biomarker panel

The Cancer Genome Atlas of 335 cutaneous melanoma patients contained gene expression information on 12 of the 14 proteins included in the final biomarker panel (**Figure 3-5** and **Figure 3-6**). SurvExpress separated the 335 melanoma patients into low (n=142, CI=60.4) and high risk (n=193, CI=51.5) cohorts based on patient survival. Cox survival analysis on the 335 patients using the 12 proteins from the 14-protein panel generated Kaplan-Meier plots with good separation of low and high-risk cohorts, *p*-value=0.0000058, concordance index of 61.65 (**Figure 3-9**). Additionally, nine of the 12 proteins had expression levels in high-risk patients that correspond to protein levels seen in Poor prognosis patients in the current study (**Figure 3-10**).

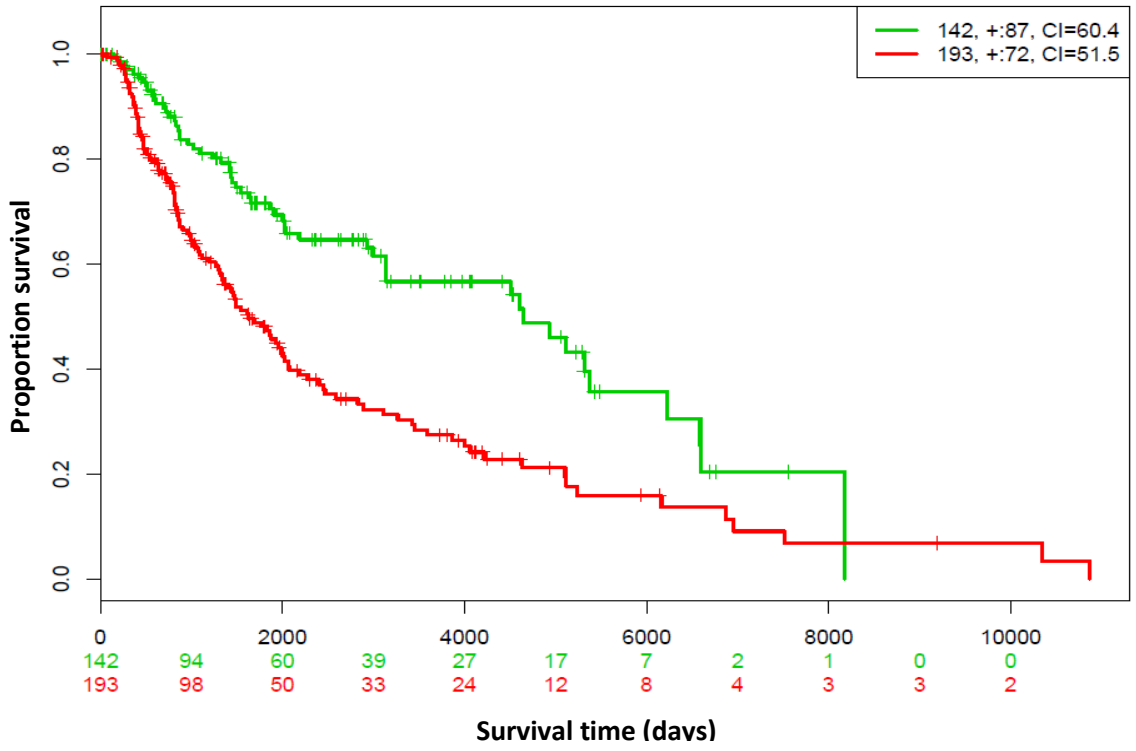

Figure 3-9. Kaplan-Meier curve of Cox survival analysis using the 14-protein biomarker panel for 331 melanoma patients by SurvExpress biomarker validation. The 14-protein panel was input into SurvExpress biomarker validation software [275] using the Cancer Genome Atlas data on 335 cutaneous melanoma patient genomics, transcriptomic and proteomic profiles [276]. Of the 14 proteins, 12 had expression level information in the database. Cox survival analysis was performed as described by Aguirre-Gamboa *et al.* [275] and patients separated into Low (n=142, green) and High (n=193, red) risk groups (*p*-value=0.000005, hazard ratio=2.07). Patient classification into risk group based on the 14-protein panel was significant, *p*-value=0.0000091. Surviving patients included in the analysis are shown on the lower X-axis.

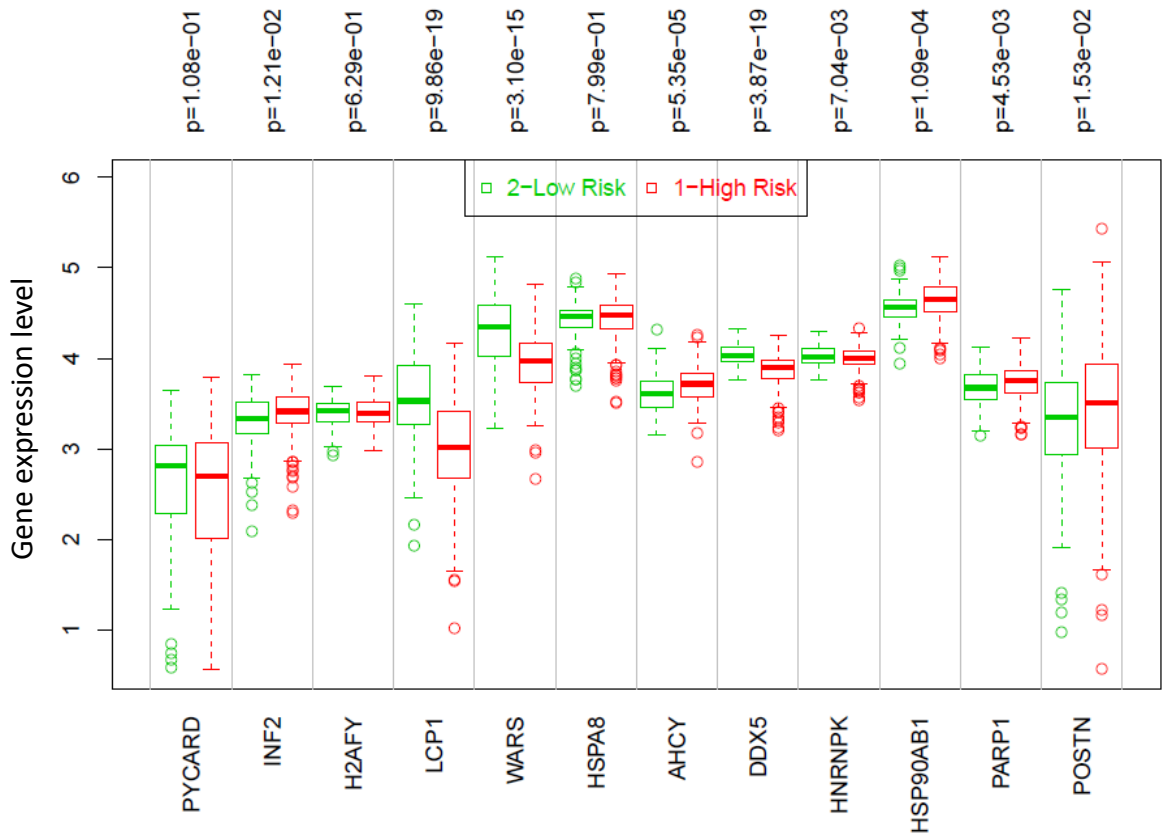

Figure 3-10. Gene expression levels of the 14-protein biomarker panel derived from 335 melanoma patients by SurvExpress biomarker validation. The 14-protein panel was input into SurvExpress biomarker validation software [275] using the Cancer Genome Atlas data on 335 cutaneous melanoma patient with mRNA and protein levels. Abundance levels of 12 of the 14 proteins were present in the data [276]. Cox survival analysis was performed as described by Aguirre-Gamboa *et al.* [275] and patients separated into High (n=168, red) and Low (n=167, green) risk groups (*p*-value=0.000044, hazard ratio=1.86). *p*-values were calculated by two-sided *t*-test on expression profiles of the two-risk groups. Circles are outliers outside the 95% CI bars.

3.4 Discussion

Treatment options for patients with stage III melanoma are limited, with variable responses, frequent emergence of resistance, and little improvement in survival [63]. AJCC staging classifies patients with stage III melanoma into groups with a broad variation in survival outcomes; methods better able to stratify patients into distinct prognostic categories are urgently required. Differentially abundant proteins could provide biomarker profiles to classify stage III melanoma patients and select better treatment strategies for individual patients. The present SRM analysis has validated a panel of ten differentially abundant proteins that discriminates between Good and Poor prognosis stage III melanoma patients. DLDA was then performed on the proteins found to be differentially abundant in Poor prognosis patients, plus proteins from our groups' previous study [269]. From analysis of the compiled proteins, a panel of 14-proteins was generated, containing 11 proteins from the previous study [269] and three of the 10 differentially abundant proteins discovered here. This protein signature is able to identify melanoma patients likely to have poor outcomes.

3.4.1 A 14-protein biomarker panel

Currently, the available biomarkers for melanoma diagnosis and prognosis exhibit low sensitivity and specificity. Melanoma does not have a single biomarker able to predict patient outcome or drug response, in contrast to the estrogen receptor and HER2 in breast cancer [347-349]. Pathological features for AJCC staging are unable to reliably predict melanoma patient outcomes, and yet this information would be critically important to treatment selection in stage III patients. Of the ten proteins found to be differentially abundant between Good and Poor prognosis stage III melanoma patients, nine have previously been identified as potential biomarkers (**Table 3-3**). However, none of these potential markers are in clinical use, as individually, these proteins exhibit low sensitivity and specificity (reviewed by Polanski and Anderson [350]). The shortcomings of the use of individual biomarker screens can be seen for HER2, an epidermal growth factor receptor (EGFR), used to predict patient response to HER2 targeted therapies. HER2 has high specificity (98%), but low sensitivity (40%) [351] and has exhibited poor reproducibility most likely due to variation in immuno-histochemical techniques [352]. By contrast, a biomarker panel collectively exhibits greater reliability and sensitivity and is able to encompass the variation in mutations found in melanoma and other cancers [353, 354].

For melanoma, the benefits of biomarker panels in diagnosis and disease monitoring can be seen in a number of studies, such as the combination of protein S-100β (S-100β) with melanoma-inhibitory activity (MIA) [355], S-100β with LDH [356] and osteopontin, MIA and S-100β [357, 358]. Only a few countries, such as the UK, recommend testing in their clinical guidelines using these markers. The 14-protein signature reported here (**Figure 3-5** and **Figure 3-6**) stratifies stage III melanoma patients into Good and Poor prognosis groups. DLDA used here combined the SRM data with proteins identified from a previous study by our group [269] to ultimately give an improved signature, using just 14 proteins compared to 22 proteins in the previous panel (*p*-value=0.0013 and *p*-value=0.00019, respectively). Additionally, the 14-protein panel showed separation of Good and Poor prognostic patients at just 3 months post-lymph-node resection (**Figure 3-6**). This would enable earlier identification of high-risk patients and earlier implementation of aggressive therapies for these patients could translate to improved outcomes. The new 14-protein panel also had fewer misclassifications of Poor prognosis patients compared to the previous 22-protein signature, with only a single Poor prognosis patient classified as Good (**Table 3-5**). The misclassification of Poor prognosis patients has greater detrimental effect than misclassification of Good prognosis individuals, as these high-risk patients would not receive the aggressive intervention they require.

The 30 patient lymph node samples had a variety of mutations (**Table 3-1** and **Supplementary Table S3-2**). Due to the significance of BRAF mutations to the oncogenic potential of melanoma, results were further analysed according to BRAF mutational status [359]. Importantly, with 15 out of 30 samples having an activating BRAF mutation (**Supplementary Table S3-2**), the panel was able to differentiate patients into Good and Poor prognostic groups independent of BRAF status. Indeed, when patients were separated by BRAF status, a Kaplan-Meier plot showed significant separation of the two cohorts (**Figure 3-7**). However, the 14-protein signature provides higher confidence when stratifying patients into prognostic groups if the metastases have a BRAF mutation, suggesting that some proteins within the panel are influenced by oncogenic BRAF mutations.

Additionally, due to the influence of sex hormones on melanoma survival, with poorer survival in males compared to females [360], the ability of the 14-protein panel to correctly classify Good and Poor prognosis in both male (n=18) and female (n=12) patients was assessed. The signature performs well in males, *p*-value=0.0078, with three out of 18 patients misclassified (**Figure 3-8**). In females the separation of the Good and Poor prognosis cohorts was not significant, *p*-value=0.16, with 4 of 12 patients misclassified. The poor performance

of the 14-protein panel in the female cohort is likely due to a single outlying patient and reflects the need for larger cohort validation.

The lack of validation from a large independent cohort of patients is one of the major impediments in the implementation of biomarkers in the clinic. To test the performance of the 14-protein panel on a larger cohort with a variety of mutations, we utilised SurvExpress, an open-access biomarker validation program [275]. The 12 proteins from the 14-protein panel that had expression level information were tested against the Cancer Genome Atlas Network cutaneous melanoma database of 335 melanoma patients' genome expression profiles. A Cox survival analysis was performed on the patients separated by risk group. The Kaplan-Meier plots show that 12 proteins from the 14-protein panel are able to classify high-risk patients in the larger cohort (**Figure 3-9**). The expression profiles contained in the database were compiled from 335 patients with all stages of melanoma, showing the potential of the 14-protein panel to have a wider application beyond stage III patients. Furthermore, the protein levels of nine of the 14-protein panel in Poor prognosis patients correlated with mRNA and protein level data in high-risk patients contained within the cutaneous melanoma database (**Figure 3-10**).

One of the factors responsible for a lack of clinically relevant melanoma biomarkers is the limited access to samples and the often small biopsies of tissue available for analysis. In this study, ten proteins were detected and quantified from 0.5 µg of whole tissue extract. Furthermore, as the amount of sample required for SRM is quite small, especially compared to genomic techniques, repeat analyses are often possible. Given the small sample required, mass spectrometry screens should be implemented in the clinic while the current AJCC staging system is still employed for prognostication. The performance of the biomarker screen can be compared to the current clinical staging after sufficient data has been collected.

The samples used in this analysis contained at least three different cell types (melanoma cells, stromal cells and leukocytes). Therefore, not all proteins detected in this study are derived from the melanoma cells. Additionally, the mixed cell population may dilute clinically relevant proteins found in one cell type and could account for the relatively low fold-changes observed in **Table 3-2**. While the ability to sort individual cell types has improved biomarker discovery and our understanding of cancer phenotypes, a whole tissue approach, as used here, may prove beneficial for biomarker discovery coupled with more sensitive methods of detection. Another benefit of a whole tissue approach is the significant contribution of the TME to the cancerous

phenotype and as such the TME is a potential source of clinical biomarkers. Additionally, whole tissue analysis streamlines diagnostic workflows and decreases costs.

As technologies in the field of proteomics become more sensitive, huge databases of proteins identified in melanoma and other cancers can be compiled [361]. New methodologies, such as Data Independent Acquisition mass spectrometry (DIA-MS), allow for quantitative information on thousands of proteins to be collected without prior knowledge of targets [362]. As more proteomic information is collected through high-throughput techniques such as SRM and combined with patient drug response profiles, melanoma could be sub-typed for prognosis and drug response, an important step toward personalised medicine. Further studies with larger patient cohorts should further compare the biomarkers in poor prognosis patients identified in this study with the administered chemotherapies and patient responses.

3.4.2 Differentially abundant proteins between Good and Poor prognosis stage III patients

Melanoma contains multiple mutations that drive proliferation and inhibit apoptosis. Here we have validated ten proteins found to be differentially abundant in Poor prognosis AJCC stage III melanoma patients identified in our groups' previous work [269]. All ten differentially abundant proteins have roles in cancer progression and metastasis. While none of the proteins reported here are currently in clinical use, nine of the ten proteins have been proposed as potential biomarkers for cancer, while only four have been identified in melanoma (**Table 3-3**). Of the ten differentially abundant proteins identified (**Table 3-2**), three were included in the final 14-protein signature and are discussed below.

The presence of proteins involved in T-cell stimulation and immunity in the 14-protein panel are of particular importance as lymph nodes are a major site of T-cell activation. Also, given the success of immunotherapies that activate T-cells against melanoma, inclusion of these proteins in biomarker screens may provide clinicians with additional information for therapeutic selection. The therapeutic antibodies, ipilimumab and tremelimumab, target T-lymphocyte antigen-4 (CLTA-4), a negative regulator of T-lymphocytes, while Nivolumab is an antibody against Programmed Death Receptor-1 (PD-1), a ligand that also decreases T-lymphocyte proliferation. One such protein is Apoptosis-associated Speck-like protein containing a CARD (ASC or PYCARD), an adaptor protein of the inflammasome. The role of the inflammasome in tumourigenesis has been a topic of considerable study of late, however

its role in tumour progression and metastasis has proved to be complex and much contrary evidence exists [363]. In melanoma, the effects of PYCARD appear to be stage specific with reduced levels observed in metastatic cells resulting in enhanced NF-κB signalling [364, 365].

High levels of stress response proteins are observed in cancer due in part to a high proliferative burden. Consistent with the link between stress and cancer progression, three stress response proteins were differentially abundant in Poor prognosis melanoma patients. Gp96 is a heat shock protein responsible for both protein folding and antigen presentation in tumour cells. Gp96 is over-expressed in a number of cancers and correlates with poor prognosis in oral, gall bladder, lung, multiple myeloma, hepatocellular and nasopharyngeal carcinomas [318-321]. Gp96 binds peptides for presentation to the major histocompatibility complex class I protein (MHC-I) thereby activating a $CD8^+$ T-cell immunogenic response [366-370]. Due to its ability to elicit a tumour specific response, new immunotherapies and vaccines based on Gp96 are under trial [371, 372]. Rivoltini *et al.* have shown that T-cells activated with melanoma cell line-derived Gp96-peptide can trigger cytotoxic activity in stage IV melanoma patients [373]. Clinical trials of Vitespan, a tumour-derived Gp96 peptide complex (Antigenics Inc, New York, NY, USA), showed that longer survival correlated with increased doses of Vitespan in a cohort of 322 stage IV melanoma patients [374]. The samples are stage III lymph node metastases and therefore the presence of a marker of T-cell immune surveillance, Gp96, in the biomarker panel has the additional benefit of identifying patients most likely to respond to Gp96-based immunotherapies.

Cytosol aminopeptidase (AMPL or LAP3), which was decreased in abundance in Poor prognosis stage III melanoma patients, catalyses the removal of N-terminal amino acids from peptides. The complex functions of aminopeptidases and their roles in cancer are not well understood, having both pro- and anti-oncogenic effects on cell migration and proliferation when on the cell surface [375]. AMPL, a cytosolic aminopeptidase, is involved in N-terminal peptide trimming for presentation of immunogenic peptides on MHC class I molecules, allowing for cytotoxic T cells to screen for neoplastic cells [376, 377]. The observed down-regulation of AMPL in poor prognosis patients may therefore promote immune evasion. In addition, a member of the same family, adipocyte-derived leucine aminopeptidase (A-LAP), has been shown to be a negative regulator of Vascular endothelial growth factor (VEGF) expression, thereby suppressing angiogenesis [378]. The decreased abundance of AMPL in poor prognosis patients may also increase VEGF signalling and promote angiogenesis.

Tryptophan tRNA ligase (WARS), which was decreased in abundance in Poor prognosis stage III melanoma patients, is an angiostatic factor for many normal cells and cancers including melanoma [322]. Splicing of the tryptophan tRNA ligase in response to anti-tumoural interferon-gamma (IFN-γ) produces two isoforms (TrpRS and T2-TrpRS) that have anti-angiogenic effects [323, 324, 379]. The decreased levels of WARS observed here could potentially result in an increased angiogenic ability in the Poor prognosis stage III melanoma patients.

Of the ten differentially abundant proteins identified (**Table 3-2**), three are involved in metabolism, Glutathione S-transferase 1 (GSTP1), Phosphoglycerate kinase 1 (PGK1) and Glucosidase subunit II β (GLU2B). GSTP1 was increased in stage III melanoma patients with Poor prognosis compared with those with longer survival. GSTP1 is a member of the glutathione S-transferase family, that catalyses the addition of hydrophobic and electrophilic compounds to reduced glutathione for removal from the body. Increased GSTP1 has been reported to correlate with progression of human melanoma [315] and drug resistance in various malignancies, including melanoma [316]. GSTP1 in combination with multidrug resistance protein 1 (MRP1), also elevated in melanoma, promotes drug resistance [380]. The increased levels of GSTP1 in Poor prognosis patients reported here could reflect an innate resistance to therapies present prior to treatment. In addition, GSTP1 protects cells from oxidative stress, common in cancer, through the removal of reactive oxygen species [381].

PGK1 is an enzyme of the glycolytic pathway that produces ATP. Increased levels of PGK1 are associated with progression and drug resistance in numerous cancers including breast, gastric and colon cancers [343, 344, 382, 383]. These previous findings are in contrast to the decreased levels of PGK1 found here in melanoma and may relate to PGK1 'moonlighting' as an inhibitor of angiogenesis. PGK1 has been found to be secreted from tumour cells where it acts as a disulfide reductase, reducing plasmin that then proteolytically cleaves and activates angiostatin, an anti-angiogenic factor [384]. PGK1 administered to tumour-bearing mice causes a decrease in tumour vascularity and a decrease in the growth rate of tumours [325]. The decreased levels of PGK1 in Poor prognosis patients reported here may reflect an increased angiogenic capacity of the tumour microenvironment leading to poor outcomes.

GLU2B is a regulatory subunit of glucosidase β involved in glycoprotein biosynthesis and fibroblast growth factor signalling [332, 333]. The decreased abundance of GLU2B

(**Table 3-2**) in whole tissue may alter cellular signalling through changes in protein glycosylation [385].

CCT7 is a component of the TCP1 ring complex (TRiC) that performs ATP-dependent protein folding. TCP1 is over-expressed in colorectal and breast cancers and has been proposed as a therapeutic target [336, 337]. Here we report overall increased levels of CCT7 in whole tissue lymph node resections from Poor prognosis stage III melanoma patients, showing a potential increased protective capacity within these tumours. In addition, levels of other TRiC members have also been found to increase in cancer [386-388].

Myosin regulatory light chain 12A (MYL12A), a subunit of myosin II, contributes to several cancer hallmarks including, replicative immortality, cell invasion and avoidance of cell death, as reviewed by Ouderkirk and Krendel [389]. The role of myosin in cancer involves a complex interplay between subunit composition, cellular localisation and activation via phosphorylation [389]. In this study, decreased levels of MYL12A were found in melanoma samples from patients with Poor outcomes (**Table 3-2**). Decreased levels of MYL12A have been reported in cancer [338]. However, due to the complex and diverse actions of myosin, further study is required to dissect its role in cancer progression and metastasis.

Of the ten differentially abundant proteins, three were found to have fold-changes that are contrary to the current literature: Thioredoxin-dependent peroxide reductase mitochondrial (PRDX3), Tenascin (TNC) and Alpha-actinin-4 (ACTN4, **Table 3-2**). PRDX3 protects cellular enzymes from oxidative damage and is critical in neoplastic transformation [390-392]. The decreased levels of PRDX3 in melanoma lymph node metastases with poor prognosis are contrary to the current literature that associate increased levels of PDRX with tumourigenesis [339, 340].

TNC, an extracellular matrix glycoprotein and ACTN4, an actin cross-linker, both mediate cellular adhesion and motility at the cell surface [326, 329]. Increased levels of both proteins are associated with a cancerous phenotype and poor outcome in various cancers, including melanoma [326-328, 330, 331, 346, 393]. However, many proteins possess dual functionality, termed a ‘moonlighting’ function, which may explain their decreased abundance found in whole tissue samples. The decreased levels of these extracellular matrix proteins observed here may also reflect alteration in the microenvironment arising from tumour remodelling.

3.5 Conclusions

In this study, we have identified a panel of 14 proteins able to collectively identify stage III melanoma patients likely to have poor survival, regardless of their BRAF mutational status. Ten proteins were validated to be differentially abundant in poor prognosis patients compared to melanoma patients with good survival. When these ten proteins were combined with the 21 differential proteins from our groups previous study, and new statistical methods applied, a new 14-protein panel was identified that could predict patient outcome with more accuracy but with fewer proteins compared to the 21-protein panel. The ability to identify high risk patients early could dramatically improve outcomes, by assisting clinicians in selecting the best treatment for individual patients.

This study was able to validate the proteins from the previous iTRAQ study which had lower fold-changes and were previously deemed to be statistically insignificance and have small biologically irrelevant changes in abundance. Ten of these proteins were orthogonally validated as differentially abundant and three were included in the final protein signature for poor prognosis. These findings, particularly the inclusion of the three proteins in the 14-protein panel, highlights the need for more sensitive instrumentation and more sophisticated statistical analysis in complex disease states such as cancer.

Protein panels overcome the limitations of single marker screens and should enable sub-typing of an individual patient's melanoma. The use of protein panels will contribute to the goal of personalised medicine with the ability to predict not only patient outcomes but also drug responses. The considerable analytical power of mass spectrometry and SRM should facilitate the translation from bench to bedside, with provision of high throughput screens from very little sample, with short processing times and high reproducibility and reliability.

Chapter 4: Changes in the melanoma proteome with activation of the Unfolded Protein Response

4.1 Introduction

A study previously conducted in our laboratory [394] investigating differentially abundant proteins in good and poor prognosis AJCC III melanoma patients elucidated several interesting molecular pathways potentially utilised by melanoma for progression and metastasis. In the previous chapter several of these protein changes were validated by SRM in the AJCC stage III patient cohort. A major pathway discovered to be up-regulated in poor prognosis stage III patients from these studies was the Unfolded Protein Response (UPR), with four of the 14-protein prognostic panel directly involved in this stress response; HSPA8, HSP90AB1, WARS and PARP1.

The UPR has been identified to be increasingly activated in many cancers including melanoma [1]. However, its contribution to melanoma pathology is not well understood. The UPR has far reaching effects even within normal cells and therefore comprehension of how these downstream effectors of the UPR are utilised by cancers is not well known. Understanding molecular mechanisms and pathways exploited by melanoma to increase its invasive potential, aid in progression and therefore its ability to metastasise to distant sites is critical for melanoma treatment.

Our previous studies focused on changes in protein abundance in stage III melanoma patients that correlate with prognosis, therefore the aim was to determine how the UPR could be aiding in melanoma progression and oncogenic transformation to a neoplasm capable of metastasis. The role of the UPR in melanoma progression and metastasis was explored in cell line models. Primary and metastatic cell lines were selected for investigation, bearing both mutant and wild-type BRAF due to its known link with the UPR, as discussed in Chapter 1. Two cell lines were treated with thapsigargin (TH), an inhibitor of endoplasmic and sarcoplasmic reticulum calcium ATPases, resulting in depletion of Ca^{2+} stores within the ER. As Ca^{2+} is an essential cofactor of many ER chaperones, this depletion leads to increased ER-stress and activation of the UPR. Increased activation of the UPR in the melanoma cell lines was investigated using quantitative mass spectrometry. A melanoma cell line model was successfully established to study the effects of increased UPR on the proteome via thapsigargin treatment which induced ER-stress. Cell lysates were labelled using isobaric tags for relative and absolute quantitation (iTRAQ) and the peptides separated by two-dimensional separation by high performance liquid chromatography (2D-HPLC) prior to mass spectrometry. In total, 66 proteins were found to be significantly differentially abundant in both cell lines with increased UPR activation, involved in cytoskeletal rearrangements, increased metabolic

potential, altered mRNA and protein processing capacity, alterations to cell signalling pathways and apoptotic proteins.

4.2 Methods

Detailed protocols are described in Chapter 2: Materials and Methods and briefly described below.

4.2.1 Cell culture IC_{50} assays

4.2.1.1 SRB assay

Melanoma cell lines MEL-RM and WMM1175 were cultured as described in Chapter 2.3 and **Table 2-1**. Cell lines were then treated with thapsigargin, a non-competitive inhibitor of sacro/endoplasmic calcium ATPase. As calcium is an important cofactor for ER chaperone functionality, thapsigargin results in an accumulation of unfolded proteins in the ER and induction of the UPR [395, 396] The sulforhodamine B (SRB) assay was used to select an optimal concentration of thapsigargin that would induce ER-stress without resulting in cell death, mimicking the conditions of *in vivo* tumour samples. The SRB dye binds to basic amino acids and is a measure of cellular protein content. As ER-stress and induction of the UPR results in global suppression of mRNA and protein synthesis, cell cycle arrest, senescence but in cancerous cells will not induce apoptosis, measuring total protein content is a more appropriate measure of induction of the UPR in cancers cells than measuring apoptosis. Detailed protocols of the SRB assay can be found in Chapter 2.3.1.1.

4.2.1.2 Sub-G1 DNA assay

To ensure melanoma cell lines were not undergoing apoptosis with thapsigargin treatment and therefore an appropriate model system had been established for *in vivo* mimic, apoptosis was measured with the Sub-G1 DNA assay. The Sub-G1 DNA assay uses the nucleic acid stain propidium iodide (PI) to assess cell viability. PI binds to DNA and can be used to measure progression through the cell cycle, with one copy of the genome at G1 phase, replication with two copies of the genome in M phase or DNA degradation to small fragments via caspases during apoptosis. Detailed protocols can be found in Chapter 2.3.1.2.

4.2.2 Western blotting

Western blots were performed as described in Chapter 2.5. Details on the antibodies, concentrations and incubations times can be found in the **Supplementary Table S2-1**.

4.2.3 Sub-cellular fractionation of melanoma cell lines

Detailed methods on the subcellular fractionation can be found in Chapter 2.3.3. In order to get increased depth in proteome coverage especially for organelles of importance for the UPR such the nuclei and mitochondria, subcellular fractionation was performed. The nuclear, mitochondrial and cytosolic fractions were isolated for MS analysis, while the membrane fraction was isolated and stored for future studies. An overview of the subcellular fractions in outlined in **Figure 4-1**.

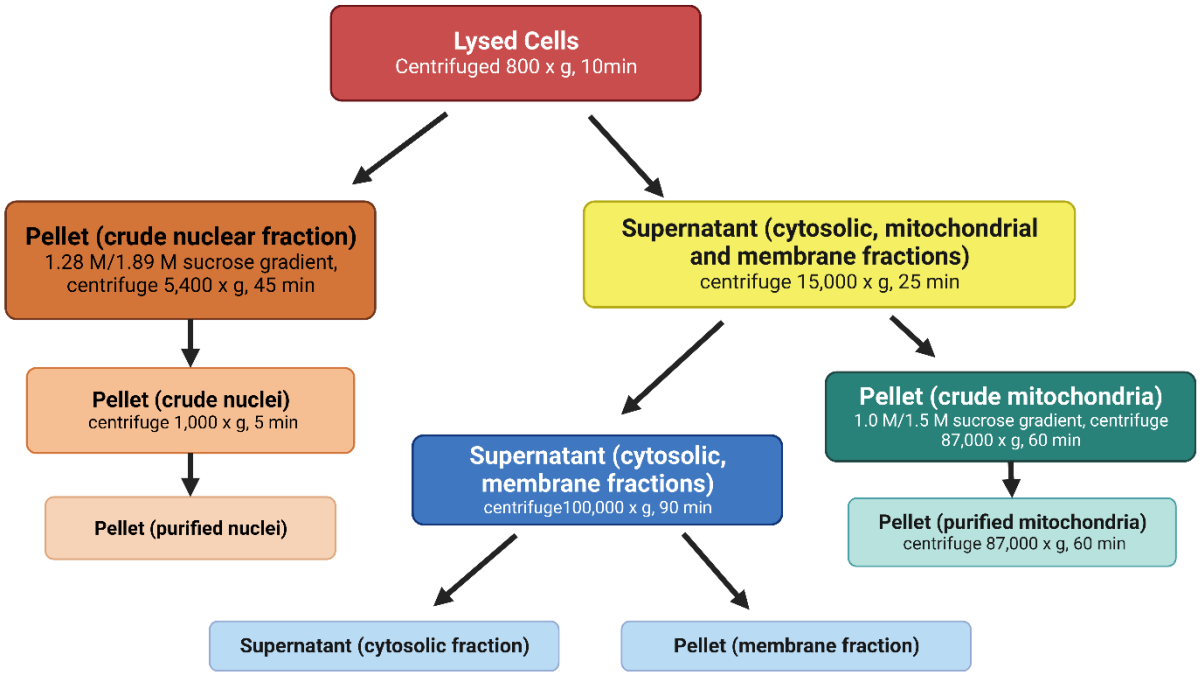

Figure 4-1. Overview of subcellular fractionation protocol. Complete methods are detailed in Chapter 2.3.3.

Briefly, cells were lysed and centrifuged separating the crude nuclear fraction as the pellet from the mitochondrial, cytosolic and membrane fractions in the supernatant. The crude nuclei pellet was isolated at the interface of a two-step sucrose gradient and purified with washing. The mitochondrial fraction was separated from the cytosolic and membrane subcellular fractions via centrifugation, the resulting crude mitochondrial pellet was isolated at the interface of a two-step sucrose gradient with ultra-centrifugation and purified with washing. The cytosolic and membrane fractions were separated via ultra-centrifugation into pelleted membrane fraction and the cytosolic fraction in the supernatant.

4.2.4 Tryptic digestion and iTRAQ labelling

The nuclear, mitochondrial and cytosolic fractions were processed for quantitative MS with iTRAQ labelling as detailed in Chapter 2.4. Briefly, nuclear, mitochondrial and cytosolic subcellular fractions were solubilised in 0.1% (w/v) SDS and treated with Benzonase nuclease to degrade DNA and RNA. Proteins were then purified and quantitated using chloroform/methanol clean up and the Qubit fluorometric protein assay. Proteins were solubilised in 0.5 M in TEAB, pH 8.0 with 0.1% (w/v), then cysteine residues reduced and alkylated with TCEP and iodoacetamide, respectively. Tryptic digestion of proteins was performed by the addition of 1:25, trypsin: protein and incubated at 37 ℃ overnight. The resulting peptides were labelled with 8-plex iTRAQ tags according to the manufacturer's instructions and labelled iTRAQ sets pooled (**Table 4-1**). Labelled peptide pools were cleaned with solid phase extraction first using cation exchange then hydrophilic-lipophilic balanced reverse phase LC columns.

Table 4-1. Assignment of 8-plex iTRAQ tags to the cytosolic, nuclear, and mitochondrial subcellular fractions of WMM1175 and Mel-RM melanoma cell lines for 2D-LC-MS/MS analysis.

	WMM1175				Mel-RM			
	Control	**TH**	**Control**	**TH**	**Control**	**TH**	**Control**	**TH**
Cytosolic	113	114	115	116	117	118	119	121
Nuclear	113	114	115	116	117	118	119	121
Mitochondrial	113	114	115	116	117	118	119	121

4.2.5 Quantitative MS analysis with iTRAQ labelling

Prior to MS analysis each set of iTRAQ labelled peptide mixtures was fractionated by strong cation exchange (SCX) chromatography over a 60 min gradient collecting fractions every 2 min. Fractions 1-5, 6-7 and 28-30 were pooled to give a total of 23 fractions for MS analysis. Each fraction was further separated by nanoflow (0.6 μL/min) reverse phase liquid chromatography with a 105 min non-linear gradient for MS analysis on the QSTAR Elite ESI with 120 min acquisitions in IDA mode with Q2 modified Enhance All mode for improved iTRAQ report tag quantitation. Acquisitions methods were set for TOF-MS survey scan acquired (*m/z* 350-1750, 0.5 s), with the three most abundant multiply charged precursor ions (2+ to 4+, counts >30) in the survey scan sequentially subjected to product ion analysis.

MS datafiles were analysed with ProteinPilot™ v4.0 software searching against the SwissProt human protein database, utilising the Paragon™ algorithm for protein identification and the Pro Group™ algorithm to perform a statistical analysis on the peptides found to

determine the minimal set of confident protein identifications [278]. A protein identification threshold of 95% confidence or greater for peptide matches, an unused ProtScore of >1.3 was imposed and a global false discovery rate (FDR) of 1%. The intensity ratios of isobaric tag reporter ion peaks were used to quantify relative peptide abundance and therefore the corresponding protein abundance. A Student's paired *t*-test was performed with equal variance to compare control to treated samples in both Mel-RM and SK-MEL-28 cell lines. Only those proteins whose change in abundance had a fold change of 1.5 or greater and a p-value < 0.05 were taken as statistically significant.

Hierarchical clustering was performed with the python package Seaborn clustermap using Euclidean distance metrics and Pearson's correlation from fastcluster [279]. Missing values were excluded from the correlation analysis so as not to introduce unwanted variance from technical missing values although values missing biologically, that may be of significance are ignored as a consequence. Principal component analysis (PCA) was carried out with the python package sklearn [280]. Data was not transformed, unit variance scaling was employed on iTRAQ ratios with Nonlinear Iterative Partial Least Squares (NIPALS) PCA method without imputation. Pathway analysis was carried out with the differentially abundant proteins using the STRING repository as described in Chapter 2.7.1

4.3 Results

4.3.1 Activation of the UPR with thapsigargin

4.3.1.1 SRB assay

An optimal inhibitory concentration of thapsigargin was determined by SRB assay. The SRB assay was selected as it is a measure of total protein, rather than cell death, as the UPR in melanoma does not induce cell death but rather reduces the total protein burden within the cell via several pathways as described in Chapter 1.

At thapsigargin concentrations from 0.1 to 5 µM at 48 h, 60% of the total cellular protein remains compared to control (**Figure 4-2** and **Figure 4-3**). At 72 h both cell lines had a marked decrease in total protein, with approximately 30% protein content compared to control.

At higher concentrations, 10 µM thapsigargin, the WMM1175 melanoma cell line exhibited greater susceptibility to thapsigargin than the Mel-RM cells, with 35% versus 55% of total protein in the control at 48 h. However, at 72 h, both cell lines have a similar reduction in total protein with 15% and 23% of the control protein for WMM1175 and Mel-RM, respectively. A concentration of 1 µM for 48 h was selected as the optimal concentration for the following experiments.

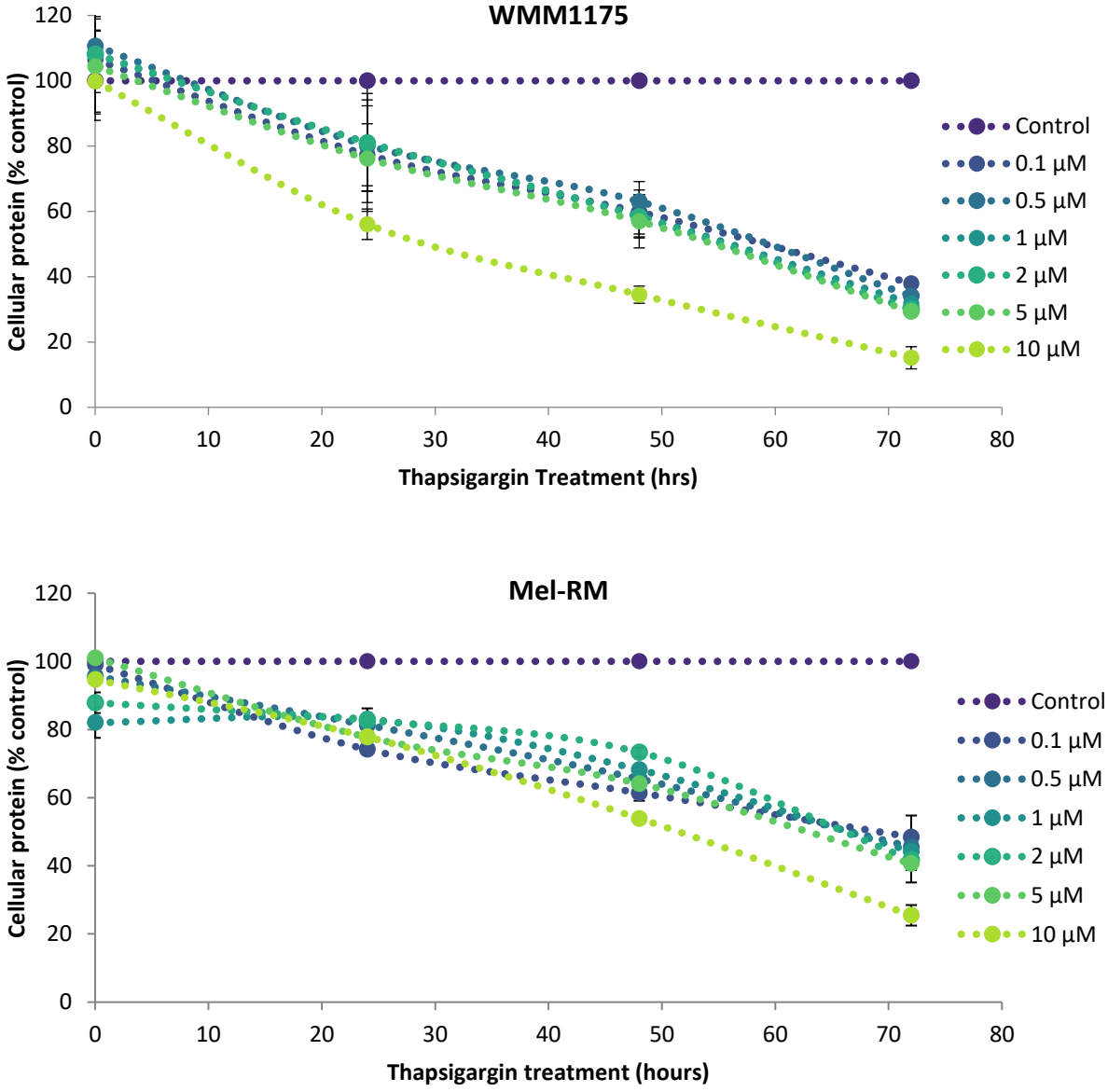

Figure 4-2. Inhibition of cellular protein content with varying thapsigargin concentrations over time in WMM1175 and Mel-RM melanoma cell lines. Melanoma cell lines, WMM1175 and Mel-RM, were treated with varying concentrations of thapsigargin (0.1 – 10 µM) up to 72 h. Total cellular protein was determine determined by SRB assay, and the data is expressed as a percent of untreated control cells. Error bars represent S.E.M. of 3 technical replicates in 3 biological replicates for each cell line.

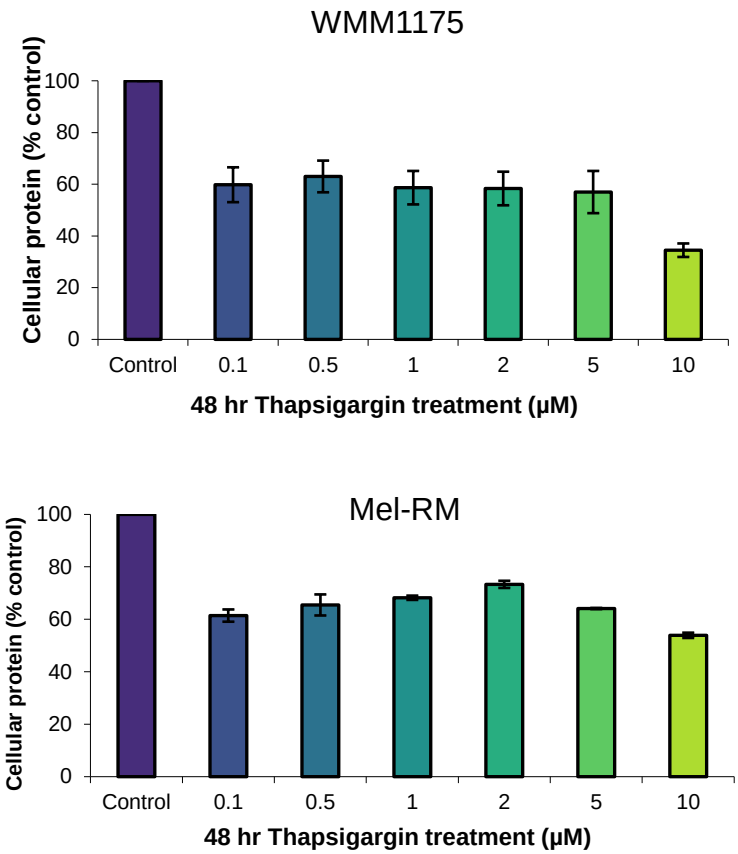

Figure 4-3. Inhibitory concentrations of thapsigargin at 48 h on WMM1175 and Mel-RM melanoma cell lines determined by SRB assay. Melanoma cell lines, Mel-RM and WMM1175, were treated with varying concentrations of thapsigargin (0.1 – 10 µM) for 48 hr. Error bars represent S.E.M. of 3 technical replicates in 3 biological replicates for each cell lines.

4.3.1.2 Cell viability with SubG1 DNA assay

ER-stress and induction of the UPR in melanoma *in vivo* does not result in apoptosis in cancerous cells as it would in normal cell types, even with acute, prolonged ER-stress, as cancer acquires resistance to UPR-induced apoptosis. The Sub G1 DNA assay was performed to ensure the inhibitor concentration of 40% determined by the SRB assay was only resulting in a reduction in protein, part of the recovery arm of the UPR, and not inducing UPR-mediated apoptosis. In the Sub-G1 assay PI binds to the DNA of fixed cells, with the amount of florescence corresponding to the amount of DNA present. This gives two peaks when measured on the flow cytometer correlating to cells in the G1/S phase of the cell cycle with a single genome and cells in G2\M phase with two copies of the genome. During apoptosis, DNA is cleaved by caspases first into high molecular weight, then low molecular weight fragments. If apoptosis has occurred, the DNA degradation can be observed as a third peak, called the Sub-G1 peak, with a corresponding low florescent signal. No apoptosis was detected in either cell lines using the optimal thapsigargin conditions (1 µM, 48 h) for either cell line (**Figure 4-4**).

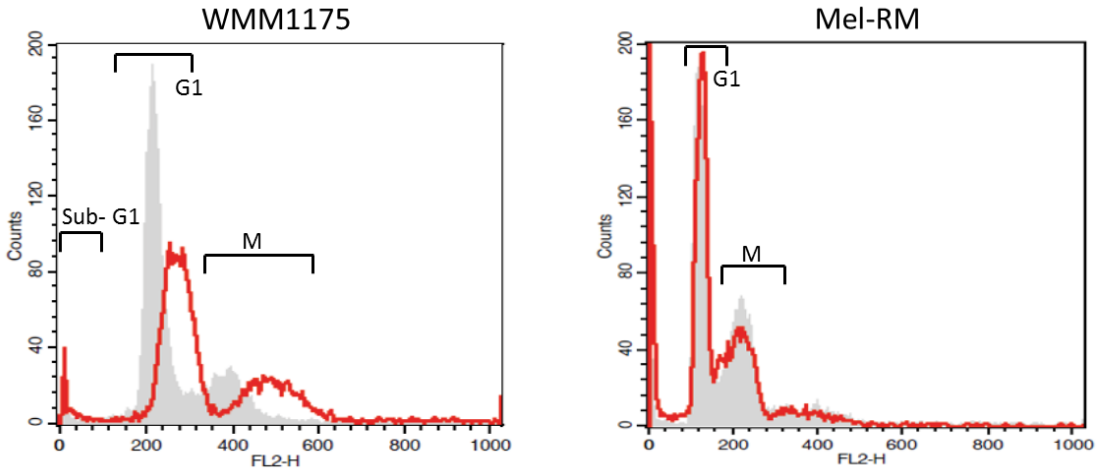

Figure 4-4. Detection of apoptotic cell death in WMM1175 and Mel-RM melanoma cell lines treated with 1 µM thapsigargin for 48 h. Sub-G1 DNA assay was used for the two cell lines and PI detection by flow cytometry is shown. Untreated control cells are shown in grey and the treated cell lines are shown in red. The figures are representative of technical replicates (n=3).

4.3.1.3 Up-regulation of UPR modulators

Increased activation of the UPR in thapsigargin-treated cells was confirmed by probing for UPR specific proteins; GRP78, XBP1 and HYOU1. GRP78, as the master regulator of the UPR, was probed for in the three subcellular fractions (**Figure 4-5).** GRP78 had greater abundance in the nucleus, cytoplasm and mitochondria upon treatment with 1 µM thapsigargin for 48 hr in both cells. The presence of GRP78 in the nuclear and mitochondrial fractions in control melanoma cells was too low to be detected via Western blotting.

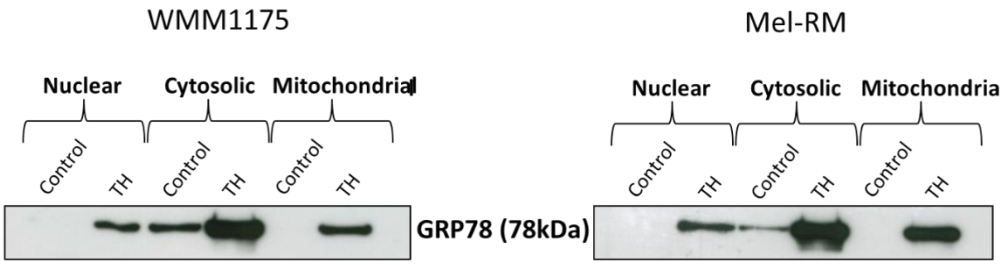

Figure 4-5. Activation of the unfolded protein response determined by up-regulation of GRP78 in the nuclear, cytosolic and mitochondrial fractions. Cell lines (WMM1175 and Mel-RM) were treated with 1 µM thapsigargin (TH) for 48 h and the nuclear, cytosolic and mitochondrial fractions isolated. Western blotting was performed by loading 10 µg of the nuclear, cytosolic and mitochondrial fractions on a 12% polyacrylamide gel probing for GRP78, the master UPR regulator. Membranes were incubated with primary anti-GRP78 (1:1000) 4ºC overnight, followed by anti-mouse secondary antibody (1:10,000) for 1 h at room temperature. Binding of the secondary antibody conjugated to peroxidase was then visualised with ECL reagent. Figure is representative of two separate membranes.

Whole cell lysates without fractionation were probed for two other ER stress related proteins. XBP-1, a transcription factor that controls the expression of UPR-related genes by binding to UPR-response elements, was probed for both its spliced and unspliced isoforms. In both melanoma cell lines the abundance of XBP-1 as determined by Western blotting decreased with increased ER-stress. The decrease was greater in the MEL-RM cell line. HYOU1 is an ER-associated chaperone also known to be increased with ER stress. The expression of HYOU1 was elevated in whole cell lysates of Mel-RM cells treated with thapsigargin (**Figure 4-6**). Several HYOU1 products of differing molecular weights were observed, either due to antibody cross-reactivity as discussed in Chapter 1, or, as they are not present in control cells, they may be potential HYOU1 isoforms. Overall, the Western blot data is consistent with thapsigargin inducing an ER stress and increased activation of the UPR.

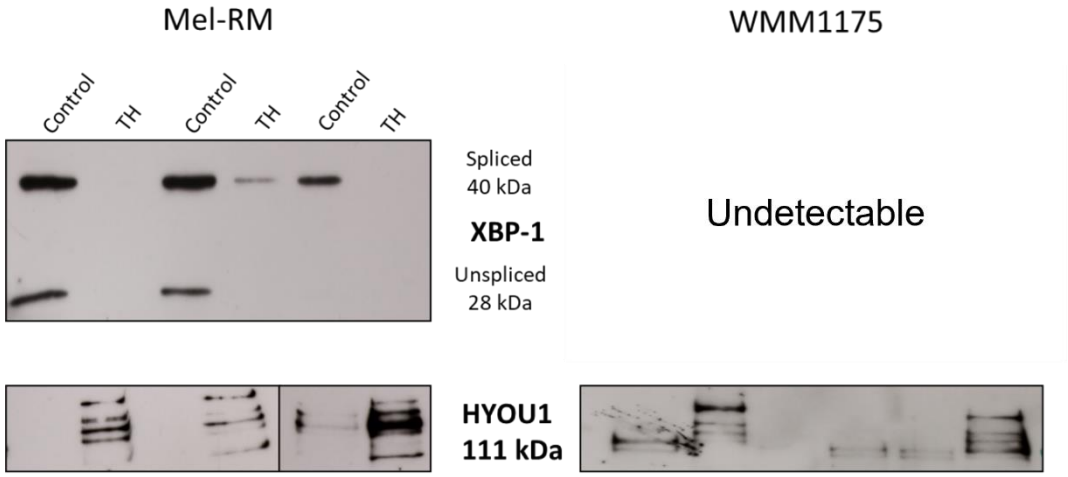

Figure 4-6. Activation of the unfolded protein response determined by western blotting of XBP-1 and HYOU1 in MEL-RM and WMM1175 melanoma cell line whole cell lysates. Cell lines (WMM1175 and Mel-RM) were treated with 1 µM thapsigargin (TH) for 48 h. Western blotting was performed by loading 10 µg of whole cell lysate on a 12% polyacrylamide gel probing for UPR regulators XBP-1 and HYOU1. Membranes were incubated with primary anti-XBP-1 (1:500) at 4ºC overnight followed by anti-rabbit secondary antibody (1:7,500) for 1 h at room temperature. Separately, membranes were incubated with anti-HYOU1 (1:500) for 1h at room temperature, followed by anti-rabbit secondary antibody (1:5,000) for 1 h at room temperature. Binding of secondary antibodies conjugated to peroxidase was then visualised with ECL reagent. Figure is representative of two separate membrane each with biological triplicates.

4.3.2 Subcellular fractionation

To confirm the subcellular fractionation method enriched the target cell compartments, subcellular specific proteins of known organelle specificity were selected for Western blotting.

Transcription factor PU.1 (PU.1) for the nuclear proteome, Succinate dehydrogenase A (SDHA) for the mitochondrial proteome and Glyceraldehyde 3-phosphate dehydrogenase (GAPDH) for the cytosolic proteome. The abundance of these marker proteins was compared between the whole cell lysates and enriched fractions by Western blotting (**Figure 4-7**). Each protein was clearly enriched in the appropriate subcellular fraction.

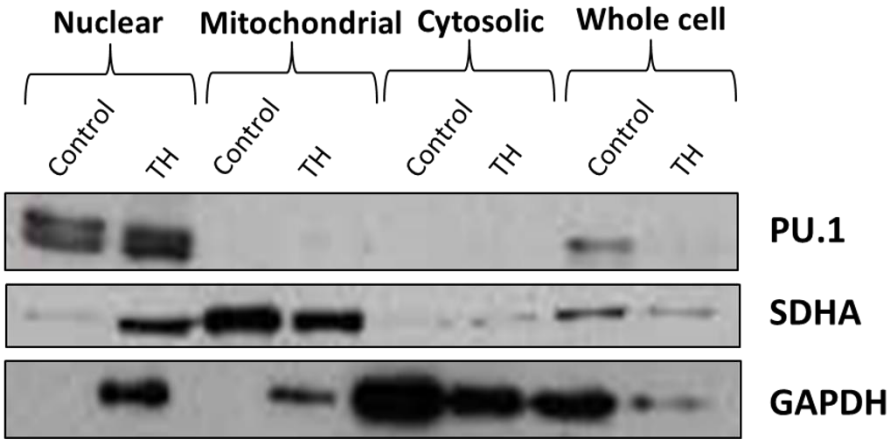

Figure 4-7: Enrichment of subcellular proteomes from ultracentrifugation over two-step sucrose gradients determined by subcellular markers. Western blotting with markers PU.1 for the nuclear, SDHA for mitochondrial and GAPDH for the cytosolic fractions. Gels were loaded with 10 µg of each subcellular fraction and a whole cell lysate sample on a 12% polyacrylamide. Separately, membranes were incubated with primary anti-PU.1 (1:1,000) for 1 h at room temperature, followed by anti-rabbit secondary antibody (1:7,500) for 1 h at room temperature. Separately, membranes were incubated with primary anti-SDHA (1:2,000) for 1 h at room temperature, followed by anti-mouse secondary antibody (1:10,000) for 1 h at room temperature. Separately, membranes were incubated with primary anti-GAPDH (1:40,000) for 1 h at room temperature, followed by anti-mouse secondary antibody (1:20,000) for 1 h at room temperature. Binding of secondary antibodies conjugated to peroxidase was then visualised with ECL reagent. Figure is representative of two separate membrane each with biological triplicates.

4.3.3 Differential proteins in melanoma cell lines in response to ER-stress analysed by 2D-LC-MS\MS with iTRAQ tags

The proteome of each subcellular fraction from the two melanoma cell lines was acquired after iTRAQ labelling by 2D-LC-MS\MS on a QSTAR Elite ESI mass spectrometer (Chapter 2.4.7). A total of 3,490 proteins (>95% confidence, three or more peptides per protein) were identified by 2D-LC-MS/MS analysis in the three subcellular fractions from the two melanoma cell lines. After thapsigargin treatment, the WMM1175 cells had 374 significantly differentially abundant proteins (114 cytosolic, 180 nuclear and 80 mitochondrial) and the Mel-RM line; 259 significant proteins (82 cytosolic, 70 nuclear and 107 mitochondrial, **Figure 4-8**).

Overall, 561 proteins were found to be differentially abundant with thapsigargin treatment in either cell line (p-value ≤ 0.05, >3 peptides, fold-change >1.5).

Of the 560 proteins differentially abundant, 71 were common between the two cell lines (**Table 4-2**, **Figure 4-8** and **Figure 4-9**). Among the 71, 66 were unique proteins across all fractions and cells, as HYOU1 was in common between the cytosol and nucleus, TIMM50 between nucleus and mitochondria, and GRP78 (HSPA5) was common to all three fractions. While all 560 proteins are therefore associated with increased ER stress and activation of the UPR, the 71 proteins in common are of greater interest, as they indicate stable changes elicited across cell lines during UPR activation. Among the 71, the direction of differential abundance, up- or down-regulated, was the same in both cell lines (**Table 4-2**), indicating good data consistency. Among the 71 proteins, 33 were up-regulated and 38 down-regulated (**Figure 4-10**, **Figure 4-11** and **Figure 4-12**). Among the up-regulated group were seven unique proteins up-regulated to the greatest extent (>5-fold, **Table 4-2**): HSPA5, HYOU1, NAMPT, RPS18, SPCS2, CISD2 and PGRMC2 (in decreasing order), all of which are part of the Cell Response to Stress pathway and five of the seven to the UPR pathway (Reactome pathways).

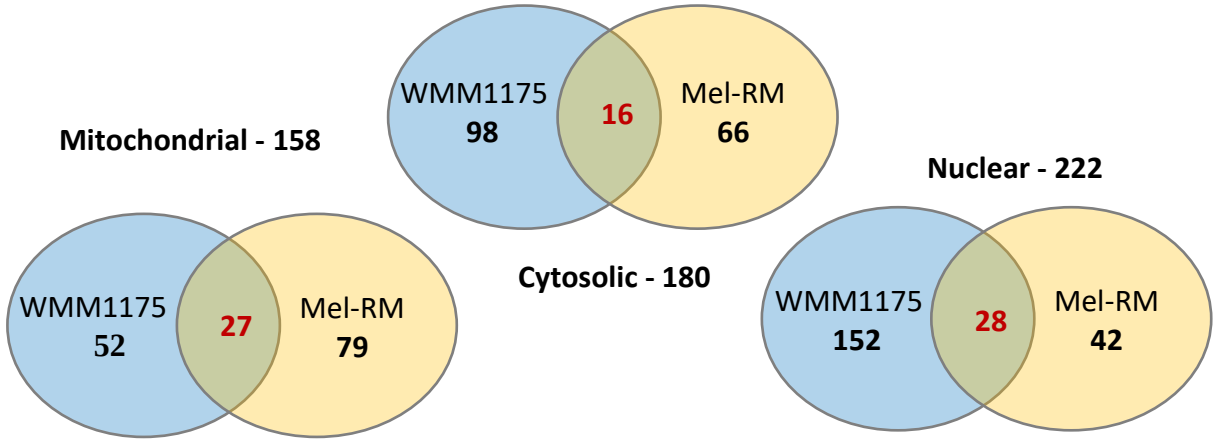

Figure 4-8. Changes in the melanoma proteome with increased UPR activation. Melanoma cell lines Mel-RM and WMM1175 were treated with TH (1 µM, 48 h). The nuclear, mitochondrial and cytosolic subcellular proteomes were isolated by differential centrifugation then analysed by LC-MS/MS with iTRAQ tags on a QSTAR Elite mass spectrometer. Protein identifications are shown only when they have three or more unique peptides (95% CI) with an Unused Protscore >1.3, a significance threshold of fold-change >1.5 and p-value ≤ 0.05. The results represent technical MS duplicates of biological replicates (n=4) for two cell lines.

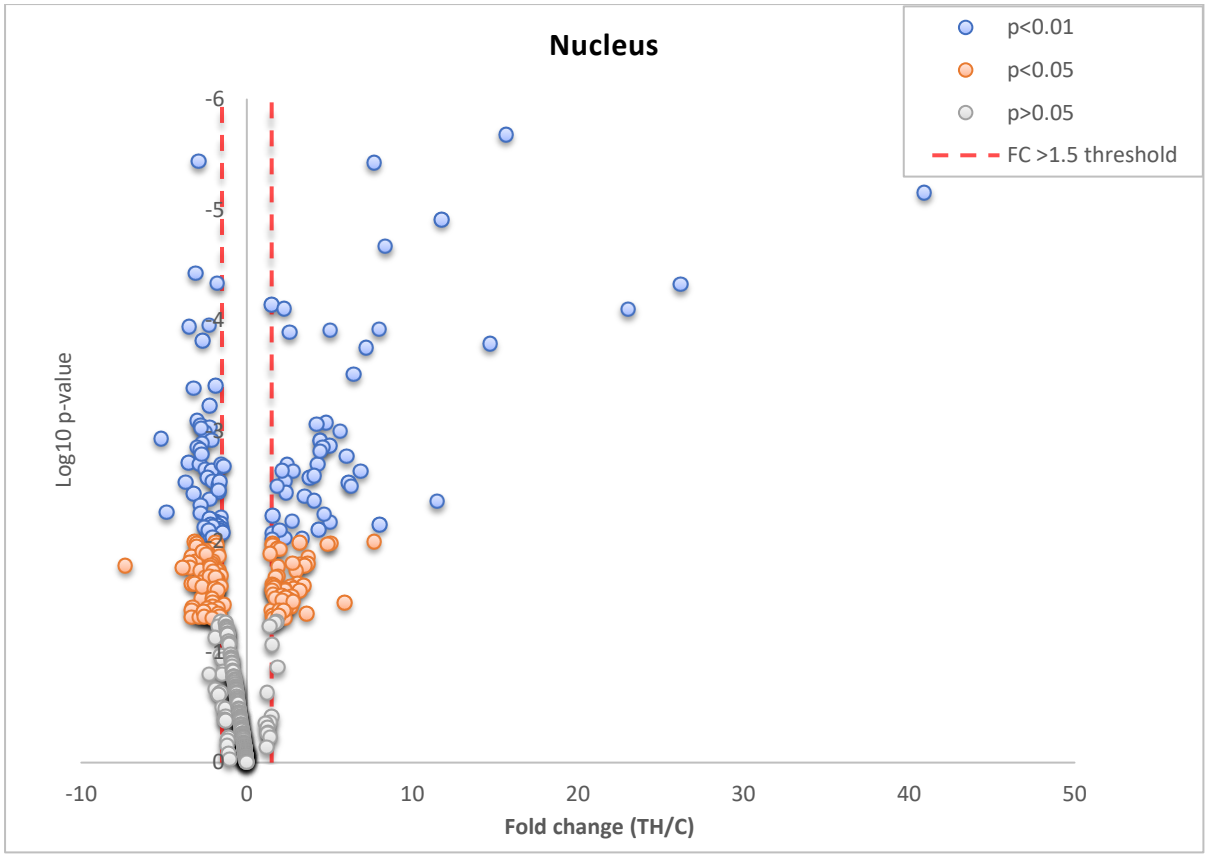
Nucleus
p<0.01
p<0.05
p>0.05
FC >1.5 threshold
Log10 p-value
-6
-5
-4
-3
-2
-1
0
-10
0
10
20
30
40
50
Fold change (TH/C)

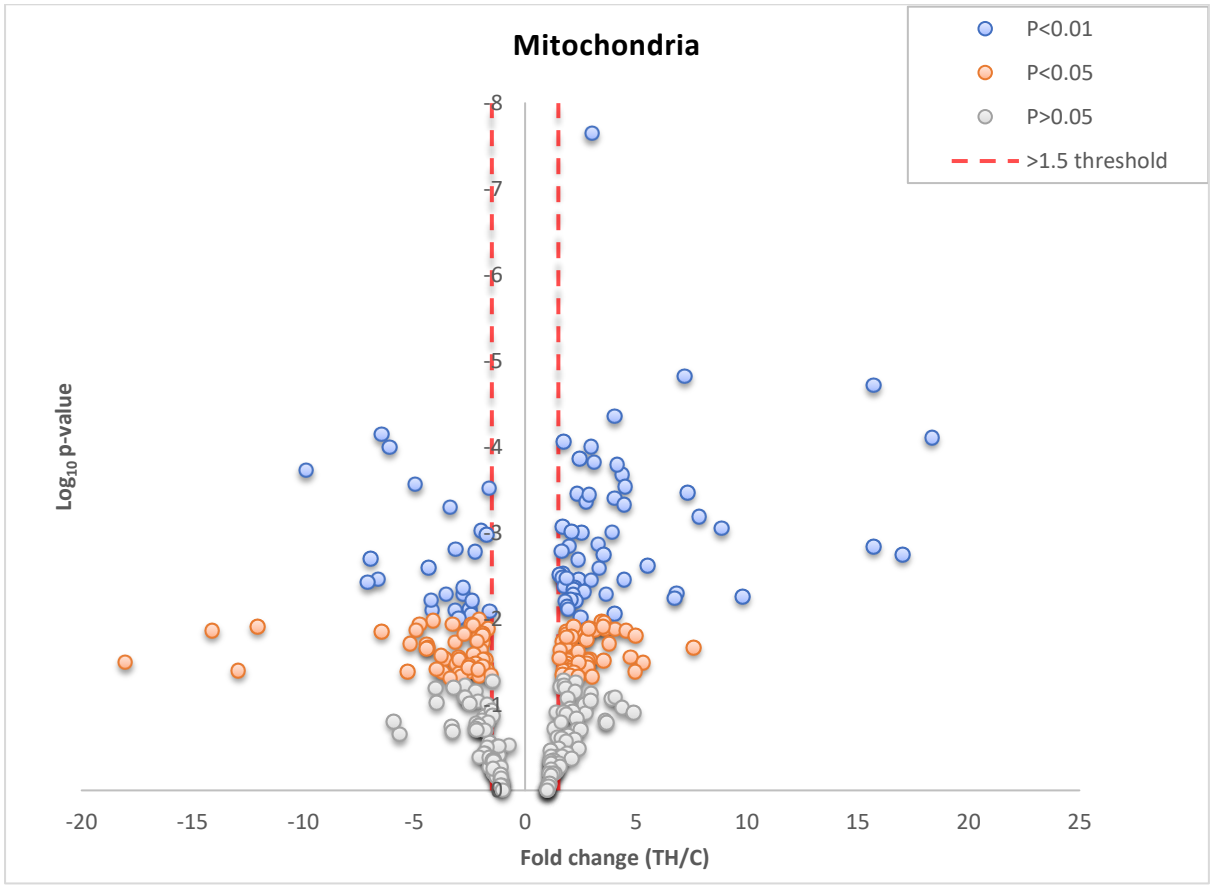
Mitochondria
P<0.01
P<0.05
P>0.05
>1.5 threshold
Log10 p-value
8
7
6
5
4
3
2
1
0
-20
-15
-10
-5
0
5
10
15
20
25
Fold change (TH/C)

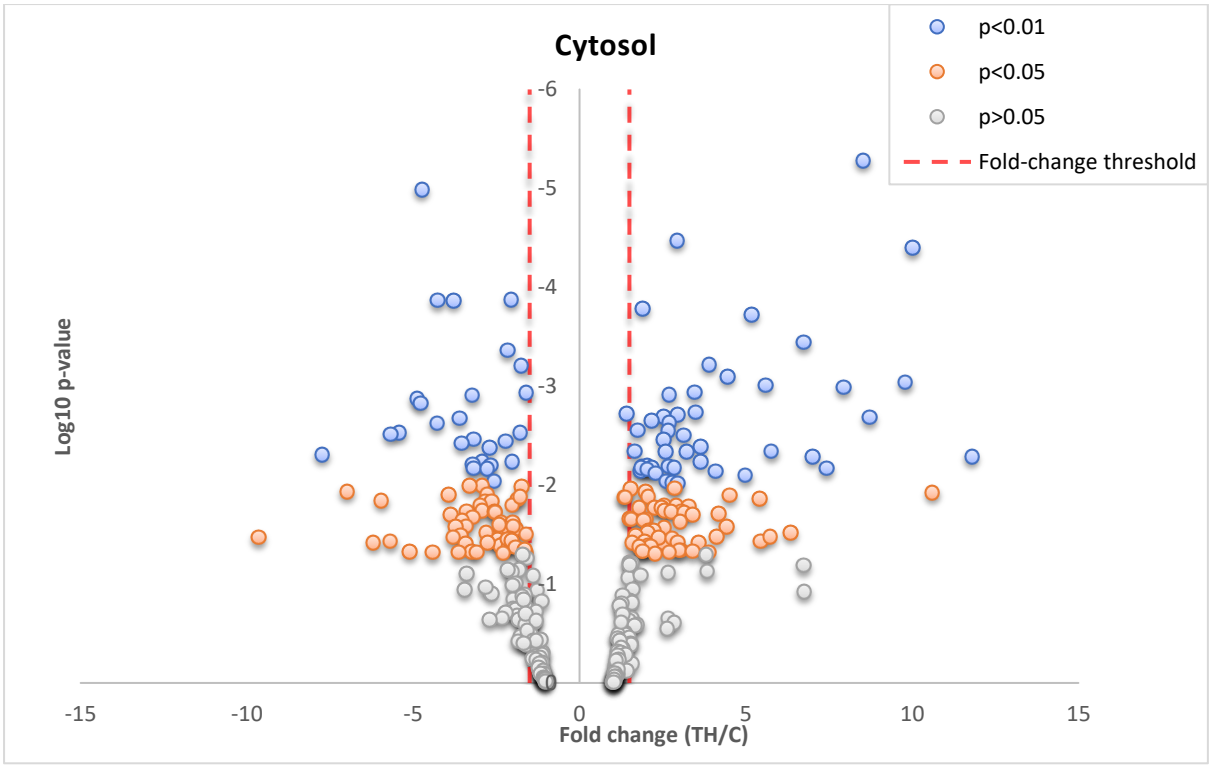

Figure 4-9. Differentially abundant proteins in Mel-RM and WMM1175 melanoma cell line nuclear, mitochondrial and cytosolic fractions after thapsigargin treatment and increased activation of the UPR. Proteins with a fold-change of >1.5 and *p*-value ≤0.05 in both Mel-RM and WMM1175 cell lines (**Table 4-2**) in response to UPR activation (1 µM TH, 48 h).

Table 4-2. Differentially abundant proteins identified by iTRAQ in the subcellular fractions of Mel-RM and WMM1175 melanoma cell lines after thapsigargin treatment and increased activation of the UPR. Melanoma cell lines Mel-RM and WMM1175 were treated with TH (1 µM, 48 h). The nuclear, mitochondrial and cytosolic subcellular proteomes were isolated by differential centrifugation then analysed by LC-MS/MS with iTRAQ tags on a QSTAR Elite mass spectrometer. Protein identifications are based on three or more unique peptide (95% CI) with an Unused Protscore >1.3, differential cut-off of fold-change >1.5 and *p*-value ≤ 0.05. The following results represent technical MS duplicates of biological replicates (n=4) for two cell lines.

Accession	Gene Name	Name	Major Function	WMM1175 Average Fold change (*p*-value)		Mel-RM Average Fold change (*p*-value)		% Protein Coverage (95% CI)
Cytosolic Proteome								
E9PL22	HYOU1	Hypoxia up-regulated protein 1	Stress response	10.01	(<0.001)	9.80	(0.001)	35.22
P43490	NAMPT	Nicotinamide phosphoribosyltransferase	Metabolic	8.53	(<0.001)	2.54	(0.002)	34.42
P62269	RPS18	40S ribosomal protein S18	RNA biogenesis	7.01	(0.005)	1.89	(0.046)	
P13667	PDIA4	Protein disulfide-isomerase A4	Protein processing	4.18	(0.019)	10.61	(0.012)	58.14
P62249	RPS16	40S ribosomal protein S16	RNA biogenesis	3.64	(0.006)	2.52	(0.038)	52.05
P14625	HSP90B1	Endoplasmin	Stress response	2.87	(0.011)	5.45	(0.037)	73.97
Q01518	CAP1	Adenylyl cyclase-associated protein 1	Cytoskeletal	2.61	(0.009)	1.84	(0.007)	25.68
P07237	P4HB	Protein disulfide-isomerase	Protein processing	2.54	(0.003)	4.43	(0.026)	84.06
P11021	HSPA5	78 kDa glucose-regulated protein	Stress response	1.52	(0.013)	1.51	(0.001)	
G5E9Q2	CSDE1	Cold shock domain containing E1	Stress response	-1.60	(0.001)	-2.02	(0.016)	5.69
F8W726	UBAP2L	Ubiquitin-associated protein 2-like	Unknown	-1.65	(0.045)	-5.68	(0.003)	4.416
P31153	MAT2A	S-adenosylmethionine synthase isoform type-2	Metabolic	-1.71	(0.050)	-3.40	(0.029)	14.94
E9PC52	RBBP7	Histone-binding protein RBBP7	Chromatin remodelling	-1.78	(0.013)	-2.48	(0.033)	15.38
O15355	PPM1G	Protein phosphatase 1G	Protein processing	-2.09	(0.035)	-6.20	(0.038)	6.78
Q13509	TUBB3	Tubulin beta-3 chain	Cytoskeletal	-2.80	(0.030)	-3.42	(0.039)	66
Q02818	NUCB1	Nucleobindin-1	Stress response	-6.98	(0.012)	-3.20	(0.006)	18
Nuclear Proteome								
P11021	HSPA5	78 kDa glucose-regulated protein	Stress response	14.69	(<0.001)	40.93	(<0.001)	77.83
J3KPF3	SLC3A2	4F2 cell-surface antigen heavy chain	Transporter	4.35	(0.008)	2.15	(0.002)	12.20

Accession	Gene Name	Name	Major Function	WMM1175 Average Fold change (*p*-value)		Mel-RM Average Fold change (*p*-value)		% Protein Coverage (95% CI)
P22087	FBL	rRNA 2'-O-methyltransferase fibrillarin	rRNA processing	2.46	(0.002)	1.97	(0042)	30.22
Q9Y4L1	HYOU1	Hypoxia up-regulated protein 1	Stress response	2.33	(0.049)	4.07	(0.003)	6.81
Q13601	KRR1	KRR1 small subunit processome component homolog	rRNA processing	2.33	(0.003)	1.52	(0.027)	9.88
P17096	HMGA1	High mobility group protein HMG-I/HMG-Y	Transcriptional regulation	1.58	(0.006)	1.86	(0.003)	40.19
P04844	RPN2	Dolichyl-diphosphooligosaccharide--protein glycosyltransferase subunit 2	Protein processing	- 1.54	(0.007)	- 2.20	(0.017)	14.10
Q96RR5	HCA90	Hepatocellular carcinoma-associated antigen 90	Cell cycle	- 1.67	(0.014)	- 2.24	(0.006)	4.85
Q96GC5	MRPL48	39S ribosomal protein L48, mitochondrial	RNA biogenesis	- 1.74	(0.013)	- 1.57	(0.025)	10.85
P08621	SNRNP70	U1 small nuclear ribonucleoprotein 70 kDa	mRNA processing	- 1.76	(0.022)	- 2.22	(0.021)	18.10
Q9H307	PNN	Pinin	Cell adhesion	- 1.82	(0.025)	- 1.69	(0.003)	6.97
J3QLR8	MRPS23	28S ribosomal protein S23, mitochondrial	Translation	- 1.87	(0.007)	- 2.40	(0.040)	14.47
Q8WU90	ZC3H15	Zinc finger CCCH domain-containing protein 15	Cell signalling	- 1.88	(0.036)	- 2.46	(0.013)	10.33
Q15459	SF3A1	Splicing factor 3A subunit 1	mRNA processing	- 1.88	(0.010)	- 2.69	(0.026)	15.26
O75475	PSIP1	PC4 and SFRS1-interacting protein	Transcriptional regulation/ stress response	- 2.04	(0.026)	- 3.67	(0.003)	12.26
O60506	SYNCRIP	Heterogeneous nuclear ribonucleoprotein Q	mRNA processing	- 2.20	(0.009)	- 2.09	(0.033)	38.20
P40227	CCT6A	T-complex protein 1 subunit zeta	Stress response	- 2.27	(<0.001)	- 2.09	(0.049)	12.60
Q92922	SMARCC1	SWI/SNF complex subunit SMARCC1	Transcriptional regulation	- 2.35	(0.008)	- 2.20	(0.007)	8.80
Q13263	TRIM28	Transcription intermediary factor 1-beta	Transcriptional regulation	- 2.37	(0.003)	-1.74	(0.028)	16.77
O75643	NRNP200	U5 small nuclear ribonucleoprotein 200 kDa helicase	mRNA processing	- 2.49	(0.001)	- 2.52	(0.012)	3.14
Q9Y3B4	SF3B14	Pre-mRNA branch site protein p14 OS=Homo sapiens	mRNA processing	- 2.53	(0.002)	- 1.53	(0.002)	32.00
P42166	TMPO	Lamina-associated polypeptide 2, isoform alpha	Chromatin structure	- 2.63	(0.047)	- 2.06	(0.038)	11.67
Q13813	SPTAN1	Spectrin alpha chain, non-erythrocytic 1	Cytoskeletal	- 2.74	(0.023)	-1.87	(0.021)	32.80
Q9UHX1	PUF60	Poly(U)-binding-splicing factor PUF60	Apoptosis	- 2.86	(0.002)	- 2.59	(0.043)	15.92

Accession	Gene Name	Name	Major Function	WMM1175 Average Fold change (*p*-value)		Mel-RM Average Fold change (*p*-value)		% Protein Coverage (95% CI)
Q9UH99	SUN2	SUN domain-containing protein 2	Cytoskeletal	- 2.91	(<0.001)	- 5.17	(0.001)	8.23
Q00341	HDLBP	Vigilin	Metabolic	- 3.09	(<0.001)	- 2.75	(0.001)	13.50
P06493	CDK1	Cyclin-dependent kinase 1	Cell cycle	- 3.33	(0.014)	- 2.12	(0.042)	11.78
Q3ZCQ8-2	TIMM50	Isoform 2 of Mitochondrial import inner membrane translocase subunit TIM50	Transporter	- 3.51	(0.002)	- 4.84	(0.005)	8.56
Mitochondrial Proteome								
P11021	HSPA5	78 kDa glucose-regulated protein	stress response	18.35	(<0.001)	15.70	(<0.001)	71.87
E9PI68	SPCS2	Signal peptidase complex subunit 2	protein processing	7.85	(<0.001)	3.56	(0.031)	31.52
Q8N5K1	CISD2	CDGSH iron-sulfur domain-containing protein 2	Metabolic	7.60	(0.022)	2.54	(0.001)	37.04
O15173	PGRMC2	Membrane-associated progesterone receptor component 2	steroid receptor	5.00	(0.016)	4.77	(0.028)	48.88
Q9BVK6	TMED9	Transmembrane emp24 domain-containing protein 9	Transporter	4.56	(0.014)	7.34	(<0.001)	45.53
H0YDT8	EMC7	ER membrane protein complex subunit 7	Metabolic	4.47	(0.004)	2.56	(0.031)	35.42
Q07065	CKAP4	Cytoskeleton-associated protein 4	Cytoskeletal	4.14	(<0.001)	5.40	(0.001)	58.14
P49755	TMED10	Transmembrane emp24 domain-containing protein 10	Transporter	4.03	(<0.001)	8.87	(0.001)	45.66
O00264	PGRMC1	Membrane-associated progesterone receptor component 1	steroid receptor	3.29	(0.001)	2.35	(<0.001)	41.54
Q70UQ0-4	IKBIP	Isoform 4 of Inhibitor of nuclear factor kappa-B kinase-interacting protein	Apoptosis	3.03	(0.048)	2.34	(0.035)	30.24
Q15006	EMC2	ER membrane protein complex subunit 2	Metabolic	3.02	(<0.001)	2.90	(0.013)	27.27
P42766	RPL35	60S ribosomal protein L35	protein processing	2.98	(<0.001)	2.94	(0.030)	7.273
P23381	WARS	Tryptophan--tRNA ligase, cytoplasmic	Protein processing\ angiogenic	2.41	(0.033)	2.22	(0.004)	12.1
H0YNG3	SEC11A	Signal peptidase complex catalytic subunit SEC11A	protein processing	2.41	(0.047)	3.80	(0.020)	26.99
Q96JB5	CDK5RAP3	CDK5 regulatory subunit-associated protein 3	cell cycle	2.21	(0.013)	2.97	(0.004)	15.61
Q9P0L0-2	VAPA	Isoform 2 of Vesicle-associated membrane protein-associated protein A	vesicle trafficking	2.07	(0.006)	3.16	(0.014)	21.77
P61009	SPCS3	Signal peptidase complex subunit 3	protein processing	1.90	(0.007)	2.41	(0.004)	18.33
P51571	SSR4	Translocon-associated protein subunit delta	Transporter	1.89	(0.016)	3.35	(0.003)	30.64

Accession	Gene Name	Name	Major Function	WMM1175 Average Fold change (*p*-value)		Mel-RM Average Fold change (*p*-value)		% Protein Coverage (95% CI)
O43707	ACTN4	Alpha-actinin-4	Cytoskeletal	-1.89	(0.030)	-4.95	(<0.001)	24.26
P25705	ATP5A1	ATP synthase subunit alpha, mitochondrial	Metabolic	-2.05	(0.010)	-1.74	(0.039)	45.03
C9JJ19	MRPS34	28S ribosomal protein S34, mitochondrial	protein processing	-2.55	(0.037)	-3.62	(0.029)	21.33
G5E9W7	MRPS22	28S ribosomal protein S22, mitochondrial	protein processing	-2.75	(0.015)	-3.14	(0.019)	11.29
P05141	SLC25A5	ADP/ATP translocase 2	Transporter	-4.23	(0.006)	-1.78	(0.030)	44.63
F8W6I7	HNRNPA1	Heterogeneous nuclear ribonucleoprotein A1	mRNA processing	-4.35	(0.003)	-13.00	(0.028)	37.19
P51991	HNRNPA3	Heterogeneous nuclear ribonucleoprotein A3	mRNA processing	-6.11	(<0.001)	-6.96	(0.002)	18.25
Q3ZCQ8-2	TIMM50	Isoform 2 of Mitochondrial import inner membrane translocase subunit TIM50	transporter	-6.46	(0.014)	-14.11	(0.014)	14.25
P22626	HNRNPA2B1	Heterogeneous nuclear ribonucleoproteins A2/B1	mRNA processing	-12.05	(0.012)	-4.14	(0.011)	44.48

The WMM1175 cell lines had an additional 302 significantly differentially abundant proteins (98 cytosolic, 152 nuclear and 52 mitochondrial) while the Mel-RM line also had an additional 187 significantly differentially abundant proteins (66 cytosolic, 42 nuclear and 79 mitochondrial) (**Figure 4-10, Figure 4-11, Figure 4-12, Supplementary Figure S4-1, Supplementary Figure S4-2** and **Supplementary Figure S4-3**). An additional 132 proteins (24 cytosolic, 42 nuclear and 62 mitochondrial) were identified to have the same response to increased UPR activation, with the same differentially abundant trend observed in both cell cells. However, for these proteins, the required significance criteria of p-value ≤ 0.05 was only met in one not both cell lines.

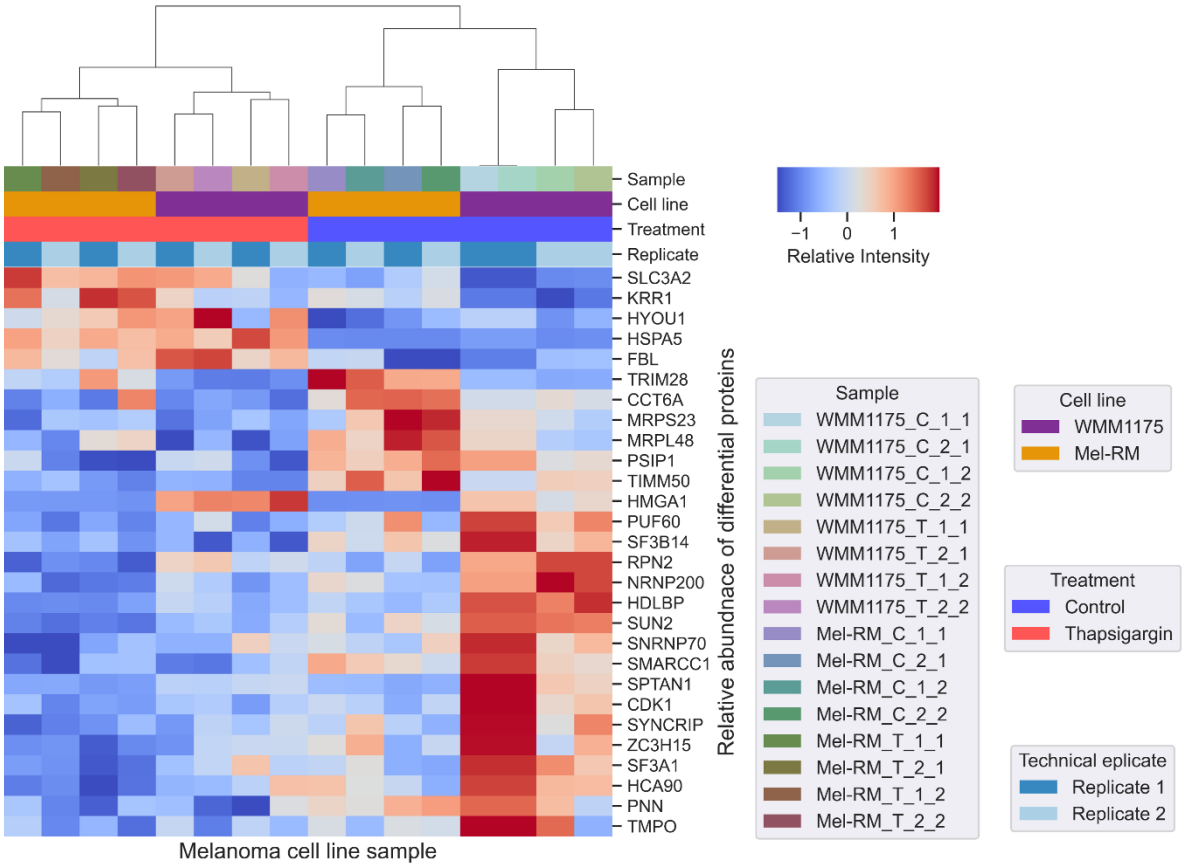

Figure 4-10: Differential nuclear proteins in WMM1175 and Mel-RM melanoma cell lines with increased ER-stress and activation of the UPR. Melanoma cell lines WMM1175 and Mel-RM were treated with TH (1 µM, 48 h). The nuclear subcellular proteome was isolated by differential centrifugation then analysed by LC-MS/MS with iTRAQ tags. Protein identifications must have three or more unique peptide (95% CI) with an Unused Protscore >1.3, differential abundance cut-off of fold-change >1.5 and p-value ≤ 0.05. The following results represent technical MS duplicates of biological replicates (n=4) for two cell lines.

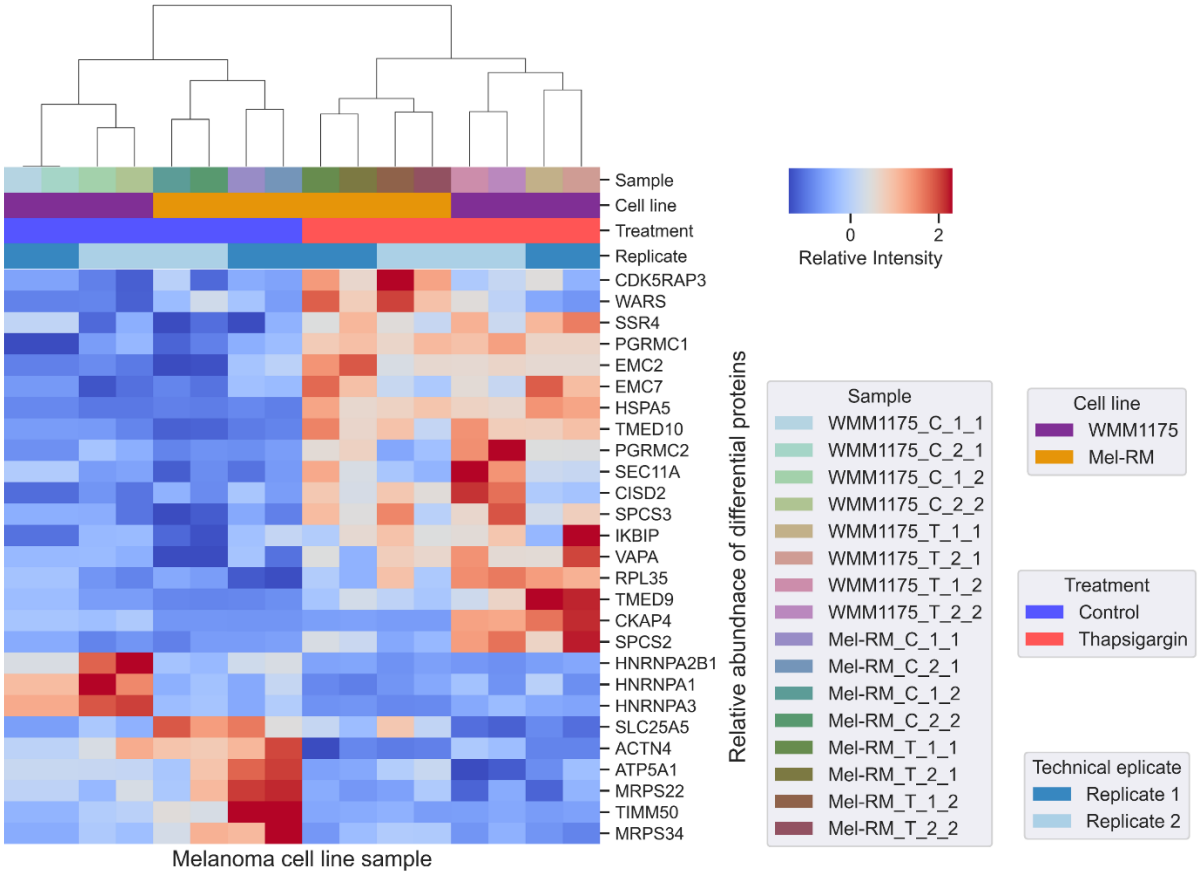

Figure 4-11: Differential mitochondrial proteins in Mel-RM and WMM1175 melanoma cell lines with increased ER-stress and activation of the UPR. Melanoma cell lines Mel-RM and WMM1175 were treated with TH (1 µM, 48 h). The cytosolic subcellular proteome was isolated by differential centrifugation then analysed by LC-MS/MS with iTRAQ tags. Protein identifications must have three or more unique peptide (95% CI) with an Unused Protscore >1.3, differential abundance cut-off of fold-change >1.5 and p-value ≤ 0.05. The following results represent technical MS duplicates of biological replicates (n=4) for two cell lines.

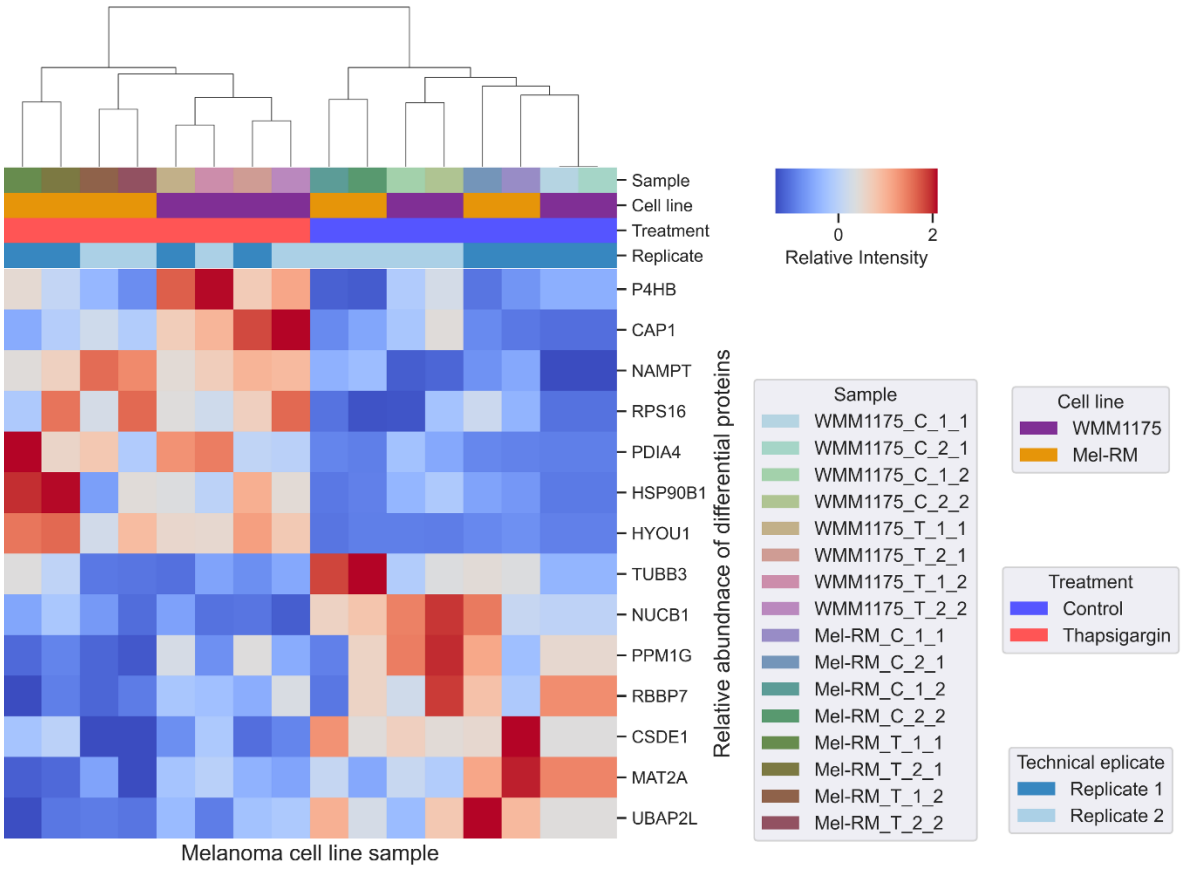

Figure 4-12: Differential cytosolic proteins in Mel-RM and WMM1175 melanoma cell lines with increased ER-stress and activation of the UPR. Melanoma cell lines Mel-RM and WMM1175 were treated with TH (1 µM, 48 h). The mitochondrial subcellular proteome was isolated by differential centrifugation then analysed by LC-MS/MS with iTRAQ tags. Protein identifications must have 3 or more unique peptide (95% CI) with an Unused Protscore >1.3, differential abundance cut-off of fold-change >1.5 and p-value ≤ 0.05. The following results represent technical MS duplicates of biological replicates (n=4) for two cell lines.

4.3.3.1 Clustering and PCA

Data analysis of the combined subcellular proteomes was used to determine the main variables within the entire dataset. The top three principal components were visualised against the other vectors (**Figure 4-13**). The top variables within the dataset with 95% confidence were found to be, in order: technical replicate, cell line and thapsigargin treatment accounting for 57.8%, 25.5% and 16.7% of the variance, respectively.

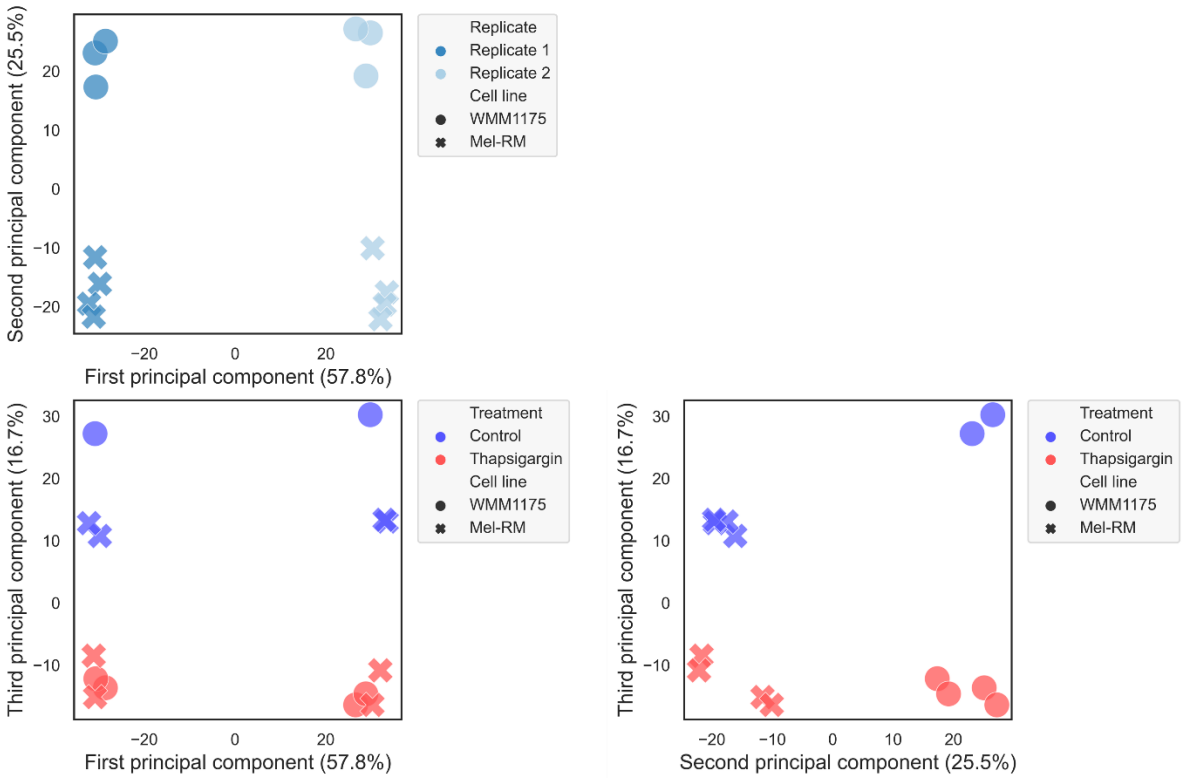

Figure 4-13: Principal component analysis of the protein expression in thapsigargin-treated MEL-RM and WMM1175 cell lines. Proteomic quantitative MS data from the iTRAQ analysis of the nuclear, cytosolic and mitochondrial fractions acquired on the QSTAR Elite ESI were combined and PCA analysis performed on iTRAQ ratios, unit variance scaling was performed on ratios without imputation before NIPAL PCA. The first principal component is technical variance between MS technical duplicates, second principal component accounts for variance in the proteome of the two cell lines and the third principal component is the variance in the proteome between control and thapsigargin treatments.

The correlation of the response between the two lines with increased UPR activation was examined with correlation analysis by Fisher's exact test and unsupervised hierarchical clustering. Correlation analysis and clustering was performed on iTRAQ ratios for all proteins, including those with missing values, identified in the cytosolic, nuclear and mitochondrial proteomes grouped together in a single analysis. Samples correlate somewhat based on cell lines and treatment, however the strongest correlation is driven by the technical replicates. (**Figure 4-13**). Hierarchical clustering shows the strong batch effect likely brought about by the 3-month gap between technical replicate acquisitions on the QSTAR which resulted in a large proportion of missing values between the MS technical replicates (**Figure 4-14**).

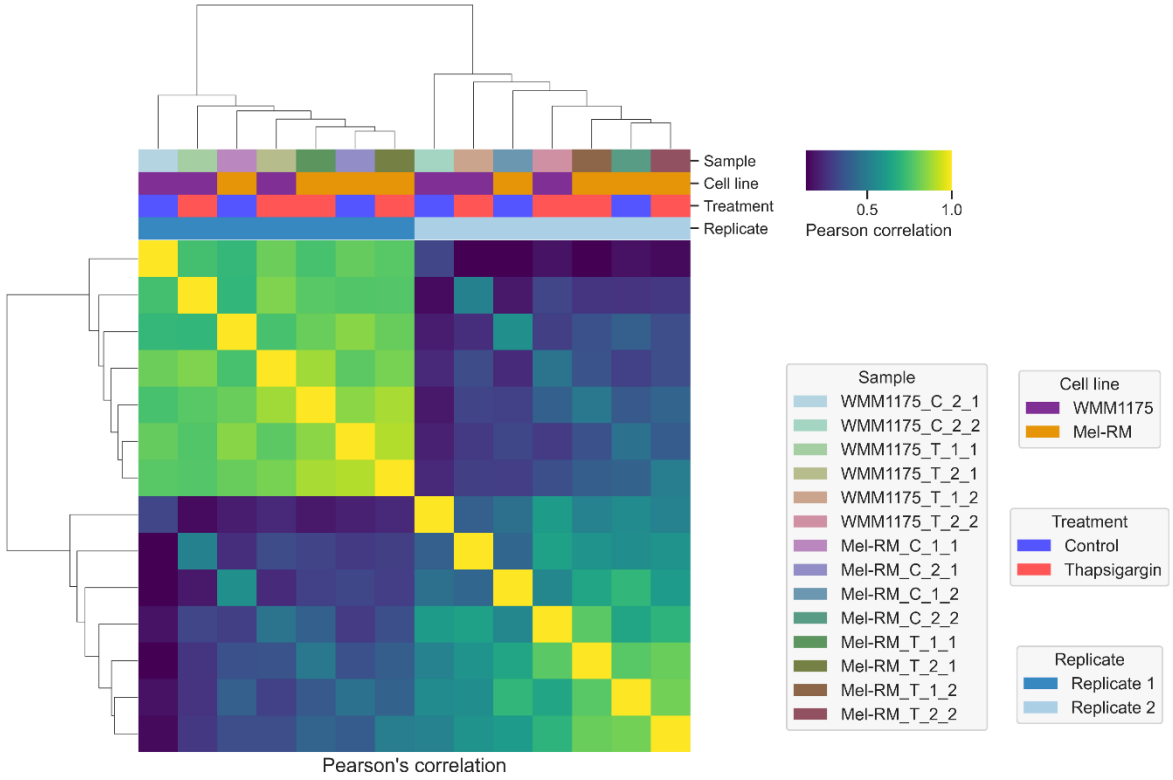

Figure 4-14: Pearson's correlation and hierarchical clustering of melanoma samples analysed by mass spectrometry utilising iTRAQ tags for quantitation. Proteomic quantitative MS data from the iTRAQ analysis of the nuclear, cytosolic and mitochondrial fractions acquired on the QSTAR Elite ESI were combined and the Pearson's correlation was calculated between all melanoma cell lines samples (control and thapsigargin treated for WMM1175 and Mel-RM) based on the entire proteomic data for all subcellular fractions. Unsupervised hierarchical clustering was then performed to visualise the correlation matrix between the samples.

4.3.4 Pathway analysis in melanoma under the UPR

Of the 64 proteins found to be differentially abundant in the two melanoma cell lines with increased UPR activation, changes occur across a broad range of biological functions; cytoskeletal rearrangement, stress responses, transcriptional regulation, metabolism, protein cellular transport, RNA processing, cell adhesion, protein processing, apoptosis, cell signalling, Chromatin structure and the cell cycle (**Figure 4-15**). To further explore the molecular functions modulated by the UPR, pathways analysis was performed to better understand the extensive effects of this stress response and what role it plays in melanoma oncogenesis.

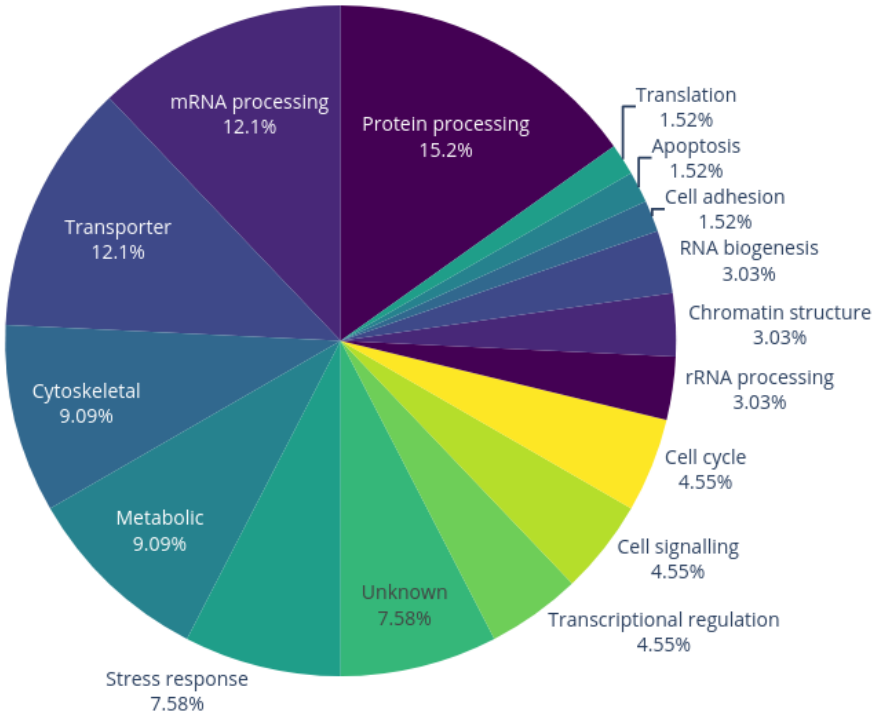

Figure 4-15: Function of UPR differentially abundant proteins. Assigned functional categories from NextProt of proteins found to be differentially abundant with UPR activation in melanoma cell lines WMM1175 and Mel-RM [397].

The 71 proteins found to be differentially abundant with increased UPR activation, 66 of which are unique protein identifications, were input into STRING pathway analysis. The overall protein-protein interaction enrichment score, which is a measure of the probability that the 64 differentially abundant proteins interact at random, was calculated to have a *p*-value = 1.0 e^{-16}. Meaning that the 64 differentially abundant proteins have a high degree of interaction. The top five biological processes associate with the differentially abundant proteins are peptide processing, protein targeting to the ER, protein localisation to the ER, mRNA splicing and protein-containing complex disassembly (**Table 4-3**). The differentially abundant proteins are strongly associated with protein localisation to the ER, most likely the of result of an arm of the UPR that increases the selective import of key chaperones and protein processing machinery into the ER, to increase the protein processing capacity of the cell.

Table 4-3. Pathway analysis of differentially abundant proteins with increased UPR showing the top five biological processes. Pathway analysis was performed by the STRING data repository reporting the gene ontology group for each biological process, the number of proteins identified that are in the biological process, the strength of the association compared to a random set of proteins and the FDR calculated *p*-value using Benjamini–Hochberg procedure [282].

GO-term	Biological process	count in network	Strength	FDR
GO:0006465	Signal peptide processing	3 of 11	1.91	0.0063
GO:0045047	Protein targeting to ER	5 of 110	1.14	0.0188
GO:0070972	Protein localisation to ER	6 of 140	1.11	0.0047
GO:0000398	mRNA splicing, via spliceosome	10 of 294	1.01	0.00025
GO:0032984	Protein-containing complex disassembly	6 of 229	0.9	0.0428

4.4 Discussion

Previous studies from our laboratory and detailed in Chapter 3, highlighted the UPR as an important cellular process in the outcome of AJCC stage III melanoma patients [269]. The work in this chapter explored the role of ER stress in melanoma and mechanisms utilised by the UPR in progression and metastasis. A model system was established to study the UPR in the subcellular compartments of melanoma cell lines using an ER-stress inducing compound, thapsigargin. The aim was to confirm the utility of this cell line model for studying increased UPR in melanoma and then to identify proteins differentially abundant with increased UPR using quantitative MS. The underlying hypothesis was that better characterisation of this complex cellular response in melanoma would increase our understanding of its contribution to neoplastic progression.

4.4.1 Increased UPR in melanoma cell lines

Strong induction of the UPR is observed in the significant differentially abundant proteins identified by MS in the subcellular compartments of the melanoma cell line UPR models (**Table 4-2**). Several critical mediators of the UPR were upregulated with thapsigargin treatment for 48 h as observed both by Western blotting and MS analysis. GRP78 the master UPR regulator was increased an average of 15-fold across the subcellular fractions of the melanoma cell lines. Other UPR regulators detailed in Chapter 1 were also upregulated indicating increased induction of the UPR, including Hypoxia upregulated protein 1 (HYOU1, 13-fold increase) and Endoplasmin (HSP90B1, 4.16-fold increase).

Nucleobindin-1 (NUCB1), a negative regulator of the UPR was down-regulated with thapsigargin treatment. NUCB1 suppresses the UPR via Site-1 protease (S1P) inhibition, thereby preventing cleavage of ATF6 in the Golgi [398]. PC4 and SFRS1-interacting protein (PSIP1) itself was found to be down-regulated in both cell lines. Down-regulation of this stress response modulator allows for the ATF6 arm of the UPR to proceed uninhibited, cleaved ATF6 will translocate to the nucleus where it promotes expression of ER chaperones [127].

Both spliced and unspliced XBP-1 however were shown to be decreased in abundance with western blotting with increased activation of the UPR (**Figure 4-6**). This would indicate that the IRE1 arm of the UPR is not activated, which is one of the two arms of the UPR responsible for relieving cellular stress and returning the cell to homeostasis [140, 141]. As the IRE1 and PERK act to give precise modulation of the UPR in higher eukaryotes [141], the absence of

spliced XBP-1 found here requires further validation followed by functional studies to understand its capacity in cancers cells.

4.4.1.1 ER-stress beyond the ER

Subcellular localisation is one of the main features by which the cell modulates protein function. As technologies improve, particularly in the field of mass spectrometry, the degree to which the cell utilises this compartmentalisation to shift protein function becomes more apparent. From this study, protein shuttling between subcellular compartments is a potential major regulatory mechanism used by the UPR. Additionally, studying subcellular compartments individually gives increased proteome coverage through separation of the more abundant cytosolic proteins from mitochondrial and nuclear proteins.

As discussed in Chapter 1, GRP78 is the master regulator of the UPR, it resides in the ER where it binds to unfolded proteins acting as a protein chaperone as proteins are processed for membrane or extracellular export [1]. When unfolded proteins accumulate beyond the cells resting capacity to re-fold these proteins, GRP78 induces multiple signalling cascades to return the cell to homeostasis. In this study GRP78 was found to be localised not only in the cytosolic fraction, which contains the ER, but also to the nucleus and mitochondria. Upon increased activation of the UPR, GRP78 increased by an average of 1.5-fold in the cytoplasm, 27.8-fold in the nucleus and 17.0-fold in the mitochondria. This localisation was validated in the Western blotting for anti-GRP78 in the subcellular fractions (**Figure 4-5**). This would not be an experimental artefact given both the lack of contamination of cytoplasmic proteins in the nuclear and mitochondrial fractions (**Figure 4-7**) and the large fold-changes observed by MS compared to the cytosolic fractions.

Subcellular shuttling of GRP78 has previously been reported to the plasma membrane, extracellular space, mitochondria and in a limited number of studies to the nucleus. Increased ER-stress has been found to promote the relocalisation of GRP78 to the cell surface in cancer cells but not in normal cells [175, 176, 399]. As such, cell surface GRP78 has been proposed as a chemotherapeutic target that may prove selective for cancer cells [400]. At the cell surface GRP78 promotes proliferation and angiogenesis through its interaction with tumour-associated macrophages and endothelial cells where it upregulates VEGF and activates Akt signalling [197, 401, 402]. However, given that the UPR is consistently activated in normal cells, although at lower levels than in cancer, it is likely that the translocation of GRP78 is also occurring

within normal cells, albeit at lower levels, that has gone undetected. Due to its emerging role in extracellular signalling, examining the membrane proteomes of these treated cells would yield insights into how melanoma cells respond to ER-stress through modulation of their microenvironment and interactions with surrounding cells.

GRP78 also exists in a cytosolic form, arising from alternate splicing of its pre-mRNA, which excludes the ER-localisation signal [195]. Cytosolic-GRP78 (GRP78va) is more abundant in cancerous cells, notably human leukaemia [403]. GRP78va has been shown to modulate the apoptotic arm of the UPR and its increased expression correlates with decreased apoptosis in cells undergoing ER-stress.

GRP78 has been observed in the mitochondria when over-expressed in response to increased ER-stress. Cross-talk between the ER and mitochondria plays a key role in UPR-mediated apoptosis and protein relocalisation is utilised by cells to modulate various apoptotic cascades [404-406]. Mitochondrial-GRP78 (mGRP78) has been shown to play a cytoprotective role mainly through modulation of Ca^{2+} efflux [407]. Increased Ca^{2+} concentrations in the mitochondria results in Cytochrome c release and apoptosis. Given GRP78 functions as a Ca^{2+} binding protein, it has been proposed that mGRP78 protects against apoptosis by sequestering calcium in the mitochondria [406, 408]. Therefore, the presence of GRP78 in the mitochondria of melanoma cells is most probably a cytoprotective mechanism and demonstrates another process by which the UPR promotes tumourigenesis and metastasis. The large increase in mGRP78 observed in this study, 18-fold in WMM1174 and 15-fold in MEL-RM, is evidence of one of the mechanisms by which melanoma prevents the apoptotic pathways of the UPR and exclusively exploit its cytoprotective arms.

Additionally, GRP78 was found upregulated in the nucleus of melanoma cells treated with thapsigargin, 15-fold in WMM1175 and 41-fold in MEL-RM cells. GRP78 has previously been reported to relocalise to the nucleus with UPR induction in a limited number of studies however the precise role of nuclear-GRP78 (nGRP78) is unknown [409-411]. Morris *et al.* found that GRP78 lacking ATPase activity translocated to the nucleus and that overexpression of this cloned GRP78 desensitised cells to apoptosis [411]. However, the mechanism by which GRP78 co-ordinates this shuttling as part of the UPR is unknown. Further studies are required into the mechanisms by which melanoma cells shuttle GRP78 to the nucleus and how it contributes to the beneficial role of the UPR in cancers. Given the large increase of this protein in the nuclear

compartment of melanoma cells undergoing ER-stress the impact of this relocalisation is likely a significant mechanism in melanoma biology.

The mechanisms underpinning the relocalisation of GRP78 are not well known, alternate splicing, protein-complex shuttling and transporter saturation are all proposed mechanisms. For cytosolic-GRP78, alternate splicing has been demonstrated as a mechanism that retains GRP78 in the cytoplasm [403]. However, due to its sequence similarity, ER- and cytosolic GRP78 are indistinguishable from each other via conventional shotgun proteomic techniques carried out in this study. More targeted MS approaches that can elucidate the mechanisms behind GRP78 protein relocalisation, such as Cy-TOF, would be of immense value in studying these protein shuttling events.

Hypoxia up-regulated 1 (HYOU1) also displays similar protein shuttling activity in response to UPR activation. HYOU1 is an ER-stress induced chaperone when localised to the ER but also influences UPR-induced apoptosis [1]. HYOU1 has three predicted translation initiation sites that would give rise to three distinct products [412]. Additionally, HYOU1 has been reported to be highly glycosylated at numerous sites [413]. Either of these mechanisms of protein functional regulation could explain the results in **Figure 4-6**. The five bands of differing molecular weighs identified by Western blotting range from 150- 200 kDa and are only present in melanoma cell with increased ER-stress.

4.4.1.2 UPR, senescence and survival

The capacity of melanoma cells to deal with high levels of ER-stress while managing to abrogate stress-induced apoptosis can be seen in **Figure 4-2**, **Figure 4-3** and **Figure 4-4**. Despite receiving 10 μM thapsigargin for 72 h a sub-population of cells remained viable and even after 216 h of treatment these cells could be revived with media replacement compared to untreated cells (data not shown). The metastatic cell line Mel-RM had less apoptosis compared to the primary WMM1175 line which had a small population of sub-G1 apoptotic cells (**Figure 4-4**). The WMM1175 cells also exhibit a shift in DNA content indicative of polyploid cells arising from senescence. Further evidence of growth arrest and potentially senescence is seen in the 3.33-fold and 2.12-fold decrease in Cyclin-dependant kinase 1 (CDK1) in WMM1175 and MEL-RM cells, respectively. CDK1, is a member of the cyclin-dependant kinase family of cell cycle regulators that mediate progression through the cell cycle. CDK1 was found to be up-regulated at the transcriptomic level in metastatic compared to primary melanomas [414, 415]. Additionally, in mice xenografts increased levels of CDK1 correlated with increased

tumourigenesis and tumour growth [416, 417]. Therefore, the decrease of CDK1 with increased UPR activation found here, demonstrates another mechanism by which the UPR could contribute to melanoma progression.

Several conditions to which cancerous cells are often exposed such as hypoxia and chemotherapeutic agents can induce cellular senescence. Senescence is characterised by growth arrest, resistance to apoptotic signalling, metabolic dysregulation, persistent DNA damage and elevated secretion of pro-inflammatory and growth factors [418]. However, tumours have been shown to be able to restore the cell from a senescent phenotype, as such senescence has been found to promote proliferation and tumour growth in several cancers [417, 419, 420] and is associated with increased invasive potential [421, 422]. Additionally, the Senescence-associated secretory phenotype (SASP) has been shown to secrete transforming growth factor beta (TGF-β) and interleukin-6 (IL-6) [423-426], both of which have an immunosuppressive role in tumourigenesis.

The UPR is intrinsically linked with activation of cellular senescence, particularly in cancers. Although, whether it is a driver of the senescent phenotype or a consequence remains unknown [427]. These findings show the potential ability of the UPR to modulate cell cycle progression in melanoma through the modulation of CDK1, a previously unreported mechanism of the UPR. This would allow the UPR to assist melanoma undergoing insult from chemotherapies or stress associated with metastasis. Additionally, activation of senescence in cancers has been hypothesised as a novel therapeutic strategy [428]. Therefore, the ability of the UPR to decrease levels of CDK1 as reported here and induce cellular senescence makes the UPR an attractive target for this therapeutic approach. Furthermore, given the current standard treatment for metastatic melanoma is anti-PD1 immunotherapy, combinatorial therapies targeting the UPR could potentially see improvements to patient outcomes.

4.4.2 Cellular pathways altered with UPR activation

Of the 3,490 proteins identified by iTRAQ labelled mass spectrometry, 561 were differentially abundant with increased UPR. Of these, 71 proteins were common between cell lines, indicating that 2% of the detected proteome was significantly and consistently modulated with thapsigargin treatment and UPR activation in melanoma cells. The considerable heterogeneity exhibited by cancers can be seen in the proteins that were differentially expressed exclusively in a one cell line with increased UPR activation; 302 proteins in WMM1175 and

187 proteins in Mel-RM. The majority of proteins were down-regulated, no doubt many of which are a consequence of the suppression of global protein synthesis, a homeostatic arm of the UPR. However, this does not diminish the effect these changes have on the cell or their contribution to the altered oncogenic capacity of the cancer.

However, 132 proteins had the same trend in differential abundance with increased UPR but did not meet the cut-off for differential significance. **Figure 4-8** shows the extent of changes in the UPR regulated proteome, however the 1.5-fold change cut-off was applied to ensure against false identification due to the relative insensitivity of iTRAQ methods coupled with the older instrumentation. Newer mass spectrometry technology would allow for more relaxed thresholding of protein fold changes.

Of the differentially abundant proteins common to the melanoma cell lines, the functions of these proteins are related to cellular processes crucial for oncogenesis and metastasis, including altered metabolism, modulation of the cell cycle, proliferation, survival and apoptosis, cellular adhesion and modulating global RNA and proteins synthesis.

4.4.2.1 Metabolic dysfunction and the UPR

An altered metabolic profiles is one of the major changes exhibited by cancerous cells and is a hallmark of cancer described by Hanhan and Weinberg in 2000 [429]. In order to meet the proliferative burden associated with neoplastic transformation, cells must alter their metabolism to meets the increased energy requirements of continuous proliferation. The atypical metabolic profile of cancers was first observed in 1930 by Warburg in which cancer cells, even in aerobic conditions preferential perform glycolysis over oxidative phosphorylation in the mitochondria [430]. The reason behind this seemingly anachronistic preference of cancer cells for ‘aerobic glycolysis’, given it is 18-times less efficient in energy production, is still poorly understood.

Seven proteins directly involved in metabolism were found to be differentially abundant in thapsigargin treated melanoma cells. Specifically, NAMPT, MAT2A, CISD2, EMC7 and EMC2 were found to be up-regulated. Increased levels of NAMPT would have profound cellular effects, as it is the rate limiting step in NAD^+ biosynthesis, an important co-factor in numerous cellular and metabolic processes [431-433]. This up-regulation would significantly increase the metabolic capacity of cancerous cells, allowing them to meet the energy requirements of neoplastic proliferation that otherwise would slow tumour growth.

4.4.2.2 BRAF and the UPR

The UPR and mutant BRAF have been found to reciprocally regulate each other's signalling pathways, which has major implication for melanoma where both of these pathways are up-regulated and have crucial roles in tumourigenesis. Constitutive activation of RAS\RAF\MEK\ERK brought on by BRAF mutations found in 50% of melanoma, promotes increased protein synthesis by perpetuating pro-survival and pro-proliferative pathways [434, 435]. With the increased protein processing requirements, ER-stress results and therefore, induction of the UPR. However, additional regulation also occurs by which members of this pathway can directly regulate UPR activity. In *Caenorhabditis elegans* Rho GTPase homologs of Ras were shown to mediate UPR induction via GRP78 transcription regulation [436]. In triple negative breast cancer mice models, MEK inhibition prevented GRP78 up-regulation upon ER-stress [437], showing that MEK can influence the levels of this master UPR regulator in the absence of ER-stress. Paradoxically, inhibition of the MEK/ERK pathway, which would reduce the protein processing burden in the cell, actually sensitises cells to UPR-induced apoptosis [438], showing MEK/ERK are couped to the recovery arms of the UPR. Additionally, continuous activation of IRE1 and ATF6 as part of the UPR, causes a reciprocal activation of MEK/ERK [166]. Importantly, cell death with MEK/ERK inhibition was induced via direct caspace-4 activation by the UPR as outlined in Chapter 1. This presents an interesting chemotherapeutic strategy which would bypass most classical apoptotic cascades to which melanoma are notoriously resistant. The protective capacity of activated MEK/ERK against UPR-induced apoptosis can be seen in the present study, with cell line WMM1175 bearing a V600E BRAF mutation while MEL-RM is wildtype for BRAF. As shown by Sub-G1 DNA assay neither melanoma cell line exhibited a significant increase in apoptosis when treated with thapsigargin. However, mutant BRAF bearing cells show altered cell cycle progression with increased UPR and show a small population of cells undergo apoptosis compared to the wildtype BRAF Mel-RM (**Figure 4-4**). Interesting, clustering analysis showed WT BRAF cells treated with thapsigargin had proteome similarities to the mutant BRAF control cells. These findings are consistent with the literature in which MEK/ERK alone can result in increased induction of the UPR. Furthermore, this provides some anecdotal evidence that MEK/ERK has crosstalk with cytoprotective portions of the UPR. Further study of the reciprocal regulation of the UPR and RAS/RAF/MEK/ERK pathways are explored in Chapter 6.

4.5 Conclusions

Here we investigated the wide actions the UPR exhibits in subcellular compartments of two melanoma cell lines using iTRAQ quantitation and contribute to the understanding of the role of the UPR within both normal cellular homeostasis, as well as its contribution to cancer progression and metastasis. In addition to direct stress response mechanism the pathways modulated by the UPR include, major cytoskeletal rearrangements, increased metabolic potential, altered mRNA and protein processing capacity, alterations to cell signalling pathways and apoptotic proteins.

The findings of this study highlight the UPR as a major drug target for the treatment of cancers and demonstrates several synergistic and combinatorial therapeutic strategies that could be exploited for the treatment of melanoma. Such as the combination of UPR inhibitors and BRAF/MEK inhibitions due to the reciprocal regulation known to exist between the MEK/ERK pathway and numerous UPR modulators.

Chapter 5: SRM validation of UPR-associated proteins in melanoma cell line models

5.1 Introduction

The broad response induced by ER-stress and activation of the UPR, makes quantifying this dynamic cellular process challenging. As reported in the previous chapter, the response induced by UPR activation varied greatly in subcellular fractions between two melanoma cell lines, with only 13% of the proteins identified to be differentially abundant with increased UPR common between the two cell lines. The varied downstream molecular changes of the UPR coupled with the vast heterogeneity seen among cancers makes finding a novel drug target or biomarker difficult. Therefore, the aim of the study in this Chapter was to validate key findings from Chapter 4 using orthogonal techniques on a larger panel of four melanoma cell lines whole cell lysates rather than subcellular fractions, in order to robustly identify proteins which are integral to this stress response in melanoma.

Firstly, a subset of proteins found to have significant biological implications in melanoma and the UPR that were identified as differentially abundant with increased UPR activation were further studied with fluorescence microscopy and validated with Western blotting. The proteins selected for further analysis were PGRMC1 (progesterone receptor membrane component 1), SLC3A2 (4F2 cell surface antigen heavy chain) and a member of the SWI/SNF chromatin remodelling family, SMARCC1. A major variable in melanoma prognosis is gender, with females having significantly thinner lesions, reduced dissemination and a 15% better 5-year survival compared to males [439, 440]. To explore the possible link between sex hormones and the UPR, PGRMC1 was further examined. SLC3A2 has been found upregulated in several cancer types and has been shown to play a role in anti-tumoural immunity [441-443]. The SWI/SNF family of chromatin remodelling complexes has been established as a major class of oncogenic mutations in melanoma, with 50% of patients found to have an inactivation mutation in one or more of its family members [444, 445]. As such, confirmation of the link between the UPR and the chromatin remodelling complex was further explored.

Then, key proteins found to be differentially abundant with increased UPR activation in subcellular fractions utilising iTRAQ quantitation from Chapter 4 (**Table 4-2**) were validated by selected reaction monitoring (SRM) in whole cells lysates. SRM assays, as discussed in Chapter 3, have greater specificity and more accurate quantitation than the shotgun proteomic approaches used for initial discovery. In order to identify UPR-associated proteins that can be targeted in a broad range of patients, orthogonal validation of the Chapter 4 iTRAQ results was performed in a broader melanoma cell line panel treated with thapsigargin, comprising four melanoma cell lines covering both primary and metastatic phenotypes as well as mutant and

wild-type BRAF (WMM1175, Mel-RM, SK-Mel-28 and WMM1125, **Table 2-1**). Forty-three proteins were then selected for validation with SRM from the differentially abundant proteins discovered by iTRAQ in Chapter 4. Proteins were selected for further analysis due to their biological importance in melanoma and association with the UPR. From the SRM analysis, eight proteins were identified as being significantly differentially abundant across all four melanoma cell lines when the UPR was increased with thapsigargin treatment. The eight proteins include six proteins with increased abundance with UPR activation; Hypoxia up-regulated protein 1 (HYOU1), Nicotinamide phosphoribosyltransferase (NAMPT), Protein disulfide-isomerase A4 (PDIA4), 4F2 cell-surface antigen heavy chain (SLC3A2), Membrane-associated progesterone receptor component 2 (PGRMC2) and Tryptophan-tRNA ligase (WARS). While two proteins were down-regulated with increased UPR; SWI/SNF complex subunit SMARCA5 (SMRCA5) and SUN domain-containing protein 2 (SUN2). These findings demonstrate that the UPR regulates a diverse set of pathways and mechanisms within melanoma. Due to their biological functions, modulation of these UPR-associated proteins could contribute to melanomas neoplastic progression and increase its metastatic potential. Furthermore, the eight UPR-associated proteins identified here are consistently regulated in different melanoma phenotypes with increased UPR activation, highlighting their potential as novel drug targets or markers of progression.

5.2 Methods

Detailed protocols are described below or can be found in Chapter 2: Materials and Methods.

5.2.1 Melanoma cell lines

Melanoma cell lines were grown and harvested as described in Chapter 2 and **Table 2-1**. Cell pellets were solublised in 0.1% (w/v) SDS with probe tip sonication for membrane and DNA disruption. Cells were then treated with Benzonase (1 Unit /20 x 10^6 cells) then protein lysates stored at -80ºC.

5.2.2 Protein isolation and digestion

Proteins were cleaned with chloroform/methanol extraction as described in Chapter 2.4.2. Tryptic digestion with SCX and HLB peptide clean-up was performed as described in Chapter 2.4.3.

5.2.3 Fluorescence microscopy

Fluorescence microscopy was performed on the melanoma cell lines WMM1175 and Mel-RM as describe in Chapter 2. PGRMC1 and SLC3A2 were examined to monitor changes in subcellular localisation with increased UPR activation.

5.2.4 Western blotting

Western blotting was carried out as described in Chapter 2.5. The differential abundance of PGRMC1 and SMARCC1 from the Chapter 4 was validated with Western blotting in the melanoma cell lines WMM1175 and Mel-RM. Details on the antibodies, buffers and incubation times for each antibody can be found in **Supplementary Table S2-1.**

5.2.5 SRM analysis

Target proteins (43) were selected for SRM validation from the 62 proteins found to be differentially abundant with UPR activation in subcellular fractions in Chapter 4 (**Table 4-2**). Proteins were selected for validation based on fold-change values, *p*-values, biological significance and the presence of proteotypic peptides conforming to the requirements of SRM

analysis. Detailed methods can be found in Chapter 2.2.3. Briefly, SRM assays were carried out on the SCIEX 5500 QTRAP run with a nano-flow LC (300 nL/min). SRM assays were schedule and collision energies optimised per precursor. Samples were spiked with synthetic ^{13}C- and ^{15}N-labelled synthetic peptides from JPT technologies at concentrations balanced to the endogenous peptide levels. Samples (0.5 µg) were loaded onto a 150mm C18 separation column via a TRAP column. Samples were acquired in duplicate in positive ion, scheduled SRM mode (detection time window: 240 s; target scan time: 1.5 s) with a total acquisition time of 30 min and 25 min linear gradient. The list of monitored transitions can be found in the Supplementary material (**Supplementary Table S5-1**). QTRAP performance was monitored with a calibration curve of increasing light:heavy peptide ratio and bovine serum albumin standard.

5.2.6 SRM data analysis

Data files (.wiff) were imported into Skyline and manually inspected for correctness. Skyline criteria were set to a mass tolerance of 0.5 Da for monoisotopic *y*- and *b*-ions generated by tryptic digestion with zero missed cleavages. Peaks were searched against a Human mass spectral database (National Institute of Standards and Technology (NIST), human consensus library with CID fragmentation, detected on a QTOF mass analyser, downloaded 2015-05-13). Total peak area ratios (ratios of the sum of three areas corresponding to three transitions) of light (L: endogenous peptides) to heavy (H: isotopically labelled peptides) were analysed by student *t*-test without normalisation.

5.3 Results

Forty-three proteins found to be differentially abundant with increased activation of the UPR utilising iTRAQ quantitation in subcellular fractions in Chapter 4, were selected for validation in whole cell lysates from four melanoma cell line with SRM. Select proteins were also validated with either Western blotting or fluorescence.

5.3.1 Decrease in SMARCC1 with the UPR

SMARCC1 was found to be down-regulated in both WMM1175 (decrease 2.35-fold, *p*-value 0.008) and Mel-RM (decrease 2.2-fold, *p*-value 0.007) cell lines with iTRAQ analysis. Due the emerging importance of the SWI/SNF chromatin remodelling family in melanoma progression, this protein was selected for validation with Western blotting [444, 446]. SMARCC1 was confirmed to be decreased in abundance with thapsigargin induced ER-stress and increased UPR activation (**Figure 5-1**).

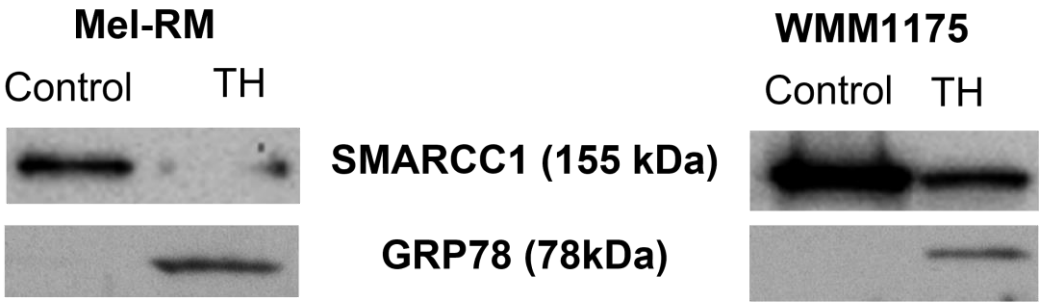

Figure 5-1. Validation of decreased SMARCC1 abundance with increased UPR activation in melanoma cell lines. Western blotting was performed with biological triplicates on the melanoma cell lines WMM1175 and Mel-RM treated with thapsigargin (TH, 1 µM, 48 h). Samples (10 µg) were loaded onto a 12% polyacrylamide gel, then eletrophoretically transferred to a nitrocellulose membrane and probed for SMARCC1 and GRP78. Membranes were incubated with primary anti-GRP78 (1:1,000) 4ºC overnight, followed by anti-mouse secondary antibody (1:10,000) for 1 h at room temperature. Stripped membranes were incubated with primary anti-SMARCC1 (1:1,000) 4ºC overnight, followed by anti-mouse secondary antibody (1:10,000) for 1 h at room temperature. Binding of the secondary antibody conjugated to peroxidase was then visualised with ECL reagent. Even sample loading was assessed with Sypro Ruby total proteins stain. The figure is representative of two separate experiments.

5.3.2 Decrease of PGRMC1 with increased UPR

Due to the established link between gender and the UPR, PGRMC1 was examined through fluorescence microscopy and Western blotting in melanoma cell lines treated with thapsigargin. PGRMC1 was found to decrease 2.8-fold with UPR activation (**Table 4-2**). The

decrease in PGRMC1 abundance with increased activation of the UPR was confirmed with Western blotting of melanoma cell lines treated with 1 μM thapsigargin for 48 h (**Figure 5-2**).

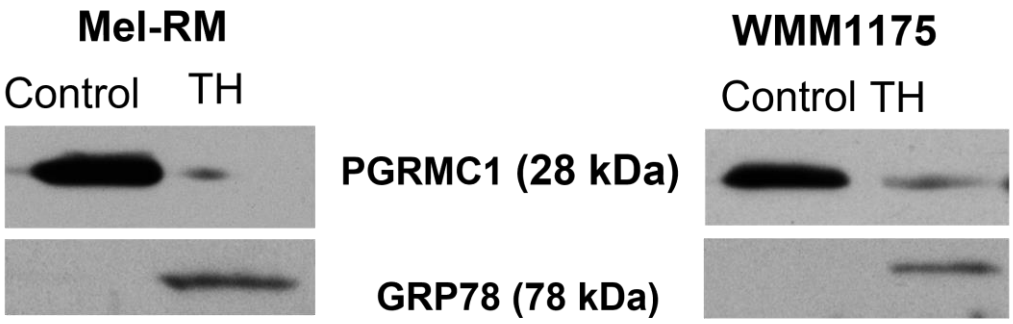

Figure 5-2. PGRMC1 decreases in abundance in melanoma cell lines with increased UPR. Western blot for PGRMC1 and GRP78 in Mel-RM and WMM1175 melanoma cell lines treated with TH (1 μM, 48 h) with biological triplicates. Samples (10 μg) were loaded onto a 12% polyacrylamide gel, eletrophoretically transferred to a nitrocellulose membrane and probed for PGRMC1 and GRP78. Membranes were incubated with primary anti-GRP78 (1:1,000) 4ºC overnight, followed by anti-mouse secondary antibody (1:10,000) for 1 h at room temperature. Stripped membranes were incubated with primary anti-PGRMC1 (1:1,000) for 1 h at room temperature, followed by anti-rabbit secondary antibody (1:5,000) for 1 h at room temperature. Binding of the secondary antibody conjugated to peroxidase was then visualised with ECL reagent. Even sample loading was assessed with Sypro Ruby total proteins stain. The figure is representative of two separate experiments.

Due the major role of subcellular shuttling in modulating cellular processes and potentially the UPR, fluorescence microscopy was performed on the melanoma cell lines with increased UPR induced by thapsigargin. A decrease in PGRMC1 abundance can be observed with fluorescence microscopy upon increased UPR activation (**Figure 5-3**). Additionally, a change in the subcellular localisation of PGRMC1 from widely diffused throughout the cytoplasm to discrete locations within the cell was observed with increased UPR.

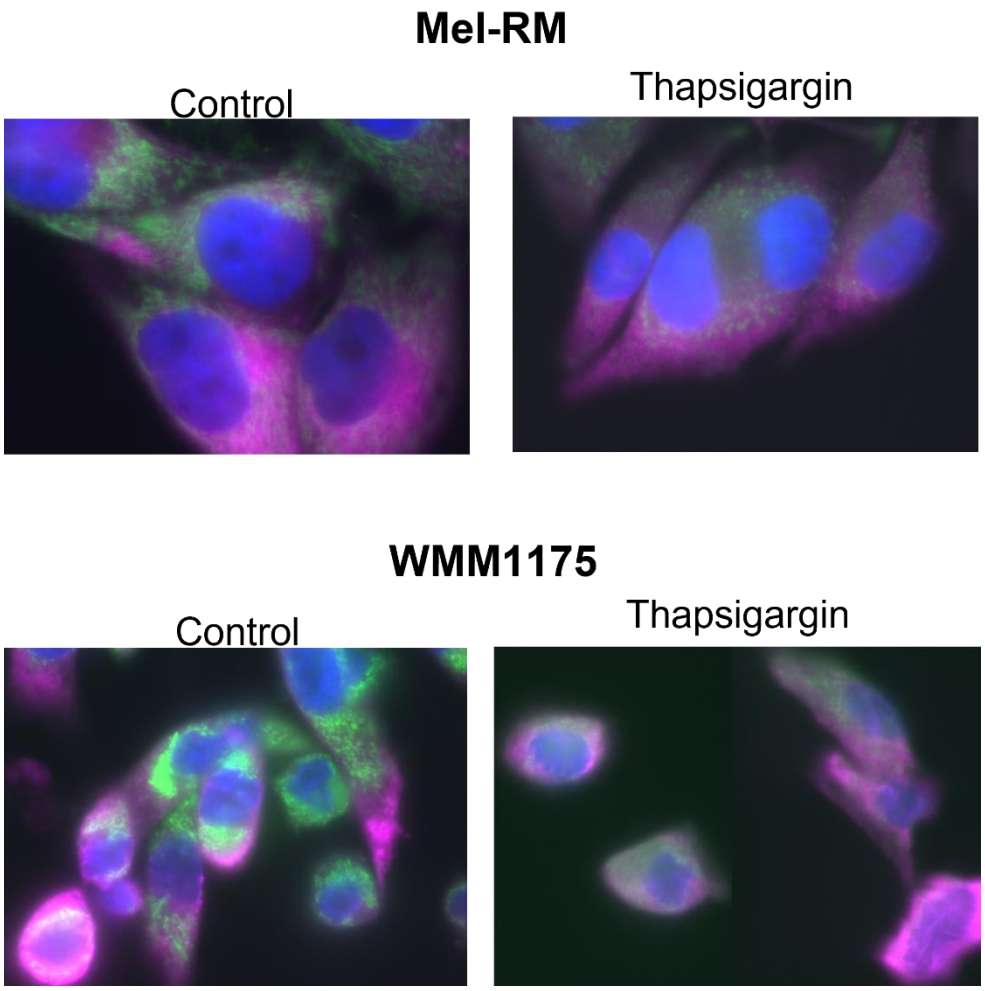

Figure 5-3. PGRMC1 decreases in abundance in melanoma cell lines with increased UPR. Fluorescence microscopy of PGRMC1 in Mel-RM and WMM1175 melanoma cell lines treated with thapsigargin (1 μM, 48 h) showing nucleus (blue), SDHA-mitochondria (purple) and PGRMC1 (green). Images were taken at 100x magnification and are representative of biological replicates (n=3).

5.3.3 Increase cell surface expression of SLC3A2 with increased UPR

4F2 cell surface antigen (SLC3A2) was increased 3.16-fold in melanoma cells with increased UPR in Chapter 4 (**Table 4-2**). Melanoma cells treated with thapsigargin when examined by fluorescence microscopy, showed an increase of SLC3A2 at the cell surface with increased UPR (**Figure 5-4**). The increase in SLC3A2 (shown red) was most evident at the adherent surface of the melanoma cells shown in the lower panel. Importantly, SLC3A2 can be seen strongly localised to membrane projecting filaments in the melanoma cells treated with thapsigargin.

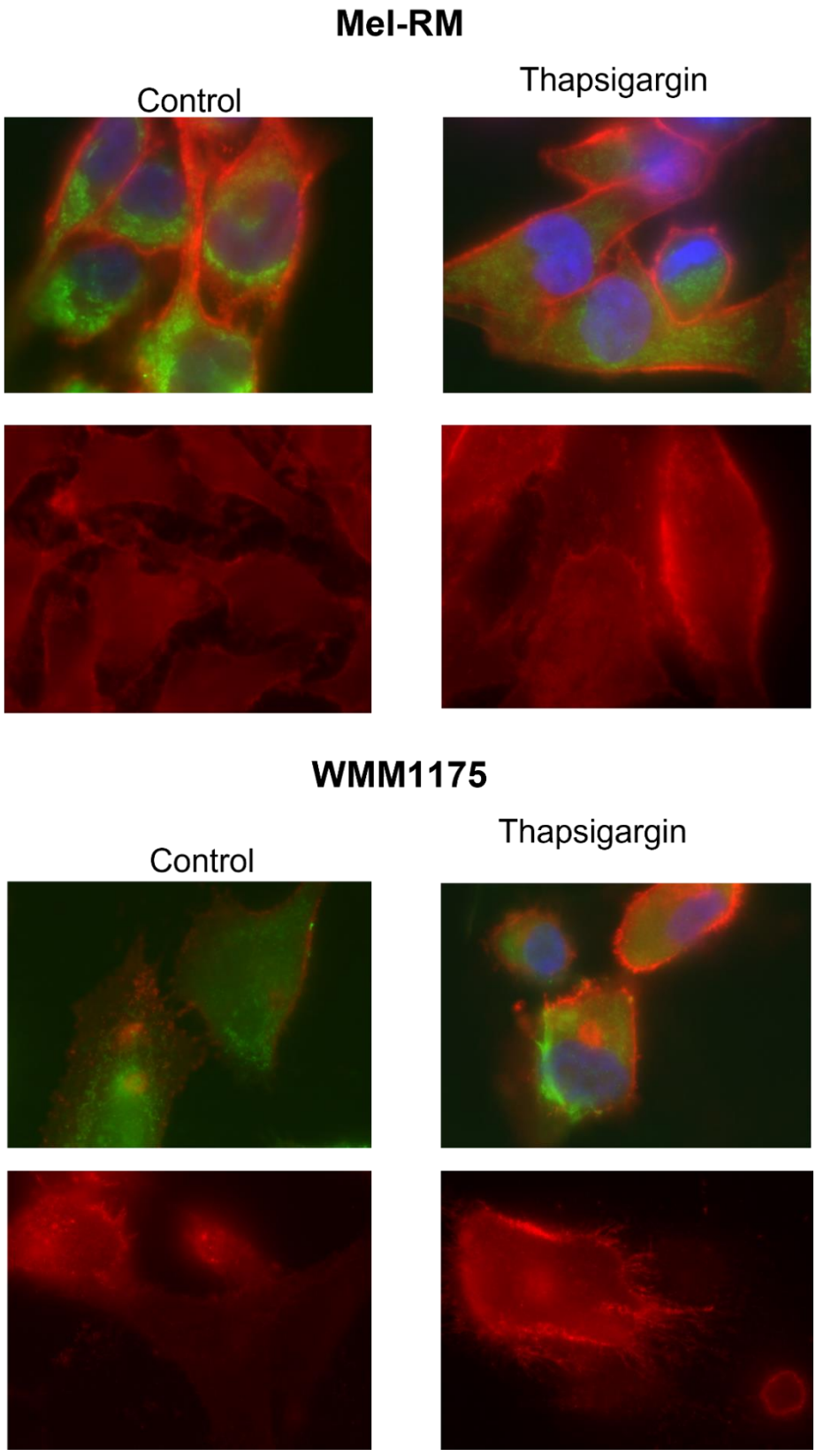

Figure 5-4. SLC3A2 cell surface antigen increases in abundance upon UPR. Fluorescence microscopy of Mel-RM and WMM1175 melanoma cell lines treated with thapsigargin (1 μM, 48 h) showing nucleus (blue), SDHB-mitochondria (green) and SLC3A2 (red). Upper panels show a cellular cross-section, lower panel show the adherent membrane plane at the culture plate surface. Images were taken at 100x magnification and are representative of biological replicates (n=3).

5.3.4 Selected Reaction Monitoring validation of iTRAQ results

Orthogonal validation of the Chapter 4 iTRAQ results in subcellular fractions was performed utilising SRM due to the increased selectivity and accuracy of this method. Of the 66 unique proteins (71 proteins differentially abundant in the subcellular fractions) found to be modulated in melanoma cell lines with increased activation of the UPR (**Table 4-2** and **Figure 4-8**), 43 were selected for validation in four melanoma cell lines, WMM1175, Mel-RM, SK-Mel-28 and WMM1125. The 43 targets were selected based on fold-change values, biological significance and suitability of candidate peptides for SRM requirements such as proteotypic peptides.

Utilising SRM, the 43 proteins were quantified in whole cell lysates of four melanoma cell lines treated with thapsigargin (1 µM, 48 h). To identify proteins that were consistently modulated in response to increased UPR activation across different melanoma phenotypes, proteins were considered significant if they adhered to a p-value <0.05 and fold-change > 1.5 in all four cells lines. All proteins were quantified using three peptides per protein except PDIA4 which utilised two peptides (**Supplementary Table S5-1**).

Eight proteins were found to be significantly differentially abundant in all four melanoma cell lines with increased UPR activation (**Figure 5-5** and **Table 5-1**). Six proteins showed increased abundance with UPR activation: Hypoxia up-regulated protein 1 (HYOU1), Nicotinamide phosphoribosyltransferase (NAMPT), Protein disulfide-isomerase A4 (PDIA4), 4F2 cell-surface antigen heavy chain (SLC3A2), Membrane-associated progesterone receptor component 2 (PGRMC2) and Tryptophan-tRNA ligase (WARS). While two proteins were down-regulated with increased UPR: SWI/SNF complex subunit SMARCA5 (SMRCA5) and SUN domain-containing protein 2 (SUN2). While an additional protein SWI/SNF complex subunit SMARCC2 (SMRCC2), was down-regulated in only one cell line but with important biological implications. The correlation between the differential abundance of the eight proteins as measured by iTRAQ compared to SRM was relatively good, with an average Pearson's correlation >0.85 for the same cell line (**Supplementary Figure S5-1**).

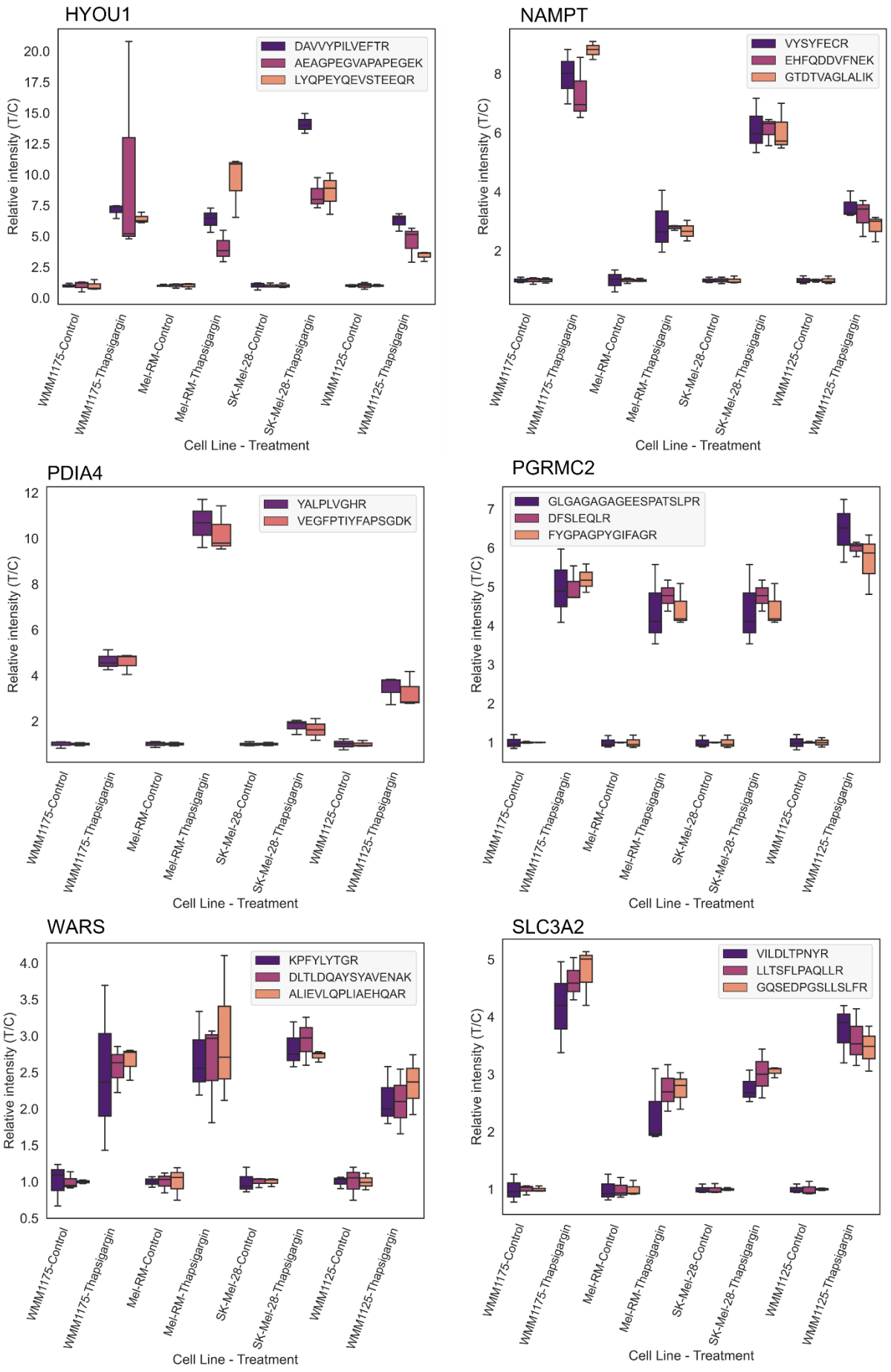
HYOU1
DAVVYPILVEFTR
AEAGPEGVAPAPEGEK
LYQPEYQEVSTEEQR
NAMPT
VYSYFECR
EHFQDDVFNEK
GTDTVAGLALIK
PDIA4
YALPLVGHR
VEGFPTIYFAPSGDK
PGRMC2
GLGAGAGAGEESPATSLPR
DFSLEQLR
FYGPAGPYGIFAGR
WARS
KPFYLYTGR
DLTLDQAYSYAVENAK
ALIEVLQPLIAEHQAR
SLC3A2
VILDLTPNYR
LLTSFLPAQLLR
GQSEDPGSLLSLFR
Relative intensity (T/C)
WMM1175-Control
WMM1175-Thapsigargin
Mel-RM-Control
Mel-RM-Thapsigargin
SK-Mel-28-Control
SK-Mel-28-Thapsigargin
WMM1125-Control
WMM1125-Thapsigargin
Cell Line - Treatment

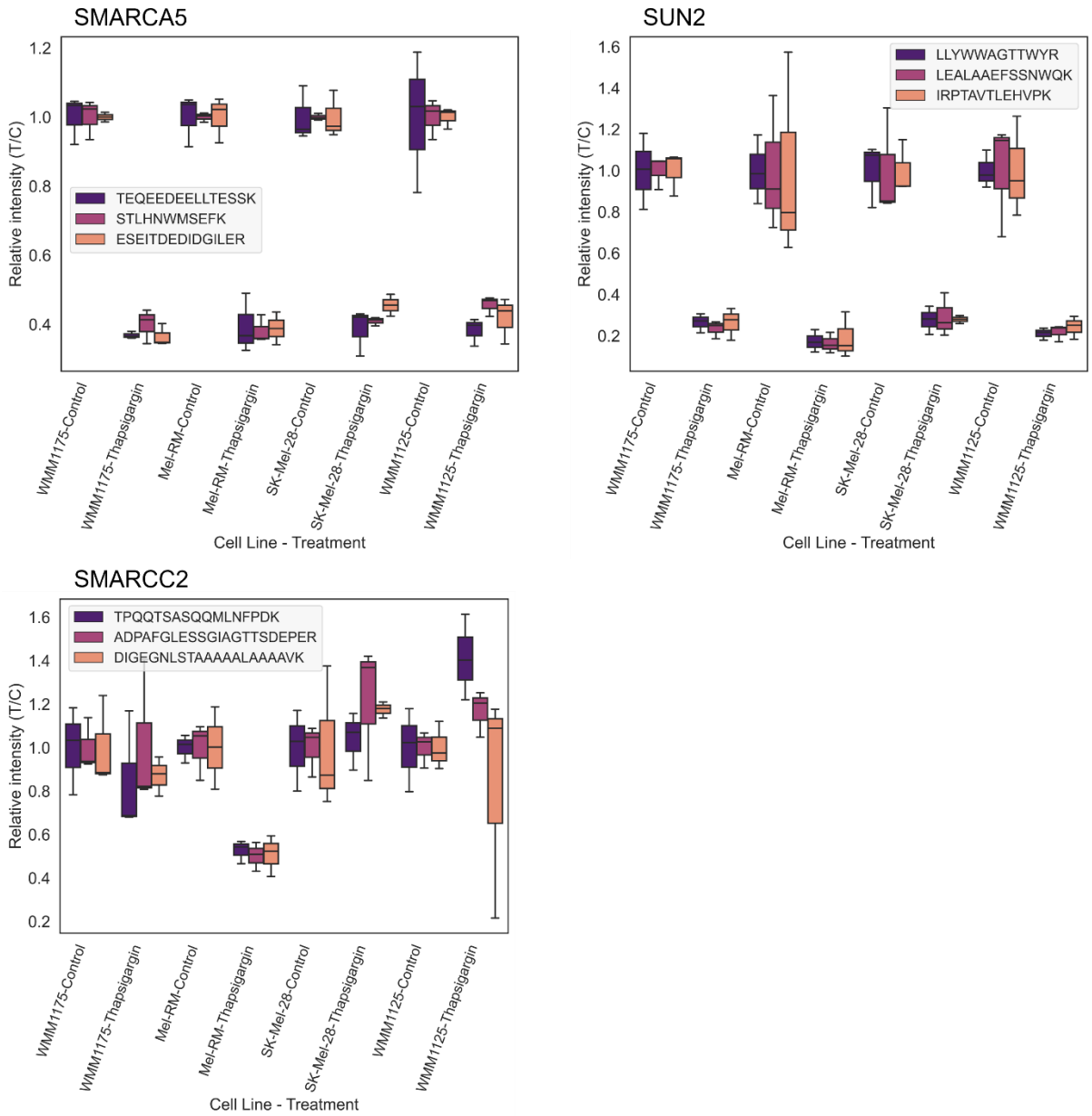

Figure 5-5. SRM validation of peptide quantitation for proteins differentially abundant with increased UPR activation in melanoma cell lines. Quantitation of peptide targets by SRM in four melanoma cell lines WMM1175, Mel-RM, SK-Mel-28 and WMM1125 treated with thapsigargin (1 µM, 48 h). Peptides had significant differential abundance (*p*-value <0.05) in all cell lines excepting for SMRCC2. The data shows relative intensity for each of the three (2 for PDIA4) proteotypic peptides used for quantitation. Horizontal lines represent the median peptide abundance and bars represent 95% confidence intervals per peptide with n=3.

Table 5-1. Eight proteins validated by SRM to be differentially abundant with increased UPR activation in four melanoma cell lines. Melanoma cell lines, WMM1175, Mel-RM, SK-Mel-28 and WMM1125, were analysed by SRM. Protein significance was determined as *p*-value <0.05 for individual peptides quantitation with biological triplicate.

Accession number	Gene name	Protein name	Major function	Average fold-change (T/C)	*p*-value
E9PL22	HYOU1	Hypoxia up-regulated protein 1	Stress response	7.36	0.005
P43490	NAMPT	Nicotinamide phosphoribosyltransferase	Metabolic	5.02	0.011
P13667	PDIA4	Protein disulfide-isomerase A4	Protein processing	5.04	0.027
O15173	PGRMC2	Membrane-associated progesterone receptor component 2	Metabolic	5.05	0.008
P23381	WARS	Tryptophan-tRNA ligase	Angiogenesis	2.59	0.027
J3KPF3	SLC3A2	4F2-cell surface antigen heavy chain	Amino acid transporter	3.42	0.009
O60264	SMARCA5	SWI/SNF complex subunit SMARCA5	Transcriptional regulation	-2.50	0.004
Q9UH99	SUN2	SUN domain-containing protein 2	Cytoskeletal	-4.27	0.018

The function of the eight proteins and their known roles in cancer were explored. As summarised in **Table 5-2** the eight UPR-associated proteins found to be differential in the whole cell lysates of the 4 melanoma cell line models of UPR are implicated in numerous roles related to cancer progression and metastasis including; increased metabolic capacity, increased invasive potential, inhibition of apoptosis and promoting cell cycle progression, inaction of the immune response and drug resistance.

Table 5-2. Protein function and known role in cancer of the eight proteins found to be differentially abundant with increased UPR activation in 4 melanoma cell lines using SRM quantitation. Eight proteins found to be significantly differentially abundant in all 4 melanoma cells lines were investigated for their known role in tumour biology. The protein functions are summarised below and discussed in detail in Section 5.4 of this Chapter.

Gene name	Abundance with UPR	Protein Function	Correlation of protein abundance with role in cancers
HYOU1	Increased	• Chaperone protein • Stress response	• Positive - Increased metabolism • Positive - Increased migratory potential
NAMPT	Increased	• Metabolism	• Positive - Increased metabolism
PDIA4	Increased	• Chaperone protein • Immune presentation	• Positive - Inhibiting apoptosis • Positive - Increased DNA repair
PGRMC2	Increased	• Steroid receptor • Signal transduction	• Positive - Drug resistance • Positive - Increased tumour progression
WARS	Increased	• Protein translation	• Positive - Increased tumour progression • Positive - Increased angiogenesis • Positive - Increased tumour progression • Positive - Increased immune activation
SLC3A2	Increased	• Protein translation • Signal transduction • Amino acid transporter	• Positive - Increased tumour progression • Positive - Increased migratory potential • Positive - Decreased immune activation
SMARCA5	Decreased	• Chromatin remodeling	• Negative - Increased tumorigenesis
SUN2	Decreased	• Cellular structure	• Negative - Increased tumour progression • Negative - Increased tumorigenesis • Negative - Increased metabolism

5.4 Discussion

Forty-three of the 66 proteins found to be differentially abundant (1.5-fold change, *p*-value <0.05) with increased activation of the UPR in melanoma cell lines treated with thapsigargin discovered in Chapter 4 with iTRAQ analysis were validated in whole cell lysates from four melanoma cell lines utilising SRM. Validation was performed with various proteomic techniques; Western blotting, fluorescence microscopy and SRM mass spectrometry. The analysis was expanded from two to four cell lines, to identify proteins that are consistently differential across a range of melanoma phenotypes and thus are likely to represent core modulators of the UPR. Identification of these core modulators gives broader utility of these proteins as potential biomarkers and drug targets for this extremely heterogenous disease. Additionally, examining the functions and known roles of these proteins in cancer (**Table 5-2**), collectively contributes to our understanding of how the UPR promotes melanoma progression.

In the larger melanoma cell line panel, the abundance of eight proteins were validated to be differentially abundant with increased ER-stress and activation of the UPR in all four cell lines; Hypoxia up-regulated protein 1 (HYOU1), Nicotinamide phosphoribosyltransferase (NAMPT), Protein disulfide-isomerase A4 (PDIA4), 4F2 cell-surface antigen heavy chain (SLC3A2), Membrane-associated progesterone receptor component 2 (PGRMC2) and Tryptophan-tRNA ligase (WARS). While two proteins were down-regulated with increased UPR; SWI/SNF complex subunit SMARCA5 (SMRCA5) and SUN domain-containing protein 2 (SUN2).

5.4.1 Validation of UPR-associated differentially abundant proteins

5.4.1.1 HYOU1

Hypoxia up-regulated protein 1, also known as ORP150, is a member of the HSP70 family of heat shock proteins involved in protein folding in the ER and maintenance of cellular homeostasis. HYOU1 was validated here to be up-regulated in cell lines models of UPR activation an average of 7.36-fold, correlating to its increased abundance in both cytosolic and nuclear fractions discovered with iTRAQ in Chapter 4. HYOU1 has been found to be upregulated in several cancers including prostate carcinoma [447], nasopharyngeal carcinoma [448], ovarian cancer [449], Kaposi's sarcoma [450], thyroid cancer [451] and breast cancer [452]. The over-expression of HYOU1 in these cancers is associated with increased progression with the mechanisms underpinning this association to carcinogenesis being

modulation of major oncogenic cell signalling pathways, altered metabolism, cytoprotection and immunodeficiency.

HYOU1 has been shown to alter metabolic capacity in cancers by stabilising LDHB mRNA, resulting in increased LDHB abundance and therefore increased glycolysis [451]. Interestingly, as discussed in Chapter 3, LDH is prognostic biomarker in the serum of metastatic melanoma patients. However, it's utility as a reliable prognostic biomarker is questionable, not only as increased LDH serum levels are present in many other disease states, but also because it is not consistently predictive across patients [453]. These findings present a potential alternative prognostic biomarker utilising the existing LDH biomarker combined with HYOU1 abundances in cancer tissues rather than serum.

A major signalling pathway shown to be modulated by HYOU1 is AKT/PI3K. In ovarian cancers increased HYOU1 modulates the epithelial to mesenchymal transition via AKT/PI3K and resulted in the reduction of N-Cadherin and Vimentin in the tumour microenvironment, promoting invasion and migration [449]. A case study in a single individual with immunodeficiency and dysregulated glucose metabolism since birth was found to have a heterozygous missense mutation in the ATP-binding region of HYOU1 [454]. The patient had altered binding affinity for several proteins compared to wild-type, indicating an altered stress response capability. However, the link between defective HYOU1 protein and the patient's systemic immunodeficiency could not be characterised but bears further investigation due to the success of immunotherapies in treating metastatic melanoma.

5.4.1.2 NAMPT

The rate limiting step in the NAD salvage pathway is the conversion of nicotinamide to nicotinamide mononucleotide (NMN) carried out by the enzyme NAMPT, which is then converted to NAD+, an essential co-factor for ATP synthesis. As such, NAMPT is critical for cancers to maintain the high levels of carbohydrate metabolism required for neoplastic growth [455]. NAD+ is also utilised in DNA repair and gene expression making it a key cellular component in oncogenesis [456, 457]. Therefore, NAMPT is a critical driver of tumourigenesis which can be observed by the high levels of NAMPT found in numerous cancers including breast, colon, prostate, thyroid, gastric, and several haematopoietic malignancies. The SRM validation of NAMPT increasing an average of 5.02-fold in the melanoma cell line models with increased UPR, positively correlating with the average 5.5-fold increase in the cytosolic fractions discovered in Chapter 4. This reveals another novel mechanism by which the UPR

may be contributing to tumourigenesis. While decreased levels of NAMPT have been reported to control the induction of mitochondrial UPR (UPRmt) [458-460], the findings from this study are the first to present a reciprocal regulation of NAMPT and the UPR.

5.4.1.3 PDIA4

PDIA4 is a protein disulfide isomerase involved in protein folding through both its ability to act as a protein chaperone and through the formation of correct disulphide bonds via oxidoreductase activity. PDIA4 was found to be increased an average of 5.84-fold in the whole cell lysates using SRM, correlating with an average 10.6-fold increase in the cytosolic fractions quantitated with iTRAQ in Chapter 4. PDIA4 is known to be regulated by the UPR and resides mainly within the ER where it ensures the correct folding of membrane and secretory proteins. As such PDIA4 has a critical role in mediating presentation to the immune system through MHC class I complexes [461]. PDIA4 also localises to the mitochondria, nucleus and extracellular membrane space where it plays a role in T-cell migration, cancer invasion and matrix remodelling [418, 462-465]. PDIA4 has a well-established link with cancer, with demonstrated involvement in progression and metastasis. In addition to its tumour promoting role through typical stress response mechanisms, PDIA4 has been shown to promote tumour progression through inactivation of caspase 3 and 7 [466], enhancing DNA repair [467] and altering the balance between cell cycle progression and apoptosis [468]. PDIA4 has also been shown to mediate resistance to several anti-cancer drugs [469-471]. These findings correlate with other studies wherein increased PDIA4 expression is linked to poor prognosis in lung cancers, ovarian cancers, and gliomas [465, 470, 472].

5.4.1.4 PGRMC1 and PGRMC2

Both PGRMC1 and PGRMC2 belong to the Membrane-associated progesterone receptors (MAPR) group of proteins which also includes neuferricin and neudesin. PGRMCs were first identified as membrane receptors that bound progesterone and were shown to mediate sex-linked progesterone effects in female reproductive organs [473]. In addition to the classical steroid receptor function that results in transcriptional regulation of downstream effector genes, a diverse range of biological functions were subsequently reported for PGRMCs including entry into the cell cycle [474], mitotic and meiotic cell division [475], regulation of apoptosis [476], alteration of metabolism and cholesterol biosynthesis [477, 478], membrane trafficking [479], autophagy [476, 480] and iron homeostasis [481]. PGRMC1 and PGRMC2 were both identified to have increased abundance, 2.82-fold and 4.89-fold, respectively, with UPR activation from the iTRAQ discovery analysis (**Table 4-2**). In this Chapter PGRMC2 was

validated with SRM to be up-regulated 5.05-fold in response to the UPR. PGRMC1 however was found to be down-regulated with Western blotting and fluorescence microscopy but was not significantly differential across the four cell lines with SRM.

PGRMC1 and PGRMC2 have no direct reported link to the UPR, although as noted above, they are associated with autophagy and specifically with ER-phagy, which are intrinsically linked to the UPR as discussed in Chapter 1. Additionally, PGRMC1 is responsible for the clearance of misfolded prohormones from the ER [482] ensuring the production and secretion of correctly folded prohormones into the tumour microenvironment. Increasing PGRMC levels are associated with increased progression of several cancers including endometrial [483], ovarian [483], head and neck [484] and breast cancers [485]. The PGRMC hormone receptors are also associated with drug resistance to several chemotherapeutics [476, 486-489]. In this study only PGRMC2 was validated as differentially abundant with SRM. This could be the result of the initial iTRAQ analysis finding both PGRMC1 and 2 have increased abundance in the mitochondrial subcellular fraction, which in later whole cell validation was no longer detectable. The increased abundance of these membrane receptors in the mitochondria during ER-stress suggests they elicit their metabolic function as part of the UPR.

Due to the increasingly evident, but not well understood, link between sex-hormones and melanoma progression discussed in Chapter 3, the association of PGRMCs with the UPR in this study are of interest. A clear link exists between sex and melanoma outcome, however the underlying mechanism remains undefined [490, 491]. A large amount of conflicting evidence exists in the literature on the molecular roles of progesterone, androgens and estrogen in melanoma biology. Additionally, hormone-targeted therapies, such as tamoxifen, that have efficacy in other hormone related-cancers have exhibited no benefit in the treatment of melanoma. Given this information, the combination of both gender, the level to which the UPR is activated and in particular the abundances of PGRMC1 and PGRMC2 could provide insights into the complex role of hormones in melanoma progression. Furthermore, the combination of these three factors as an integrated single biomarker could potentially be utilised for melanoma prognosis, and potentially, treatment selection from hormone-targeted therapies. Due to the inability of cell cultures to accurately model systemic hormonal effects however, the findings here in cell line models have not been further investigated and further research is required, ideally on patient samples.

5.4.1.5 WARS

Tryptophanyl-tRNA synthetase (WARS) is the enzyme responsible for ligation of tryptophan to its tRNA during translation. WARS was found to be upregulated 2.59-fold with SRM, consistent with the 3.32-fold increase found with iTRAQ quantitation. Overexpression of this protein is associated with several human disease states such as infection, neurological diseases and cancer. It is overexpressed in several malignancies compared to normal tissues including uveal melanoma [189, 492-495]. Additionally, increased levels of WARS are seen in metastatic lesions compared to primary tumours [189, 496]. These previous findings are consistent with this study which found WARS to be upregulated in melanoma cell line models with increased UPR, re-enforcing the role of this stress response in melanoma progression.

These findings in the cell line models of UPR are contrary to the biomarker study on patient samples in Chapter 3, that found decreased levels of WARS to be a biomarker for poor prognosis in stage III melanoma patients [2]. These contrary findings may be explained by methodological artefacts or the diverse roles carried out by this protein which include immune modulation, regulation of angiogenesis, lymphogenesis and metabolism. These diverse functions were gained through evolution, with the acquisition of five additional protein domains [497]. In addition to these domains, WARS exhibits altered functionality through alternate splicing, proteolytic cleavage and PTMs [498, 499]. Secretion of full-length WARS mediates increased immune activation via chemokine released from macrophage and eliciting innate immune responses [500]. Alternately, secreted WARS can be cleaved proteolytically to produce protein fragments. One fragment (T2-WARS) has been shown to act as an angiostatic factor, through inhibition of VEGF preventing endothelial cell proliferation and migration in the extracellular space. In this capacity, increased levels of WARS would act contrary to the findings of this study which proposes that increased WARS as a consequence of increased UPR acts to promote tumour progression.

However, other studies correlate with the findings here, associating increased WARS levels with tumour progression and poor outcome. WARS has been shown to mediate the adaption of cancer cell to nutritional stress, a state which occurs mostly during metastasis. Tryptophan (Trp) is both an essential amino acid and the least abundant in the genetic code. Therefore, to meet their proliferative burden cancer cells must be able to incorporate a ready supply of Trp in protein production. However, simultaneously cancers cells compete to utilise degraded Trp products to suppress immune cells. Trp catabolites induce apoptosis in T-regulatory cells and cell cycle arrest of CD8+ T-cells thereby supressing antitumour immune responses [501]. This

mechanism of immune evasion has been shown to be exploited by melanoma, which has increased abundance of tryptophan degrading enzymes [502]. Therefore, it has been proposed that in order to both utilise the immune-suppressive effects of degraded Trp while also maintaining high levels of protein production, cancer cells increase the levels of cytoplasmic and mitochondrial WARS to capture low abundant Trp and sequester it as Trp-tRNA [503].

5.4.1.6 SLAC3A2

4F2 cell-surface antigen heavy chain (SLAC3A2) is an amino acid transporter found on the cell surface bound to SLC7A5 and SLC7A11, where it acts as a chaperone to stabilise the protein complex. This transporter complex mediates the import of leucine coupled to the efflux of L-glutamine. In additional to membrane transportation, SLC3A2 has a dual role as a receptor for signal transduction, leading to the term transceptor. Transportation of cargo by SLC3A2 across the membrane also mediates activation of the mammalian target of rapamycin complex 1 (mTORC1) signalling and promotes cellular growth [504]. SLC3A2 validated here to be increased in abundance with increased UPR with a 3.42-fold increase quantified by SRM, corresponding to the 3.25-fold increase observed in the nuclear fraction with iTRAQ. SLC3A2 is a known upstream regulator of the several branches of the UPR by mediating levels of downstream UPR effects, ATF4, ATF6 and XBP-1 through activation of mTOR [505]. This correlates with the findings reported here that SLC3A2 is upregulated in response to ER-stress.

Significantly, a correlation of increased SLC3A2 levels with cancer progression has been seen in various cancers including gastric [442], osteosarcoma [506] and breast cancer [507]. Furthermore, SLC3A2 binds to and activates β1-integrin, an adhesion receptor that regulates cellular migration and invasion, therefore increased SLC3A2 promotes metastasis [508]. Florescence microscopy on melanoma cells showed an increase of SLC3A2 with increased UPR at the adherent membrane interface and particularly localised at structures on the cell membrane (**Figure 5-4**). However, due to the limited specificity and semi-quantitative nature of fluorescence microscopy, further validation and localisation studies are required to confirm these findings. Together this data supports a possible role of the UPR in promoting the metastatic potential of tumours. These finders are further explored in Chapter 6 with bioinformatic analysis on transcriptomic data from 460 melanoma patients which revealed SLC3A2 and WARS are significantly predictive of overall patient survival (**Figure 6-7**).

SLC3A2 has also been associated with immune suppression within the tumour microenvironment. Given that the standard treatment for metastatic melanoma is currently

either single or combinatorial immunotherapies; anti-PD1 and anti-CTLA4, this upregulation in melanoma is of potential clinical significance. Cancerous cells make the tumour microenvironment inhospitable for infiltrating immune cells by creating an acidic, hypoxic and nutrient deprived environment resulting in decreased anti-tumoural activity [441]. With the increase in immunotherapies such as those mentioned above and CAR T-cell therapies, tumour recognition and infiltration is only part of the challenge. The activated immune cells must be able to proliferate and meet their energy requirements in order to carry out their anti-tumoural effects. Increased sequestering of amino acids by cancerous cells through increased SLC3A2 abundance, may perpetuate the harsh conditions in the tumour microenvironment and further suppresses the ability of immune cells to clear neoplastic cells.

5.4.1.7 SMARCA5

SMARCA5 is a member of the SWItch/Sucrose Non-Fermentable (SWI/SNF) chromatin remodelling family. Members of the SWI/SNF family assemble into a complex comprising at least six protein subunits that surround the nucleosome [509]. The complex participates in chromatin remodelling through ATP hydrolysis to relax chromatin packaging, increasing the affinity of transcription factors and transcriptional machinery to specific regions of DNA. In mammals there are 29 genes encoding members of the SWI/SNF family, the assembled complex contains one of two core members SMARCA2 (BRM) or SMARCA4 (BRG1) in different combinations with other family members. The large complex (~2 MDa) also participates in altering gene expression through the recruitment of transcription factors to their binding sites. The assembled SWI/SNF complex can associate with transcription factors such as histone deacetylase HDAC3, Rb and Ikaros [510, 511]. Other proteins that exhibit major cellular control such as BRCA1 have also been found bound to SWI/SNF complexes [512]. Gene expression within the cell can be altered depending on the composition of the members in the assembled SWI/SNF complex through differential DNA binding affinities and affinities for different transcription factors [513].

The iTRAQ analysis in Chapter 4 found that SMARCC1 was down-regulated with ER-stress an average of 2.28-fold, SMARCA4 was significantly down-regulated 1.58-fold in one cell line and SMARCA5 significantly down-regulated 1.96-fold in the other cell line (**Table 4-2** and **Supplementary Figure S4-1**). These three proteins and other member of the SWI/SNF family were targeted for SRM analysis in this Chapter, however due to high sequence homology, low abundance and expansion of biological replicates to examine whole cell protein lysates, very few of these members could be detected by SRM. With SRM quantitation

SMARCA5 was detected to decreased in abundance 2.50-fold in all four melanoma cell lines, while SMARCC2 was only decreased in abundance in Mel-RM cells (**Figure 5-5**). The iTRAQ findings for the decreased abundance of SMARCC1 with UPR activation were confirmed with Western blotting (**Figure 5-1**).

With the era of large meta-analyses and multi-omic studies, it was revealed that the SWI/SNF complex played a significant role in oncogenesis and cancer progression. Various members of the SWI/SNF complex have been found to be mutated in 20% of malignancies [514] and 30% of melanomas [444, 446]. It was not until the family members were examined collectively and in large studies that the impact of this chromatin remodelling family in cancer became clear. Subsequently, SMARCB1 was identified as a tumour suppressor protein, in which SMARCB1 knock-downs resulted in lymphomas or rhabdoid tumours in mice models [515]. Loss of SMARCB1 is however rare in human tumours, with most loss of function mutations seen in the core catalytic subunits SMARCA2 and SMARCA4, found in ~15% of all tumour types. In cancers the loss of one or more of the SWI/SNF subunits, results in altered composition of the complex, therefore altered binding affinity to chromatin sites and altered gene expression. The role of individual SWI/SNF family members has since been extensively studied however there are numerous discrepancies within the literature. SMARCA4 was initially identified as a tumour suppressor protein, with inactivating mutations found in numerous cancers [516-519]. However, SMARCA4 levels have been positively correlated with oncogenic activation in liver cancer [520]. A pan-cancer study on SMARCA4 transcriptomic data showed levels both positively and negatively correlated with prognosis depending on cancer type [521]. SMARCB1 has been proposed as a tumour suppressor gene, the loss of which results in oncogenesis [522], with decreased levels correlate with increased progression and poor patient outcome [523]. Contrary to these findings, SMARCB1 is also reported as essential for DNA repair and melanoma survival [524]. These contrary findings are likely the result of the study of individual SWI/SNF members rather than studies focusing on the functional complex. While mechanistic studies using model systems have provided contrary findings, meta-analyses of patient data overwhelmingly show loss of the abundance of SWI/SNF family members is associated with increased progression and poor survival in melanoma patients [444, 522, 525-534].

Collectively, the findings presented here indicated that the UPR may potentially exert broad transcriptional control through the modulation of these chromatin remodelling factors. A later study reported the SWI/SNF complexes regulated the unfolded protein response in

Saccharomyces cerevisiae, in particular the arm of the UPR responsible for global suppression of protein synthesis [535]. The findings presented here demonstrate that potentially mutations alone are not responsible for the decrease of SWI/SNF seen in many cancers, that the UPR may also contributes to the decreased protein abundance of this chromatin remodelling family in cancer. In this study four SWI/SNF family members were found to be altered as part of the UPR. As such, studies examining the role of SWI/SNF in human cancers should not just focus on mutations but also include techniques for protein quantitation in order to gain a comprehensive understanding. Studies should also focus on the dysregulation of this protein family collectively, examining all family members, as the dysregulation is seen on the level of the complex not in its separate protein subunits.

5.4.1.8 SUN2

SUN2 is a member of the inner nuclear membrane LINC complex which mediates the attachment of nuclear lamina to the cytoskeleton [536]. SUN2 was validated by SRM to be decreased in abundance in response to increased UPR activation, with an average 4.27-fold decrease across the four melanoma cell lines (**Table 5-1**), correlating to an average 4.04-fold decrease in the nuclear fractions with iTRAQ analysis in Chapter 4. Decreased levels of SUN2 have been reported in various cancers. In colorectal cancers, SUN2 has decreased abundance in neoplastic tissue, reduced SUN2 levels are associated with increased invasive potential and poorer overall survival [537]. The same decreased levels of SUN2 are observed in patient breast cancer samples compared to normal mammary tissue [538]. Reduced SUN2 levels promote the growth of oral, ovarian, embryonal, prostate and lung cancers [235, 539-541]. Lung cancer patients with lower SUN2 levels have shorter overall survival [542]. Additionally, SUN2 can suppress the Warburg effect by inhibiting the expression of GLUT1 and LDHA [542]. Therefore, decreased SUN2 levels as part of the UPR could potentially elevate the metabolic capacity of cancer cells. SUN1 and SUN2 are both critical for DNA damage repair through the recruitment of nuclear factors [543], therefore decreased SUN2 levels as a consequence of UPR activation could increase the genomic plasticity of cancers, promoting oncogenesis and more aggressive phenotypes.

5.5 Conclusions

The eight UPR-associated proteins validated by SRM as differentially abundant with increased UPR activation are targets of the UPR that are consistent across cell line models. As such they represent proteins which are integral to this stress response in melanoma. The proteins (HYOU1, NAMPT, PDIA4, PGRMC2, WARS, SLC3A2, SMARCA5 and SUN2) are involved in a range of cellular processes including metabolism, cellular migration, immune suppression, angiogenesis, chromatin remodelling, protein folding, signalling, DNA repair, drug resistance and cytoprotection (**Table 5-2**). In a biological context, the known function of all eight proteins could contribution to progression and metastasis of melanoma and cancers in general. Additional, significant evidence exists within the literature to demonstrate these proteins play a role in cancer progression and patient outcome in a broader range of cancer types beyond melanoma, which is explored further in the following chapter. Furthermore, the consistent modulation of these proteins by the UPR makes them potential targets for future development of therapeutic strategies that exploit the reliance of cancers on this stress response.

Chapter 6: *in silico* validation of UPR associated proteins in melanoma and pan-cancer patient cohorts

6.1 Introduction

In recent years the field of cancer research has moved into the era of big data, seeking to utilise large pan-cancer studies to comprehend this complex disease. These large multi-study, multi-omic analyses have provided the layered information and large numbers required to understand this heterogenous disease. Several of these studies have sought to reshape the way in which we classify cancers. These analyses seek to move away from traditional histological subtypes, that classify cancers based on cell of origin and tissue type, into molecular subtypes, that classify cancers based upon the molecular dysfunctions driving the cancer.

The aim of the following bioinformatic analysis was to utilise publicly available transcriptomic and proteomic data from melanoma and pan-cancer patients, to assess if the UPR-associated proteins identified in Chapters 4 and 5 are modulated in response to increased UPR in independent dataset and other cancer types. Additionally, to determine if the UPR is one type of molecular dysfunction commonly observed across cancer types that can be used as part of a broader molecular biomarker signatures to select the most effective treatments or to predict patient outcome, in order to strengthen the potential connection of the UPR with patient outcome, initially identified in Chapter 3 and expanded in Chapters 4 and 5.

Firstly, given the reciprocal regulation between MEK/ERK activation and the UPR discussed in previous chapters, a proteomic dataset from ten melanoma cell lines treated with MEKi was used to examine the relationship between the UPR-associated proteins, GRP78 (the master regulator of the UPR) and MEKi resistance. SWATH-MS data for the MEKi treated cell lines contained quantitative data for 47 of the 66 UPR-associated proteins discovered in Chapter 4. Five of the UPR-associated proteins were found to correlate with MEKi resistance, reaffirming the relationship between MEK/ERK signalling and the UPR. Additionally, the analysis highlights the potential use of these proteins and UPR activation as biomarkers for treatment selection in melanoma.

Secondly, due to the known relationship between increased UPR activation and poor prognosis in melanoma patients, the abundances of the 66 UPR-associated proteins discovered in Chapter 4 in melanoma cell lines with iTRAQ analysis was examined in a SWATH-MS dataset of 32 stage III melanoma patients with known survival outcomes. Quantitative data was obtained for 43 of the 66 UPR-associated proteins, and using GRP78 as a marker of UPR activation, their protein abundance was correlated to UPR activation. Ten proteins found to be differentially abundant in melanoma cell lines with increased UPR from Chapter 4 were

discovered to have the same differential abundance with increased UPR activation in melanoma patients. The abundance of the 43 UPR-associated proteins was examined to determine if similar changes in abundance that occur with increased UPR in cell lines correlated with poor survival in melanoma patients from public data. Twenty-two of the UPR-associated proteins from Chapter 4, including six of the eight validated in Chapter 5, were found to correlate with patient prognosis, although very few to a statistically significant degree. These finding in patient data further demonstrate a link between increased UPR activation and poor prognosis in melanoma patients.

Thirdly, the eight UPR-associated markers from melanoma cell lines validated in Chapter 5 were examined in publicly available melanoma transcriptomic data to determine if their correlation with UPR activation also correlated with patient survival. RNA-Seq data from 460 stage I to IV melanoma patient was obtained from the TCGA. The transcriptomic abundances of the eight UPR-associated proteins were correlated with UPR activation using GRP78 as a marker for UPR induction. The abundance of the eight UPR-associated proteins was able to cluster patients based upon the levels of UPR induction and two proteins (SLC3A2 and WARS) were able to act as potential prognostic markers that significantly predict outcome in melanoma patients.

Fourthly, as the UPR is associated with tumour progression and poor outcome, not just in melanoma but other solid cancer types, the eight UPR-associated proteins were examined in RNA-Seq data of 6,176 cancer patients representing sixteen cancer types, for their potential association with overall patient survival. All eight of the UPR-associated proteins were found to be significantly associated with patient outcome, demonstrating that the UPR has a major role in cancer progression. Overall, these findings highlight the potential future use of the UPR-associated proteins discovered in this study as prognostic biomarkers in solid tumours.

6.2 Methods

6.2.1 Correlation of the UPR associated protein with MEK inhibitor resistance in melanoma cell lines

Proteomic data acquired with SWATH-MS by the Molloy group was mined for an association between the UPR and the RAS/RAF/MEK/ERK pathway via correlation with MEKi sensitivity in a panel of melanoma cell lines established from stage III cutaneous melanoma patient samples [284]. The sensitivity of ten melanoma cell lines were determined by the Molloy group through cell viability on cells treated with the MEKi, selumetinib. Of the 64 UPR-associated proteins discovered in Chapter 4, 47 proteins had quantitative data used in the following analysis. Proteins were calculated to correlate with MEKi sensitivity by comparing the topmost sensitive lines with the most resistant line. UPR-associated proteins were deemed to contribute to MEKi resistance if they exhibited a correlation >0.5 to the relative resistance of the ten cell lines. Unsupervised hierarchical clustering was performed to evaluate if the UPR-associated proteins could group samples based on MEKi sensitivity. A graphical summary of the method can be found in **Supplementary Figure S6-1**.

6.2.2 Prognostic significance of UPR-associated proteins in melanoma patient proteomic data

Proteomic data of 32 stage III melanoma patients also generated by the Molloy group [284] was examined to validate the association of the 64 proteins identified in Chapter 4 with the UPR in an *in vivo* context with patient clinical data. Of the 64 UPR-associated proteins, 43 had quantitative data in the melanoma patient dataset and were used for subsequent analysis. Pearson correlation was calculated for the UPR-associated proteins with the levels of GRP78 being used to identify any association of that target with the UPR. To determine if the UPR-associated proteins correlate with patient survival, the cohort was split into good (>4-year OS) and poor prognostic (<1 year OS) groups and log rank *p*-values calculated with a two-tailed *t*-test. A graphical summary of the method can be found in **Supplementary Figure S6-2**.

6.2.3 Prognostic significance of the eight UPR-associated proteins in melanoma patient transcriptomic data – TCGA data

Publicly available RNA-Seq data from 460 melanoma patients from the TCGA-SKCM dataset with corresponding clinical data was downloaded from the cSurvival data repository

[286, 287]. This repository maintains curated and quality-controlled patient data from the TCGA and removes problematic samples, e.g. prior treatment, failed QC, withdrawn patient consent. Survival analysis with KM survival curves, Hazard ratio and 95% confidence interval were calculated by univariate Cox regression on each of the eight UPR-associated proteins as a predictor of overall survival using the python package lifelines [288]. Clusters in the RNA-seq data were determined with k-means clustering using the python package sklearn [544]. The number of clusters were optimised using Silhouette scoring, in which the Silhouette correlation was calculated for increasing numbers of clusters, using a random subset of samples (n=100). The full RNA-seq dataset was then fit to the optimised number of clusters using the k-means++ Lloyd algorithm performed over 100 iterations with a random centroid state of 1. Pearson's correlation and unsupervised hierarchical clustering was then used to determine whether there may be an association with UPR activation clusters in melanoma patients. A graphical summary of the method can be found in **Supplementary Figure S6-3**.

6.2.4 Prognostic significance of the eight UPR-associated protein in a pan-cancer RNA-Seq dataset

Publicly available RNA-Seq data from the TCGA was downloaded from the cSurvival data repository listed above [286, 287]. Sixteen solid tumour cohort comprising a total of 6,176 patients were selected for analysis; Bladder carcinoma (n=404), Breast cancers (n=725), Cervical carcinomas (n=304), Oesophageal adenocarcinomas (n=80), Head and Neck squamous cell carcinomas (n=499), Renal clear cell carcinomas (n=530), Hepatocellular carcinomas (n=370), Lung adenocarcinomas (n=504), Lung squamous cell carcinomas (n=495), Ovarian carcinomas (n=373), Pancreatic adenocarcinomas (n=177), Rectal adenocarcinomas (n=165), Sarcomas (n=259), Stomach adenocarcinomas (n=247), Thyroid cancers (n=502) and Uterine endometrial carcinomas (n=542). Survival analysis with KM survival curves, Hazard ratio and 95% confidence intervals were calculated by univariate Cox regression on each of the eight UPR-associated proteins as a predictor of overall survival using the python package lifelines. Cancer cohorts were first analysed by cancer type, then tumour types grouped for the final analysis when individually predictive of survival. A graphical summary of the method can be found in Supplementary material **Supplementary Figure S6-4**.

6.3 Results

6.3.1 Association of UPR-differentially abundant proteins with resistance to MEKi in proteomic data from melanoma cell line models

Due to the reciprocal regulation of the UPR and MAPK pathway activation discussed in Chapter 4, publicly available proteomic data from melanoma cell line models treated with a MEKi were analysed. The 66 UPR-associated proteins found to be differentially abundant with increased UPR activation induced by thapsigargin in subcellular fraction of two melanoma cell lines with iTRAQ analysis were examined to determine if a correlation exists between the UPR and MEKi resistance. Of the 66 unique UPR-associated proteins discovered in the thapsigargin treated cell line models in Chapter 4 (**Table 4-2** and **Figure 4-8**), 47 were also found in the MEKi cell line SWATH-MS data. Seven proteins were found to have an association with MEKi resistance in untreated melanoma cell lines with a Pearson's correlation >0.5 (**Figure 6-1**). The seven proteins; ATP synthase subunit alpha, mitochondrial (ATPA), Protein disulfide-isomerase A4 (PDIA4), Endoplasmin (ENPL or HSP90B1), 78 kDa glucose-regulated protein (GRP78), Heterogeneous nuclear ribonucleoprotein A2 (ROA2), High mobility group protein HMG-I/HMG-Y (HMGA1) and Alpha-actinin-4 (ACTN4); were able to separate the cell lines into clusters according to sensitivity or resistance with unsupervised hierarchical clustering (**Figure 6-2**).

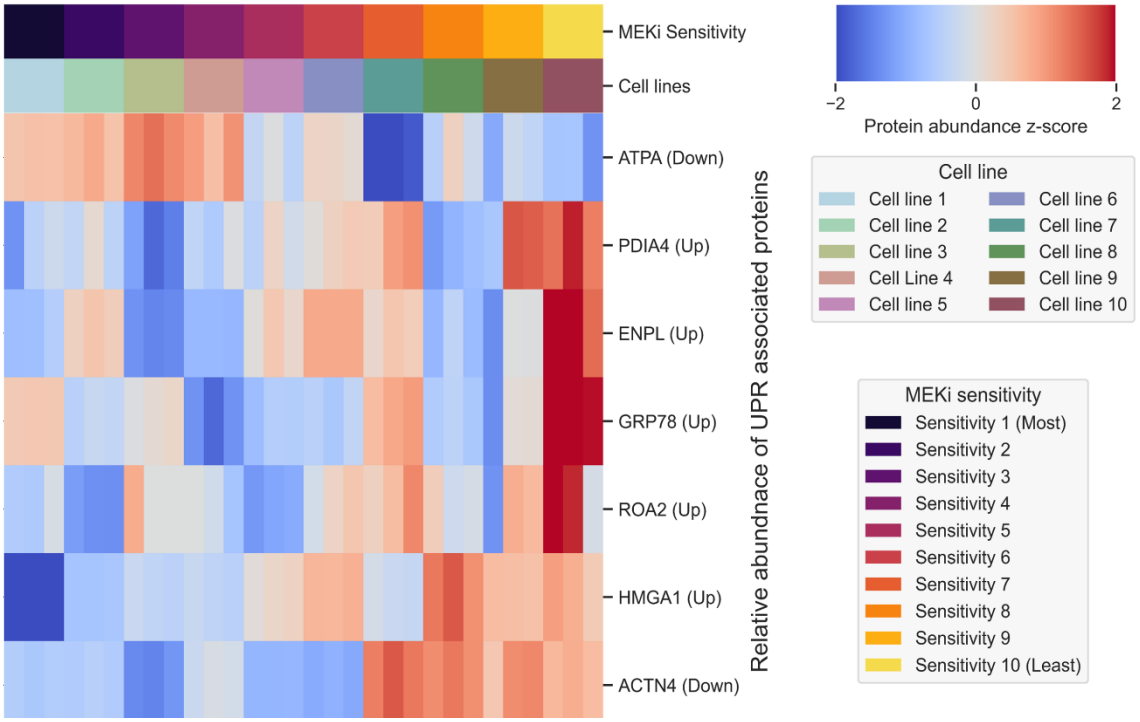

Figure 6-1. **Correlation of UPR-associated proteins with MEK inhibitor (MEKi) resistance in 10 melanoma cell lines.** The 66 proteins identified to be differentially abundant with UPR activation in Chapter 4 were examined in publicly available proteomic data of 10 melanoma cell lines treated with a MEKi [284]. The abundance of seven proteins was found to be associated with MEKi resistance (Pearson's correlation of >0.5). The heatmap shows the abundance (z-score) of the seven proteins and their association with the MEKi sensitivity of individual cell lines.

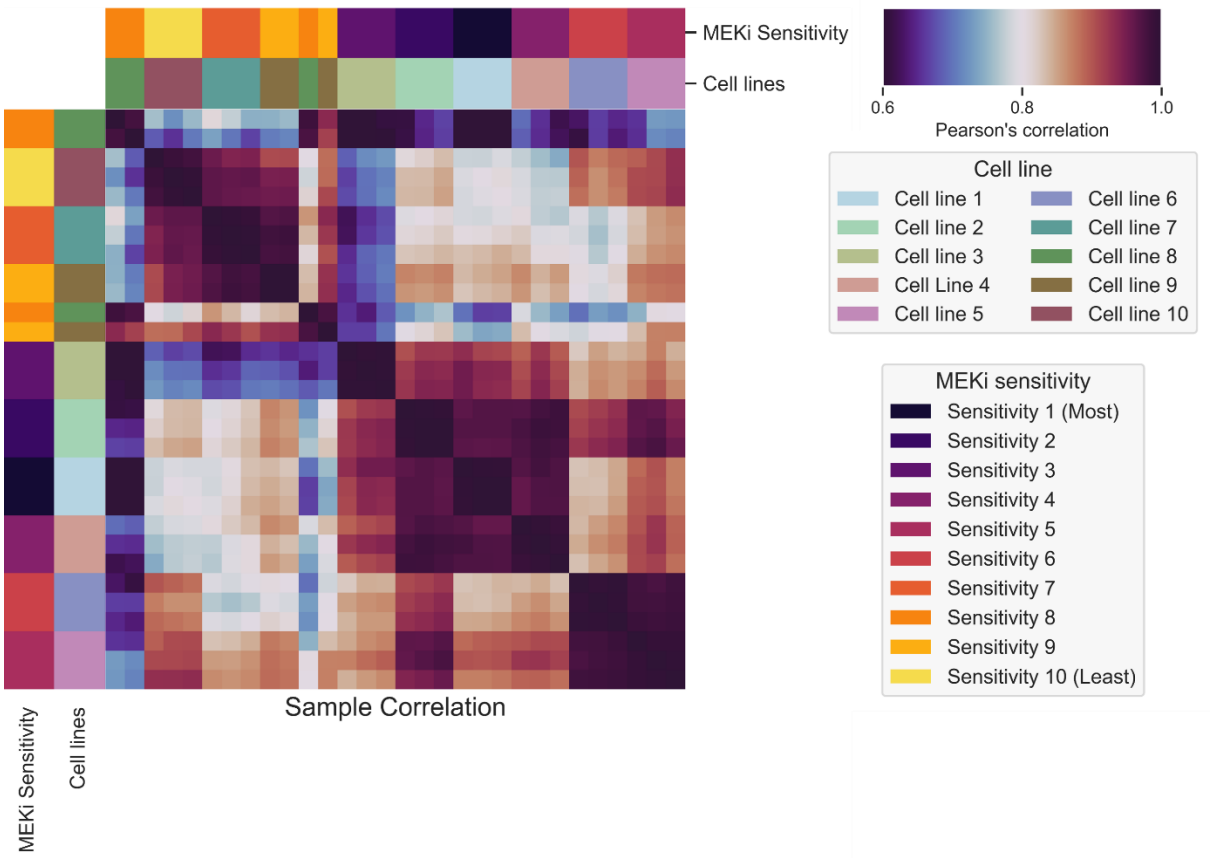

Figure 6-2. **Clustering of melanoma cell lines by UPR-associated proteins correlates with MEK inhibitor resistance.** The 66 proteins identified to be differentially abundant with UPR activation were examined in public proteomic data of 10 melanoma cell lines treated with a MEKi [284]. The abundance of seven proteins were found to be associated with MEKi resistance (Pearson's correlation of >0.5). Pearson's correlation comparing the cell line samples with unsupervised hierarchical clustering shows clustering by MEKi sensitivity and resistance based upon the abundances of seven UPR-associated proteins.

6.3.2 Correlation of UPR-associated proteins with UPR-activation in melanoma patient proteomic data

To determine if the 66 UPR-associated proteins discovered in the melanoma cell line subcellular fractions in Chapter 4 using iTRAQ analysis (**Table 4-2**), is reflective of the changes that occur in patient samples, publicly available proteomic data from melanoma patient tumours was analysed. First, the 66 UPR-associated proteins were correlated against GRP78 levels, as a marker of UPR activation, in public stage III melanoma acquired with SWATH-MS [284]. Forty three of the 66 proteins identified in the iTRAQ analysis were also identified in the stage III melanoma patient data. Ten of UPR-associated proteins were found to correlate with GRP78 levels in 32 melanoma patients, nine of which had the same trend in abundance (i.e., up- or down-regulated) seen in the cell line models (**Figure 6-3**). This correlates with our previous observations that these proteins are differentially abundant with increased UPR activation. Furthermore, the results reveal that the findings from Chapter 4 utilising cell line

models may be translated to patient tumours in some cases. Of interest, are the two patients for which their GRP78 levels do not correlate with the 10 UPR-associated proteins in **Figure 6-3**. In these two patients, despite high levels of GRP78, the cancers exhibit low HYOU1, NAMPT, PDIA4, PDIA1, KCAP4 and high FBRL, ATPA and ADT2 (**Figure 6-3**). This might suggest that despite high levels of GRP78, the master UPR regulator, the UPR pathway may not be highly activated in these tumours.

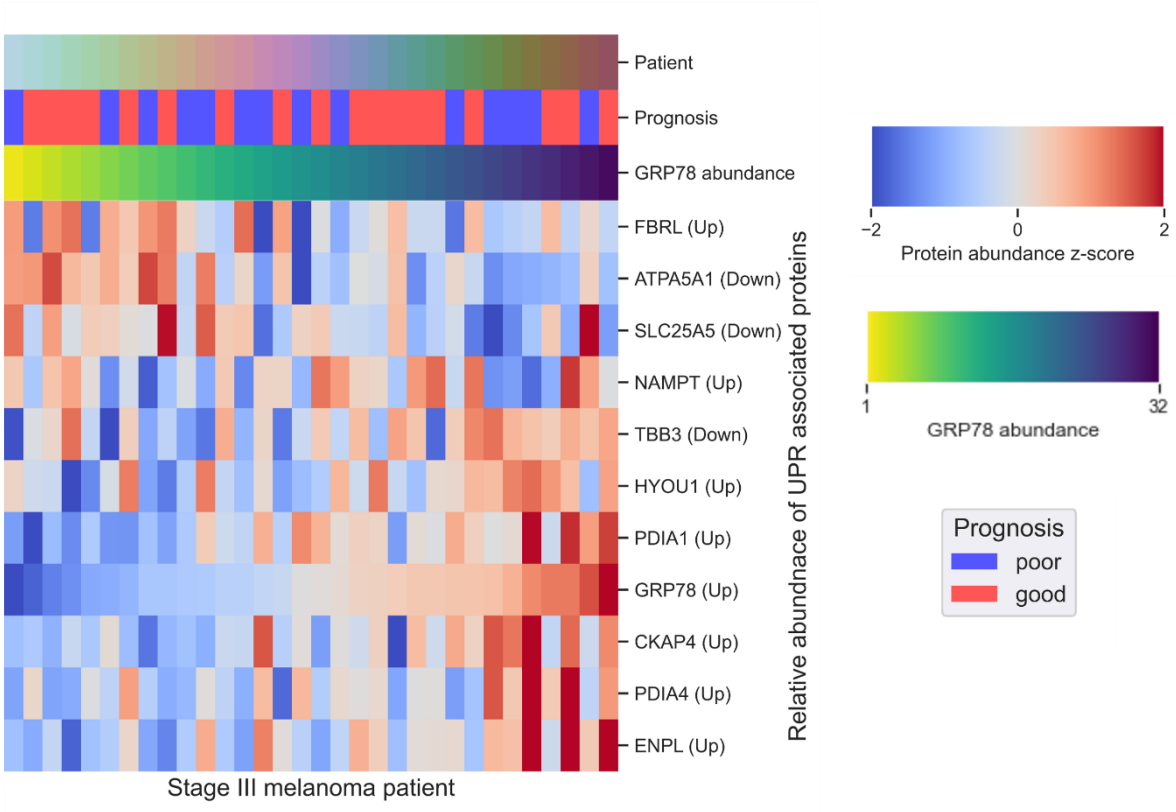

Figure 6-3. Differential abundance of 10 UPR-associated proteins from cell line models correlate with UPR activation in melanoma patient data. Proteomic data from 32 stage III melanoma patients was taken from publicly available data. Quantitative data from 43 of the 66 UPR-associated proteins found in the melanoma patient data was examined for its correlation to GRP78 levels as a marker of UPR activation. Ten UPR-associated proteins discovered in Chapter 4 were found to correlate with GRP78 levels in proteomic data of stage III melanoma patients, nine of which with the same trend in abundance.

Secondly, the 10 UPR-associated proteins found to be differentially abundant with increased UPR activation in cell lines (**Figure 6-3**) were used collectively as a panel to cluster cancers from different patients based on the level of UPR activation as demonstrated with unsupervised hierarchical clustering (**Figure 6-4**). Melanoma patients with high levels of GRP78, and therefore increased UPR activation, can be grouped based upon the abundances of the 10

proteins. This revealed that 10 of the 66 UPR-associated proteins discovered in cell line models in Chapter 4 are also associated with the UPR in patient tumours.

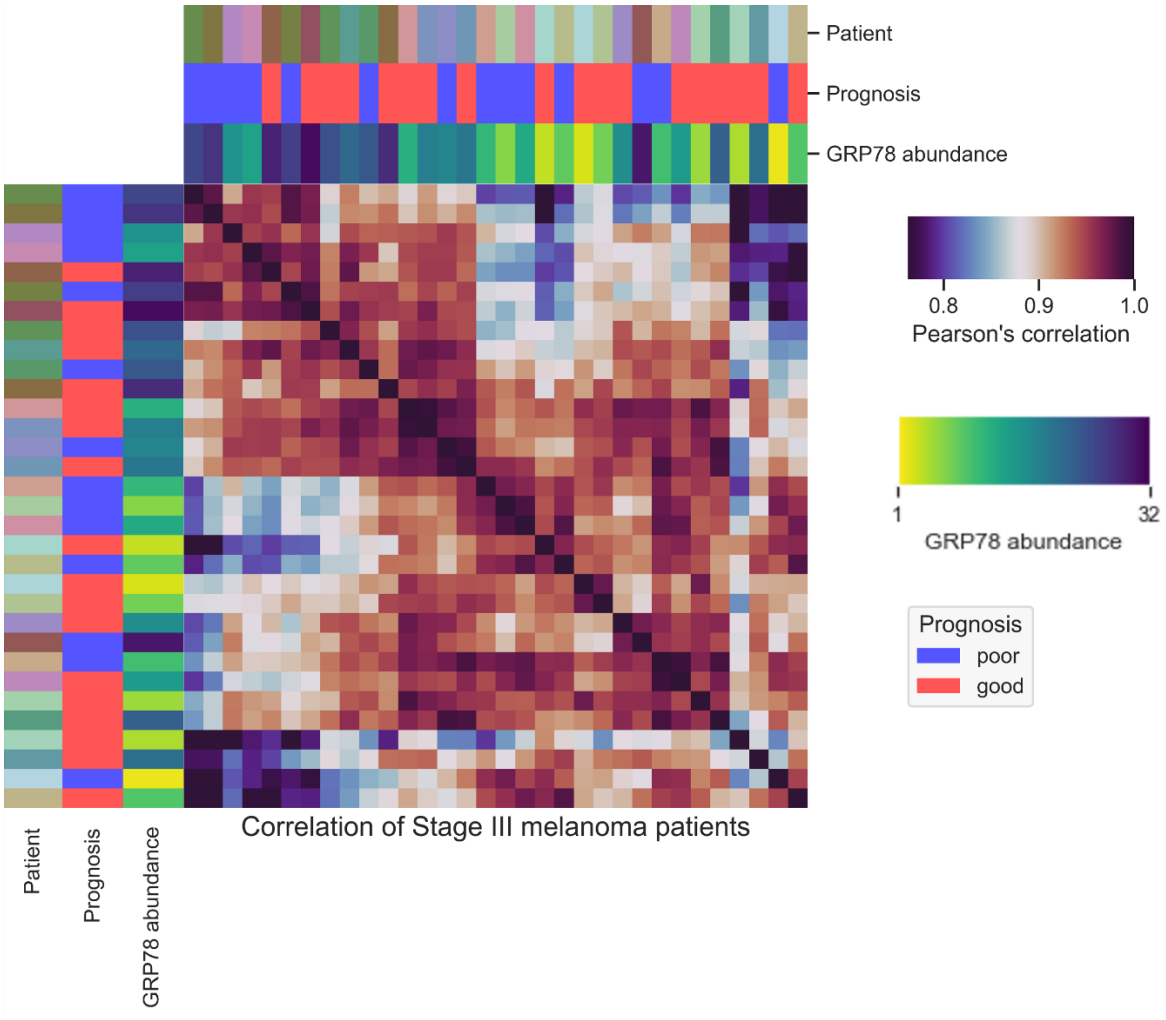

Figure 6-4. Clustering of melanoma patients based on UPR-activation utilising 10 UPR-associated proteins. Proteomic data from 32 stage III melanoma patients was taken from publicly available data. Quantitative data from 43 of the 64 UPR-associated proteins found in the melanoma patient data was examined for its correlation to GRP78 levels as a marker of UPR activation. Ten proteins were found to have a correlation with GRP78 levels (**Figure 6-3**). Using the abundances of the 10 proteins collectively the Pearson's correlation between the stage III melanoma patients was calculated and unsupervised hierarchical performed. Using the 10 UPR-associated proteins together, patients broadly cluster based on the level of UPR activation.

6.3.3 Correlation of UPR-associated proteins with survival of stage III melanoma patients – SWATH-MS proteomic dataset

Having demonstrated that the ten UPR-associated proteins correlate with UPR activation, as determined by GRP78 levels in Section 6.3.2, the next aim was to assess if increased activation of the UPR correlates with patient survival, using the UPR-associated proteins

discovered in Chapter 4. The 66 proteins found to be differentially abundant with increased UPR activation using iTRAQ analysis in subcellular fractions from two melanoma cell lines from Chapter 4 were correlated against stage III melanoma patient's prognosis from SWATH-MS analysis carried out by the Molloy laboratory [284]. Forty-three of the 66 proteins were identified in the 32 stage III melanoma patients' proteomic data. Among these, 22 proteins had a correlation between increased UPR and poor prognostic outcome (**Table 6-1**). The observed correlation of the UPR-associated proteins however suffers from a lack of statistical significance. This could be due to the UPR having a small or partial influence on patient survival, as many factors contribute to patient outcome including various molecular pathways. Additionally, it could be a result of tumour heterogeneity or the small size of the cohort, factors that are commonly problematic in cancer biomarker studies. Activation of the UPR alone is not a prognostic factor when used in isolation without any additional biomarkers as demonstrated in **Figure 6-3**, **Figure 6-4** and **Table 6-1**. Of the 22 UPR-associated proteins that correlate with patient outcome, six proteins (HYOU1, NAMPT, PDIA4, HSPA5, PGRMC2 and WARS) are among the eight UPR-associated proteins identified by iTRAQ in Chapter 4 then validated by SRM in Chapter 5 (**Table 5-1**). The eight UPR-associated proteins were found to represent a core group of proteins consistently modulated with UPR activation in a wider melanoma cell line panel. Combined with the findings here, the eight UPR-associated proteins were selected for analysed further in publicly available transcriptomic data from melanoma and pan-cancer patient tumours.

Table 6-1. **Correlation of differentially abundant proteins with increased UPR from iTRAQ analysis of melanoma cell lines with stage III melanoma patient prognosis.** Twenty-two of the 66 UPR-associated proteins discovered in melanoma cell line models in Chapter 4 correlate with poor outcome in proteomic data of 32 stage III melanoma patients. Values were calculated by two-tailed Student's *t*-test and Pearson's correlation analysis. Six of the eight of the UPR-associated proteins which were discovered by iTRAQ and validated by SRM in Chapter 5 are shown in bold.

Accession	Gene Name	Name	Major Function	Fold-change with poor prognosis	*p*-value in SWATH	Protein abundance with increased UPR	UPR correlation to poor prognosis
E9PL22	**HYOU1**	**Hypoxia up-regulated protein 1**	**Stress response**	**2.09**	**0.366**	**Increased**	**Yes**
P43490	**NAMPT**	**Nicotinamide phosphoribosyltransferase**	**Metabolic**	**1.73**	**0.005**	**Increased**	**Yes**
P62269	RPS18	40S ribosomal protein S18	Protein processing	1.97	0.483	Increased	Yes
P13667	**PDIA4**	**Protein disulfide-isomerase A4**	**Protein processing**	**2.04**	**0.704**	**Increased**	**Yes**
P62249	RPS16	40S ribosomal protein S16	Protein processing	1.97	0.510	Increased	Yes
P14625	HSP90B1	Endoplasmin	Stress response	2.04	0.528	Increased	Yes
Q01518	CAP1	Adenylyl cyclase-associated protein 1	Cytoskeletal	1.98	0.708	Increased	Yes
P07237	P4HB	Protein disulfide-isomerase	Protein processing	2.08	0.300	Increased	Yes
P11021	**HSPA5**	**78 kDa glucose-regulated protein**	**Stress response**	**1.99**	**0.940**	**Increased**	**Yes**
P22087	FBL	rRNA 2'-O-methyltransferase fibrillarin	rRNA processing	1.85	0.297	Increased	Yes
P17096	HMGA1	High mobility group protein HMG-I/HMG-Y	Transcriptional regulation	5.06	0.504	Increased	Yes
Q8N5K1	CISD2	CDGSH iron-sulfur domain-containing protein 2	Metabolic	2.00	0.998	Increased	Yes
O15173	**PGRMC2**	**Membrane-associated progesterone receptor component 2**	**Steroid receptor**	**1.85**	**0.448**	**Increased**	**Yes**
Q9BVK6	TMED9	Transmembrane emp24 domain-containing protein 9	Vesicular trafficking	2.33	0.387	Increased	Yes
Q07065	CKAP4	Cytoskeleton-associated protein 4	Cytoskeletal	2.22	0.153	Increased	Yes
P49755	TMED10	Transmembrane emp24 domain-containing protein 10	Transporter	2.16	0.434	Increased	Yes
O00264	PGRMC1	Membrane-associated progesterone receptor component 1	Steriod receptor	2.04	0.849	Increased	Yes
Q15006	EMC2	ER membrane protein complex subunit 2	Metabolic	2.32	0.092	Increased	Yes
P42766	RPL35	60S ribosomal protein L35	Protein processing	1.78	0.470	Increased	Yes

P23381	**WARS**	**Tryptophan--tRNA ligase, cytoplasmic**	**Protein processing\ angiogenic**	**1.88**	**0.425**	Increased	**Yes**
Q96JB5	CDK5RAP 3	CDK5 regulatory subunit-associated protein 3	Cell cycle	1.84	0.212	Increased	Yes
P51571	SSR4	Translocon-associated protein subunit delta	Transporter	1.87	0.490	Increased	Yes

6.3.4 Correlation of eight UPR-associated proteins with melanoma disease specific survival in stage I – IV melanoma patients RNA-Seq data

The above correlation of the UPR-associated proteins with patient prognosis in section 6.3.3 above with a small proteomic dataset of 32 melanoma patients, while correlating with changes in abundance that are observed in cell line models of UPR activation, suffered from a lack of statistical power. In order to overcome tumour heterogeneity and analyse a large melanoma patient cohort, bioinformatic analysis was carried out on publicly available transcriptomic data from 460 melanoma patient samples.

The eight UPR-associated proteins, listed in **Table 5-1,** were examined in patient transcriptomic data to determine if their abundance levels were modulated with UPR activation in a pattern consistent with the cell line model findings from Chapter 5. RNA-Seq data from the TCGA melanoma dataset (TCGA-SKCM) from 460 melanoma patients was examined and the abundance levels of the eight UPR-associated proteins (HYOU1, NAMPT, PDIA4, PGRMC2, WARS, SLC3A2, SMARCA5 and SUN2) were used to fit samples into UPR-activation clusters using k-means clustering. The optimal number of clusters was determined to be four using Silhouette coefficient, in which four clusters were found to give the highest degree of separation between clusters, while minimising dissimilarity within a single cluster (**Supplementary Figure S6-5**). Melanoma patients were fit into the four clusters based upon the levels of the eight UPR-associated proteins (**Figure 6-5**). Each cluster was assigned a level of UPR activation using GRP78 abundance as the discriminator. The cluster with high UPR activation was therefore characterised by high GRP78 abundance, Cluster 4, has correlating abundance level for six of the eight UPR-associated proteins. In Cluster 4 high GRP78 is associated with high HYOU1, NAMPT, PDIA4, PGRMC2, SLC3A2 and low SUN2, with only SMARCA5 and WARS having conflicting abundance (up- or down-regulation) to the cell line model (**Figure 6-5**). Further confirming that these proteins are modulated as a result of UPR activation and demonstrating the changes in the UPR-associated proteins from Chapter 4 and 5 are similarly differential in patient samples. Additionally, Cluster 3, characterised by medium GRP78 abundance and therefore classified as mid-level UPR activation, has increased levels of HYOU1, NAMPT and PDIA4. The pattern of the UPR-associated proteins in Cluster 2 correlating with the findings of previous chapters. Furthermore, it matches the known regulation of the UPR as having highly nuanced modulation and can be active at low levels to repeal low level cellular stress without inducing apoptosis [1, 437].

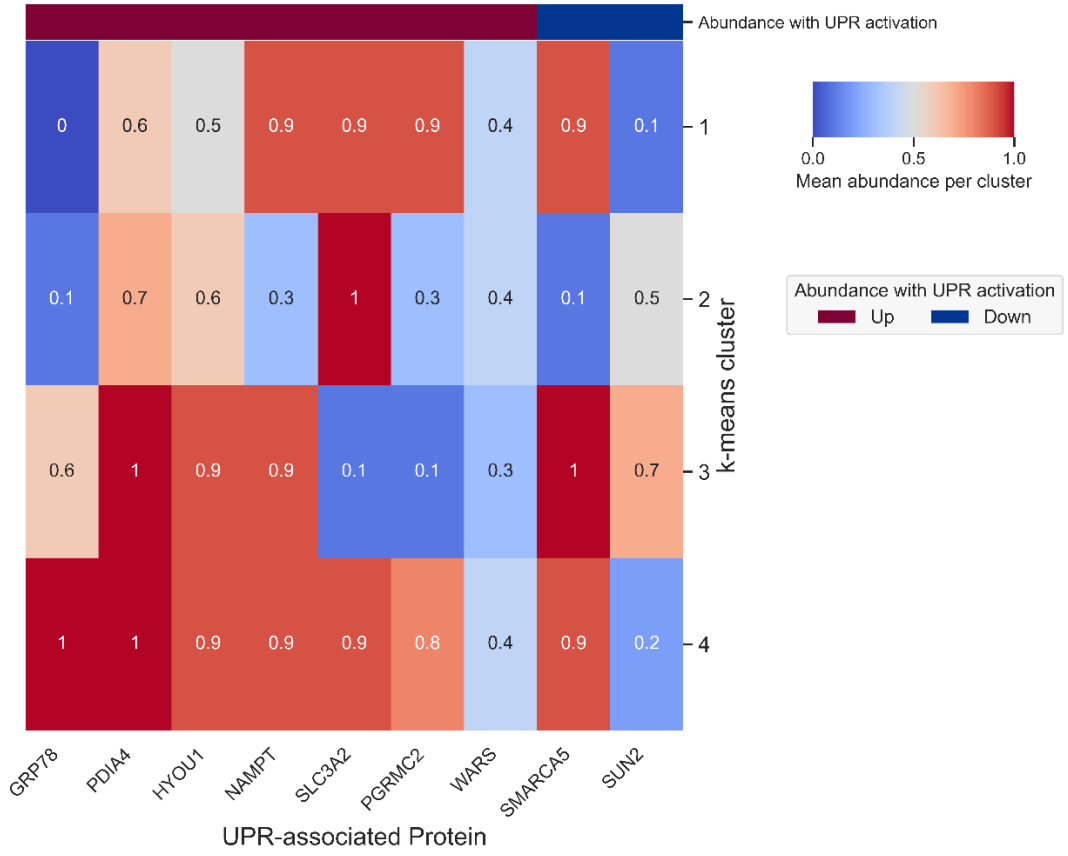

Figure 6-5. Clustering of melanoma patients into UPR-activation clusters based on RNA-Seq abundance levels of the eight **UPR-associated proteins.** RNA-Seq abundance levels of the eight UPR-associated proteins were analysed from 460 melanoma patients from the TCGA-SKCM cutaneous melanoma dataset. Clustering of the 460 melanoma patients was performed using k-means clustering, fitting the patients into four clusters based upon the abundances of the eight UPR-associated proteins. Abundance levels of the eight UPR-associated proteins in RNA-Seq patient data correlated with the cell lines model of UPR activation discovered in previous chapters. Cluster 4, characterised by high GRP78 levels and therefore high UPR activation, has abundance levels of PDIA4, HYOU1, NAMPT, SCL3A2, PGRMC2 and SUN2 from patient transcriptomic data that correlate with the proteomic cell lines model of UPR activation.

Unsupervised hierarchical clustering of the 460 stage I-IV melanoma patients was then performed using the transcriptomic data from the TCGA melanoma dataset (TCGA-SKCM) for the eight UPR associated targets. Correlating the clusters with the abundance of GRP78, the master regulator of the UPR, patients broadly cluster into groups of high (Clusters 3 and 4) and low (Cluster 1 and 2) UPR activation (**Figure 6-6**). The correlation of the eight proteins with GRP78 levels, as observed with the proteomic data, again provides further evidence that these proteins are changed in abundance with increased UPR.

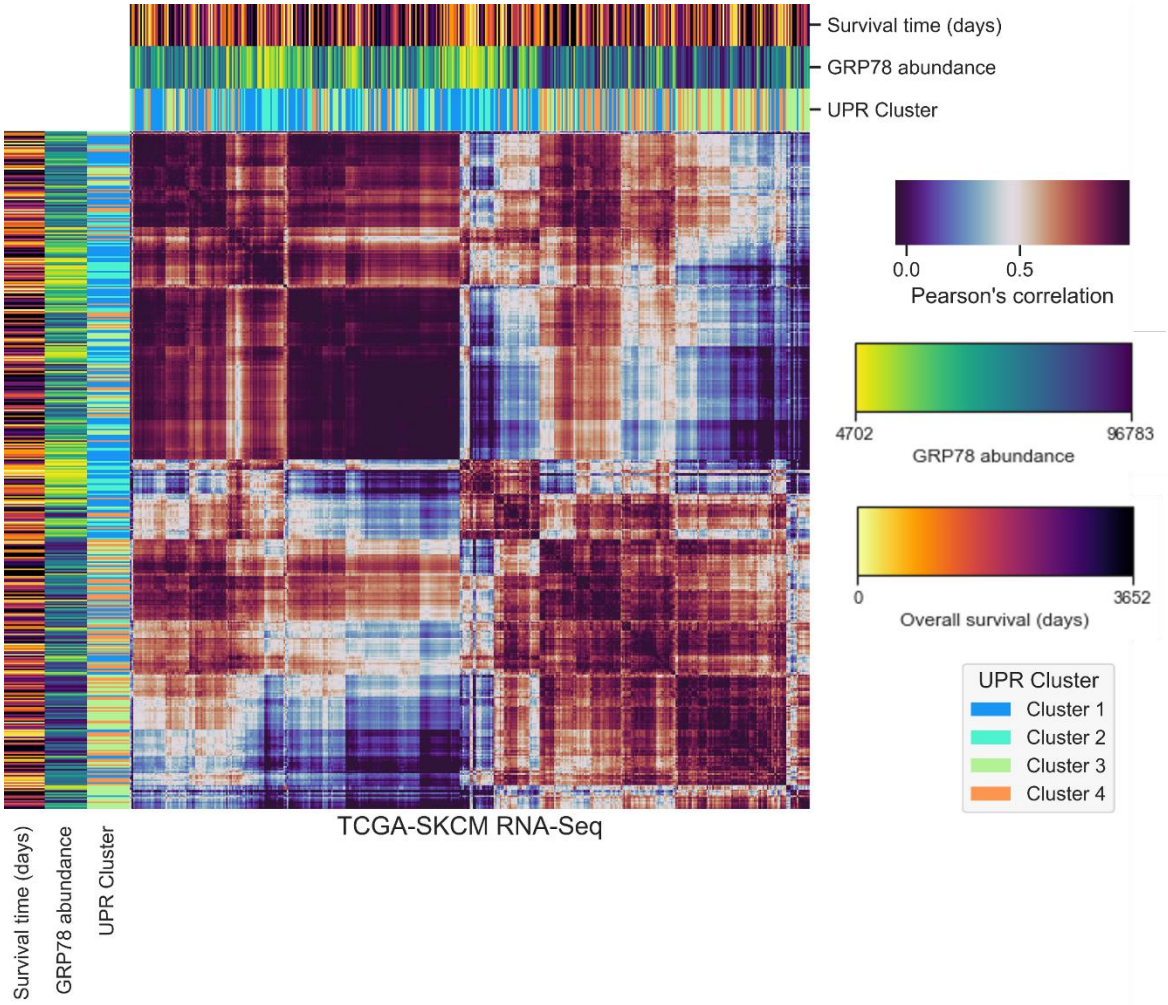

Figure 6-6. **Unsupervised correlation clustering of RNA-Seq data from 460 melanoma patients based on the abundance of the eight UPR-associated proteins and GRP78.** Pearson's correlation was carried out between all 460 melanoma patients with RNA-Seq data for the 8-UPR associated proteins. Unsupervised clustering was used to reveal UPR-activation groupings correlating with GRP78 abundance and with the k-means clusters (**Figure 6-5**) representing UPR activation in melanoma patients.

Due to the known association of the UPR with melanoma progression and metastasis, the eight UPR-associated proteins found to be differentially abundant with increased UPR activation were examined for their potential correlation with overall survival in melanoma patients. When used collectively, the RNA-Seq abundance levels of the eight UPR-associated proteins did not correlate with overall patient survival (**Figure 6-6)**. However, univariate Cox proportional hazard testing revealed that two of the 8-UPR associated proteins have significant prognostic predictive ability in transcriptomic data for melanoma patients, with increased levels of SLC3A2 and decreased levels of WARS associated with poor prognosis (**Figure 6-7 and Figure 6-8**). SLC3A2 has a hazard ratio of 1.733 (95% CI 1.22-2.45), meaning increased mRNA abundance of this target increased the risk of a patient having a poor outcome by 73.3%, with both significant *p*-values (<0.005) and Wald z-score (3.05). WARS had a hazard ratio of

0.517 (95% CI 0.30-0.70), showing patients had a 48.3% increased risk of a poor outcome with decreased WARS mRNA abundance (*p*-value <0.005, z-score=4.36).

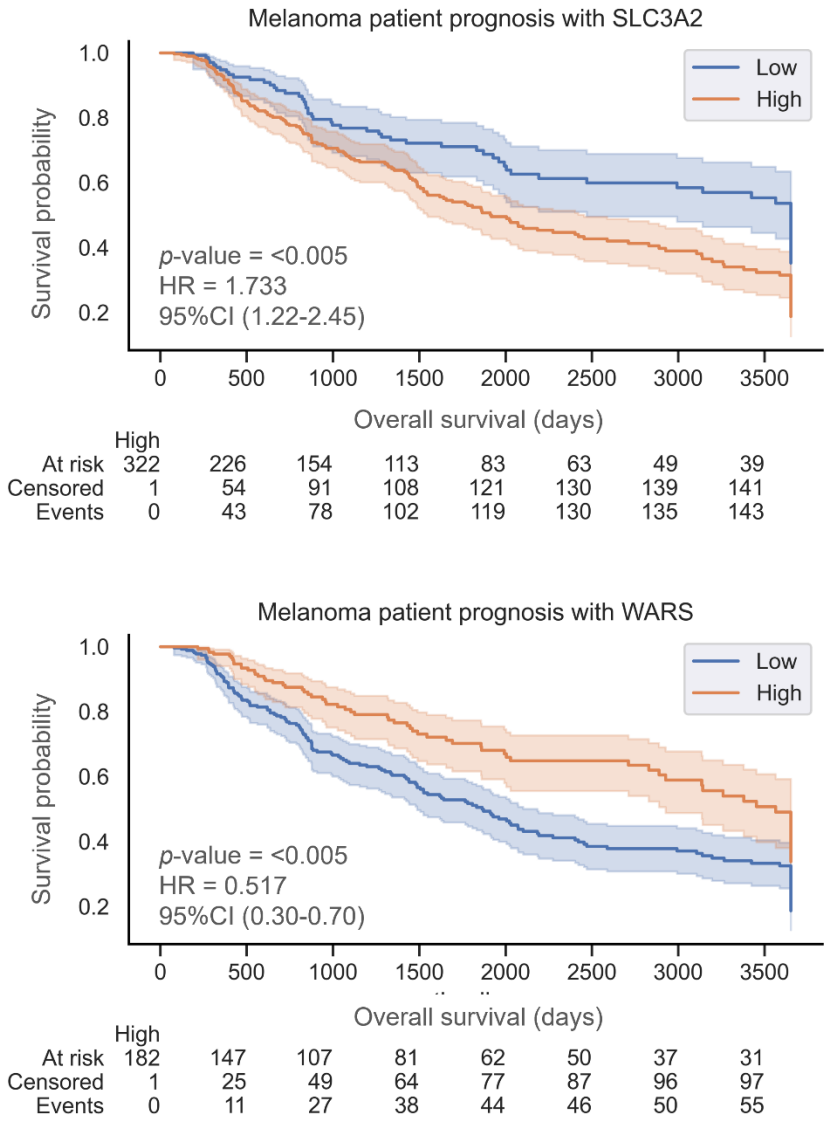

Figure 6-7. **Kaplan-Meier curves of two of the eight UPR-associated proteins, SLC3A2 and WARS, are predictive of poor prognosis in melanoma patients.** Transcriptomic data from 460 melanoma patients from stages I-IV was analysed for a correlation with UPR-associated proteins and patient outcome. Patients were divided into high and low expression groups with overall survival used as a binary outcome. Univariate Cox proportional hazard testing was performed used RNA-Seq abundance levels of the eight UPR-associated proteins. The table below each plot lists the number of patients with high abundance levels for the target at each time interval of 500 days. In the table, at risk is the number of patients alive, events are the number of patients that died specifically from melanoma and censored is the number of patients removed from the analysis due to causes such as unknown cause of death or no follow-up. As shown by the KM plots, the RNA-Seq data revealed that SLAC3A2 and WARS are significantly predictive of patient overall survival. Increased abundance of SLAC3A2 and decreased levels of WARS are associated with poor outcome, *p*-value < 0.005.

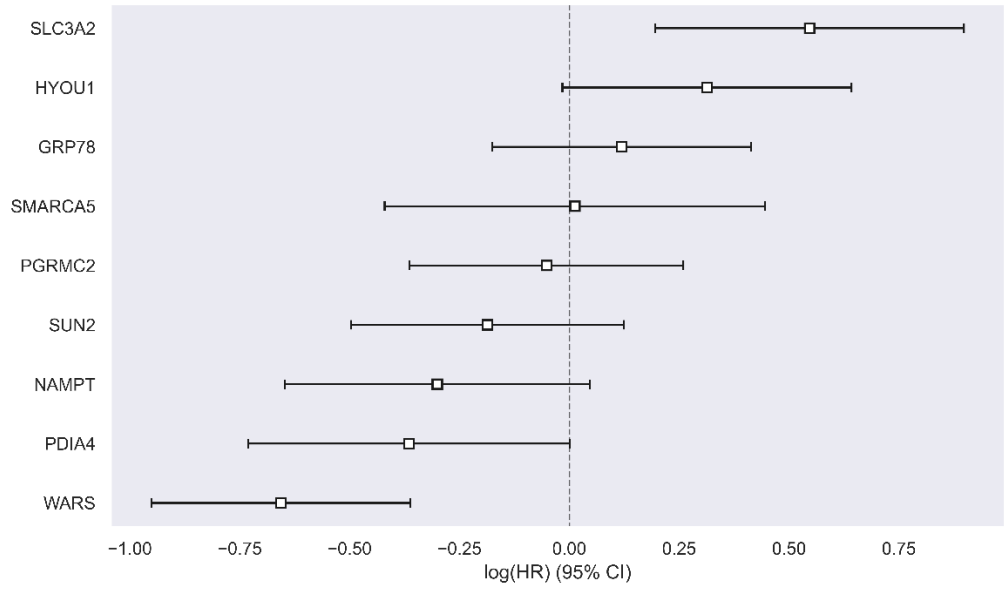

Figure 6-8: **Hazard ratios of the ability of the eight UPR-associated proteins from cell line models to predict melanoma patient outcome from RNA-Seq data.** The ability of the eight UPR-associated proteins derived from melanoma cell line models to predict patient survival outcome was tested using transcriptomic data from 460 melanoma patients from stages I-IV. Patients were divided into high and low expression groups for each of the eight UPR-associated proteins and overall survival was used as a binary outcome. Univariate Cox proportional hazard testing revealed that increased abundance of SLAC3A2 and decreased levels of WARS were significantly predictive of poor overall survival in patients, both *p*-value < 0.005 and HR=1.733 and 0.517, respectively.

6.3.5 Correlation of the eight UPR-associated proteins with survival from a pan-cancer transcriptomic dataset - Human Protein Atlas

To broaden the investigate of the importance of the eight UPR-associated proteins differentially abundant with UPR activation, the Human Protein Atlas (HPA) database was used for *in silico* validation on a pan-cancer scale. The database contains transcriptomic data on thousands of cancer patient samples, enabling the assessment of the UPR proteins identified in cell line models in progression and survival outcomes in cancer patients.

Mining the results from the independent survival analysis carried out by the HPA, of the eight UPR-associated proteins found to be differentially abundant with UPR activation in cell line models, five (HYOU1, NAMPT, PDIA4, SLC3A2 and WARS) were found to individually correlate with patient survival in one or more different cancer types (**Table 6-2**). Increased levels of HYOU1, NAMPT, PDIA4, SLC3A2 and WARS, were identified in the HPA survival analysis as correlating with poor survival in cancer patients shown in the table, with a 5-year overall survival threshold for good prognosis. Importantly, increased abundance of GRP78, the main regulator of ER-stress, which is increased with the UPR, also correlated with poor patient

survival for renal cancer. In addition to GRP78, three UPR-associated proteins (HYOU1, NAMPT and PDIA4) were all associated with poor patient survival in renal cancer.

In contrast, increased levels of PGRMC2, which were associated with increased UPR activation in cell line models, had a positive correlation with patient survival in endometrial and renal cancers, being associated with good patient outcome. For the proteins SUN2 and SMARCA5 no correlation to overall survival was seen in the transcriptome of patients of any cancer type.

Table 6-2. **Correlation of validated UPR proteins with overall survival of cancer patients using survival analyses of transcriptomic data from the Human Protein Atlas.** Survival analyses performed by the HPA using KM survival estimators carried out by the Human Protein Atlas with patients divided into groups for poor and good outcome based on 5-year overall survival. Changes in abundance of the 8 UPR-associated proteins were examined in the HPA survival analyses. Cancer in which the change in the correlated with the UPR cell line model and had a significant association with patient survival (p-value <0.001) are shown.

UPR-associated protein	Change in cell line UPR model	Cancer type with correlation to poor survival	Change in HPA with poor survival	Number of patients
HYOU1	Increased	Renal Cancer	Increased	877
		Thyroid	Increased	501
GRP78	Increased	Renal Cancer	Increased	877
NAMPT	Increased	Renal Cancer	Increased	877
		Pancreatic Cancer	Increased	176
		Cervical Cancer	Increased	291
		Head and Neck Cancer	Increased	499
PDIA4	Increased	Renal Cancer	Increased	877
		Glioma	Increased	153
SLC3A2	Increased	Urothelial Cancer	Increased	406
		Liver Cancer	Increased	365
WARS	Increased	Liver Cancer	Increased	365

6.3.6 Correlation of the eight UPR-associated proteins with patient survival from pan-cancer dataset - TCGA RNA-Seq data

Finally, the expression levels of the eight UPR-associated proteins were correlated with patient survival in the largest publicly available transcriptomic database from the TCGA. For the pan-cancer analysis sixteen tumour types were selected for investigation to expand the study and encompass the diverse tumour heterogeneity. The selection of data was made to include solid state tumours where the UPR has been shown to play a greater role in progression, common cancer types and cancer cohorts with sufficiently large patient numbers (>50 patients) to provide meaningful statistical analysis. The cohorts used in the pan-cancer analysis total 6,176 patients and include; bladder carcinomas (n=404), breast cancers (n=725), cervical

carcinomas (n=304), oesophageal adenocarcinomas (n=80), head and neck squamous cell carcinomas (n=499), renal clear cell carcinomas (n=530), hepatocellular carcinomas (n=370), lung adenocarcinomas (n=504), lung squamous cell carcinomas (n=495), ovarian carcinomas (n=373), pancreatic adenocarcinomas (n=177), rectal adenocarcinomas (n=165), sarcomas (n=259), stomach adenocarcinomas (n=247), thyroid cancers (n=502) and uterine endometrial carcinomas (n=542).

The prognostic value of GRP78 (**Figure 6-9**), HYOU1 (**Figure 6-10**), NAMPT (**Figure 6-11**), PDIA4 (**Figure 6-12**), PGRMC2 (**Figure 6-13**), SLC3A2 (**Figure 6-14**), SMARCA5 (**Figure 6-15**), WARS (**Figure 6-16**) and SUN2 (**Figure 6-17**) at predicting overall survival in patients with various tumour types was assessed. Each cancer cohort was divided into groups based on expression of the UPR-associated proteins then KM plots were used to compare overall survival of the high and low expression groups. KM plots for individual cancer types can be found in **Supplementary Figures S6-6** to **S6-14**. Cohorts with significant predictive values (**Figure 6-18**) were then grouped for the final analysis (**Figure 6-9** through **Figure 6-17**).

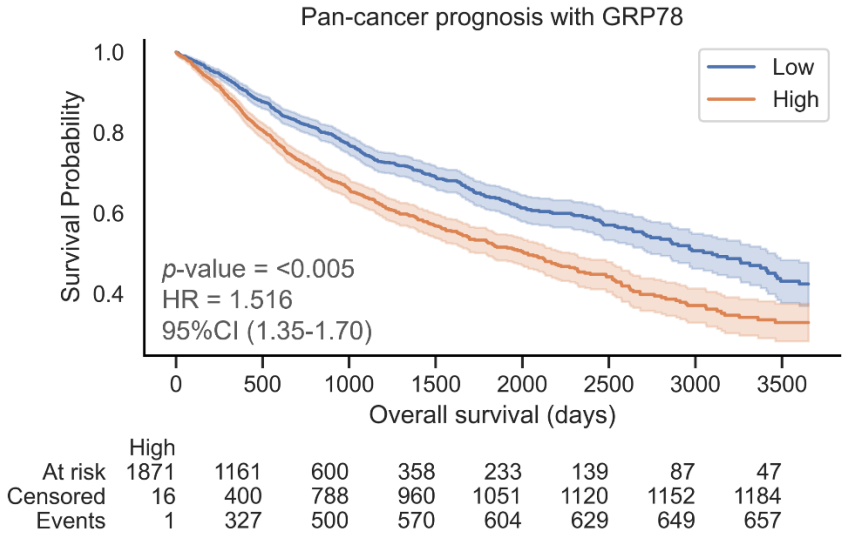

Figure 6-9. **Pan-cancer survival analysis with GRP78 abundance**. GRP78 as a predictor of survival in bladder adenocarcinomas, infiltrating breast carcinomas, cervical squamous cell carcinomas, head and neck squamous cell carcinomas, hepatocellular carcinomas, lung adenocarcinomas, lung squamous cell carcinomas and sarcomas utilising RNA-Seq and patient survival data from the TCGA (n=3,776 patients).

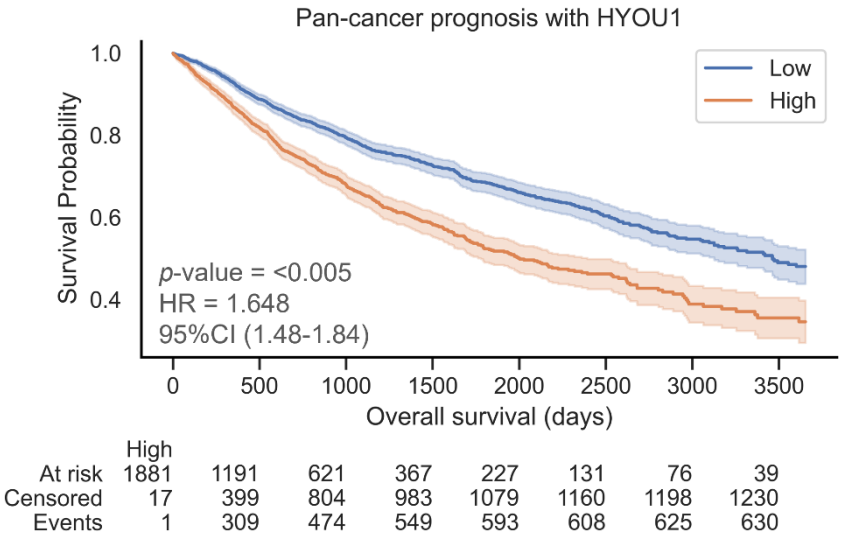

Figure 6-10. **Pan-cancer survival analysis with HYOU1 abundance**. HYOU1 expression as a predictor of survival in bladder adenocarcinomas, infiltrating breast carcinomas, cervical squamous cell carcinomas, head and neck squamous cell carcinomas, renal clear cell carcinomas, hepatocellular carcinomas, lung adenocarcinomas, lung squamous cell carcinomas, sarcomas and thyroid carcinomas utilising RNA-Seq and patient survival data from the TCGA (n = 4,747 patients).

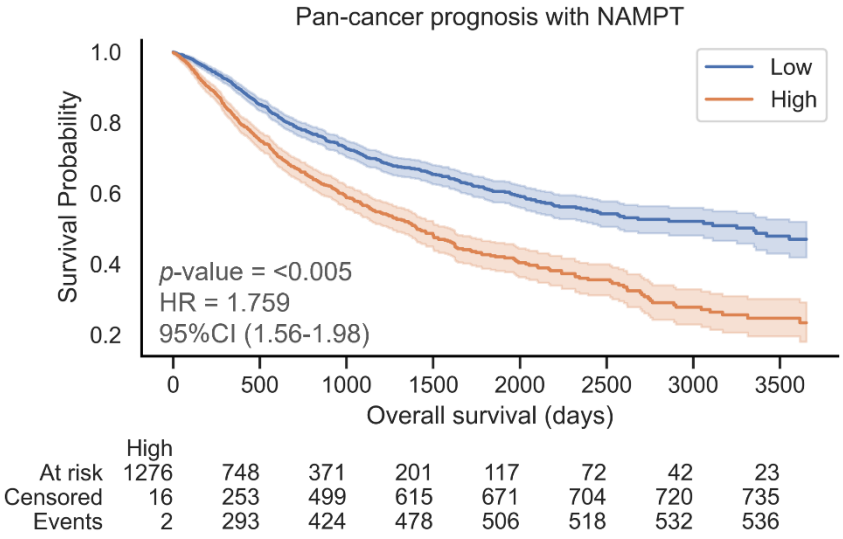

Figure 6-11. **Pan-cancer survival analysis with NAMPT abundance**. NAMPT expression as a predictor of survival in cervical squamous cell carcinomas, oesophageal adenocarcinomas, head and neck squamous cell carcinomas, renal clear cell carcinomas, lung adenocarcinomas, pancreatic adenocarcinomas, sarcomas, stomach adenocarcinomas and uterine carcinomas utilising RNA-Seq and patient survival data from the TCGA (n=3,235 patients).

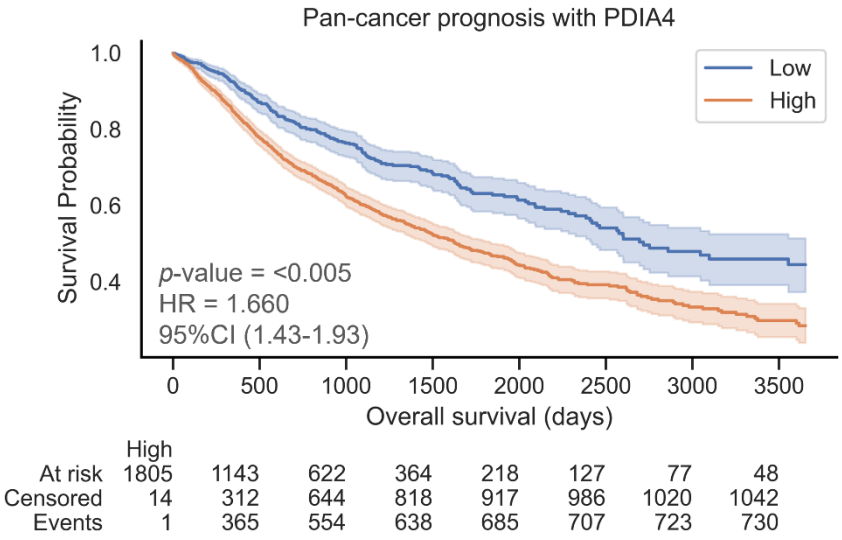

Figure 6-12. **Pan-cancer survival analysis with PDIA4 abundance**. PDIA4 expression as a predictor of survival in cervical squamous cell carcinomas, head and neck squamous cell carcinomas, renal clear cell carcinomas, lung adenocarcinomas, lung squamous cell carcinomas, pancreatic adenocarcinomas and sarcomas utilising RNA-Seq and patient survival data from the TCGA (n=2,600 patients).

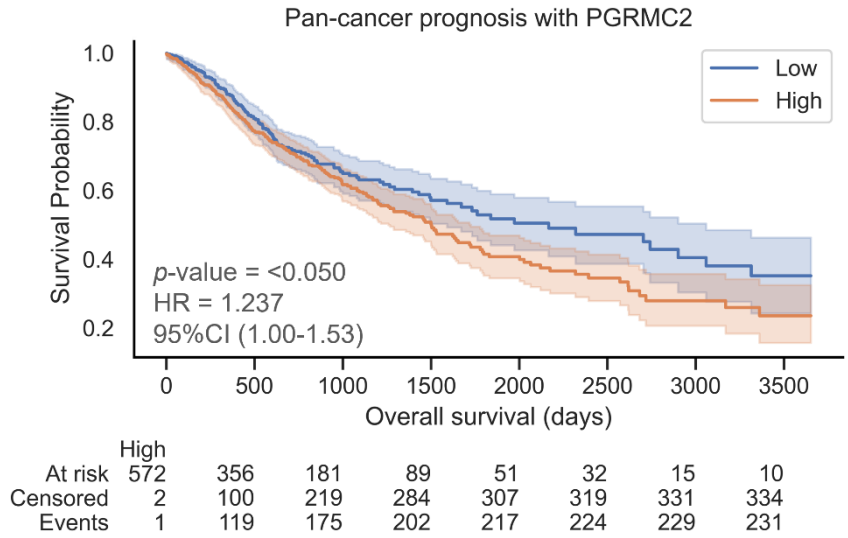

Figure 6-13. Pan-cancer survival analysis with PGRMC2 abundance. PGRMC2 expression as a predictor of survival in head and neck squamous cell carcinomas and lung adenocarcinomas utilising RNA-Seq and patient survival data from the TCGA (n=958 patients).

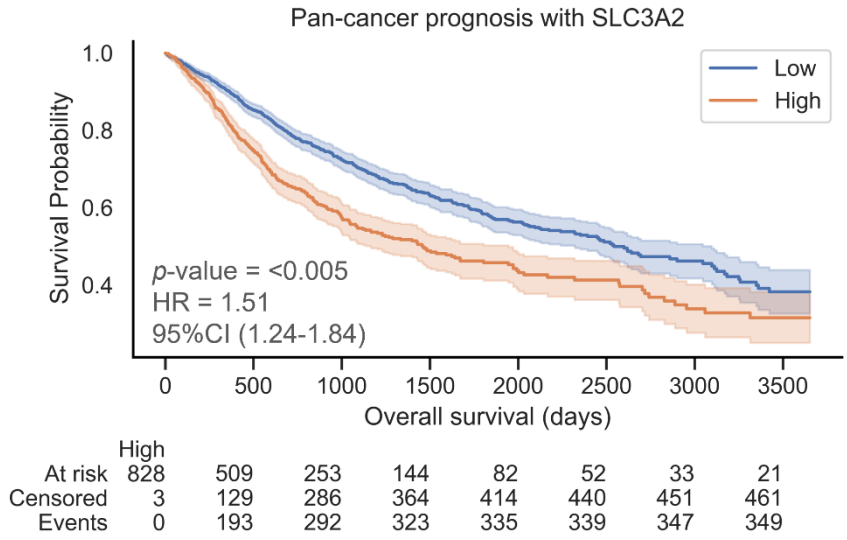

Figure 6-14. Pan-cancer survival analysis with SLC3A2 abundance. SLC3A2 expression as a predictor of survival in bladder adenocarcinomas, cervical squamous cell carcinomas, head and neck squamous cell carcinomas, hepatocellular carcinomas, lung adenocarcinomas, sarcomas and uterine carcinomas utilising RNA-Seq and patient survival data from the TCGA (n=2,769 patients).

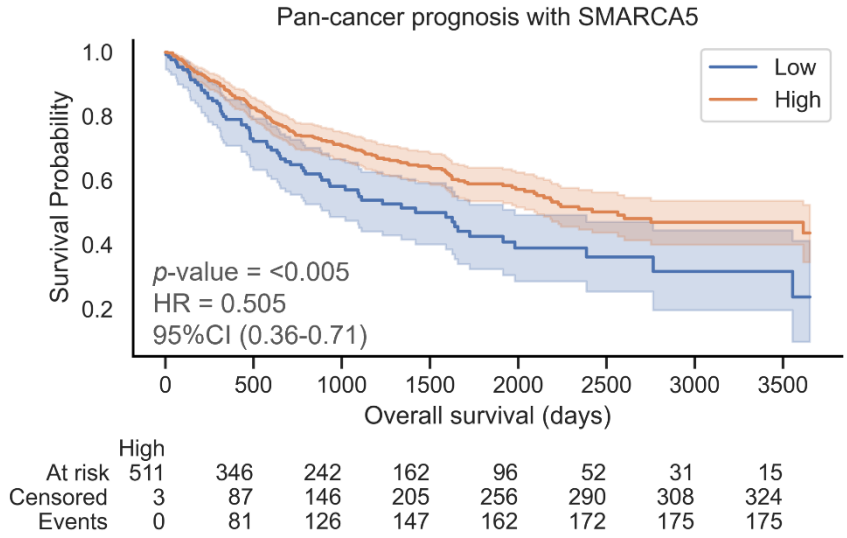

Figure 6-15. **Pan-cancer survival analysis with SMARCA5 abundance**. SMARCA5 expression as a predictor of survival in renal clear cell carcinomas and pancreatic adenocarcinomas utilising RNA-Seq and patient survival data from the TCGA (n=643 patients).

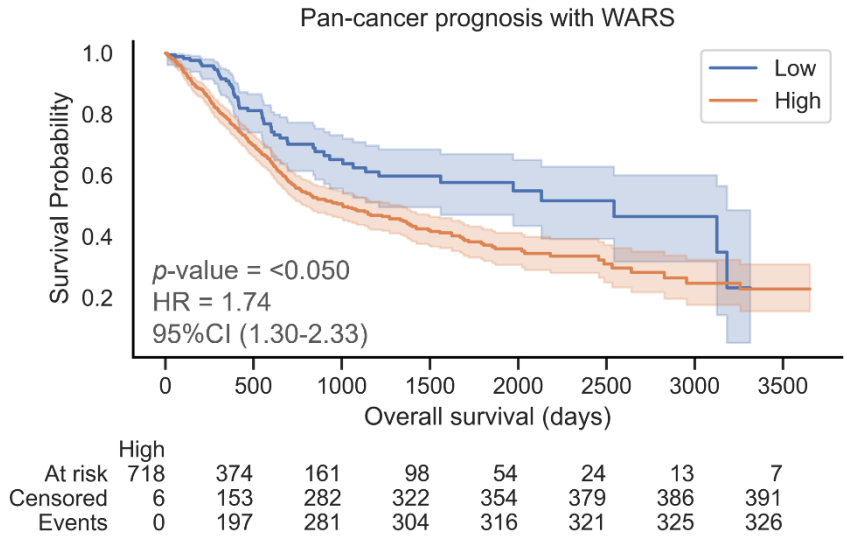

Figure 6-16. **Pan-cancer survival analysis with WARS abundance**. WARS expression as a predictor of survival in bladder adenocarcinomas, hepatocellular carcinomas and pancreatic adenocarcinomas utilising RNA-Seq and patient survival data from the TCGA (n=906 patients).

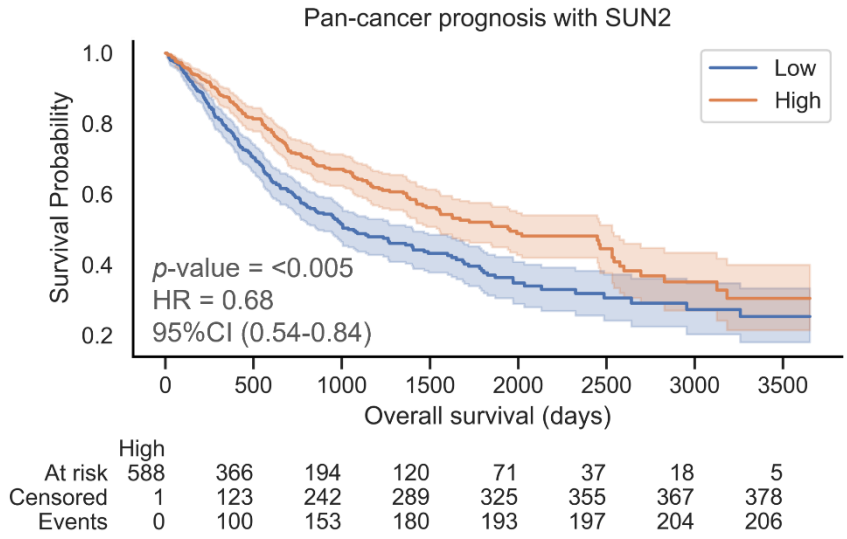

Figure 6-17. Pan-cancer survival analysis with SUN2 abundance. SUN2 expression as a predictor of survival in bladder adenocarcinomas, oesophageal adenocarcinomas, hepatocellular carcinomas and sarcomas utilising RNA-Seq and patient survival data from the TCGA (n=1,179 patients).

All eight UPR-associated proteins and GRP78 were predictive of overall patient survival in at least two cancer types. The prognostic value of the eight UPR-associated proteins were consistent with their protein abundance levels (up- or down-regulated) that were observed with increased UPR activation in the melanoma cell line models. (**Figure 6-18**). However, five of the eight plus GRP78 (HYOU1, NAMPT, PDIA4, SLC3A2, SUN2, and GRP78) were the most predictive across cancer types and had the greatest number of positive correlations with elevated GRP78 as a measure of UPR activation UPR activation.

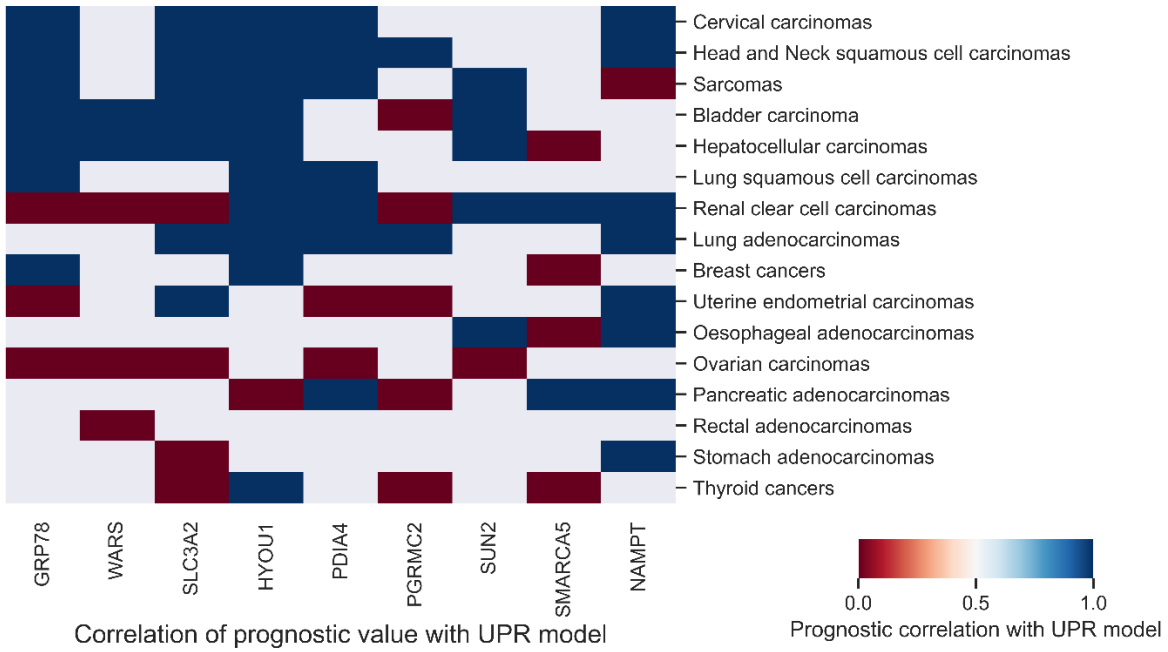

Figure 6-18. Prognostic ability of eight UPR-associated proteins and GRP78 at predicting overall survival in cancer patient RNA-Seq data and its correlation to the UPR activation cell line model. Individual UPR-associated proteins were analysed by KM plots to determine their prognostic value for overall survival in cancer patients of 16 tumour types. UPR-associated proteins were considered prognostic with log rank *p*-values <0.05. Proteins targets which had significant prognostic value and protein abundance correlates with the UPR cell line model. Protein targets with significant prognostic values but abundance levels with negative correlation with the UPR cell line model are shown in red. Blank values indicate no significant prognostic value.

The ability of the subsets of the UPR-associated proteins to predict patient outcome was stronger in certain cancer types; head and neck squamous cell carcinomas, lung adenocarcinomas, sarcomas, cervical carcinomas and hepatocellular carcinomas, suggesting that the UPR has a more prominent role in progression for these cancers (**Figure 6-18**). The correlation between the prognostic values of the eight UPR-associated proteins relative to the trend in abundance expected with activation of the UPR is shown in **Figure 6-19**. Overall, the eight UPR-associated proteins were prognostic and matched the abundance pattern of UPR activation in 53 incidences across all 16 cancer types.

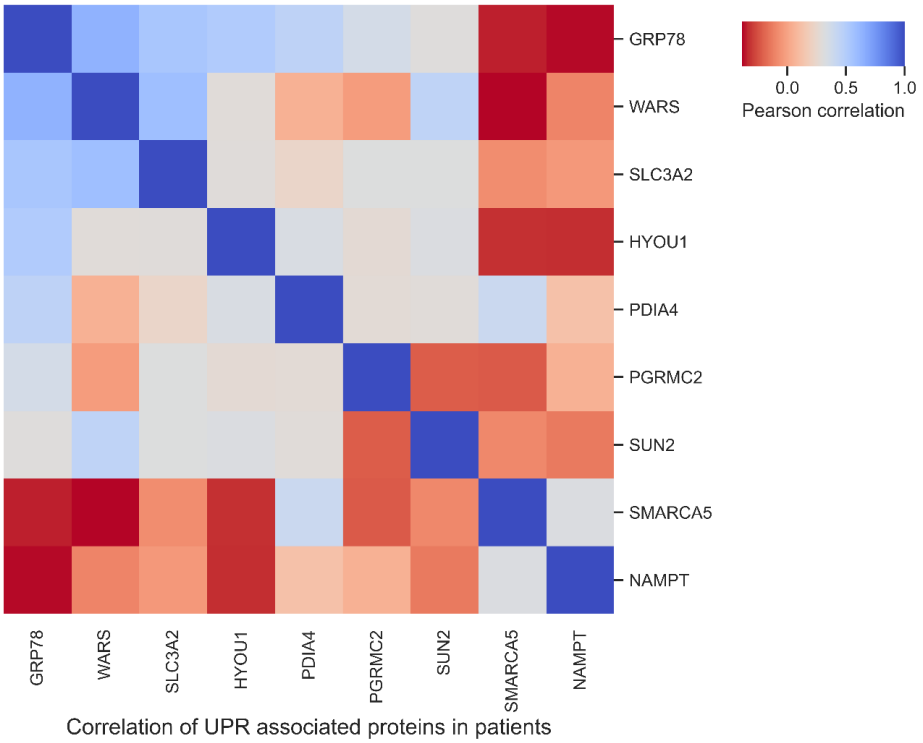

Figure 6-19. Correlation of the eight UPR-associated proteins with prognostic value in cancer patients from the TCGA RNA-Seq dataset. The correlation of the prognostic value of the eight UPR-associated proteins in all 6,176 cancer patients independent of cancer type with RNA-Seq data from the TCGA.

6.4 Discussion

In recent years, the study of cancer has moved into an era of big data. Historically, -omic studies utilising genomics, transcriptomics or proteomics have always been handicapped by cancer heterogeneity and the need for large cohort numbers to clarify the wide biological variability seen across cancer, even of the same tumour type. This has seen an increase in recent years towards large pan-cancer multi-omic studies, that seek to provide new insights into cancer biology by identifying patterns that would be invisible in smaller cohorts.

Many of these pan-cancer studies have also attempted to reshape the way in which cancers are classified into tumour types [545-547]. Cancer is currently classified by a pathologist into cancer types and subtypes, based on the location of the primary tumours and cell type of origin. For example, lung adenocarcinoma are cancers that have arisen from cells within the lung of an epithelial lineage or in the case of cutaneous melanoma, melanocyte cells within the epidermis. This classification has seen most cancer studies siloed by cancer types. Molecular clustering seeks to reclassify cancers based on the major pathways or mechanisms that exhibit dysfunction or are exploited in a single cancer regardless of the cell type of origin [547, 548]. Molecular clustering has the potential to reshape the way in which cancers are classified and seeks to explain the vast heterogeneity of tumours. The eight UPR-associated protein identified here are a potential core functional cluster of proteins that could be used as markers of UPR activation in cancer.

This *in silico* analysis performed in this Chapter capitalises on the accumulated knowledge to strengthen the findings from Chapter 3, 4 and 5. Select proteins found to be differentially abundant (1.5-fold change, *p*-value <0.05) with increased activation of the UPR in melanoma cell lines treated with thapsigargin discovered in Chapter 4 with iTRAQ analysis were independently confirmed with a range of proteomic techniques including Western blotting, fluorescence microscopy and SRM mass spectrometry. The change in abundance of eight proteins were validated to be differentially abundant with increased ER-stress and activation of the UPR. Six of the proteins were increased in abundance (HYOU1, NAMPT, PDIA4, SLC3A2, PGRMC2 and WARS), while two proteins were decreased (SMARCA5 and SUN). In this Chapter, the outcomes from the melanoma cell line model of UPR activation was tested in patient data. The eight UPR-associated proteins were the focus of further *in silico* bioinformatic analysis utilising publicity available proteomic and transcriptomic data, to characterise the relationship between the UPR and cellular response to MEKi's and the association of the UPR with patient survival outcomes.

6.4.1 UPR as a marker for MEK inhibitor resistance

As outlined in Chapter 1 there is known reciprocal activation of the UPR and Ras/Raf/MEK/ERK signalling. As discussed previously, this relationship could potentially be exploited with combinatorial therapies targeting BRAF/MEK and UPR pathways. To test if any of the 64 UPR-associated proteins discovered in Chapter 4 are associated with MEKi sensitivity, publicly available proteomic data from 10 melanoma cell lines, characterised for MEKi sensitivity were analysed. From the analysis of the SWATH-MS data, changes in abundance of seven UPR-associated proteins (ATPA, PDIA4, ENPL, GRP78, ROA2, HMGA1 and ACTN4) were found to correlate with MEKi sensitivity and were able to separate the cell lines into sensitive or resistance clusters. As such these seven UPR-associated proteins are potential markers for MEKi treatment selection.

The current treatment for metastatic melanoma is combinatorial BRAF inhibitors (BRAFi) and MEKi's for mutant-BRAF malignancies or immunotherapies targeting PD-1 and CTLA4. For patients with mutant-BRAF melanomas the ASCO guidelines currently recommend one of three combinatorial BRAFi/MEKi treatments; dabrafenib/trametinib, encorafenib/binimetinib and vemurafenib/cobimetinib [549]. Immunotherapies, pilimumab plus nivolumab, nivolumab alone, or pembrolizumab as a single agent, are also equally recommended for both mutant and wildtype BRAF melanoma [549]. Treatment selection between these therapies is based upon BRAF mutational status, patient comorbidities and overall health, previous treatments and predicted toxicity to treatment. However, there is no accurate predictor of which patients will have better outcome under which treatment [103]. The correlation found here between activation of the UPR and MEKi inhibitor sensitivity (**Figure 6-1** and **Figure 6-2**) in melanoma cell lines bears further studies in patients. If the findings are consistent with patient melanomas, it could prove to be a valuable contribution to screen for patients likely to respond to therapies targeting MEK signalling by utilising downstream effectors of the UPR as biomarkers. Furthermore, the results reported here also lend weight to the therapeutic strategy proposed in Chapter 3, to combinatorially target MAPK signalling and the UPR. Similar to triplet treatment strategies combining BRAFi, MEKi and PD-1 targeted immunotherapies, that have demonstrated increased survival benefits in late-stage melanoma patients, targeting the Ras/Raf/MEK/ERK pathway with BRAFi and MEKi while also targeting the UPR could potentially exhibit increased drug efficacy.

6.4.2 UPR-activation clusters

Utilising publicly available proteomic and transcriptomic data, the 66 UPR-associated proteins previously discovered, particularly the subset of eight UPR-associated proteins validated by SRM, can be used to identify cancers with high levels of UPR activation as inferred from GRP78 levels. As seen with unsupervised clustering of SWATH-MS and RNA-Seq data, patient tumours could be separated into groups based on GRP78 levels used as a marker of UPR activation (**Figure 6-4** and **Figure 6-6**). Interestingly, in the proteomic data from stage III melanoma patients when using a subset of 10 UPR-associated proteins, two patients can be distinguished with high levels of GRP78 but low levels of UPR activation (**Figure 6-4**). In the larger TCGA RNA-Seq cohort, which is better able to encompass cancer heterogeneity, patients were clustered into high and low UPR-activation groups based on the eight UPR-associated proteins, supporting the hypothesis from the cell line models in Chapter 4 and 5 that these proteins are consistent effectors of the UPR (**Figure 6-6**).

The eight UPR-associated proteins consistently modulated by the UPR in cell line models were examined in other cancer types in a pan-cancer *in silico* analysis. Comparing the levels of UPR-associated proteins across 6,176 patients, WARS, SLC3A2, HYOU1 and PDIA4 were positively correlated and NAMPT and SMARCA5 negatively correlated both with GRP78 and with the other UPR-associated proteins (**Figure 6-19**). Again, supporting the hypothesis that the eight UPR-associated proteins may be modulated in response to activation of the UPR across a broad range of cancer types beyond melanoma. The clustering is by no means perfect, possibly reflective of the diversity of this stress response with cancer heterogeneity.

These findings highlight the strength of using molecular pathways as single biomarkers or to characterise cancer phenotypes. Cell signalling acts cumulatively to produce a specific phenotype, often exhibiting a high degree of redundancy within pathways to produce the same molecular outcome within the cell. The analysis of large multi-cohort studies has challenged the traditional pathological classification of cancers [287, 546]. Cancers, regardless of their pathological category, often exploit the same molecular pathways to gain oncogenic potential and a neoplastic phenotype [545, 547, 548, 550]. However, enormous heterogeneity exists within tumours, with various ways to exploit the same pathway and numerous different combinations of oncogenic signalling contributing to a single phenotype. Molecular clusters, similar to the UPR cluster found here, can group cancers according to molecular dysfunction

and which pathways particular cancers rely most heavily upon for growth and survival. This molecular classification not only gives new biological insights into cancers but can also be used for treatment selection for individual patients. A pan-cancer study using genomic mutational data was able to classify cancers according to nine functional mutational clusters [545]. Another study utilising both proteomic and genomic data was able to classify cancers into eleven clusters based on the molecular profiles [548].

6.4.3 UPR-associated proteins as markers of patient prognosis in melanoma

As the elevated activation of the UPR is known to correlate with poor outcome in many cancer types including melanoma, the eight UPR-associated proteins were examined as markers for prognosis in both proteomic and transcriptomic melanoma datasets. The proteomic data comprising SWATH-MS analysis on 32 stage III melanoma patients was not able to correlate the eight UPR-associated proteins with patient outcome (**Figure 6-3** and **Figure 6-4**). This could be a due to an incorrect hypothesis; that the eight UPR-associated proteins are not consistent, key modulators of the UPR across tumours. It is most likely a result of cancer heterogeneity and small cohort size being unable to provide statistically significant results. In contrast, analysing the TCGA melanoma dataset with transcriptomic data on 460 melanoma patients from stage I-IV, two of the UPR-associated proteins were found to be strong predictors of melanoma patient survival. Increased expression of SLC3A2 and decreased expression of WARS were markers of poor outcome in melanoma patients (**Figure 6-7** and **Figure 6-8**).

Increased levels of SLC3A2 as a marker of poor overall survival in patients correlates with the previous observations in Chapter 4 and 5, in which SLC3A2 protein abundance increased with activation of the UPR as discovered through iTRAQ (**Table 4-2**), validated with SRM (**Table 5-1**) and was observed to localise to invasive plasma membrane structures with fluorescence microscopy (**Figure 5-4**).

Decreased levels of WARS was prognostic of poor overall survival in melanoma patient transcriptomic data, which is the opposite of its abundance levels with UPR activation, WARS was found to increase in abundance in response to ER-stress in cell lines with both iTRAQ and SRM. However, decreased abundance of WARS is one of the markers in the 14-protein prognostic panel for stage III melanoma patients quantitated by SRM (**Figure 3-2**). Therefore, both transcriptomic and proteomic data correlate in melanoma patients. The discrepancy seen

in the data between melanoma cell lines and patient samples, could be due to the diverse functionality of WARS. WARS functions as an immune modulator, regulates angiogenesis and lymphogenesis and alters metabolism, eliciting these different roles through its five structural domains, alternate splicing, proteolytic cleavage and PTMs [497-500]. The difference seen in the cell line versus patient data is potentially due to the effects of the tumour microenvironment (TME), which is not modelled for in cell line studies. Secretion of full-length WARS into the TME mediates increased immune activation via macrophage chemokine release [500]. Therefore, decreased levels of WARS would assist in immune evasion. Additionally, secreted WARS is cleaved proteolytically in the TME into the protein fragment T2-WARS [499]. T2-WARS inhibits VEGF, acting as an angiostatic factor thereby preventing endothelial cell proliferation. Decreased WARS would therefore allow for greater tumour angiogenesis and promote tumour metastasis. To determine the exact role of WARS in the UPR and melanoma progression, more detailed studies are required to characterise the molecular status of this protein, including its spliced isoform, cleavage state and any PTMs, all of which lead to altered functionality of this protein. WARS was potentially not detected as a prognostic marker in the SWATH-MS data due to the less sensitive and reproducible nature of this technique compared to SRM.

The large cohort size used in the transcriptomic data analysis highlights the diversity of the UPR, with four major clusters observed using only the eight UPR-associated proteins examined here (**Figure 6-6**). The approach used here shows the potential utility of molecular clusters comprising multiple marker panels over a single biomarker for diagnosis, prognosis and treatment selection in cancers. Furthermore, this work highlights a novel approach which could be employed in future biomarker panels, utilising the activation or deactivation of whole molecular pathways as single markers within a larger panel rather than individual proteins. For example, in the case of the UPR, the eight UPR-associated proteins could be used together to determine the activation state of the UPR within a tumour, then the activation state of this whole molecular mechanism would represent a molecular cluster that could be used collectively as a single marker within a panel in combination with other molecular biomarkers such as activation of MEK/ERK. This strategy could potentially overcome cancer heterogeneity in which neoplasms can use diverse measures to achieve the same molecular outcome.

Interestingly, a good correlation exists between the abundance levels measured by transcriptomic and proteomic techniques for UPR-associated proteins. Several meta-studies

comparing proteomic and transcriptomic data have found a poor overall correlation between abundance levels but a general concordance of up- or down-regulation [551, 552]. The correlation between the mRNA and proteins could be due to two of the major mechanisms of regulation of the UPR being exerted at the transcriptional level through global suppression of mRNA synthesis and selective mRNA degradation.

6.4.4 UPR-associated proteins as markers of patient prognosis in a pan-cancer analysis

The eight UPR-associated proteins plus GRP78 were examined in TCGA transcriptomic data for 16 solid tumour types to determine if the UPR had a role in cancer progression in other cancer types. All of the UPR related proteins were predictive of patient prognosis in at least two different cancer types (**Figure 6-9** through **Figure 6-17**). Several cancer types appear to be more highly reliant on the UPR, utilising this stress response in cancer progression: head and neck squamous cell carcinomas, lung adenocarcinomas, sarcomas, cervical carcinomas, bladder carcinomas and hepatocellular carcinomas (**Figure 6-18**). The reliance of these cancers on the UPR and as a predictor of poor prognosis can be seen in other studies for head and neck SCC [553-556], lung adenocarcinomas [557-559], sarcomas [560, 561], cervical carcinomas [562, 563], bladder carcinomas [564-567] and hepatocellular carcinomas [568-571].

Proteins HYOU1, GRP78, NAMPT, PDIA4 and SLC3A2, were more strongly associated with poor prognosis across numerous cancers. These five UPR-associated proteins had the greatest prognostic ability across the widest range of cancer types while positively correlating with abundance changes associated with activation of the UPR discovered in previous chapters (**Figure 6-18**). These findings suggest the five proteins are integral for perpetuating the pro-survival and pro-proliferative branches of the UPR, although the contribution of other proteins is not excluded or diminished. Additionally, it is possible that the proteins are more consistently modulated in the activation of the UPR across cancer types and across individual tumours. The functions of these proteins and their potential contribution to cancer progression is discussed in Chapter 5.

The use of large cohorts is critical when validating biomarkers in heterogenous diseases like cancer. Currently, large pan-cancer cohorts exist for genomic and transcriptomic data. As proteomic technologies improve, bringing high-throughput technology coupled with standardisation of the field, an increase in large proteomic datasets has been possible. In the

coming years publicly, available proteomic data will approach that of transcriptomic and genomic datasets, giving new large-scale insights into cancer biology. The use of these pan-cancer datasets are not without issue. For example, in the above study, overall survival was used as the endpoint for prognosis across the various cancer types. However, overall survival is not of clinical relevance at follow-up for some cancer types, resulting in discrepancies when comparing across different cancers [287].

6.5 Conclusions

The discoveries made in proteomic data of cell line models in Chapters 4 and 5 have been explored further with bioinformatic analysis for their relationship with drug resistance and patient survival. Examining publicly available proteomic data on melanoma cell lines with varying MEKi sensitivity, a relationship was observed between the UPR-associated proteins and response to MEKi's. Seven of the UPR-associated proteins were able to cluster samples by drug sensitivity, revealing a potential for these proteins as markers for MEKi treatment selection in patients.

Publicly available melanoma patient proteomic data revealed the abundance of 10 UPR-associated proteins were correlated with UPR activation in a trend consistent with the cell line models from Chapter 4 and 5. These findings demonstrate the potential of translating results from *in vitro* models into patient data.

As is seen in a large number of biomarker studies, the proteomic data for melanoma patients suffered from a lack of statistical power due to small cohort size. Therefore, transcriptomic data for a melanoma and a pan-cancer cohort was analysed for an association between the core eight UPR-associated proteins and patient survival. In the melanoma patient transcriptomic data two UPR-associated proteins SLC3A2 and WARS were both predictive of patient outcome. While in the larger transcriptomic pan-cancer dataset of 6,176 patients, all eight UPR-associated were predictive of patient survival in two or more cancer types.

Chapter 7: Summary and future directions

7.1 Purpose of the study

Cutaneous melanoma is an aggressive tumour, with a 5-year survival rate of 61% and 26%, for stage III and stage IV disease, respectively. Melanoma is also one of the few remaining cancers with an increasing incidence rate, with an estimated doubling of new cases by 2040 [12]. While major advancements in the treatment of metastatic melanoma have occurred in the last decade, innate and acquired resistance remains a major issue. Currently, there are two therapeutic strategies used for the treatment of metastatic melanoma, MAPK inhibitors and immunotherapies. However, on average only 50% of melanoma patients will respond and only a small subset will go on to have longer term benefit. As such, new methods are needed that can identify patients that will respond to particular therapeutic strategies, especially given the serious side effects. Additionally, new novel drugs or drug combinations with increased efficacy are required to improve patient response and outcome.

The first aim of this study was to identify a protein panel able to distinguish stage III cutaneous melanoma patients that are likely to have poor outcome. For stage III melanoma patient, approximately half of patients will die from melanoma within 1 year after surgical intervention while the other half of patients will live beyond five years. A clinical test is required to identify patients likely to have poor prognosis and therefore require aggressive follow up treatment. Additionally, there is a need to prevent patients that do not require adjuvant treatment from receiving unnecessary therapies with serious detrimental side effects. SRM was selected to validate potential biomarkers identified in an earlier study, as the selectivity, reproducibility and robustness of this technique makes it suitable for clinical application [572, 573]. Utilising SRM on a stage III melanoma patient cohort, 10 proteins (GSTP1, Q59FC6, CCT7, MYL12A, PRDX3, GLU2B, ACTN4, PGK1, WARS and TNC) were orthogonally validated to be differentially abundant in Good (n=16, >4 years survival post-resection) and Poor (n=14, <2 years survival) prognostic groups. Combining these ten proteins with previously identified putative biomarkers, an SRM panel of 14-proteins was identified that could predict patients likely to have poor survival outcome of less than 1 year (*p*-value=0.00019). The 14-protein panel could be used in the future to identify patients likely to have poor outcome and therefore require aggressive therapeutic strategies post-resection.

From the 14-protein SRM panel derived from melanoma patient samples and previous work conducted in our laboratory, activation of the UPR was found to be increased in patients with poor outcome. These findings coupled with the known literature, the UPR was identified as a major contributor to melanoma progression. The UPR is known to play a role in cancer

progression and metastasis but how cancers exploit this widespread dynamic stress response is not well characterised. Therefore, the role of the UPR in melanoma progression was investigated with proteomic analysis utilising cell line models for ER-stress and the UPR. To mimic the induction of the UPR observed in patient melanoma samples, a melanoma cell line model of the UPR was successfully established with the drug thapsigargin. Quantitative proteomic analysis with iTRAQ labelling was employed to identifying proteins differentially abundant in melanoma cell line subcellular fractions with increased UPR activation. Of the 3,490 proteins identified, 561 were differentially abundant with thapsigargin treatment and increased UPR (p-value < 0.05, fold-change >1.5). A total of 66 unique proteins (71 proteins with 16 cytosolic, 28 nuclear and 27 mitochondrial) were differentially abundant in both melanoma cell lines with increased UPR activation. The identified differentially abundant proteins are involved in major cytoskeletal rearrangements, increased metabolic potential, altered mRNA and protein processing capacity, alterations to cell signalling pathways and apoptotic proteins. The pathways and mechanisms identified to be modulated by UPR activation in this model cell line system are known to contribute to cancer progression and metastasis. Furthermore, several potential novel mechanisms of UPR modulation were identified, including subcellular shuttling of GRP78 to the nucleus, metabolic regulation through NAMPT and cell cycle progression through CDK1. Further mechanistic studies are required to confirm these hypotheses and could contributing to our understanding of how the UPR carries out its homeostatic functions.

Orthogonal validation was performed to confirm the differential abundance of the proteins identified with shotgun mass spectrometry methodologies. A range of proteomics techniques were selected, Western blotting, fluorescence microscopy and chiefly, SRM mass spectrometry. The melanoma cell line model with thapsigargin treatment was expanded to include four melanoma cell lines, both primary and metastatic with mutant and wildtype BRAF. A core set of eight UPR-associated proteins were validated as differentially abundant across all melanoma cell line models. The eight UPR-associated proteins include six proteins with increased abundance (HYOU1, NAMPT, PDIA4, SLC3A2, PGRMC2 and WARS) and two proteins with decreased abundance (SMRCA5 and SUN2). These eight UPR-associated proteins which are consistently modulated across the four cell lines with increased UPR have biological significance for melanoma progression, increasing the proliferative and metabolic capacity, promoting drug resistance, favourably altering the survival/apoptotic balance, altering the tumour microenvironment and promoting cellular migration and invasion.

To address the shortcomings seen in many proteomic and biomarkers studies with small cohort size and lack validation cohorts, publicly available transcriptomic and proteomic data was used for *in silico* validation and bioinformatic analyses. To determine if the identified UPR-associated proteins, particular the core eight UPR-associated proteins, have potential utility as markers of progression and drug resistance. Seven of the total 66 UPR-associated proteins (ATPA, PDIA4, ENPL or HSP90B1, GRP78, ROA2, HMGA1, ACTN4) were found to be associated with MEKi resistance in melanoma cell line proteomic data. MEKi in combination with BRAFi is one of the two treatment options for metastatic melanoma, however resistance is a significant issue in gaining longer term benefit for patients. The seven UPR-associated proteins identified here could contribute to the future formation of a proteomic panel to select effective treatment for melanoma patients.

To determine if the differentially abundant proteins found in cell line models could be translated to patients, publicly available proteomic data from melanoma patients was analysed for the abundance of the 66 UPR-associated proteins. Nine of the 66 proteins (FBRL, ATPA5A1, SLC25A5, NAMPT, HYOU1, PDIA1, CKAP4, PDIA4, ENPL) from the cell line models correlate with UPR activation in melanoma patient samples. Demonstrating that the cell line model of UPR-activation established here and the resulting findings, are in part reflective of patient biology.

The core eight UPR-associated proteins were examined for an association with patient prognosis in melanoma and pan-cancer transcriptomic data. In melanoma patient RNA-Seq data (n=460), SLC3A2 and WARS were both predictive of patient outcome (*p-value* <0.005, HR=1.733 and 0.517, respectively). SLC3A2 expression levels in the RNA-Seq data correlated with abundance change observed in the UPR cell line model. However, WARS had the opposite change in expression level but did correlate with change in abundance found in the 14-protein SRM panel for melanoma patient prognosis. In the pan-cancer cohort transcriptomic data all eight UPR-associated proteins were significantly associated with poor patient outcome in two or more cancer types, with changes in expression being consistent with change in protein abundance seen in the cell line model of the UPR. Given what is known in the literature on the important role of the UPR in cancer progression, these findings highlight the potential utility of the eight UPR-associated proteins as biomarkers for patient prognosis in a broad range of cancer types.

7.2 Future directions

When the results from this study are combined with the known literature, described in the introduction, it is evident the UPR is exploited by cancers, particularly melanoma, to aid in progression and metastasis. The role of the UPR in cancer bears further study, particularly in large patient cohorts, to characterise its contribution to progression and to identify novel drug targets.

As discussed in Chapter 1 the UPR was the target of several clinical trials in various cancers. Agents that target the UPR in isolation have so far not been of significant benefit to patient outcome. As with most therapies, these UPR targeting agents may exhibit greater efficacy when used in combination with other therapies. Combinatorial drugs largely exhibit greater efficacy, have a larger proportion of responders and have decreased drug resistance. Given the reciprocal activation of the UPR and MAPK pathway, studies into combinatorial and potentially even synergistic drug action with UPR targeting drugs and BRAFi/MEKi should be explored. Additionally, biomarker that can select for cancers that exploit and rely on the UPR, such as the eight UPR-associated proteins identified in this study, could be beneficial in identify patients that would benefit from this combinatorial approach.

Cancer is a sum of its individual parts, with the cumulative action of numerous signalling pathways and enormous numbers of minute alterations to proteins contributing to a distinct phenotype. Many diagnostic tests and drug strategies fail to acknowledge this, for example targeting of mutant BRAF for inhibition in metastatic melanoma, as discussed in Chapter 1. Due to parallel signalling pathways and other cellular mechanism, downstream MEK and ERK were reactivated, resulting in many patients acquiring drug resistance and a more aggressive cancer phenotype. This is also seen in single biomarker screens, which fail to encompass the heterogeneity of cancers. This has led an attempt to reclassify cancer groups based on molecular clustering. Molecular clustering seeks to reclassify cancers based on the major pathways or mechanisms that exhibit dysfunction or are exploited in a single cancer regardless of the cell type of origin. Molecular clustering has the potential to reshape the way in which cancers are classified and seeks to explain the vast heterogeneity of tumours. A major example is the Pan-cancer Atlas, which profiled over 10,000 tumours from 33 cancer types, resulting in 29 papers classifying tumours based on key molecular features, common genetic mutations, epigenetic regulation patterns, immunogenic profiles and oncogenic signalling pathways [286, 546, 574-580]. Molecular clustering can also reveal novel drug targets and more importantly

could reshape the way in which treatments are selected for specific cancer patients, a step toward personalised medicine [581].

An example of where characterising the activation state of an entire molecular pathway would assist in treatment selection, is the use of BRAFi and MEKi in melanoma patients. Currently, melanoma patients are predicted to respond to BRAFi/MEKi treatment based upon BRAF mutational status. However, as discussed in Chapter 1, the MAPK pathway that these inhibitors target can be activated downstream, resulting in either innate or acquired resistance. Characterising the entire MAPK pathway and is associated adjacent pathways, could assist in identifying patients that would have innate resistance to BRAFi/MEKi and those that are likely to acquire resistance. This study identifies a core set of eight UPR-associated proteins that could potentially be used to identify which cancers exhibit a high level of UPR activation and are therefore likely reliant on exploiting the UPR as part of its neoplastic capacity. The eight UPR-associated proteins are therefore one such molecular cluster that could potentially be used to categorise a cancer and select an appropriate treatment. If such a selection criterion was employed for patients entering UPR targeting drug trials, which have exhibited little success to date (**Table 1-1**), greater patient response and success of the trails may be gained.

Characterising the role of the UPR in melanoma biology would greatly benefit from proteomic studies in patient samples, ideally in a large cohort. However, obtaining these large cohorts with well annotated data is often extremely difficult. Large pan-cancer studies layer together datatypes and datasets to provide a more comprehensive understanding of cancer biology. The most recent layer of data added into pan-cancer studies is proteomic datasets, which continue to grow as proteomics is more widely utilised and technologies advance [547, 550, 582]. As proteomic datasets continue to grow, reviewing earlier proteomic findings may help to validate the large amounts of research done in the field of cancer. An overwhelming number of protein biomarker studies have been published in recent years, the increase of which coincides with the advancement of proteomic technologies, particularly mass spectrometry and its uptake within the scientific community. Despite the large number of putative protein biomarkers identified, most have failed to enter the clinic. This is in large part due to the lack of validation studies required for clinical implementation, particularly for a heterogenous disease such as cancer. Other factors include improper study design, lack of comparison to current clinic standards and lack of clinically relevant aims [573, 583]. This is exemplified by the 1,000 plus manuscripts published every year in the field of proteomic biomarkers, a number

that continues to grow, yet the vast majority do not come close to meeting the requirements for clinical application [573].

The issue with the large number of unvalidated biomarkers in the literature exists to the extent that some experts in the field have suggested that further discoveries studies are no longer needed and that focus should be redirect to validating the plethora of putative biomarkers already reported in the literature [573]. To implement this proposed strategy, i*n silico* validation studies on large datasets can be implemented. These large-scale meta-analyses could help to identify candidates most likely to have biological relevance before larger scale validation studies are carried out. These large datasets are also key to understanding heterogenous diseases such as cancer particularly in detecting common pathways and mechanisms across cancer types and individuals, opening up the possibility for personalised medicine.

Due the issue of translating proteomic biomarker discovery into the clinical, several experts in the field have proposed strategies to help facilitate entry into the clinic. A clear clinical use must be outline, with the clinical need met by the biomarker clearly defined and clinical context of its use. A comparison to the current clinic biomarker or index must be implemented to show improvement over the current standard. And lastly but most challengingly, a plan for clinical implementation must be considered from the outset. This last point is considered the most challenging, especially as most researchers have no knowledge of the requirements for clinical translation. Assessing the clinical feasibility of a biomarker is costly and requires years to confidently evaluate its health benefit. To this end, it is suggested that early in the study multidisciplinary translation groups should be consulted comprising cancer biologists, clinicians, statisticians, health economists, representatives of patient groups, health insurance, pharmaceutical companies, biobanks, and regulatory agencies [583, 584].

It is widely agreed that quantitative proteomics with mass spectrometry should be implemented through targeted MS approaches, mainly SRM. While others propose a hybrid DIA and targeted approach like Parallel Reaction Monitoring (PRM), providing quantitation of high value targets while capturing information on the remaining proteome. SRM has several features which make it highly applicable for clinical quantitation, with SRM assays currently already in clinical use for small molecule screening, such as routine newborn screening for metabolic deficiencies. This MS technique is highly selective, specific and robust. The use of internal heavy labelled standards gives accurate identification and quantification of proteins,

while also ensuring inter and intra-laboratory reproducibility. Competing technologies for the application of proteomics in the clinic include O-link proximity extension assays, a single molecule protein microarray platform offered by Nautilus and CyTOF mass cytometry [585-587]. These platforms have some distinct benefits over SRM, the O-link proximity assay allows for signal amplification, the Nautilus protein microarray offers single molecular detection and CyTOF allows for protein localisation. Interestingly, these three platforms all rely on one or more antibodies for protein detection, which can lack reproducibility and use a single epitope for identification lending to reduced specificity. This lack of specificity depending on the antibody, lack of reproducibility and antibody batch variation, can lead to high rates of false negative and positives. For this reason, SRM which uses multiple peptides for both identification and quantitation has a distinct advantage.

Despite the challenges of clinical proteomic biomarkers, the collective implementation of the strategies outlined above with the numerous advancements made in the field, make its clinical application feasible. Improvements in rapid, robust sample preparation, peptide separation and sample introduction into the MS, more sensitive MS instrumentation, implementation of rigorous quality control measures and improved data analysis including the use of machine learning and neural networks, are collectively moving the field of proteomics towards the clinic. The marked advantage of proteomics is its ability to accurately quantify hundreds of proteins in a single screen, allowing for a more comprehensive understanding of a complex disease state, such as the UPR activation state of cancers proposed in this study. The ability of the proteome to explain complex disease phenotype, while also providing methods for accurate biomarker quantitation could prove to be enormously beneficially for the diagnosis, prognosis and treatment selection of cancer patients.

Reference list

1. Sykes, E.K., S. Mactier, and R.I. Christopherson, *Melanoma and the Unfolded Protein Response.* Cancers (Basel), 2016. **8**(3).
2. Sykes, E.K., et al., *A 14-Protein Signature for Rapid Identification of Poor Prognosis Stage III Metastatic Melanoma.* Proteomics Clin Appl, 2018. **12**(3): p. e1700094.
3. Schiaffino, M.V., *Signaling pathways in melanosome biogenesis and pathology.* Int J Biochem Cell Biol, 2010. **42**(7): p. 1094-104.
4. Upadhyay, P.R., T. Ho, and Z.A. Abdel-Malek, *Participation of Keratinocyte-and Fibroblast-derived factors in melanocyte homeostasis, the response to UV, and pigmentary disorders.* Pigment cell & melanoma research, 2021. **34**(4): p. 762-776.
5. Cronin, K.A., et al., *Annual report to the nation on the status of cancer, part 1: National cancer statistics*, N.c. statistics, Editor. 2022. p. 4251-4284.
6. Abdel-Malek, Z.A., A.L. Kadekaro, and V.B. Swope, *Stepping up melanocytes to the challenge of UV exposure.* 2010. **23**(2): p. 171-186.
7. Plettenberg, A., et al., *Human melanocytes and melanoma cells constitutively express the Bcl-2 proto-oncogene in situ and in cell culture.* Am J Pathol, 1995. **146**(3): p. 651-9.
8. Böhm, M., et al., *α-Melanocyte-stimulating hormone protects from ultraviolet radiation-induced apoptosis and DNA damage.* Journal of Biological Chemistry, 2005. **280**(7): p. 5795-5802.
9. Manga, P. and N. Choudhury, *The unfolded protein and integrated stress response in melanoma and vitiligo.* Pigment Cell Melanoma Res., 2021. **34**(2): p. 204-211.
10. Zhang, X.D., et al., *Mechanisms of resistance of normal cells to TRAIL induced apoptosis vary between different cell types.* FEBS Lett, 2000. **482**(3): p. 193-9.
11. Sung, H., et al., *Global Cancer Statistics 2020: GLOBOCAN Estimates of Incidence and Mortality Worldwide for 36 Cancers in 185 Countries.* 2021. **71**(3): p. 209-249.
12. Arnold, M., et al., *Global Burden of Cutaneous Melanoma in 2020 and Projections to 2040.* JAMA Dermatology, 2022. **158**(5): p. 495-503.
13. Balch, C.M., et al., *Final Version of 2009 AJCC Melanoma Staging and Classification.* Journal of Clinical Oncology, 2009. **27**(36): p. 6199-6206.
14. Keung, E.Z. and J.E. Gershenwald, *The eighth edition American Joint Committee on Cancer (AJCC) melanoma staging system: implications for melanoma treatment and care.* Expert Rev Anticancer Ther, 2018. **18**(8): p. 775-784.
15. Damsky, W.E., L.E. Rosenbaum, and M. Bosenberg, *Decoding melanoma metastasis.* Cancers (Basel), 2010. **3**(1): p. 126-63.
16. Moan, J., A.C. Porojnicu, and A. Dahlback, *Ultraviolet Radiation and Malignant Melanoma*, in *Sunlight, Vitamin D and Skin Cancer*, J. Reichrath, Editor. 2008, Springer New York: New York, NY. p. 104-116.
17. Østerlind, A., et al., *The Danish case-control study of cutaneous malignant melanoma. II. Importance of UV-light exposure.* Int J Cancer, 1988. **42**(3): p. 319-324.
18. *Genomic Classification of Cutaneous Melanoma.* Cell, 2015. **161**(7): p. 1681-96.
19. Matthews, N.H., et al., *Epidemiology of melanoma*. Exon Publications. 2017. 3-22.
20. Carli, P., A. Biggeri, and B. Giannotti, *Malignant melanoma in Italy: risks associated with common and clinically atypical melanocytic nevi.* J Am Acad Dermatol, 1995. **32**(5 Pt 1): p. 734-9.
21. Rhodes, A.R., et al., *Dysplastic melanocytic nevi in histologic association with 234 primary cutaneous melanomas.* J Am Acad Dermatol, 1983. **9**(4): p. 563-574.

22. Duray, P.H. and M.S. Ernstoff, *Dysplastic nevus in histologic contiguity with acquired nonfamilial melanoma: Clinicopathologic experience in a 100-bed hospital.* Archives of dermatology, 1987. **123**(1): p. 80-84.
23. Gruber, S.B., et al., *Nevomelanocytic proliferations in association with cutaneous malignant melanoma: a multivariate analysis.* J Am Acad Dermatol, 1989. **21**(4): p. 773-780.
24. Bauer, J. and C. Garbe, *Acquired Melanocytic Nevi as Risk Factor for Melanoma Development. A Comprehensive Review of Epidemiological Data.* Pigment Cell Res., 2003. **16**(3): p. 297-306.
25. Tucker, M.A., et al., *Clinically recognized dysplastic nevi: a central risk factor for cutaneous melanoma.* JAMA Dermatology, 1997. **277**(18): p. 1439-1444.
26. Health, A.I.o. and Welfare, *Cancer data in Australia*. 2022, AIHW: Canberra.
27. De Giorgi, V., et al., *Estrogens, estrogen receptors and melanoma.* Expert Rev Anticancer Ther, 2011. **11**(5): p. 739-747.
28. Still, R. and S. Brennecke, *Melanoma in pregnancy.* Obstet Med, 2017. **10**(3): p. 107-112.
29. Byrom, L., et al., *Increased mortality for pregnancy-associated melanoma: systematic review and meta-analysis.* Journal of the European Academy of Dermatology Venereology, 2015. **29**(8): p. 1457-1466.
30. Lee, Y., et al., *Incidence and outcomes of pregnancy-associated cancer in Australia, 1994–2008: a population-based linkage study.* BJOG: An International Journal of Obstetrics Gynaecology, 2012. **119**(13): p. 1572-1582.
31. Khosrotehrani, K., et al., *Pregnancy promotes melanoma metastasis through enhanced lymphangiogenesis.* 2011. **178**(4): p. 1870-1880.
32. Enninga, E.A., et al., *Immunomodulatory effects of sex hormones: requirements for pregnancy and relevance in melanoma.* Mayo Clin Proc, 2014. **89**(4): p. 520-35.
33. Dadras, S.S., et al., *Tumor lymphangiogenesis predicts melanoma metastasis to sentinel lymph nodes.* Journal of Cutaneous Pathology, 2005. **32**(1): p. 84-84.
34. Greene, M.H., *The genetics of hereditary melanoma and nevi. 1998 update.* Cancer, 1999. **86**(11 Suppl): p. 2464-77.
35. Rossi, M., et al., *Familial Melanoma: Diagnostic and Management Implications.* Dermatol Pract Concept, 2019. **9**(1): p. 10-16.
36. Gandini, S., et al., *Meta-analysis of risk factors for cutaneous melanoma: III. Family history, actinic damage and phenotypic factors.* European Journal of Cancer, 2005. **41**(14): p. 2040-59.
37. Raimondi, S., et al., *MC1R variants, melanoma and red hair color phenotype: a meta-analysis.* Int J Cancer, 2008. **122**(12): p. 2753-60.
38. Goldstein, A.M., et al., *Features associated with germline CDKN2A mutations: a GenoMEL study of melanoma-prone families from three continents.* Journal of Medical Genetics, 2007. **44**(2): p. 99.
39. Fargnoli, M.C., et al., *MC1R variants increase melanoma risk in families with CDKN2A mutations: A meta-analysis.* European Journal of Cancer, 2010. **46**(8): p. 1413-1420.
40. Flanagan, N., et al., *Pleiotropic effects of the melanocortin 1 receptor (MC1R) gene on human pigmentation.* Hum Mol Genet, 2000. **9**(17): p. 2531-7.
41. Fang, S., et al., *Joint Effect of Multiple Common SNPs Predicts Melanoma Susceptibility.* PLOS ONE, 2014. **8**(12): p. e85642.
42. Rendleman, J., et al., *Melanoma risk loci as determinants of melanoma recurrence and survival.* Journal of Translational Medicine, 2013. **11**(1): p. 279.

43. Hirobe, T., *How are proliferation and differentiation of melanocytes regulated?* Pigment Cell Melanoma Res., 2011. **24**(3): p. 462-478.
44. Bennett, D.C. and E.E. Medrano, *Molecular Regulation of Melanocyte Senescence.* Pigment Cell Res., 2002. **15**(4): p. 242-250.
45. Marais, R. and C.J. Marshall, *Control of the ERK MAP kinase cascade by Ras and Raf.* Journal of Cancer Survivorship, 1996. **27**: p. 101-25.
46. Daum, G., et al., *The ins and outs of Raf kinases.* Trends in Biochemical Sciences, 1994. **19**(11): p. 474-480.
47. Whitwam, T., et al., *Differential oncogenic potential of activated RAS isoforms in melanocytes.* Oncogene, 2007. **26**(31): p. 4563-4570.
48. Taparowsky, E., et al., *Structure and activation of the human N-ras gene.* Cell, 1983. **34**(2): p. 581-586.
49. Omholt, K., et al., *Screening of N-ras Codon 61 Mutations in Paired Primary and Metastatic Cutaneous Melanomas.* Clinical Cancer Research, 2002. **8**(11): p. 3468-3474.
50. Bennett, D.C. and E.E. Medrano, *Molecular Regulation of Melanocyte Senescence.* Pigment Cell Research, 2002. **15**(4): p. 242-250.
51. Daniotti, M., et al., *BRAF alterations are associated with complex mutational profiles in malignant melanoma.* Oncogene, 2004. **23**(35): p. 5968-5977.
52. Tsao, H., et al., *Genetic Interaction Between NRAS and BRAF Mutations and PTEN/MMAC1 Inactivation in Melanoma.* Journal of Investigative Dermatology, 2004. **122**(2): p. 337-341.
53. Zhang, W. and H.T. Liu, *MAPK signal pathways in the regulation of cell proliferation in mammalian cells.* Cell Research, 2002. **12**(1): p. 9-18.
54. Maloney, R.C., et al., *The mechanism of activation of monomeric B-Raf V600E.* Comput Struct Biotechnol J, 2021. **19**: p. 3349-3363.
55. Köhler, M., et al., *Activation loop phosphorylation regulates B-Raf in vivo and transformation by B-Raf mutants.* Embo j, 2016. **35**(2): p. 143-61.
56. Wan, P.T.C., et al., *Mechanism of Activation of the RAF-ERK Signaling Pathway by Oncogenic Mutations of B-RAF*. Cell, 2004. **116**(6): p. 855-867.
57. Yoon, S. and R. Seger, *The extracellular signal-regulated kinase: Multiple substrates regulate diverse cellular functions.* Growth Factors, 2006. **24**(1): p. 21-44.
58. Gray-Schopfer, V.C., S.d.R. Dias, and R. Marais, *The role of B-RAF in melanoma.* Cancer and Metastasis Reviews, 2005. **24**(1): p. 165-183.
59. Zuber, J., et al., *A genome-wide survey of RAS transformation targets.* Nature genetics, 2000. **24**(2): p. 144-152.
60. Mercer, K.E. and C.A. Pritchard, *Raf proteins and cancer: B-Raf is identified as a mutational target.* Biochimica et Biophysica Acta - Reviews on Cancer, 2003. **1653**(1): p. 25-40.
61. Liu, J., et al., *Oncogenic BRAF regulates beta-Trcp expression and NF-kappaB activity in human melanoma cells.* Oncogene, 2007. **26**(13): p. 1954-8.
62. Basseres, D.S. and A.S. Baldwin, *Nuclear factor-[kappa]B and inhibitor of [kappa]B kinase pathways in oncogenic initiation and progression.* Oncogene, 2006. **25**(51): p. 6817-6830.
63. Gollob, J.A., et al., *Role of Raf Kinase in Cancer: Therapeutic Potential of Targeting the Raf/MEK/ERK Signal Transduction Pathway.* Seminars in Oncology, 2006. **33**(4): p. 392-406.
64. Ou, M., et al., *MDM2 induces EMT via the B-Raf signaling pathway through 14-3-3.* Oncol Rep, 2021. **46**(1).

65. Wellbrock, C. and R. Marais, *Elevated expression of MITF counteracts B-RAF-stimulated melanocyte and melanoma cell proliferation.* Journal of Cell Biology, 2005. **170**: p. 703-708.
66. Wellbrock, C., et al., *Oncogenic BRAF regulates melanoma proliferation through the lineage specific factor MITF.* PLOS ONE, 2008. **3**(7).
67. Levy, C., M. Khaled, and D.E. Fisher, *MITF: master regulator of melanocyte development and melanoma oncogene.* Trends in Molecular Medicine, 2006. **12**: p. 406-414.
68. Garraway, L.A., *Integrative genomic analyses identify MITF as a lineage survival oncogene amplified in malignant melanoma.* Nature, 2005. **436**: p. 117-122.
69. Chang, D.Z., et al., *Clinical significance of BRAF mutations in metastatic melanoma.* Journal of Translational Medicine, 2004. **2**(1): p. 46.
70. Sumimoto, H., et al., *Inhibition of growth and invasive ability of melanoma by inactivation of mutated BRAF with lentivirus-mediated RNA interference.* Oncogene, 2004. **23**(36): p. 6031-6039.
71. Mattei, S., et al., *Expression of cytokine/growth factors and their receptors in human melanoma and melanocytes.* Int J Cancer, 1994. **56**(6): p. 853-857.
72. Alqathama, A., *BRAF in malignant melanoma progression and metastasis: potentials and challenges.* Am J Cancer Res, 2020. **10**(4): p. 1103-1114.
73. Ascierto, P.A., et al., *The role of BRAF V600 mutation in melanoma.* Journal of Translational Medicine, 2012. **10**: p. 85.
74. Cohen, C., et al., *Mitogen-actived Protein Kinase Activation Is an Early Event in Melanoma Progression.* Clinical Cancer Research, 2002. **8**(12): p. 3728-3733.
75. Pollock, P.M., et al., *High frequency of BRAF mutations in nevi.* Nature genetics, 2003. **33**(1): p. 19-20.
76. Breslow, A., *Prognosis in cutaneous melanoma: tumor thickness as a guide to treatment.* Pathol Annu, 1980. **15**(Pt 1): p. 1-22.
77. Breslow, A., *Prognostic factors in the treatment of cutaneous melanoma.* Journal of Cutaneous Pathology, 1979. **6**(3): p. 208-12.
78. Atallah, E. and L. Flaherty, *Treatment of metastatic malignant melanoma.* Curr Treat Options Oncol, 2005. **6**(3): p. 185-93.
79. Ascierto, P.A., et al., *Phase II trial (BREAK-2) of the BRAF inhibitor dabrafenib (GSK2118436) in patients with metastatic melanoma.* Journal of Clinical Oncology, 2013. **31**(26): p. 3205-11.
80. Kim, K.B., et al., *Phase II study of the MEK1/MEK2 inhibitor Trametinib in patients with metastatic BRAF-mutant cutaneous melanoma previously treated with or without a BRAF inhibitor.* Journal of Clinical Oncology, 2013. **31**(4): p. 482-9.
81. Holderfield, M., et al., *Targeting RAF kinases for cancer therapy: BRAF-mutated melanoma and beyond.* Nature Reviews Cancer, 2014. **14**(7): p. 455-67.
82. Roesch, A., et al., *Phenotypic tumour cell plasticity as a resistance mechanism and therapeutic target in melanoma.* European Journal of Cancer, 2016. **59**: p. 109-112.
83. Su, F., et al., *Resistance to selective BRAF inhibition can be mediated by modest upstream pathway activation.* Cancer Res, 2012. **72**(4): p. 969-78.
84. Greger, J.G., et al., *Combinations of BRAF, MEK, and PI3K/mTOR Inhibitors Overcome Acquired Resistance to the BRAF Inhibitor GSK2118436 Dabrafenib, Mediated by NRAS or MEK Mutations.* Molecular Cancer Therapeutics, 2012. **11**(4): p. 909-920.
85. Poulikakos, P.I., et al., *RAF inhibitor resistance is mediated by dimerization of aberrantly spliced BRAF(V600E).* Nature, 2011. **480**(7377): p. 387-90.

86. Nazarian, R., et al., *Melanomas acquire resistance to B-RAF(V600E) inhibition by RTK or N-RAS upregulation.* Nature, 2010. **468**(7326): p. 973-7.
87. Villanueva, J., et al., *Acquired resistance to BRAF inhibitors mediated by a RAF kinase switch in melanoma can be overcome by cotargeting MEK and IGF-1R/PI3K.* Cancer Cell, 2010. **18**(6): p. 683-95.
88. Straussman, R., et al., *Tumour micro-environment elicits innate resistance to RAF inhibitors through HGF secretion.* Nature, 2012. **487**(7408): p. 500-4.
89. Anforth, R., et al., *Factors influencing the development of cutaneous squamous cell carcinoma in patients on BRAF inhibitor therapy.* J Am Acad Dermatol, 2015. **72**(5): p. 809-815.e1.
90. Zhong, J., et al., *BRAF Inhibitor Resistance in Melanoma: Mechanisms and Alternative Therapeutic Strategies.* Curr Treat Options Oncol, 2022. **23**(11): p. 1503-1521.
91. Gowrishankar, K., et al., *Acquired Resistance to BRAF Inhibition Can Confer Cross-Resistance to Combined BRAF/MEK Inhibition.* Journal of Investigative Dermatology, 2012. **132**(7): p. 1850-1859.
92. Algazi, A.P., et al., *Continuous versus intermittent BRAF and MEK inhibition in patients with BRAF-mutated melanoma: a randomized phase 2 trial.* Nature Medicine, 2020. **26**(10): p. 1564-1568.
93. van Not, O.J., et al., *BRAF and NRAS Mutation Status and Response to Checkpoint Inhibition in Advanced Melanoma.* JCO Precis Oncol, 2022. **6**: p. e2200018.
94. Chen, D., et al., *Response and outcomes after anti-CTLA4 versus anti-PD1 combined with stereotactic body radiation therapy for metastatic non-small cell lung cancer: retrospective analysis of two single-institution prospective trials.* J Immunother Cancer, 2020. **8**(1).
95. Hodi, F.S., et al., *Improved survival with ipilimumab in patients with metastatic melanoma.* N Engl J Med, 2010. **363**(8): p. 711-23.
96. Robert, C., et al., *Ipilimumab plus dacarbazine for previously untreated metastatic melanoma.* N Engl J Med, 2011. **364**(26): p. 2517-26.
97. Eroglu, Z., et al., *Long term survival with cytotoxic T lymphocyte-associated antigen 4 blockade using tremelimumab.* European Journal of Cancer, 2015. **51**(17): p. 2689-97.
98. Hamid, O., et al., *Five-year survival outcomes for patients with advanced melanoma treated with pembrolizumab in KEYNOTE-001.* Annals of Oncology, 2019. **30**(4): p. 582-588.
99. Ascierto, P.A., et al., *Overall survival (OS) and safety results from a phase 3 trial of ipilimumab (IPI) at 3 mg/kg vs 10 mg/kg in patients with metastatic melanoma (MEL).* Annals of Oncology, 2016. **27**(suppl_6): p. 1106O-1106O.
100. Zang, X. and J.P. Allison, *The B7 family and cancer therapy: costimulation and coinhibition.* Clinical Cancer Research, 2007. **13**(18): p. 5271-5279.
101. Larkin, J., et al., *Combined Nivolumab and Ipilimumab or Monotherapy in Untreated Melanoma.* N Engl J Med, 2015. **373**(1): p. 23-34.
102. Betof Warner, A., et al., *Long-Term Outcomes and Responses to Retreatment in Patients With Melanoma Treated With PD-1 Blockade.* Journal of Clinical Oncology, 2020. **38**(15): p. 1655-1663.
103. Hamid, O., et al., *Efficacy, Safety, and Tolerability of Approved Combination BRAF and MEK Inhibitor Regimens for BRAF-Mutant Melanoma.* Cancers (Basel), 2019. **11**(11): p. 1642.
104. Wolchok, J.D., et al., *Nivolumab plus ipilimumab in advanced melanoma.* New England Journal of Medicine, 2013. **369**: p. 122-133.
105. Postow, M.A., et al., *Nivolumab and ipilimumab versus ipilimumab in untreated melanoma.* New England Journal of Medicine, 2015. **372**(21): p. 2006-2017.

106. Ascierto, P.A., et al., *Adjuvant nivolumab versus ipilimumab in resected stage IIIB–C and stage IV melanoma (CheckMate 238): 4-year results from a multicentre, double-blind, randomised, controlled, phase 3 trial.* The lancet oncology, 2020. **21**(11): p. 1465-1477.
107. Roh, W., et al., *Integrated molecular analysis of tumor biopsies on sequential CTLA-4 and PD-1 blockade reveals markers of response and resistance.* Sci Transl Med, 2017. **9**(379): p. eaah3560.
108. Seidel, J.A., A. Otsuka, and K. Kabashima, *Anti-PD-1 and Anti-CTLA-4 Therapies in Cancer: Mechanisms of Action, Efficacy, and Limitations.* Frontiers in Oncology, 2018. **8**.
109. Kakavand, H., et al., *Negative immune checkpoint regulation by VISTA: a mechanism of acquired resistance to anti-PD-1 therapy in metastatic melanoma patients.* Modern Pathology, 2017. **30**(12): p. 1666-1676.
110. Lei, Q., et al., *Resistance Mechanisms of Anti-PD1/PDL1 Therapy in Solid Tumors.* Frontiers in Cell and Developmental Biology, 2020. **8**.
111. Liu, Y., E.G. Shepherd, and L.D. Nelin, *MAPK phosphatases — regulating the immune response.* Nature Reviews Immunology, 2007. **7**(3): p. 202-212.
112. Huang, G., L.Z. Shi, and H. Chi, *Regulation of JNK and p38 MAPK in the immune system: Signal integration, propagation and termination.* Cytokine, 2009. **48**(3): p. 161-169.
113. Welti, M., et al., *Triple Combination of Immune Checkpoint Inhibitors and BRAF/MEK Inhibitors in BRAFV600 Melanoma: Current Status and Future Perspectives.* Cancers (Basel), 2022. **14**(22).
114. Hu-Lieskovan, S., et al., *Improved antitumor activity of immunotherapy with BRAF and MEK inhibitors in BRAF(V600E) melanoma.* Sci Transl Med, 2015. **7**(279): p. 279ra41.
115. Deken, M.A., et al., *Targeting the MAPK and PI3K pathways in combination with PD1 blockade in melanoma.* Oncoimmunology, 2016. **5**(12): p. e1238557.
116. Schadendorf, D., et al., *STARBOARD: encorafenib + binimetinib + pembrolizumab for first-line metastatic/unresectable BRAF V600-mutant melanoma.* Future Oncology, 2022. **18**(17): p. 2041-2051.
117. Sullivan, R.J., et al., *Atezolizumab plus cobimetinib and vemurafenib in BRAF-mutated melanoma patients.* Nature Medicine, 2019. **25**(6): p. 929-935.
118. Ribas, A., et al., *Pembrolizumab (pembro) plus dabrafenib (dab) and trametinib (tram) in BRAFV600E/K-mutant melanoma: Long-term follow-up of KEYNOTE-022 parts 1, 2, and 3.* Journal of Clinical Oncology, 2022. **40**(16_suppl): p. 9516-9516.
119. Almen, M.S., et al., *Mapping the human membrane proteome: a majority of the human membrane proteins can be classified according to function and evolutionary origin.* BMC Biol, 2009. **7**: p. doi: 10.1186/1741-7007-7-50.
120. Wang, M., et al., *Role of the Unfolded Protein Response Regulator GRP78/BiP in Development, Cancer, and Neurological Disorders.* Antioxidants & Redox Signaling, 2009. **11**(9): p. 2307-2316.
121. Prischi, F., et al., *Phosphoregulation of Ire1 RNase splicing activity.* Nature Communications, 2014. **5**.
122. Kondratyev, M., et al., *PERK-dependent compartmentalization of ERAD and unfolded protein response machineries during ER stress.* Exp Cell Res, 2007. **313**(16): p. 3395-407.
123. Tam, A.B., A.C. Koong, and M. Niwa, *Ire1 has distinct catalytic mechanisms for XBP1/HAC1 splicing and RIDD.* Cell Rep, 2014. **9**(3): p. 850-8.
124. Rzymski, T., et al., *Role of ATF4 in regulation of autophagy and resistance to drugs and hypoxia.* Cell Cycle, 2009. **8**(23): p. 3838-3847.

125. Novoa, I., et al., *Feedback Inhibition of the Unfolded Protein Response by GADD34-Mediated Dephosphorylation of eIF2α.* The Journal of Cell Biology, 2001. **153**(5): p. 1011-1022.
126. Boyce, M., et al., *A Selective Inhibitor of eIF2α Dephosphorylation Protects Cells from ER Stress.* Science, 2005. **307**(5711): p. 935-939.
127. Shen, J., et al., *ER Stress Regulation of ATF6 Localization by Dissociation of BiP/GRP78 Binding and Unmasking of Golgi Localization Signals.* Developmental Cell, 2002. **3**(1): p. 99-111.
128. Teske, B.F., et al., *The eIF2 kinase PERK and the integrated stress response facilitate activation of ATF6 during endoplasmic reticulum stress.* Molecular Biology of the Cell, 2011. **22**(22): p. 4390-4405.
129. Yoshida, H., et al., *XBP1 mRNA Is Induced by ATF6 and Spliced by IRE1 in Response to ER Stress to Produce a Highly Active Transcription Factor.* Cell, 2001. **107**(7): p. 881-891.
130. Chen, Y. and F. Brandizzi, *IRE1: ER stress sensor and cell fate executor.* Trends Cell Biol, 2013. **23**(11): p. 547-55.
131. Proud, C.G., *eIF2 and the control of cell physiology.* Seminars in Cell & Developmental Biology, 2005. **16**(1): p. 3-12.
132. Yamasaki, S. and P. Anderson, *Reprogramming mRNA translation during stress.* Current Opinion in Cell Biology, 2008. **20**(2): p. 222-226.
133. Acosta-Alvear, D., et al., *XBP1 Controls Diverse Cell Type- and Condition-Specific Transcriptional Regulatory Networks.* Molecular Cell, 2007. **27**(1): p. 53-66.
134. Ameri, K. and A.L. Harris, *Activating transcription factor 4.* Int J Biochem Cell Biol, 2008. **40**(1): p. 14-21.
135. Shen, J. and R. Prywes, *ER stress signaling by regulated proteolysis of ATF6.* Methods, 2005. **35**(4): p. 382-389.
136. Harding, H.P., et al., *An Integrated Stress Response Regulates Amino Acid Metabolism and Resistance to Oxidative Stress.* Molecular Cell, 2003. **11**(3): p. 619-633.
137. Kilberg, M.S., J. Shan, and N. Su, *ATF4-dependent transcription mediates signaling of amino acid limitation.* Trends in Endocrinology & Metabolism, 2009. **20**(9): p. 436-443.
138. Dickhout, J.G., et al., *Integrated Stress Response Modulates Cellular Redox State via Induction of Cystathionine γ-Lyase.* Journal of Biological Chemistry, 2012. **287**(10): p. 7603-7614.
139. Merksamer, P.I., A. Trusina, and F.R. Papa, *Real-Time Redox Measurements during Endoplasmic Reticulum Stress Reveal Interlinked Protein Folding Functions.* Cell, 2008. **135**(5): p. 933-947.
140. Ma, Y. and L.M. Hendershot, *The Unfolding Tale of the Unfolded Protein Response.* Cell, 2001. **107**(7): p. 827-830.
141. Ron, D. and P. Walter, *Signal integration in the endoplasmic reticulum unfolded protein response.* Nature Reviews Molecular Cell Biology, 2007. **8**(7): p. 519-529.
142. Vembar, S.S. and J.L. Brodsky, *One step at a time: endoplasmic reticulum-associated degradation.* Nature Reviews Molecular Cell Biology, 2008. **9**(12): p. 944-57.
143. Kaneko, M., et al., *Human HRD1 protects against ER stress-induced apoptosis through ER-associated degradation.* FEBS Lett, 2002. **532**(1): p. 147-152.
144. Kong, B., et al., *A common genetic variation of melanoma inhibitory activity-2 labels a subtype of pancreatic adenocarcinoma with high endoplasmic reticulum stress levels.* Scientific Reports, 2015. **5**: p. 8109.

145. Ding, W.-X., et al., *Linking of Autophagy to Ubiquitin-Proteasome System Is Important for the Regulation of Endoplasmic Reticulum Stress and Cell Viability.* Am J Pathol, 2007. **171**(2): p. 513-524.
146. Ding, W.X., et al., *Differential effects of endoplasmic reticulum stress-induced autophagy on cell survival.* J Biol Chem, 2007. **282**(7): p. 4702-10.
147. Ogata, M., et al., *Autophagy is activated for cell survival after endoplasmic reticulum stress.* Molecular Cell Biology, 2006. **26**(24): p. 9220-31.
148. Ma, X.-H., et al., *Measurements of Tumor Cell Autophagy Predict Invasiveness, Resistance to Chemotherapy, and Survival in Melanoma.* Clinical Cancer Research, 2011. **17**(10): p. 3478-3489.
149. Mathew, R., V. Karantza-Wadsworth, and E. White, *Role of autophagy in cancer.* Nature Reviews Cancer, 2007. **7**(12): p. 961-967.
150. White, E., *Deconvoluting the context-dependent role for autophagy in cancer.* Nature Reviews Cancer, 2012. **12**(6): p. 401-410.
151. Matsumoto, M., et al., *Ectopic expression of CHOP (GADD153) induces apoptosis in M1 myeloblastic leukemia cells.* FEBS Lett, 1996. **395**(2–3): p. 143-147.
152. Maytin, E.V., et al., *Stress-Inducible Transcription Factor CHOP/gadd153 Induces Apoptosis in Mammalian Cells via p38 Kinase-Dependent and -Independent Mechanisms.* Exp Cell Res, 2001. **267**(2): p. 193-204.
153. McCullough, K.D., et al., *Gadd153 sensitizes cells to endoplasmic reticulum stress by down-regulating Bcl2 and perturbing the cellular redox state.* Molecular Cell Biology, 2001. **21**(4): p. 1249-59.
154. Hetz, C., et al., *Proapoptotic BAX and BAK modulate the unfolded protein response by a direct interaction with IRE1alpha.* Science, 2006. **312**(5773): p. 572-6.
155. Urano, F., et al., *Coupling of Stress in the ER to Activation of JNK Protein Kinases by Transmembrane Protein Kinase IRE1.* Science, 2000. **287**(5453): p. 664-666.
156. Nakagawa, T., et al., *Caspase-12 mediates endoplasmic-reticulum-specific apoptosis and cytotoxicity by amyloid-beta.* Nature, 2000. **403**(6765): p. 98-103.
157. Yoneda, T., et al., *Activation of Caspase-12, an Endoplastic Reticulum (ER) Resident Caspase, through Tumor Necrosis Factor Receptor-associated Factor 2-dependent Mechanism in Response to the ER Stress.* Journal of Biological Chemistry, 2001. **276**(17): p. 13935-13940.
158. Daneshmand, S., et al., *Glucose-regulated protein GRP78 is up-regulated in prostate cancer and correlates with recurrence and survival.* Human Pathology, 2007. **38**(10): p. 1547-52.
159. Xing, X., et al., *Overexpression of glucose-regulated protein 78 in colon cancer.* Clinica Chimica Acta, 2006. **364**(1): p. 308-315.
160. Zhang, J., et al., *Association of elevated GRP78 expression with increased lymph node metastasis and poor prognosis in patients with gastric cancer.* Clinical & experimental metastasis, 2006. **23**(7-8): p. 401-410.
161. Bini, L., et al., *Protein expression profiles in human breast ductal carcinoma and histologically normal tissue.* Electrophoresis, 1997. **18**(15): p. 2832-2841.
162. Fernandez, P.M., et al., *Overexpression of the glucose-regulated stress gene GRP78 in malignant but not benign human breast lesions.* Breast cancer research and treatment, 2000. **59**(1): p. 15-26.
163. Koomägi, R., J. Mattern, and M. Volm, *Glucose-related protein (GRP78) and its relationship to the drug-resistance proteins P170, GST-pi, LRP56 and angiogenesis in non-small cell lung carcinomas.* Anticancer research, 1998. **19**(5B): p. 4333-4336.
164. Zhuang, L., et al., *Expression of glucose-regulated stress protein GRP78 is related to progression of melanoma.* Histopathology, 2009. **54**(4): p. 462-470.

165. Guan, M., et al., *MDA-9 and GRP78 as potential diagnostic biomarkers for early detection of melanoma metastasis.* Tumour Biology, 2015. **36**(4): p. 2973-2982.
166. Tay, K.H., et al., *Sustained IRE1 and ATF6 signaling is important for survival of melanoma cells undergoing ER stress.* Cell Signal, 2014. **26**(2): p. 287-94.
167. Fu, Y., et al., *Pten null prostate tumorigenesis and AKT activation are blocked by targeted knockout of ER chaperone GRP78/BiP in prostate epithelium.* Proceedings of the National Academy of Sciences, 2008. **105**(49): p. 19444-19449.
168. Dong, D., et al., *Critical role of the stress chaperone GRP78/BiP in tumor proliferation, survival, and tumor angiogenesis in transgene-induced mammary tumor development.* Cancer Res, 2008. **68**(2): p. 498-505.
169. Croft, A., et al., *Oncogenic activation of MEK/ERK primes melanoma cells for adaptation to endoplasmic reticulum stress.* Journal of Investigative Dermatology, 2014. **134**(2): p. 488-97.
170. Romero-Ramirez, L., et al., *XBP1 is essential for survival under hypoxic conditions and is required for tumor growth.* Cancer Res, 2004. **64**(17): p. 5943-7.
171. Romero-Ramirez, L., et al., *X Box-Binding Protein 1 Regulates Angiogenesis in Human Pancreatic Adenocarcinomas.* Translational Oncology, 2009. **2**(1): p. 31-38.
172. Drogat, B., et al., *IRE1 signaling is essential for ischemia-induced vascular endothelial growth factor-A expression and contributes to angiogenesis and tumor growth in vivo.* Cancer Res, 2007. **67**(14): p. 6700-7.
173. Bi, M., et al., *ER stress-regulated translation increases tolerance to extreme hypoxia and promotes tumor growth.* Embo j, 2005. **24**(19): p. 3470-81.
174. Blais, J.D., et al., *Perk-dependent translational regulation promotes tumor cell adaptation and angiogenesis in response to hypoxic stress.* Molecular Cell Biology, 2006. **26**(24): p. 9517-32.
175. Mintz, P.J., et al., *Fingerprinting the circulating repertoire of antibodies from cancer patients.* Nature Biotechnology, 2003. **21**(1): p. 57-63.
176. Chinni, S.R., et al., *Humoral immune responses to cathepsin D and glucose-regulated protein 78 in ovarian cancer patients.* Clinical Cancer Research, 1997. **3**(9): p. 1557-64.
177. Selim, M.A., et al., *Changes in oligosaccharide chains of autoantibodies to GRP78 expressed during progression of malignant melanoma stimulate melanoma cell growth and survival().* Melanoma research, 2011. **21**(4): p. 323-334.
178. Jamora, C., G. Dennert, and A.S. Lee, *Inhibition of tumor progression by suppression of stress protein GRP78/BiP induction in fibrosarcoma B/C10ME.* Proc Natl Acad Sci U S A, 1996. **93**(15): p. 7690-4.
179. Sun, Q., et al., *Expressions of GRP78 and Bax associate with differentiation, metastasis, and apoptosis in non-small cell lung cancer.* Mol Biol Rep, 2012. **39**(6): p. 6753-61.
180. Chang, Y.J., et al., *Glucose-regulated protein 78 (GRP78) regulates colon cancer metastasis through EMT biomarkers and the NRF-2/HO-1 pathway.* Tumour Biology, 2015. **36**(3): p. 1859-69.
181. Zhao, G., et al., *High Expression of GRP78 Promotes Invasion and Metastases in Patients with Esophageal Squamous Cell Carcinoma.* Dig Dis Sci, 2015. **60**(9): p. 2690-9.
182. Teng, Y., et al., *Mitochondrial ATAD3A combines with GRP78 to regulate the WASF3 metastasis-promoting protein.* Oncogene, 2016. **35**(3): p. 333-43.
183. Zhang, X.X., et al., *The cell surface GRP78 facilitates the invasion of hepatocellular carcinoma cells.* Biomed Res Int, 2013. **2013**: p. 917296.

184. Li, Z., et al., *Cell-surface GRP78 facilitates colorectal cancer cell migration and invasion.* Int J Biochem Cell Biol, 2013. **45**(5): p. 987-94.
185. Jamora, C., G. Dennert, and A.S. Lee, *Inhibition of tumor progression by suppression of stress protein GRP78/BiP induction in fibrosarcoma B/C10ME.* Proceedings of the National Academy of Sciences, 1996. **93**(15): p. 7690-7694.
186. Su, R., et al., *Grp78 promotes the invasion of hepatocellular carcinoma.* BMC Cancer, 2010. **10**(1): p. doi 10.1155/2013/917296.
187. Zhuang, L., et al., *Progression in melanoma is associated with decreased expression of death receptors for tumor necrosis factor–related apoptosis-inducing ligand.* Human Pathology, 2006. **37**(10): p. 1286-1294.
188. Papalas, J.A., et al., *Patterns of GRP78 and MTJ1 expression in primary cutaneous malignant melanoma.* Modern Pathology, 2010. **23**(1): p. 134-43.
189. Lee, C.-W., et al., *Overexpressed tryptophanyl-tRNA synthetase, an angiostatic protein, enhances oral cancer cell invasiveness.* Oncotarget, 2015. **6**(26): p. 21979.
190. Zhang, X.-X., et al., *The Cell Surface GRP78 Facilitates the Invasion of Hepatocellular Carcinoma Cells.* Biomed Res Int, 2013. **2013**: p. doi 10.1155/2013/917296.
191. Li, H., et al., *XBP1 induces snail expression to promote epithelial- to-mesenchymal transition and invasion of breast cancer cells.* Cell Signal, 2015. **27**(1): p. 82-89.
192. Caramel, J., et al., *A switch in the expression of embryonic EMT-inducers drives the development of malignant melanoma.* Cancer Cell, 2013. **24**(4): p. 466-80.
193. Alonso, S.R., et al., *A High-Throughput Study in Melanoma Identifies Epithelial-Mesenchymal Transition as a Major Determinant of Metastasis.* Cancer Res, 2007. **67**(7): p. 3450-3460.
194. Arap, M.A., et al., *Cell surface expression of the stress response chaperone GRP78 enables tumor targeting by circulating ligands.* Cancer Cell, 2004. **6**(3): p. 275-284.
195. Ni, M., Y. Zhang, and A. Lee, *Beyond the endoplasmic reticulum: atypical GRP78 in cell viability, signalling and therapeutic targeting.* Biochemical Journal, 2011. **434**: p. 181-188.
196. Rajabi, P., et al., *The role of VEGF in melanoma progression.* Journal of Research in Medical Sciences, 2012. **17**(6): p. 534-9.
197. Karali, E., et al., *VEGF Signals through ATF6 and PERK to promote endothelial cell survival and angiogenesis in the absence of ER stress.* Molecular Cell, 2014. **54**(4): p. 559-72.
198. Kern, J., et al., *GRP-78 secreted by tumor cells blocks the antiangiogenic activity of bortezomib.* Blood, 2009. **114**(18): p. 3960-3967.
199. Ghosh, R., et al., *Transcriptional Regulation of VEGF-A by the Unfolded Protein Response Pathway.* PLOS ONE, 2010. **5**(3): p. e9575.
200. Katanasaka, Y., et al., *Cancer antineovascular therapy with liposome drug delivery systems targeted to BiP/GRP78.* Int J Cancer, 2010. **127**(11): p. 2685-2698.
201. Dong, D., et al., *Spontaneous and Controllable Activation of Suicide Gene Expression Driven by the Stress-Inducible Grp78 Promoter Resulting in Eradication of Sizable Human Tumors.* Human Gene Therapy, 2004. **15**(6): p. 553-561.
202. Tsai, Y.C. and A.M. Weissman, *The Unfolded Protein Response, Degradation from the Endoplasmic Reticulum, and Cancer.* Genes & Cancer, 2010. **1**(7): p. 764-778.
203. Kenific, C., A. Thorburn, and J. Debnath, *Autophagy and Metastasis: Another double-edged sword.* Current Opinion in Cell Biology, 2010. **22**(2): p. 241-245.
204. Ossowski, L. and J.A. Aguirre-Ghiso, *Dormancy of metastatic melanoma.* Pigment cell & melanoma research, 2010. **23**(1): p. 41.

205. Eskelin, S., et al., *Tumor doubling times in metastatic malignant melanoma of the uvea: tumor progression before and after treatment.* Ophthalmology, 2000. **107**(8): p. 1443-9.
206. Logan, P.T., et al., *Single-cell tumor dormancy model of uveal melanoma.* Clinical & experimental metastasis, 2008. **25**(5): p. 509-16.
207. Hirsch, C., et al., *The ubiquitylation machinery of the endoplasmic reticulum.* Nature, 2009. **458**(7237): p. 453-60.
208. Platz, A., et al., *Human cutaneous melanoma; a review of NRAS and BRAF mutation frequencies in relation to histogenetic subclass and body site.* Molecular Oncology, 2008. **1**(4): p. 395-405.
209. Davies, H., et al., *Mutations of the BRAF gene in human cancer.* Nature, 2002. **417**(6892): p. 949-54.
210. Bilanges, B. and D. Stokoe, *Mechanisms of translational deregulation in human tumors and therapeutic intervention strategies.* Oncogene, 2007. **26**(41): p. 5973-5990.
211. Jiang, C.C., et al., *Inhibition of MEK Sensitizes Human Melanoma Cells to Endoplasmic Reticulum Stress-Induced Apoptosis.* Cancer Res, 2007. **67**(20): p. 9750-9761.
212. Beck, D., et al., *Vemurafenib potently induces endoplasmic reticulum stress-mediated apoptosis in BRAFV600E melanoma cells.* Sci Signal, 2013. **6**(260): p. doi: 10.1126/scisignal.2003057.
213. Al-Rawashdeh, F.Y., et al., *Unfolded protein response activation contributes to chemoresistance in hepatocellular carcinoma.* Eur J Gastroenterol Hepatol, 2010. **22**(9): p. 1099-105.
214. Dong, D., et al., *Vascular targeting and antiangiogenesis agents induce drug resistance effector GRP78 within the tumor microenvironment.* Cancer Res, 2005. **65**(13): p. 5785-91.
215. Vincent, L.-A., et al., *Lysosomes and unfolded protein response, determinants of differential resistance of melanoma cells to vinca alkaloids.* Fundamental & Clinical Pharmacology, 2015. **29**(2): p. 164-177.
216. Shannon, A.M., et al., *Tumour hypoxia, chemotherapeutic resistance and hypoxia-related therapies.* Cancer Treatment Reviews, 2003. **29**(4): p. 297-307.
217. Gray, L.H., et al., *The Concentration of Oxygen Dissolved in Tissues at the Time of Irradiation as a Factor in Radiotherapy.* The British Journal of Radiology, 1953. **26**(312): p. 638-648.
218. Lefranc, F., V. Mathieu, and R. Kiss, *Galectin-1-mediated biochemical controls of melanoma and glioma aggressive behavior.* World Journal of Biological Chemistry, 2011. **2**(9): p. 193-201.
219. Lee, J.H., M.L. Choy, and P.A. Marks, *Mechanisms of resistance to histone deacetylase inhibitors.* Advanced Cancer Research, 2012. **116**: p. 39-86.
220. Fiskus, W., et al., *Molecular and biologic characterization and drug sensitivity of pan-histone deacetylase inhibitor–resistant acute myeloid leukemia cells.* Blood, 2008. **112**(7): p. 2896-2905.
221. Dedes, K.J., et al., *Acquired vorinostat resistance shows partial cross-resistance to 'second-generation' HDAC inhibitors and correlates with loss of histone acetylation and apoptosis but not with altered HDAC and HAT activities.* Anti-cancer drugs, 2009. **20**(5): p. 321-333.
222. Lai, F., et al., *Cotargeting histone deacetylases and oncogenic BRAF synergistically kills human melanoma cells by necrosis independently of RIPK1 and RIPK3.* Cell Death & Disease, 2013. **4**: p. e655.

223. Lai, F., et al., *Histone deacetylases (HDACs) as mediators of resistance to apoptosis in melanoma and as targets for combination therapy with selective BRAF inhibitors.* Advances in Pharmacology and Pharmacy, 2012. **65**: p. 27-43.
224. Baumeister, P., et al., *Transcriptional induction of GRP78/BiP by histone deacetylase inhibitors and resistance to histone deacetylase inhibitor-induced apoptosis.* Molecular Cancer Therapeutics, 2009. **8**(5): p. 1086-1094.
225. Hensel, F., et al., *Early development of PAT-SM6 for the treatment of melanoma.* Melanoma research, 2013. **23**(4): p. 264-75.
226. Rasche, L., et al., *The Natural Human IgM Antibody PAT-SM6 Induces Apoptosis in Primary Human Multiple Myeloma Cells by Targeting Heat Shock Protein GRP78.* PLOS ONE, 2013. **8**(5): p. e63414.
227. Fasano, E., et al., *DHA induces apoptosis by altering the expression and cellular location of GRP78 in colon cancer cell lines.* Biochim Biophys Acta, 2012. **1822**(11): p. 1762-72.
228. Lee, C.Y., et al., *The cell cycle effects of docosahexaenoic acid on human metastatic hepatocellular carcinoma proliferation.* Int J Oncol, 2010. **36**(4): p. 991-8.
229. Bougnoux, P., et al., *Improving outcome of chemotherapy of metastatic breast cancer by docosahexaenoic acid: a phase II trial.* British Journal of Cancer, 2009. **101**(12): p. 1978-1985.
230. Albino, A.P., et al., *Cell Cycle Arrest and Apoptosis of Melanoma Cells by Docosahexaenoic Acid: Association with Decreased pRb Phosphorylation.* Cancer Res, 2000. **60**(15): p. 4139-4145.
231. Horrocks, L.A. and Y.K. Yeo, *Health benefits of docosahexaenoic acid (DHA).* Pharmacol Res, 1999. **40**(3): p. 211-25.
232. Kato, T., N. Kolenic, and R.S. Pardini, *Docosahexaenoic Acid (DHA), a Primary Tumor Suppressive Omega-3 Fatty Acid, Inhibits Growth of Colorectal Cancer Independent of p53 Mutational Status.* Nutrition and Cancer, 2007. **58**(2): p. 178-187.
233. Iigo, M., et al., *Inhibitory effects of docosahexaenoic acid on colon carcinoma 26 metastasis to the lung.* British Journal of Cancer, 1997. **75**(5): p. 650-655.
234. Awale, S., et al., *Identification of arctigenin as an antitumor agent having the ability to eliminate the tolerance of cancer cells to nutrient starvation.* Cancer Res, 2006. **66**(3): p. 1751-7.
235. Hsieh, T.-H., et al., *Downregulation of SUN2, a novel tumor suppressor, mediates miR-221/222-induced malignancy in central nervous system embryonal tumors.* Carcinogenesis, 2014. **35**(10): p. 2164-2174.
236. Sun, S., et al., *Arctigenin suppresses unfolded protein response and sensitizes glucose deprivation-mediated cytotoxicity of cancer cells.* Planta Med, 2011. **77**(2): p. 141-5.
237. Atkins, C., et al., *Characterization of a novel PERK kinase inhibitor with antitumor and antiangiogenic activity.* Cancer Res, 2013. **73**(6): p. 1993-2002.
238. Axten, J.M., et al., *Discovery of 7-methyl-5-(1-{[3-(trifluoromethyl)phenyl]acetyl}-2,3-dihydro-1H-indol-5-yl)-7H-p yrrolo[2,3-d]pyrimidin-4-amine (GSK2606414), a potent and selective first-in-class inhibitor of protein kinase R (PKR)-like endoplasmic reticulum kinase (PERK).* J Med Chem, 2012. **55**(16): p. 7193-207.
239. Park, H.-R., et al., *Effect on Tumor Cells of Blocking Survival Response to Glucose Deprivation.* Journal of the National Cancer Institute, 2004. **96**(17): p. 1300-1310.
240. Park, H.-R., et al., *Versipelostatin, a novel GRP78/Bip molecular chaperone down-regulator of microbial origin.* Tetrahedron Letters, 2002. **43**(39): p. 6941-6945.
241. Bedikian, A.Y., et al., *Phase 3 study of docosahexaenoic acid–paclitaxel versus dacarbazine in patients with metastatic malignant melanoma.* Annals of Oncology, 2011. **22**(4): p. 787-793.

242. Homsi, J., et al., *Phase 2 open-label study of weekly docosahexaenoic acid–paclitaxel in patients with metastatic uveal melanoma.* Melanoma research, 2010. **20**(6): p. 507-510.
243. Mimura, N., et al., *Blockade of XBP1 splicing by inhibition of IRE1α is a promising therapeutic option in multiple myeloma.* Blood, 2012. **119**(24): p. 5772-81.
244. Das Thakur, M., et al., *Modelling vemurafenib resistance in melanoma reveals a strategy to forestall drug resistance.* Nature, 2013. **494**(7436): p. 251-5.
245. Yao, X., et al., *Arctigenin enhances chemosensitivity of cancer cells to cisplatin through inhibition of the STAT3 signaling pathway.* J Cell Biochem, 2011. **112**(10): p. 2837-49.
246. Lindskog, M., et al., *Neuroblastoma cell death in response to docosahexaenoic acid: Sensitization to chemotherapy and arsenic-induced oxidative stress.* Int J Cancer, 2006. **118**(10): p. 2584-2593.
247. Colas, S., et al., *Sensitization by Dietary Docosahexaenoic Acid of Rat Mammary Carcinoma to Anthracycline: A Role for Tumor Vascularization.* Clinical Cancer Research, 2006. **12**(19): p. 5879-5886.
248. Narayanan, B.A., et al., *Effects of a combination of docosahexaenoic acid and 1,4-phenylene bis(methylene) selenocyanate on cyclooxygenase 2, inducible nitric oxide synthase and β-catenin pathways in colon cancer cells.* Carcinogenesis, 2004. **25**(12): p. 2443-2449.
249. Chiu, L.C.M., K.F. Tong, and V.E.C. Ooi, *Cytostatic and cytotoxic effects of cyclooxygenase inhibitors and their synergy with docosahexaenoic acid on the growth of human skin melanoma A-375 cells.* Biomedicine & Pharmacotherapy, 2005. **59, Supplement 2**: p. S293-S297.
250. Newman, M.J., *Inhibition of carcinoma and melanoma cell growth by type 1 transforming growth factor beta is dependent on the presence of polyunsaturated fatty acids.* Proceedings of the National Academy of Sciences, 1990. **87**(14): p. 5543-5547.
251. Qiao, S., et al., *D-Penicillamine targets metastatic melanoma cells with induction of the unfolded protein response (UPR) and Noxa (PMAIP1)-dependent mitochondrial apoptosis.* Apoptosis, 2012. **17**(10): p. 1079-94.
252. Jiang, C.C., et al., *Glucose-regulated protein 78 antagonizes cisplatin and adriamycin in human melanoma cells.* Carcinogenesis, 2009. **30**(2): p. 197-204.
253. Corazzari, M., et al., *Targeting homeostatic mechanisms of endoplasmic reticulum stress to increase susceptibility of cancer cells to fenretinide-induced apoptosis: the role of stress proteins ERdj5 and ERp57.* British Journal of Cancer, 2007. **96**(7): p. 1062-71.
254. Qin, J.-Z., et al., *Proteasome Inhibitors Trigger NOXA-Mediated Apoptosis in Melanoma and Myeloma Cells.* Cancer Res, 2005. **65**(14): p. 6282-6293.
255. Amiri, K.I., et al., *Augmenting Chemosensitivity of Malignant Melanoma Tumors via Proteasome Inhibition: Implication for Bortezomib (VELCADE, PS-341) as a Therapeutic Agent for Malignant Melanoma.* Cancer Res, 2004. **64**(14): p. 4912-4918.
256. Jiang, C.C., et al., *Tunicamycin Sensitizes Human Melanoma Cells to Tumor Necrosis Factor–Related Apoptosis-Inducing Ligand–Induced Apoptosis by Up-regulation of TRAIL-R2 via the Unfolded Protein Response.* Cancer Res, 2007. **67**(12): p. 5880-5888.
257. de Wilt, L.H.A.M., et al., *Bortezomib and TRAIL: A perfect match for apoptotic elimination of tumour cells?* Critical Reviews in Oncology/Hematology, 2013. **85**(3): p. 363-372.
258. Nikrad, M., et al., *The proteasome inhibitor bortezomib sensitizes cells to killing by death receptor ligand TRAIL via BH3-only proteins Bik and Bim.* Molecular Cancer Therapeutics, 2005. **4**(3): p. 443-449.

259. Lecis, D., et al., *Novel SMAC-mimetics synergistically stimulate melanoma cell death in combination with TRAIL and Bortezomib.* British Journal of Cancer, 2010. **102**(12): p. 1707-1716.
260. Lovat, P.E., et al., *Increasing melanoma cell death using inhibitors of protein disulfide isomerases to abrogate survival responses to endoplasmic reticulum stress.* Cancer Res, 2008. **68**(13): p. 5363-9.
261. Hill, D.S., et al., *Combining the ER-stress inducing agents bortezomib and fenretinide as a novel therapeutic strategy for metastatic melanoma.* Clinical cancer research : an official journal of the American Association for Cancer Research, 2009. **15**(4): p. 1192-1198.
262. Martin, S., et al., *Targeting GRP78 to enhance melanoma cell death.* Pigment cell & melanoma research, 2010. **23**(5): p. 675-682.
263. Chapman, P.B., et al., *Improved Survival with Vemurafenib in Melanoma with BRAF V600E Mutation.* New England Journal of Medicine, 2011. **364**(26): p. 2507-2516.
264. Sosman, J.A., et al., *Survival in BRAF V600–Mutant Advanced Melanoma Treated with Vemurafenib.* New England Journal of Medicine, 2012. **366**(8): p. 707-714.
265. Hartsough, E.J. and A.E. Aplin, *A STATement on Vemurafenib-Resistant Melanoma.* The Journal of investigative dermatology, 2013. **133**(8): p. 1928-1929.
266. Ma, X.-H., et al., *Targeting ER stress–induced autophagy overcomes BRAF inhibitor resistance in melanoma.* The Journal of Clinical Investigation, 2014. **124**(3): p. 1406-1417.
267. Prasad, V., et al., *Chemical induction of unfolded protein response enhances cancer cell killing through lytic virus infection.* J Virol, 2014. **88**(22): p. 13086-98.
268. Kim, Y., et al., *Targeting Heat Shock Proteins on Cancer Cells: Selection, Characterization, and Cell-Penetrating Properties of a Peptidic GRP78 Ligand†.* Biochemistry, 2006. **45**(31): p. 9434-9444.
269. Mactier, S., et al., *Protein signatures correspond to survival outcomes of AJCC stage III melanoma patients.* Pigment Cell Melanoma Res, 2014. **27**(6): p. 1106-16.
270. MacLean, B., et al., *Skyline: an open source document editor for creating and analyzing targeted proteomics experiments.* Bioinformatics, 2010. **26**(7): p. 966-8.
271. Kusebauch, U., et al., *Human SRMAtlas: A Resource of Targeted Assays to Quantify the Complete Human Proteome.* Cell, 2016. **166**(3): p. 766-78.
272. Maclean, B., et al., *Effect of collision energy optimization on the measurement of peptides by selected reaction monitoring (SRM) mass spectrometry.* Anal Chem, 2010. **82**(24): p. 10116-24.
273. Jacob, L., J.A. Gagnon-Bartsch, and T.P. Speed, *Correcting gene expression data when neither the unwanted variation nor the factor of interest are observed.* Biostatistics, 2016. **17**(1): p. 16-28.
274. Strbenac, D., et al., *ClassifyR: an R package for performance assessment of classification with applications to transcriptomics.* Bioinformatics, 2015. **31**(11): p. 1851-3.
275. Aguirre-Gamboa, R., et al., *SurvExpress: An Online Biomarker Validation Tool and Database for Cancer Gene Expression Data Using Survival Analysis.* PLOS ONE, 2013. **8**(9): p. e74250.
276. Akbani, R., et al., *Genomic Classification of Cutaneous Melanoma.* Cell. **161**(7): p. 1681-1696.
277. Bairoch, A., *The Cellosaurus, a Cell-Line Knowledge Resource.* J Biomol Tech, 2018. **29**(2): p. 25-38.

278. Shilov, I.V., et al., *The Paragon Algorithm, a next generation search engine that uses sequence temperature values and feature probabilities to identify peptides from tandem mass spectra.* Molecular & cellular proteomics, 2007. **6**(9): p. 1638-55.
279. Waskom, M.L., *Seaborn: statistical data visualization.* Journal of Open Source Software, 2021. **6**(60): p. 3021.
280. Komer, B., J. Bergstra, and C. Eliasmith, *Hyperopt-sklearn*, in *Automated Machine Learning*. 2019, Springer, Cham. p. 97-111.
281. Towbin, H., T. Staehelin, and J. Gordon, *Electrophoretic transfer of proteins from polyacrylamide gels to nitrocellulose sheets: procedure and some applications.* Proc Natl Acad Sci U S A, 1979. **76**(9): p. 4350-4.
282. Szklarczyk, D., et al., *STRING v11: protein-protein association networks with increased coverage, supporting functional discovery in genome-wide experimental datasets.* Nucleic Acids Res, 2019. **47**(D1): p. D607-d613.
283. von Mering, C., et al., *STRING: known and predicted protein-protein associations, integrated and transferred across organisms.* Nucleic Acids Res, 2005. **33**(Database issue): p. D433-7.
284. Krisp, C., et al., *Proteomic phenotyping of metastatic melanoma reveals putative signatures of MEK inhibitor response and prognosis.* British Journal of Cancer, 2018. **119**(6): p. 713-723.
285. Müllner, D., *fastcluster: Fast Hierarchical, Agglomerative Clustering Routines for R and Python.* Journal of Statistical Software, 2013. **53**(9): p. 1 - 18.
286. Hoadley, K.A., et al., *Cell-of-Origin Patterns Dominate the Molecular Classification of 10,000 Tumors from 33 Types of Cancer.* Cell, 2018. **173**(2): p. 291-304.e6.
287. Liu, J., et al., *An Integrated TCGA Pan-Cancer Clinical Data Resource to Drive High-Quality Survival Outcome Analytics.* Cell, 2018. **173**(2): p. 400-416.e11.
288. Davidson-Pilon, C., *lifelines, survival analysis in Python*. https://github.com/camDavidsonPilon/lifelines.
289. Nestle, M. and H. Carol, *Melanoma*. Dermatology. 2003, Mosby. New York, New York, USA. .
290. AIHW, *Australian Cancer Incidence and Mortaility (ACIM): Melanoma of the skin*. 2017, Australina Institute of Health and Welfare: Canberra.
291. Whiteman, D.C., A.C. Green, and C.M. Olsen, *The Growing Burden of Invasive Melanoma: Projections of Incidence Rates and Numbers of New Cases in Six Susceptible Populations through 2031.* Journal of Investigative Dermatology, 2016. **136**(6): p. 1161-71.
292. Moreno Nogueira, J.A., M. Valero Arbizu, and R. Pérez Temprano, *Adjuvant Treatment of Melanoma.* ISRN Dermatology, 2013. **2013**: p. 545631.
293. Sahin, S., et al., *Predicting ten-year survival of patients with primary cutaneous melanoma.* Cancer, 1997. **80**(8): p. 1426-1431.
294. Bedrosian, I., et al., *Incidence of sentinel node metastasis in patients with thin primary melanoma (< or = 1 mm) with vertical growth phase.* Ann Surg Oncol, 2000. **7**(4): p. 262-7.
295. Khan, M.K., et al., *Future of radiation therapy for malignant melanoma in an era of newer, more effective biological agents.* OncoTargets and therapy, 2011. **4**: p. 137-148.
296. Jonasch, E., et al., *Adjuvant high-dose interferon alfa-2b in patients with high-risk melanoma.* Cancer, 2000. **6**(3): p. 139-45.
297. Schadendorf, D., et al., *Melanoma.* Nature Reviews Disease Primers, 2015. **1**: p. 15003.
298. Eggermont, A.M.M., et al., *Prolonged Survival in Stage III Melanoma with Ipilimumab Adjuvant Therapy.* New England Journal of Medicine, 2016. **375**(19): p. 1845-1855.

299. Mann, G.J., et al., *BRAF mutation, NRAS mutation, and the absence of an immune-related expressed gene profile predict poor outcome in patients with stage III melanoma.* Journal of Investigative Dermatology, 2013. **133**(2): p. 509-17.
300. Balch, C.M., et al., *Final version of the American Joint Committee on Cancer staging system for cutaneous melanoma.* Journal of Clinical Oncology, 2001. **19**(16): p. 3635-48.
301. Morton, D.L., et al., *Multivariate analysis of the relationship between survival and the microstage of primary melanoma by clark level and breslow thickness.* Cancer, 1993. **71**(11): p. 3737-3743.
302. Jonsson, G., et al., *Gene expression profiling-based identification of molecular subtypes in stage IV melanomas with different clinical outcome.* Clinical Cancer Research, 2010. **16**(13): p. 3356-67.
303. Tembe, V., et al., *MicroRNA and mRNA expression profiling in metastatic melanoma reveal associations with BRAF mutation and patient prognosis.* Pigment Cell Melanoma Res, 2015. **28**(3): p. 254-66.
304. Journe, F., et al., *TYRP1 mRNA expression in melanoma metastases correlates with clinical outcome.* British Journal of Cancer, 2011. **105**(11): p. 1726-32.
305. Brunner, G., et al., *A nine-gene signature predicting clinical outcome in cutaneous melanoma.* J Cancer Res Clin Oncol, 2013. **139**(2): p. 249-58.
306. Cheng, Y., et al., *Stage-specific prognostic biomarkers in melanoma.* Oncotarget, 2015. **6**(6): p. 4180-4189.
307. Wang, E., et al., *Prospective Molecular Profiling of Melanoma Metastases Suggests Classifiers of Immune Responsiveness.* Cancer Res, 2002. **62**(13): p. 3581-3586.
308. Ugurel, S., J. Utikal, and J.C. Becker, *Tumor biomarkers in melanoma.* Cancer control: journal of the Moffitt Cancer Center, 2009. **16**(3): p. 219.
309. Tarhini, A.A., et al., *Prognostic Significance of Serum S100B Protein in High-Risk Surgically Resected Melanoma Patients Participating in Intergroup Trial ECOG 1694.* Journal of Clinical Oncology, 2009. **27**(1): p. 38-44.
310. Palmer, S.R., et al., *Circulating Serologic and Molecular Biomarkers in Malignant Melanoma.* Mayo Clin Proc, 2011. **86**(10): p. 981-990.
311. Vereecken, P., et al., *A synopsis of serum biomarkers in cutaneous melanoma patients.* Dermatol Res Pract, 2012. **2012**: p. 260643.
312. Finck, S.J., A.E. Giuliano, and D.L. Morton, *LDH and melanoma.* Cancer, 1983. **51**(5): p. 840-3.
313. Hofmann, M.A., et al., *Diagnostic value of melanoma inhibitory activity serum marker in the follow-up of patients with stage I or II cutaneous melanoma.* Melanoma research, 2009. **19**(1): p. 17-23.
314. Hofmann, M.A., et al., *Impact of lymph node metastases on serum level of melanoma inhibitory activity in stage III melanoma patients.* J Dermatol, 2011. **38**(9): p. 880-6.
315. Schadendorf, D., et al., *Glutathione and related enzymes in tumor progression and metastases of human melanoma.* Journal of Investigative Dermatology, 1995. **105**(1): p. 109-12.
316. Townsend, D.M. and K.D. Tew, *The role of glutathione-S-transferase in anti-cancer drug resistance.* Oncogene, 0000. **22**(47): p. 7369-7375.
317. Rebbeck, T.R., *Molecular epidemiology of the human glutathione S-transferase genotypes GSTM1 and GSTT1 in cancer susceptibility.* Cancer Epidemiology Biomarkers & Prevention, 1997. **6**(9): p. 733-743.
318. Lin, C.-Y., et al., *GP96 is over-expressed in oral cavity cancer and is a poor prognostic indicator for patients receiving radiotherapy.* Radiation Oncology, 2011. **6**(1): p. 136.

319. Chen, Y., et al., *Expression of heat-shock protein gp96 in gallbladder cancer and its prognostic clinical significance.* International Journal of Clinical and Experimental Pathology, 2015. **8**(2): p. 1946-1953.
320. Tanaka, K., et al., *Enhanced expression of mRNAs of antisecretory factor-1, gp96, DAD1 and CDC34 in human hepatocellular carcinomas.* Biochimica et Biophysica Acta, 2001. **1536**(1): p. 1-12.
321. Wang, Q., et al., *Expression of endoplasmic reticulum molecular chaperon GRP94 in human lung cancer tissues and its clinical significance.* Chinese medical journal, 2002. **115**(11): p. 1615-1619.
322. Ghanipour, A., et al., *The Prognostic Significance of Tryptophanyl-tRNA Synthetase in Colorectal Cancer.* Cancer Epidemiology Biomarkers & Prevention, 2009. **18**(11): p. 2949.
323. Wakasugi, K., et al., *A human aminoacyl-tRNA synthetase as a regulator of angiogenesis.* Proceedings of the National Academy of Sciences, 2002. **99**(1): p. 173-177.
324. Rubin, B.Y., et al., *Interferon induces tryptophanyl-tRNA synthetase expression in human fibroblasts.* Journal of Biological Chemistry, 1991. **266**(36): p. 24245-8.
325. Lay, A.J., et al., *Phosphoglycerate kinase acts in tumour angiogenesis as a disulphide reductase.* Nature, 2000. **408**(6814): p. 869-873.
326. Miyanaga, A., et al., *Diagnostic and prognostic significance of the alternatively spliced ACTN4 variant in high-grade neuroendocrine pulmonary tumours.* Annals of Oncology, 2013. **24**(1): p. 84-90.
327. Fukushima, S., et al., *Immunohistochemical actinin-4 expression in infiltrating gliomas: association with WHO grade and differentiation.* Brain Tumor Pathology, 2014. **31**(1): p. 11-16.
328. Yamamoto, S., et al., *Actinin-4 expression in ovarian cancer: a novel prognostic indicator independent of clinical stage and histological type.* Modern Pathology, 2007. **20**(12): p. 1278-1285.
329. Oberhauser, A.F., et al., *The molecular elasticity of the extracellular matrix protein tenascin.* Nature, 1998. **393**(6681): p. 181-185.
330. Herlyn, M., et al., *Characterization of tenascin secreted by human melanoma cells.* Cancer Res, 1991. **51**(18): p. 4853-8.
331. Ilmonen, S., et al., *Tenascin-C in primary malignant melanoma of the skin.* Histopathology, 2004. **45**(4): p. 405-11.
332. Arendt, C.W. and H.L. Ostergaard, *Two distinct domains of the beta-subunit of glucosidase II interact with the catalytic alpha-subunit.* Glycobiology, 2000. **10**(5): p. 487-92.
333. Goh, K.C., et al., *Identification of p90, a Prominent Tyrosine-phosphorylated Protein in Fibroblast Growth Factor-stimulated Cells, as 80K-H.* Journal of Biological Chemistry, 1996. **271**(10): p. 5832-5838.
334. Dumache, R., et al., *DNA methylation of GSTP1, a promising biomarker in early detection of prostate cancer.* Toxicology Letters, 2009. **189, Supplement**: p. S161.
335. Wang, X.P., et al., *Expression and significance of heat shock protein 70 and glucose-regulated protein 94 in human esophageal carcinoma.* World Journal of Gastroenterology, 2005. **11**.
336. Coghlin, C., et al., *Characterization and over-expression of chaperonin t-complex proteins in colorectal cancer.* J Pathol, 2006. **210**(3): p. 351-7.

337. Guest, S.T., et al., *Two members of the TRiC chaperonin complex, CCT2 and TCP1 are essential for survival of breast cancer cells and are linked to driving oncogenes.* Exp Cell Res, 2015. **332**(2): p. 223-35.
338. Yu, H.-J., et al., *Tumor Stiffness Is Unrelated to Myosin Light Chain Phosphorylation in Cancer Cells.* PLOS ONE, 2013. **8**(11): p. e79776.
339. Noh, D.Y., et al., *Overexpression of peroxiredoxin in human breast cancer.* Anticancer research, 2001. **21**(3b): p. 2085-90.
340. Duan, J., et al., *siRNA targeting of PRDX3 enhances cisplatin-induced apoptosis in ovarian cancer cells through the suppression of the NF-κB signaling pathway.* Molecular Medicine Reports, 2013. **7**: p. 1688-1694.
341. Forough, R., et al., *Elevated 80K-H protein in breast cancer: a role for FGF-1 stimulation of 80K-H.* Int J Biol Markers, 2003. **18**(2): p. 89-98.
342. Honda, K., et al., *Actinin-4, a Novel Actin-bundling Protein Associated with Cell Motility and Cancer Invasion.* The Journal of Cell Biology, 1998. **140**(6): p. 1383-1393.
343. Ahmad, S.S., et al., *Phosphoglycerate kinase 1 as a promoter of metastasis in colon cancer.* Int J Oncol, 2013. **43**(2): p. 586-90.
344. Sun, S., et al., *Phosphoglycerate kinase-1 is a predictor of poor survival and a novel prognostic biomarker of chemoresistance to paclitaxel treatment in breast cancer.* British Journal of Cancer, 2015. **112**(8): p. 1332-1339.
345. Yan, H., et al., *Over-expression of cofilin-1 and phosphoglycerate kinase 1 in astrocytomas involved in pathogenesis of radioresistance.* CNS Neurosci Ther, 2012. **18**(9): p. 729-36.
346. Tuominen, H. and M. Kallioinen, *Increased tenascin expression in melanocytic tumors.* Journal of Cutaneous Pathology, 1994. **21**(5): p. 424-9.
347. Ross, J.S., *Breast cancer biomarkers and HER2 testing after 10 years of anti-HER2 therapy.* Drug News Perspect, 2009. **22**(2): p. 93-106.
348. Piccart, M., et al., *The predictive value of HER2 in breast cancer.* Oncology, 2001. **61 Suppl 2**: p. 73-82.
349. Weigel, M.T. and M. Dowsett, *Current and emerging biomarkers in breast cancer: prognosis and prediction.* Endocrine-Related Cancer, 2010. **17**(4): p. R245-R262.
350. Polanski, M. and N.L. Anderson, *A List of Candidate Cancer Biomarkers for Targeted Proteomics.* Biomarker Insights, 2006. **1**: p. 1-48.
351. Cook, G.B., et al., *Clinical utility of serum HER-2/neu testing on the Bayer Immuno 1 automated system in breast cancer.* Anticancer research, 2001. **21**(2b): p. 1465-70.
352. Rhodes, A., et al., *Frequency of oestrogen and progesterone receptor positivity by immunohistochemical analysis in 7016 breast carcinomas: correlation with patient age, assay sensitivity, threshold value, and mammographic screening.* J Clin Pathol, 2000. **53**(9): p. 688-96.
353. Mor, G., et al., *Serum protein markers for early detection of ovarian cancer.* Proc Natl Acad Sci U S A, 2005. **102**(21): p. 7677-82.
354. Cheang, M.C.U., et al., *Basal-Like Breast Cancer Defined by Five Biomarkers Has Superior Prognostic Value than Triple-Negative Phenotype.* Clinical Cancer Research, 2008. **14**(5): p. 1368-1376.
355. Schmitz, C., et al., *Comparative study on the clinical use of protein S-100B and MIA (melanoma inhibitory activity) in melanoma patients.* Anticancer research, 2000. **20**(6d): p. 5059-63.
356. Kluger, H.M., et al., *Plasma Markers for Identifying Patients with Metastatic Melanoma.* Clinical Cancer Research, 2011. **17**(8): p. 2417-2425.
357. Barak, V., et al., *Serum Markers to Detect Metastatic Uveal Melanoma.* Anticancer research, 2007. **27**(4A): p. 1897-1900.

358. Barak, V., et al., *The dynamics of serum tumor markers in predicting metastatic uveal melanoma (part 1).* Anticancer research, 2011. **31**(1): p. 345-9.
359. Hayward, N.K., et al., *Whole-genome landscapes of major melanoma subtypes.* Nature, 2017. **advance online publication**.
360. Stidham, K.R., J.L. Johnson, and H.F. Seigler, *Survival superiority of females with melanoma: A multivariate analysis of 6383 patients exploring the significance of gender in prognostic outcome.* Archives of Surgery, 1994. **129**(3): p. 316-324.
361. Van Eyk, J.E., et al., *Highlights of the Biology and Disease-driven Human Proteome Project, 2015–2016.* Journal of proteome research, 2016. **15**(11): p. 3979-3987.
362. Rosenberger, G., et al., *A repository of assays to quantify 10,000 human proteins by SWATH-MS.* Scientific Data, 2014. **1**: p. 140031.
363. Guo, B., et al., *Targeting inflammasome/IL-1 pathways for cancer immunotherapy.* Scientific Reports, 2016. **6**: p. 36107.
364. Okamoto, M., et al., *Constitutively active inflammasome in human melanoma cells mediating autoinflammation via caspase-1 processing and secretion of interleukin-1beta.* J Biol Chem, 2010. **285**(9): p. 6477-88.
365. Liu, W., et al., *Dual role of apoptosis-associated speck-like protein containing a CARD (ASC) in tumorigenesis of human melanoma.* Journal of Investigative Dermatology, 2013. **133**(2): p. 518-27.
366. Arnold-Schild, D., et al., *Cutting Edge: Receptor-Mediated Endocytosis of Heat Shock Proteins by Professional Antigen-Presenting Cells.* The Journal of Immunology, 1999. **162**(7): p. 3757.
367. Janetzki, S., N.E. Blachere, and P.K. Srivastava, *Generation of tumor-specific cytotoxic T lymphocytes and memory T cells by immunization with tumor-derived heat shock protein gp96.* Journal of immunotherapy, 1998. **21**(4): p. 269-276.
368. Chandawarkar, R.Y., M.S. Wagh, and P.K. Srivastava, *The Dual Nature of Specific Immunological Activity of Tumor-derived gp96 Preparations.* The Journal of Experimental Medicine, 1999. **189**(9): p. 1437.
369. Zhou, J., et al., *Upregulation of Gp96 correlates with the radiosensitivity and five-year survival rate of nasopharyngeal carcinoma.* ORL, 2012. **74**(3): p. 164-171.
370. Chhabra, S., et al., *High expression of endoplasmic reticulum chaperone grp94 is a novel molecular hallmark of malignant plasma cells in multiple myeloma.* Journal of Hematology & Oncology, 2015. **8**(1): p. 77.
371. Przepiorka, D. and P.K. Srivastava, *Heat shock protein–peptide complexes as immunotherapy for human cancer.* Molecular medicine today, 1998. **4**(11): p. 478-484.
372. Heikema, A., et al., *Generation of heat shock protein-based vaccines by intracellular loading of gp96 with antigenic peptides.* Immunology letters, 1997. **57**(1): p. 69-74.
373. Rivoltini, L., et al., *Human Tumor-Derived Heat Shock Protein 96 Mediates In Vitro Activation and In Vivo Expansion of Melanoma- and Colon Carcinoma-Specific T Cells.* The Journal of Immunology, 2003. **171**(7): p. 3467.
374. Testori, A., et al., *Phase III Comparison of Vitespen, an Autologous Tumor-Derived Heat Shock Protein gp96 Peptide Complex Vaccine, With Physician's Choice of Treatment for Stage IV Melanoma: The C-100-21 Study Group.* Journal of Clinical Oncology, 2008. **26**(6): p. 955-962.
375. Nanus, D.M., *Of peptides and peptidases: the role of cell surface peptidases in cancer.* Clinical Cancer Research, 2003. **9**(17): p. 6307-9.
376. Beninga, J., K.L. Rock, and A.L. Goldberg, *Interferon-γ Can Stimulate Post-proteasomal Trimming of the N Terminus of an Antigenic Peptide by Inducing Leucine Aminopeptidase.* Journal of Biological Chemistry, 1998. **273**(30): p. 18734-18742.

377. Saric, T., et al., *An IFN-gamma-induced aminopeptidase in the ER, ERAP1, trims precursors to MHC class I-presented peptides.* Nat Immunol, 2002. **3**(12): p. 1169-76.
378. Watanabe, Y., et al., *Adipocyte-Derived Leucine Aminopeptidase Suppresses Angiogenesis in Human Endometrial Carcinoma via Renin-Angiotensin System.* Clinical Cancer Research, 2003. **9**(17): p. 6497-6503.
379. Reano, A., et al., *Gamma interferon potently induces tryptophanyl-tRNA synthetase expression in human keratinocytes.* Journal of Investigative Dermatology, 1993. **100**(6): p. 775-779.
380. Depeille, P., et al., *Combined effects of GSTP1 and MRP1 in melanoma drug resistance.* British Journal of Cancer, 2005. **93**(2): p. 216-223.
381. Nagai, F., E. Kato, and H.-o. Tamura, *Oxidative Stress Induces GSTP1 and CYP3A4 Expression in the Human Erythroleukemia Cell Line, K562.* Biological and Pharmaceutical Bulletin, 2004. **27**(4): p. 492-495.
382. Zieker, D., et al., *PGK1 a prospect marker for peritoneal dissemination in gastric cancer.* Journal of Clinical Oncology, 2008. **26**(90150): p. 22171-22171.
383. Duan, Z., et al., *Overexpression of human phosphoglycerate kinase 1 (PGK1) induces a multidrug resistance phenotype.* Anticancer research, 2002. **22**(4): p. 1933-41.
384. Lay, A.J., et al., *Plasmin Reduction by Phosphoglycerate Kinase Is a Thiol-independent Process.* Journal of Biological Chemistry, 2002. **277**(11): p. 9062-9068.
385. Al-Eisawi, Z., et al., *Changes in the in vitro activity of platinum drugs when administered in two aliquots.* BMC Cancer, 2016. **16**(1): p. 688.
386. Cui, X., et al., *Overexpression of chaperonin containing TCP1, subunit 3 predicts poor prognosis in hepatocellular carcinoma.* World Journal of Gastroenterology, 2015. **21**(28): p. 8588-8604.
387. Bassiouni, R., et al., *Chaperonin Containing TCP-1 Protein Level in Breast Cancer Cells Predicts Therapeutic Application of a Cytotoxic Peptide.* Clinical Cancer Research, 2016. **22**(17): p. 4366-79.
388. Huang, X., et al., *Chaperonin containing TCP1, subunit 8 (CCT8) is upregulated in hepatocellular carcinoma and promotes HCC proliferation.* Journal of Pathology, Microbiology and Immunology, 2014. **122**(11): p. 1070-1079.
389. Ouderkirk, J.L. and M. Krendel, *Non-muscle myosins in tumor progression, cancer cell invasion, and metastasis.* Cytoskeleton, 2014. **71**(8): p. 447-463.
390. Wonsey, D.R., K.I. Zeller, and C.V. Dang, *The c-Myc target gene PRDX3 is required for mitochondrial homeostasis and neoplastic transformation.* Proc Natl Acad Sci U S A, 2002. **99**(10): p. 6649-54.
391. Rhee, S.G. and H.A. Woo, *Multiple functions of peroxiredoxins: peroxidases, sensors and regulators of the intracellular messenger H(2)O(2), and protein chaperones.* Antioxidants & Redox Signaling, 2011. **15**(3): p. 781-94.
392. Klaunig, J.E., L.M. Kamendulis, and B.A. Hocevar, *Oxidative stress and oxidative damage in carcinogenesis.* Toxicol Pathol, 2010. **38**(1): p. 96-109.
393. Fukunaga-Kalabis, M., et al., *Tenascin-C promotes melanoma progression by maintaining the ABCB5-positive side population.* Oncogene, 2010. **29**(46): p. 6115-6124.
394. Mactier, S., et al., *Protein signatures correspond to survival outcomes of AJCC stage III melanoma patients.* 2014. **27**(6): p. 1106-1116.
395. Oslowski, C.M. and F. Urano, *Measuring ER stress and the unfolded protein response using mammalian tissue culture system.* Methods Enzymol, 2011. **490**: p. 71-92.
396. Jaskulska, A., A.E. Janecka, and K. Gach-Janczak, *Thapsigargin—From Traditional Medicine to Anticancer Drug.* 2021. **22**(1): p. 4.

397. Zahn-Zabal, M., et al., *The neXtProt knowledgebase in 2020: data, tools and usability improvements.* Nucleic Acids Res, 2019. **48**(D1): p. D328-D334.
398. Tsukumo, Y., et al., *Nucleobindin 1 controls the unfolded protein response by inhibiting ATF6 activation.* J Biol Chem, 2007. **282**(40): p. 29264-72.
399. Vig, S., et al., *Cytokine-induced translocation of GRP78 to the plasma membrane triggers a pro-apoptotic feedback loop in pancreatic beta cells.* Cell Death & Disease, 2019. **10**(4): p. 309.
400. Arap, M.A., et al., *Cell surface expression of the stress response chaperone GRP78 enables tumor targeting by circulating ligands.* Cancer Cell, 2004. **6**(3): p. 275-84.
401. Kern, J., et al., *GRP-78 secreted by tumor cells blocks the antiangiogenic activity of bortezomib.* Blood, 2009. **114**(18): p. 3960-7.
402. Ni, M., Y. Zhang, and A.S. Lee, *Beyond the endoplasmic reticulum: atypical GRP78 in cell viability, signalling and therapeutic targeting.* Biochemical Journal, 2011. **434**(2): p. 181-8.
403. Ni, M., et al., *Regulation of PERK signaling and leukemic cell survival by a novel cytosolic isoform of the UPR regulator GRP78/BiP.* PLOS ONE, 2009. **4**(8): p. e6868-e6868.
404. Ferri, K.F. and G. Kroemer, *Organelle-specific initiation of cell death pathways.* Nat Cell Biol, 2001. **3**(11): p. E255-63.
405. Breckenridge, D.G., et al., *Regulation of apoptosis by endoplasmic reticulum pathways.* Oncogene, 2003. **22**(53): p. 8608-18.
406. Sun, F.-C., et al., *Localization of GRP78 to mitochondria under the unfolded protein response.* Biochemical Journal, 2006. **396**(1): p. 31-39.
407. Hayashi, T. and T.P. Su, *Sigma-1 receptor chaperones at the ER-mitochondrion interface regulate Ca(2+) signaling and cell survival.* Cell, 2007. **131**(3): p. 596-610.
408. Ouyang, Y.-B., et al., *Overexpressing GRP78 influences Ca2+ handling and function of mitochondria in astrocytes after ischemia-like stress.* Mitochondrion, 2011. **11**(2): p. 279-286.
409. Ogata, S., et al., *Expressions of ATF6, XBP1, and GRP78 in normal tissue, atypical adenomatous hyperplasia, and adenocarcinoma of the lung.* Human Pathology, 2019. **83**: p. 22-28.
410. Jiang, Q., et al., *Crosstalk Between Nuclear Glucose-Regulated Protein 78 and Tumor Protein 53 Contributes to the Lipopolysaccharide Aggravated Apoptosis of Endoplasmic Reticulum Stress-Responsive Porcine Intestinal Epithelial Cells.* Cellular Physiology and Biochemistry, 2018. **48**(6): p. 2441-2455.
411. Morris, J.A., et al., *Immunoglobulin binding protein (BiP) function is required to protect cells from endoplasmic reticulum stress but is not required for the secretion of selective proteins.* J Biol Chem, 1997. **272**(7): p. 4327-34.
412. Kaneda, S., T. Yura, and H. Yanagi, *Production of three distinct mRNAs of 150 kDa oxygen-regulated protein (ORP150) by alternative promoters: preferential induction of one species under stress conditions.* J Biochem, 2000. **128**(3): p. 529-38.
413. Park, J., et al., *The chaperoning properties of mouse grp170, a member of the third family of hsp70 related proteins.* Biochemistry, 2003. **42**(50): p. 14893-902.
414. Jaeger, J., et al., *Gene expression signatures for tumor progression, tumor subtype, and tumor thickness in laser-microdissected melanoma tissues.* Clinical Cancer Research, 2007. **13**(3): p. 806-15.
415. Abdullah, C., X. Wang, and D. Becker, *Expression analysis and molecular targeting of cyclin-dependent kinases in advanced melanoma.* Cell Cycle, 2011. **10**(6): p. 977-88.
416. Ravindran Menon, D., et al., *CDK1 Interacts with Sox2 and Promotes Tumor Initiation in Human Melanoma.* Cancer Res, 2018. **78**(23): p. 6561-6574.

417. Fisher, D.T., M.M. Appenheimer, and S.S. Evans, *The two faces of IL-6 in the tumor microenvironment.* Semin Immunol, 2014. **26**(1): p. 38-47.
418. Wang, Z., H. Zhang, and Q. Cheng, *PDIA4: The basic characteristics, functions and its potential connection with cancer.* Biomedicine & Pharmacotherapy, 2020. **122**: p. 109688.
419. Krtolica, A., et al., *Senescent fibroblasts promote epithelial cell growth and tumorigenesis: a link between cancer and aging.* Proc Natl Acad Sci U S A, 2001. **98**(21): p. 12072-7.
420. Xue, W., et al., *Senescence and tumour clearance is triggered by p53 restoration in murine liver carcinomas.* Nature, 2007. **445**(7128): p. 656-60.
421. Coppé, J.-P., et al., *Senescence-Associated Secretory Phenotypes Reveal Cell-Nonautonomous Functions of Oncogenic RAS and the p53 Tumor Suppressor.* PLOS Biology, 2008. **6**(12): p. e301.
422. Liu, D. and P.J. Hornsby, *Senescent Human Fibroblasts Increase the Early Growth of Xenograft Tumors via Matrix Metalloproteinase Secretion.* Cancer Res, 2007. **67**(7): p. 3117.
423. Ruhland, M.K., et al., *Stromal senescence establishes an immunosuppressive microenvironment that drives tumorigenesis.* Nature Communications, 2016. **7**: p. 11762.
424. Hoare, M., et al., *NOTCH1 mediates a switch between two distinct secretomes during senescence.* Nat Cell Biol, 2016. **18**(9): p. 979-92.
425. Ito, Y., M. Hoare, and M. Narita, *Spatial and Temporal Control of Senescence.* Trends Cell Biol, 2017. **27**(11): p. 820-832.
426. Prieto, L.I. and D.J. Baker, *Cellular Senescence and the Immune System in Cancer.* Gerontology, 2019. **65**(5): p. 505-512.
427. Pluquet, O., A. Pourtier, and C. Abbadie, *The unfolded protein response and cellular senescence. A Review in the Theme: Cellular Mechanisms of Endoplasmic Reticulum Stress Signaling in Health and Disease.* American Journal of Physiology-Cell Physiology, 2015. **308**(6): p. C415-C425.
428. Wang, L., L. Lankhorst, and R. Bernards, *Exploiting senescence for the treatment of cancer.* Nature Reviews Cancer, 2022. **22**(6): p. 340-355.
429. Hanahan, D. and R.A. Weinberg, *The Hallmarks of Cancer.* Cell, 2000. **100**(1): p. 57-70.
430. Warburg, O.H., F. Dickens, and B. Kaiser-Wilhelm-Institut für, *The metabolism of tumours; investigations from the Kaiser Wilhelm institute for biology, Berlin-Dahlem.* 1930, London: Constable & Co. Ltd.
431. Johnson, S. and S.-I. Imai, *NAD (+) biosynthesis, aging, and disease*. Vol. 7. 2018: Research Limited. 132-132.
432. Imai, S. and L. Guarente, *NAD+ and sirtuins in aging and disease.* Trends Cell Biol, 2014. **24**(8): p. 464-71.
433. Revollo, J.R., et al., *Nampt/PBEF/Visfatin regulates insulin secretion in beta cells as a systemic NAD biosynthetic enzyme.* Cell Metab, 2007. **6**(5): p. 363-75.
434. Zaman, A., W. Wu, and T.G. Bivona, *Targeting Oncogenic BRAF: Past, Present, and Future.* Cancers (Basel), 2019. **11**(8): p. 1197.
435. Pratilas, C.A., F. Xing, and D.B. Solit, *Targeting oncogenic BRAF in human cancer.* Current topics in microbiology and immunology, 2012. **355**: p. 83-98.
436. Caruso, M.-E., et al., *GTPase-Mediated Regulation of the Unfolded Protein Response in Caenorhabditis elegans Is Dependent on the AAA⁺ ATPase CDC-48.* Mol Cell Biol, 2008. **28**(13): p. 4261.

437. Ghosh, S., et al., *Cross-talk between endoplasmic reticulum (ER) stress and the MEK/ERK pathway potentiates apoptosis in human triple negative breast carcinoma cells: role of a dihydropyrimidone, nifetepimine.* J Biol Chem, 2015. **290**(7): p. 3936-3949.
438. Yang, F., et al., *Inhibition of mitogen-activated protein kinase signaling pathway sensitizes breast cancer cells to endoplasmic reticulum stress-induced apoptosis.* Oncol Rep, 2016. **35**(4): p. 2113-2120.
439. Hieken, T.J., et al., *Sex-Based Differences in Melanoma Survival in a Contemporary Patient Cohort.* Journal of women's health, 2020. **29**(9): p. 1160-1167.
440. Bellenghi, M., et al., *Sex and Gender Disparities in Melanoma.* Cancers (Basel), 2020. **12**(7): p. 1819.
441. Nachef, M., et al., *Targeting SLC1A5 and SLC3A2/SLC7A5 as a Potential Strategy to Strengthen Anti-Tumor Immunity in the Tumor Microenvironment.* Frontiers in Immunology, 2021. **12**.
442. Yang, Y., et al., *Discovery of SLC3A2 cell membrane protein as a potential gastric cancer biomarker: implications in molecular imaging.* Journal of proteome research, 2012. **11**(12): p. 5736-47.
443. Estrach, S., et al., *CD98hc (SLC3A2) loss protects against ras-driven tumorigenesis by modulating integrin-mediated mechanotransduction.* Cancer Res, 2014. **74**(23): p. 6878-89.
444. Dreier, M.R. and I.L. de la Serna, *SWI/SNF Chromatin Remodeling Enzymes in Melanoma.* Epigenomes, 2022. **6**(1).
445. Mehrotra, A., et al., *SWI/SNF chromatin remodeling enzymes in melanocyte differentiation and melanoma.* Crit Rev Eukaryot Gene Expr, 2014. **24**(2): p. 151-61.
446. Mehrotra, A., et al., *SWI/SNF chromatin remodeling enzymes in melanocyte differentiation and melanoma.* Epigenomes, 2014. **24**(2).
447. Tsui, K.-H., et al., *Hypoxia upregulates the gene expression of mitochondrial aconitase in prostate carcinoma cells %J Journal of Molecular Endocrinology.* 2013. **51**(1): p. 131-141.
448. Zhou, Y., et al., *HYOU1, Regulated by LPLUNC1, Is Up-Regulated in Nasopharyngeal Carcinoma and Associated with Poor Prognosis.* Cancer, 2016. **7**(4): p. 367-76.
449. Li, X., et al., *HYOU1 promotes cell growth and metastasis via activating PI3K/AKT signaling in epithelial ovarian cancer and predicts poor prognosis.* Eur Rev Med Pharmacol Sci, 2019. **23**(10): p. 4126-4135.
450. Giffin, L., et al., *Modulation of Kaposi's sarcoma-associated herpesvirus interleukin-6 function by hypoxia-upregulated protein 1.* J Virol, 2014. **88**(16): p. 9429-41.
451. Wang, J.-M., et al., *HYOU1 facilitates proliferation, invasion and glycolysis of papillary thyroid cancer via stabilizing LDHB mRNA.* Journal of Cellular and Molecular Medicine, 2021. **25**(10): p. 4814-4825.
452. Stojadinovic, A., et al., *HYOU1/Orp150 expression in breast cancer.* Med Sci Monit, 2007. **13**(11): p. Br231-239.
453. Li, C., et al., *The value of melanoma inhibitory activity and LDH with melanoma patients in a Chinese population.* Medicine - observational study, 2021. **100**(8): p. e24840.
454. Haapaniemi, E.M., et al., *Combined immunodeficiency and hypoglycemia associated with mutations in hypoxia upregulated 1.* Journal of Allergy and Clinical Immunology, 2017. **139**(4): p. 1391-1393.e11.
455. Gasparrini, M. and V. Audrito, *NAMPT: A critical driver and therapeutic target for cancer.* Int J Biochem Cell Biol, 2022. **145**: p. 106189.

456. Kennedy, B.E., et al., *NAD(+) salvage pathway in cancer metabolism and therapy.* Pharmacol Res, 2016. **114**: p. 274-283.
457. Chiarugi, A., et al., *The NAD metabolome--a key determinant of cancer cell biology.* Nature Reviews Cancer, 2012. **12**(11): p. 741-52.
458. Lockett, A., et al., *Nicotinamide Phosphoribosyltransferase Activates the Mitochondrial Unfolded Protein Response to Promote Pulmonary Arterial Endothelial Cell Proliferation*, in *Lung vascular biology and mechanisms of pulmonary arterial hypertension*. 2022, American Thoracic Society. p. A4606-A4606.
459. Zhou, Q., et al., *Nicotinamide Riboside Enhances Mitochondrial Proteostasis and Adult Neurogenesis through Activation of Mitochondrial Unfolded Protein Response Signaling in the Brain of ALS SOD1G93A Mice.* International Journal of Biological Sciences, 2020. **16**(2): p. 284-297.
460. Gariani, K., et al., *Eliciting the mitochondrial unfolded protein response by nicotinamide adenine dinucleotide repletion reverses fatty liver disease in mice.* Hepatology, 2016. **63**(4): p. 1190-1204.
461. Peaper, D.R. and P. Cresswell, *Regulation of MHC class I assembly and peptide binding.* Annual review of cell developmental biology, 2008. **24**: p. 343-368.
462. Donoghue, N., et al., *Presence of closely spaced protein thiols on the surface of mammalian cells.* Protein Science, 2000. **9**(12): p. 2436-2445.
463. Reinhardt, C., et al., *Protein disulfide isomerase acts as an injury response signal that enhances fibrin generation via tissue factor activation.* The Journal of Clinical Investigation, 2008. **118**(3): p. 1110-1122.
464. Bi, S., et al., *Galectin-9 binding to cell surface protein disulfide isomerase regulates the redox environment to enhance T-cell migration and HIV entry.* Proceedings of the National Academy of Sciences, 2011. **108**(26): p. 10650-10655.
465. Goplen, D., et al., *Protein disulfide isomerase expression is related to the invasive properties of malignant glioma.* Cancer Res, 2006. **66**(20): p. 9895-9902.
466. Kuo, T.-F., et al., *Protein disulfide isomerase a4 acts as a novel regulator of cancer growth through the procaspase pathway.* Oncogene, 2017. **36**(39): p. 5484-5496.
467. Fahrmann, J.F., et al., *Proteomic profiling of lung adenocarcinoma indicates heightened DNA repair, antioxidant mechanisms and identifies LASP1 as a potential negative predictor of survival.* Clinical Proteomics, 2016. **13**(1): p. 1-12.
468. Joo, J.H., et al., *Farnesol-induced apoptosis in human lung carcinoma cells is coupled to the endoplasmic reticulum stress response.* Cancer Res, 2007. **67**(16): p. 7929-7936.
469. Tufo, G., et al., *The protein disulfide isomerases PDIA4 and PDIA6 mediate resistance to cisplatin-induced cell death in lung adenocarcinoma.* Cell Death Differ, 2014. **21**(5): p. 685-95.
470. Samanta, S., et al., *Expression of protein disulfide isomerase family members correlates with tumor progression and patient survival in ovarian cancer.* Oncotarget, 2017. **8**(61).
471. Rahman, N.S.A., et al., *Functions and mechanisms of protein disulfide isomerase family in cancer emergence.* Cell & Bioscience, 2022. **12**(1): p. 129.
472. Li, H., et al., *PDIA4 Correlates with Poor Prognosis and is a Potential Biomarker in Glioma.* Onco Targets Ther, 2021. **14**: p. 125-138.
473. Peluso, J., *Progesterone receptor membrane component 1 and its role in ovarian follicle growth.* Frontiers in Neuroscience, 2013. **7**.
474. Peluso, J.J., et al., *Progesterone Receptor Membrane Component-1 (PGRMC1) and PGRMC-2 Interact to Suppress Entry into the Cell Cycle in Spontaneously Immortalized Rat Granulosa Cells1.* Biology of Reproduction, 2014. **91**(5).

475. Lodde, V., et al., *Insights on the Role of PGRMC1 in Mitotic and Meiotic Cell Division.* Cancers (Basel), 2022. **14**(23): p. 5755.
476. Zhu, X., et al., *PGRMC1-dependent autophagy by hyperoside induces apoptosis and sensitizes ovarian cancer cells to cisplatin treatment.* Int J Oncol, 2017. **50**(3): p. 835-846.
477. Thejer, B.M., et al., *PGRMC1 effects on metabolism, genomic mutation and CpG methylation imply crucial roles in animal biology and disease.* BMC Molecular and Cell Biology, 2020. **21**(1): p. 26.
478. Furuhata, R., et al., *Progesterone receptor membrane associated component 1 enhances obesity progression in mice by facilitating lipid accumulation in adipocytes.* Communications Biology, 2020. **3**(1): p. 479.
479. Cahill, M.A. and sterility, *Choose your partners for the next dance: implied PGRMC1 roles in membrane trafficking and mitochondrial modulation.* Fertility, 2020. **113**(5): p. 938-941.
480. He, Y., et al., *Ultrasound-triggered microbubble destruction enhances the radiosensitivity of glioblastoma by inhibiting PGRMC1-mediated autophagy in vitro and in vivo.* Military Medical Research, 2022. **9**(1): p. 1-20.
481. McGuire, M.R. and P.J. Espenshade, *PGRMC1: An enigmatic heme-binding protein.* Pharmacology Therapeutics, 2022: p. 108326.
482. Chen, Y.-J., et al., *PGRMC1 acts as a size-selective cargo receptor to drive ER-phagic clearance of mutant prohormones.* Nature Communications, 2021. **12**(1): p. 5991.
483. Peluso, J.J. and J.K. Pru, *Progesterone Receptor Membrane Component (PGRMC)1 and PGRMC2 and Their Roles in Ovarian and Endometrial Cancer.* Cancers (Basel), 2021. **13**(23).
484. Zhao, Y. and X. Ruan, *Identification of PGRMC1 as a Candidate Oncogene for Head and Neck Cancers and Its Involvement in Metabolic Activities.* Frontiers in Bioengineering and Biotechnology, 2020. **7**.
485. Ruan, X. and A.O. Mueck, *Clinical Importance of PGRMC1 in Hormone Responsive Breast Cancer*. Breast Care, 2022.
486. Willibald, M., et al., *High level of progesteron receptor membrane component 1 (PGRMC 1) in tissue of breast cancer patients is associated with worse response to anthracycline-based neoadjuvant therapy.* Hormone Metabolic Research, 2017. **49**(08): p. 595-603.
487. Thieffry, C., *Progesterone Receptor Membrane Component (PGRMC) 1: Study of its expression, regulation and potential functions in the human endometrium and in endometriosis*. 2022, UCL-Université Catholique de Louvain.
488. Lin, S.-T., et al., *PGRMC1 contributes to doxorubicin-induced chemoresistance in MES-SA uterine sarcoma.* Cellular molecular life sciences, 2015. **72**(12): p. 2395-2409.
489. Hanamuro, S., et al., *Progesterone receptor membrane component 2 expression leads to erlotinib resistance in lung adenocarcinoma cells.* Die Pharmazie-An International Journal of Pharmaceutical Sciences, 2021. **76**(12): p. 602-605.
490. Dika, E., et al., *Estrogen Receptors and Melanoma: A Review.* Cells, 2019. **8**(11).
491. Scoggins, C.R., et al., *Gender-related differences in outcome for melanoma patients.* Ann Surg, 2006. **243**(5): p. 693-8; discussion 698-700.
492. Ghanipour, A., et al., *The prognostic significance of tryptophanyl-tRNA synthetase in colorectal cancer.* Cancer epidemiology, biomarkers & prevention, 2009. **18**(11): p. 2949-2956.

493. Paley, E.L., et al., *Hypoxia signature of splice forms of tryptophanyl-tRNA synthetase marks pancreatic cancer cells with distinct metastatic abilities.* Pancreas, 2011. **40**(7): p. 1043-1056.
494. Lu, S., et al., *Expression of indoleamine 2, 3-dioxygenase 1 (IDO1) and tryptophanyl-tRNA synthetase (WARS) in gastric cancer molecular subtypes.* Applied immunohistochemistry molecular morphology: AIMM, 2020. **28**(5): p. 360.
495. Yang, P.-P., X.-H. Yu, and J. Zhou, *Tryptophanyl-tRNA synthetase (WARS) expression in uveal melanoma – possible contributor during uveal melanoma progression.* Bioscience, Biotechnology, and Biochemistry, 2020. **84**(3): p. 471-480.
496. Chi, L.-M., et al., *Enhanced interferon signaling pathway in oral cancer revealed by quantitative proteome analysis of microdissected specimens using 16O/18O labeling and integrated two-dimensional LC-ESI-MALDI tandem MS.* Molecular cellular proteomics, 2009. **8**(7): p. 1453-1474.
497. Pang, Y.L.J., K. Poruri, and S.A. Martinis, *tRNA synthetase: tRNA aminoacylation and beyond.* Wiley Interdisciplinary Reviews: RNA, 2014. **5**(4): p. 461-480.
498. Wei, Z., et al., *Alternative splicing creates two new architectures for human tyrosyl-tRNA synthetase.* Nucleic Acids Res, 2016. **44**(3): p. 1247-1255.
499. Park, M.C., et al., *Secreted human glycyl-tRNA synthetase implicated in defense against ERK-activated tumorigenesis.* Proceedings of the National Academy of Sciences, 2012. **109**(11): p. E640-E647.
500. Ahn, Y.H., et al., *Secreted tryptophanyl-tRNA synthetase as a primary defence system against infection.* 2016. **2**(1): p. 1-13.
501. Munn, D.H., et al., *GCN2 kinase in T cells mediates proliferative arrest and anergy induction in response to indoleamine 2, 3-dioxygenase.* Immunity, 2005. **22**(5): p. 633-642.
502. Théate, I., et al., *Extensive Profiling of the Expression of the Indoleamine 2, 3-Dioxygenase 1 Protein in Normal and Tumoral Human TissuesIDO1 Expression Profiling in Normal and Tumoral Tissues.* Cancer immunology research, 2015. **3**(2): p. 161-172.
503. Adam, I., et al., *Upregulation of tryptophanyl-tRNA synthethase adapts human cancer cells to nutritional stress caused by tryptophan degradation.* Oncoimmunology, 2018. **7**(12): p. e1486353.
504. Bond, P., *Regulation of mTORC1 by growth factors, energy status, amino acids and mechanical stimuli at a glance.* Journal of the International Society of Sports Nutrition, 2016. **13**(1): p. 8.
505. Liu, C., et al., *SLC3A2 is a novel endoplasmic reticulum stress-related signaling protein that regulates the unfolded protein response and apoptosis.* PLOS ONE, 2018. **13**(12): p. e0208993.
506. Zhu, B., et al., *SLC3A2 is upregulated in human osteosarcoma and promotes tumor growth through the PI3K/Akt signaling pathway.* Oncol Rep, 2017. **37**(5): p. 2575-2582.
507. El Ansari, R., et al., *The multifunctional solute carrier 3A2 (SLC3A2) confers a poor prognosis in the highly proliferative breast cancer subtypes.* British Journal of Cancer, 2018. **118**(8): p. 1115-1122.
508. Poettler, M., et al., *CD98hc (SLC3A2) drives integrin-dependent renal cancer cell behavior.* Molecular Cancer, 2013. **12**(1): p. 169.
509. Dingwall, A.K., et al., *The Drosophila snr1 and brm proteins are related to yeast SWI/SNF proteins and are components of a large protein complex.* Molecular Biology of the Cell, 1995. **6**(7): p. 777-91.

510. Kim, J., et al., *Ikaros DNA-binding proteins direct formation of chromatin remodeling complexes in lymphocytes.* Immunity, 1999. **10**(3): p. 345-55.
511. Underhill, C., et al., *A novel nuclear receptor corepressor complex, N-CoR, contains components of the mammalian SWI/SNF complex and the corepressor KAP-1.* J Biol Chem, 2000. **275**(51): p. 40463-40470.
512. Bochar, D.A., et al., *BRCA1 is associated with a human SWI/SNF-related complex: linking chromatin remodeling to breast cancer.* Cell, 2000. **102**(2): p. 257-65.
513. Mathur, R., et al., *ARID1A loss impairs enhancer-mediated gene regulation and drives colon cancer in mice.* Nature genetics, 2017. **49**(2): p. 296-302.
514. Kadoch, C., et al., *Proteomic and bioinformatic analysis of mammalian SWI/SNF complexes identifies extensive roles in human malignancy.* Nature genetics, 2013. **45**(6): p. 592-601.
515. Roberts, C.W., et al., *Highly penetrant, rapid tumorigenesis through conditional inversion of the tumor suppressor gene Snf5.* Cancer Cell International, 2002. **2**(5): p. 415-425.
516. Schoenfeld, A.J., et al., *The Genomic Landscape of SMARCA4 Alterations and Associations with Outcomes in Patients with Lung Cancer.* Clinical Cancer Research, 2020. **26**(21): p. 5701-5708.
517. Fernando, T.M., et al., *Functional characterization of SMARCA4 variants identified by targeted exome-sequencing of 131,668 cancer patients.* Nature Communications, 2020. **11**(1): p. 5551.
518. Moes-Sosnowska, J., et al., *Germline SMARCA4 mutations in patients with ovarian small cell carcinoma of hypercalcemic type.* Orphanet Journal of Rare Diseases, 2015. **10**(1): p. 32.
519. Zhang, L., et al. *SMARCA4-mutated lung adenocarcinoma, a distinctive non-small cell lung cancer with worse prognosis*. in *ASCO Annual Meeting*. 2021.
520. Kim, S.Y., et al., *SMARCA4 oncogenic potential via IRAK1 enhancer to activate Gankyrin and AKR1B10 in liver cancer.* Oncogene, 2021. **40**(28): p. 4652-4662.
521. Mardinian, K., et al., *SMARCA4: Implications of an Altered Chromatin-Remodeling Gene for Cancer Development and Therapy.* Molecular Cancer Therapeutics, 2021. **20**(12): p. 2341-2351.
522. Guidi, C.J., et al., *Disruption of Ini1 leads to peri-implantation lethality and tumorigenesis in mice.* Molecular cellular biology, 2001. **21**(10): p. 3598-3603.
523. Lin, H., et al., *Loss of SNF5 expression correlates with poor patient survival in melanoma.* Clinical Cancer Research, 2009. **15**(20): p. 6404-6411.
524. Ray, A., et al., *Human SNF5/INI1, a component of the human SWI/SNF chromatin remodeling complex, promotes nucleotide excision repair by influencing ATM recruitment and downstream H2AX phosphorylation.* Molecular cellular biology, 2009. **29**(23): p. 6206-6219.
525. Mendiratta, G., E. Ke, and M. Aziz, *Cancer gene mutation frequencies for the US population. Nat Commun 12: 5961*. 2021.
526. Shain, A.H., et al., *Abstract NG07: Genomic and transcriptomic analysis reveals incremental disruption of key signaling pathways during melanoma evolution.* Cancer Res, 2018. **78**(13_Supplement): p. NG07-NG07.
527. Váraljai, R., et al., *Integrative genomic analyses of patient-matched intracranial and extracranial metastases reveal a novel brain-specific landscape of genetic variants in driver genes of malignant melanoma.* Cancers (Basel), 2021. **13**(4): p. 731.
528. Becker, T.M., et al., *The chromatin remodelling factor BRG1 is a novel binding partner of the tumor suppressor p16INK4a.* Molecular Cancer, 2009. **8**(1): p. 1-12.

529. Versteege, I., et al., *Truncating mutations of hSNF5/INI1 in aggressive paediatric cancer.* Nature, 1998. **394**(6689): p. 203-206.
530. Roberts, C.W., et al., *Haploinsufficiency of Snf5 (integrase interactor 1) predisposes to malignant rhabdoid tumors in mice.* Proceedings of the National Academy of Sciences, 2000. **97**(25): p. 13796-13800.
531. Hadfield, K.D., et al., *Molecular characterisation of SMARCB1 and NF2 in familial and sporadic schwannomatosis.* Journal of Medical Genetics, 2008. **45**(6): p. 332-339.
532. Schaefer, I.-M., et al., *Recurrent SMARCB1 inactivation in epithelioid malignant peripheral nerve sheath tumors.* The American journal of surgical pathology, 2019. **43**(6): p. 835.
533. Ticha, I., et al., *A comprehensive evaluation of pathogenic mutations in primary cutaneous melanomas, including the identification of novel loss-of-function variants.* Scientific Reports, 2019. **9**(1): p. 1-15.
534. Lee, J.J., et al., *Targeted next-generation sequencing reveals high frequency of mutations in epigenetic regulators across treatment-naive patient melanomas.* Clinical epigenetics, 2015. **7**(1): p. 1-17.
535. Sahu, R.K., et al., *SWI/SNF chromatin remodelling complex contributes to clearance of cytoplasmic protein aggregates and regulates unfolded protein response in Saccharomyces cerevisiae.* The FEBS Journal, 2020. **287**(14): p. 3024-3041.
536. Meinke, P., T.D. Nguyen, and M.S. Wehnert, *The LINC complex and human disease.* Biochemical Society Transactions, 2011. **39**(6): p. 1693-1697.
537. Liu, L., et al., *Downregulation of SUN2 promotes metastasis of colon cancer by activating BDNF/TrkB signalling by interacting with SIRT1.* J Pathol, 2021. **254**(5): p. 531-542.
538. Matsumoto, A., et al., *Global loss of a nuclear lamina component, lamin A/C, and LINC complex components SUN 1, SUN 2, and nesprin-2 in breast cancer.* Cancer medicine, 2015. **4**(10): p. 1547-1557.
539. Liao, Y., et al., *Elevated Sad1 and UNC84 Domain Containing 2 (SUN2) level inhibits cell growth and aerobic glycolysis in oral cancer through reducing the expressions of glucose transporter 1 (GLUT1) and lactate dehydrogenase A (LDHA).* Journal of Dental Sciences, 2021. **16**(1): p. 460-466.
540. Ji, J., et al., *FBXO2 targets glycosylated SUN2 for ubiquitination and degradation to promote ovarian cancer development.* Cell Death & Disease, 2022. **13**(5): p. 1-9.
541. Yajun, C., et al., *Loss of Sun2 promotes the progression of prostate cancer by regulating fatty acid oxidation.* Oncotarget, 2017. **8**(52): p. 89620.
542. Lv, X.-b., et al., *SUN2 exerts tumor suppressor functions by suppressing the Warburg effect in lung cancer.* Scientific Reports, 2015. **5**(1): p. 17940.
543. Lei, K., et al., *Inner Nuclear Envelope Proteins SUN1 and SUN2 Play a Prominent Role in the DNA Damage Response.* Current Biology, 2012. **22**(17): p. 1609-1615.
544. Pedregosa, F.a.V., Gaël and Gramfort, Alexandre and Michel, Vincent and Thirion, Bertrand and Grisel, Olivier and Blondel, Mathieu and Müller, Andreas and Nothman, Joel and Louppe, Gilles and Prettenhofer, Peter and Weiss, Ron and Dubourg, Vincent and Vanderplas, Jake and Passos, Alexandre and Cournapeau, David and Brucher, Matthieu and Perrot, Matthieu and Duchesnay, Édouard, *Scikit-learn: Machine Learning in Python*. 2012.
545. Kim, H. and Y.-M. Kim, *Pan-cancer analysis of somatic mutations and transcriptomes reveals common functional gene clusters shared by multiple cancer types.* Scientific Reports, 2018. **8**(1): p. 6041.
546. Berger, A.C., et al., *A Comprehensive Pan-Cancer Molecular Study of Gynecologic and Breast Cancers.* Cancer Cell, 2018. **33**(4): p. 690-705.e9.

547. Chen, F., et al., *Pan-Cancer Molecular Classes Transcending Tumor Lineage Across 32 Cancer Types, Multiple Data Platforms, and over 10,000 Cases.* Clinical Cancer Research, 2018. **24**(9): p. 2182-2193.
548. Zhang, Y., et al., *Proteogenomic characterization of 2002 human cancers reveals pan-cancer molecular subtypes and associated pathways.* Nature Communications, 2022. **13**(1): p. 2669.
549. Seth, R., et al., *Systemic Therapy for Melanoma: ASCO Guideline.* 2020. **38**(33): p. 3947-3970.
550. Arora, A., et al., *Pan-cancer identification of clinically relevant genomic subtypes using outcome-weighted integrative clustering.* Genome Medicine, 2020. **12**(1): p. 110.
551. Narayanan, R. and W. Van de Ven, *Transcriptome and proteome analysis: a perspective on correlation.* MOJ Proteomics Bioinform, 2014. **1**(5): p. 00027.
552. Maier, T., M. Güell, and L. Serrano, *Correlation of mRNA and protein in complex biological samples.* FEBS Lett, 2009. **583**(24): p. 3966-3973.
553. Cole, D.W., et al., *Targeting the unfolded protein response in head and neck and oral cavity cancers.* Exp Cell Res, 2019. **382**(1): p. 111386.
554. Nagelkerke, A., et al., *Hypoxic regulation of the PERK/ATF4/LAMP3-arm of the unfolded protein response in head and neck squamous cell carcinoma.* Head & neck, 2015. **37**(6): p. 896-905.
555. Garshott, D.M., et al., *The unfolded protein response as a therapeutic target for head and neck squamous cell Carcinoma*, in *Targeting Oral Cancer*. 2016, Springer. p. 225-261.
556. Chen, J. and B. Zhang. *Development and validation of an unfolded protein response-related gene signature to predict overall survival in HNSCC*. in *ASCO Annual Meeting*. 2021. Wolters Kluwer Health.
557. Jorgensen, E., et al., *Cigarette smoke induces endoplasmic reticulum stress and the unfolded protein response in normal and malignant human lung cells.* BMC Cancer, 2008. **8**(1): p. 1-30.
558. Yang, H., et al., *HSP90/AXL/eIF4E-regulated unfolded protein response as an acquired vulnerability in drug-resistant KRAS-mutant lung cancer*. Oncogenesis, 2019. **8**(9): p. 1-13.
559. Zhang, M., et al., *Deregulation of HSF1-mediated endoplasmic reticulum unfolded protein response promotes cisplatin resistance in lung cancer cells.* The FEBS Journal, 2022.
560. Briggs, J.W., et al., *Activation of the unfolded protein response in sarcoma cells treated with rapamycin or temsirolimus.* PLOS ONE, 2017. **12**(9): p. e0185089.
561. McCarthy, N., et al., *The IRE1 and PERK arms of the unfolded protein response promote survival of rhabdomyosarcoma cells.* Cancer Letters, 2020. **490**: p. 76-88.
562. Taguchi, Y., et al., *Novel prosurvival function of Yip1A in human cervical cancer cells: constitutive activation of the IRE1 and PERK pathways of the unfolded protein response.* Cell death & disease, 2017. **8**(3): p. e2718-e2718.
563. Ozfiliz-Kilbas, P., et al., *Cyclin-dependent kinase inhibitors, roscovitine and purvalanol, induce apoptosis and autophagy related to unfolded protein response in HeLa cervical cancer cells.* Mol Biol Rep, 2018. **45**(5): p. 815-828.
564. Wu, C.-H., et al., *Bladder cancer extracellular vesicles drive tumorigenesis by inducing the unfolded protein response in endoplasmic reticulum of nonmalignant cells.* Journal of Biological Chemistry, 2019. **294**(9): p. 3207-3218.

565. Yan, X., et al., *Effect of unfolded protein response on the immune infiltration and prognosis of transitional cell bladder cancer.* Annals of medicine, 2021. **53**(1): p. 1049-1059.
566. Zhu, K., et al., *Identification of a novel signature based on unfolded protein response-related gene for predicting prognosis in bladder cancer.* Human Genomics, 2021. **15**(1): p. 1-23.
567. Atala, A., *Re: Bladder Cancer Extracellular Vesicles Drive Tumorigenesis by Inducing the Unfolded Protein Response in Endoplasmic Reticulum of Nonmalignant Cells.* Journal of Urology, 2019. **202**(6): p. 1101.
568. Patel, A., et al., *The unfolded protein response is associated with cancer proliferation and worse survival in hepatocellular carcinoma.* Cancers (Basel), 2021. **13**(17): p. 4443.
569. Al-Rawashdeh, F.Y., et al., *Unfolded protein response activation contributes to chemoresistance in hepatocellular carcinoma.* European journal of gastroenterology, 2010. **22**(9): p. 1099-1105.
570. Vandewynckel, Y.-P., et al., *Modulation of the unfolded protein response impedes tumor cell adaptation to proteotoxic stress: a PERK for hepatocellular carcinoma therapy.* Hepatology, 2015. **9**(1): p. 93-104.
571. Fang, L., et al., *MICA/B expression is inhibited by unfolded protein response and associated with poor prognosis in human hepatocellular carcinoma.* Journal of Experimental Clinical Cancer Research, 2014. **33**(1): p. 1-8.
572. Macklin, A., S. Khan, and T. Kislinger, *Recent advances in mass spectrometry based clinical proteomics: applications to cancer research.* Clinical Proteomics, 2020. **17**(1): p. 17.
573. Frantzi, M., et al., *Clinical Proteomics: Closing the Gap from Discovery to Implementation.* Proteomics, 2018. **18**(14): p. 1700463.
574. Malta, T.M., et al., *Machine Learning Identifies Stemness Features Associated with Oncogenic Dedifferentiation.* Cell, 2018. **173**(2): p. 338-354.e15.
575. Campbell, J.D., et al., *Genomic, Pathway Network, and Immunologic Features Distinguishing Squamous Carcinomas.* Cell Rep, 2018. **23**(1): p. 194-212.e6.
576. Ding, L., et al., *Perspective on Oncogenic Processes at the End of the Beginning of Cancer Genomics.* Cell, 2018. **173**(2): p. 305-320.e10.
577. Bailey, M.H., et al., *Comprehensive Characterization of Cancer Driver Genes and Mutations.* Cell, 2018. **173**(2): p. 371-385.e18.
578. Thorsson, V., et al., *The Immune Landscape of Cancer.* Immunity, 2018. **48**(4): p. 812-830.e14.
579. Wang, Z., et al., *lncRNA Epigenetic Landscape Analysis Identifies EPIC1 as an Oncogenic lncRNA that Interacts with MYC and Promotes Cell-Cycle Progression in Cancer.* Cancer Cell, 2018. **33**(4): p. 706-720.e9.
580. Sanchez-Vega, F., et al., *Oncogenic Signaling Pathways in The Cancer Genome Atlas.* Cell, 2018. **173**(2): p. 321-337.e10.
581. Gao, Q., et al., *Driver Fusions and Their Implications in the Development and Treatment of Human Cancers.* Cell Rep, 2018. **23**(1): p. 227-238.e3.
582. Hoadley, K.A., et al., *Multiplatform analysis of 12 cancer types reveals molecular classification within and across tissues of origin.* Cell, 2014. **158**(4): p. 929-944.
583. Mischak, H., et al., *Implementation of proteomic biomarkers: making it work.* Eur J Clin Invest, 2012. **42**(9): p. 1027-36.

584. Nkuipou-Kenfack, E., P. Zürbig, and H. Mischak, *The long path towards implementation of clinical proteomics: Exemplified based on CKD273.* Proteomics Clin Appl, 2017. **11**(5-6): p. 1600104.
585. Solier, C. and H. Langen, *Antibody-based proteomics and biomarker research - current status and limitations.* Proteomics, 2014. **14**(6): p. 774-83.
586. Iyer, A., A.A.J. Hamers, and A.B. Pillai, *CyTOF(®) for the Masses.* Front Immunol, 2022. **13**: p. 815828.
587. Spitzer, M.H. and G.P. Nolan, *Mass Cytometry: Single Cells, Many Features.* Cell, 2016. **165**(4): p. 780-91.

Supplementary material

Table S2-1. Details on individual antibodies used for Western blotting and fluorescence microscopy from Chapter 2.5 and 2.6.

Antigen target	Species	Incubation	Dilution	Manufacturer
GAPDH	Mouse monoclonal IgG	1 h room temperature	1:40,000	Millipore, Massachusetts, USA
PU.1	Rabbit polyclonal IgG	1 h room temperature	1:1,000	Santa Cruz Biotechnology, Santa Cruz, CA, USA
SDHA	Mouse monoclonal IgG	1 h room temperature	1:2,000	Santa Cruz Biotechnology, Santa Cruz, CA, USA
GRP78	Mouse monoclonal IgG	4ºC overnight	1:1,000	Abcam, Waterloo, NSW, Australia
XBP-1	Rabbit monoclonal IgG	4ºC overnight	1:500	Santa Cruz Biotechnology, Santa Cruz, CA, USA
SMARCC1	Mouse monoclonal IgG	4ºC overnight	1:1,000	Abcam, Waterloo, NSW, Australia
PGRMC1	Rabbit monoclonal IgG	1 h room temperature	1:1,000	Millipore, Massachusetts, USA
Anti-Rabbit-HRP	Donkey polyclonal	1 h room temperature	1:5,000	Abcam, Waterloo, NSW, Australia
Anti-Mouse-HRP	Goat polyclonal	1 h room temperature	1:10,000	Santa Cruz Biotechnology, Santa Cruz, CA, USA
PGRMC1	Rabbit polyclonal IgG	4ºC overnight	1:500	Abcam, Waterloo, NSW, Australia
SLC3A2	Rabbit monoclonal IgG	4ºC overnight	1:700	Cell Signalling Technology, Danvers, Massachusetts, USA

Table S3-1. Melanoma patient demographics, primary pathology, lymph node recurrence and survival parameters from Chapter 3

Patient demographics			Culprit primary melanoma						Lymph node metastases					Survival
No.	Sex	Age	Site	T stage	Breslow thickness (mm)	Mitotic rate /mm^2	Clark level	Histology	Ulc.	AJCC stage	No. of nodes	Size (mm)	Extranodal spread	Days
Poor prognosis patients														
PP1	M	65	Lower arm	T3a	2	3	4	NM	No	Stage III	40	30	no	27
PP2	F	78	Lower leg	T3a	2.7	20	4	SSM	Yes	Stage III	13	25	yes	43
PP3	M	53	Acral- sole	T3a	2	1	4	Acral lentiginous	No	Stage III	3	50	no	67
PP4	M	69	Chest	T3a	2.2	2	3	SSM	No	Stage III	16	30	yes	70
PP5	F	46	Occult	TX	NA	NA	NA	Not known	NA	Stage III	4	80	yes	176
PP6	F	57	Back	T3a	1.8	4	4	NM	No	Stage III	63	15	no	183
PP7	M	54	Upper leg	T4a	4.5	1	4	SSM	Yes	Stage III	2	25	no	189
PP8	F	74	Upper leg	T2	1.36	5	4	SSM	No	Stage III	6	70	yes	190
PP9	M	77	Acral - toe	T4a	6.75	25	5	Acral lentiginous	Yes	Stage III	1	40	no	193
PP10	M	67	Chest	T3b	3.4	2	5	NM	No	Stage III	11	50	yes	215
PP11	M	75	Back	T1	0.6	3	2	SSM	No	Stage III	20	50	yes	235
PP12	M	56	Lower leg	T3a	3	13	3	Not classified	Yes	Stage III	20	25	no	275
PP13	F	57	Lower leg	T3a	1.7	1	3	SSM	No	Stage III	2	35	no	326
PP14	F	53	Chest	T3a	2.2	2	4	SSM	No	Stage III	9	58	yes	344
PP15	M	47	Lower leg	TX	NA	NA	NA	NA	NA	Stage IV	1	85	no	380
PP16	M	52	Occult	T0	NA	NA	NA	Not known	NA	Stage IV	5	60	yes	408
PP17	M	59	Upper arm	T3a	2.2	6	4	SSM	No	Stage IV	3	47	no	430
PP18	M	66	Chest	T2	1	0	3	SSM	No	Stage III	4	40	yes	454
PP19	M	59	Acral - toe	T3b	4	6	5	Acral lentiginous	Yes	Stage III	2	32	yes	714
PP21	**M**	**52**	**Upper leg**	**T2**	**0.85**	**10**	**4**	**Not known**	**No**	**Stage III**	**1**	**35**	**yes**	**2893**
PP22	**M**	**40**	**Occult**	**T0**	**NA**	**NA**	**NA**	**Not known**	**NA**	**Stage III**	**5**	**25**	**no**	**2932**
Good prognosis patients														
GP2	M	76	Back	TX	1.6	NA	NA	NM	NA	Stage IV	24	40	yes	1286
GP5	M	47	Occult	T0	NA	NA	NA	Not known	NA	Stage III	1	40	no	1499
GP7	M	66	Back	T1	0.55	0	2	SSM	No	Stage III	3	60	no	1913

Patient demographics			Culprit primary melanoma						Lymph node metastases					Survival
No.	Sex	Age	Site	T stage	Breslow thickness (mm)	Mitotic rate /mm^2	Clark level	Histology	Ulc.	AJCC stage	No. of nodes	Size (mm)	Extranodal spread	Days
GP8	M	63	Back	T4b	11	8	5	NM	No	Stage III	3	25	no	1929
GP9	M	30	Occult	T0	NA	NA	NA	Not known	NA	Stage III	1	95	no	2115
GP10	M	30	Upper arm	T4a	6.2	8	5	SSM	No	Stage III	2	30	yes	2408
GP11	F	67	Lower leg	T2	0.8	0	3	SSM	No	Stage III	7	40	yes	2764
GP12	M	51	Lower leg	T4a	4.2	5	4	SSM	Yes	Stage III	4	15	no	2939
GP13	M	64	Back	T1	0.7	0	2	NM	No	Stage III	4	45	no	2969
GP14	F	40	Lower leg	T2	1	2	3	SSM	No	Stage III	1	35	no	2974
GP15	F	22	Upper leg	T4a	5.2	8	4	NM (Spitz)	No	Stage III	2	65	no	3357
GP17	F	75	Lower leg	T2	1.5	0	4	SSM	No	Stage III	1	35	no	3528
GP18	F	64	Lower leg	T4b	4.5	21	4	NM	No	Stage III	2	20	no	3650
GP19	F	44	Occult	T0	NA	NA	NA	Not known	NA	Stage III	1	24	yes	3921
GP20	M	61	Lower arm	T1	0.4	0	2	SSM	No	Stage III	10	120	no	4357

Table S3-2. Mutational status of patients with AJCC stage III melanoma from Chapter 3.

Patient	Mutational status							Survival
No.	BRAF	NRAS	FLT3	MET	PIK3CA	PDGFRA	EGFR	(Days)
Poor prognosis patients								
PP1	No	**Yes**	No	No	No	No	No	27
PP2	No	**Yes**	No	No	No	**Yes**	No	43
PP3	**Yes**	No	No	No	No	No	No	67
PP4	**Yes**	No	No	No	No	No	No	70
PP5	**Yes**	No	No	No	No	No	No	176
PP6	No	**Yes**	No	No	No	No	No	183
PP7	**Yes**	No	No	No	No	No	No	189
PP8	No	No	No	No	No	No	No	190
PP9	No	No	No	No	**Yes**	No	No	193
PP10	**Yes**	No	No	No	No	No	No	215
PP11	No	No	No	No	No	No	No	235
PP12	No	**Yes**	No	No	No	No	No	275
PP13	**Yes**	No	No	No	No	No	No	326
PP14	No	No	No	No	No	No	No	344
PP15	**Yes**	No	No	No	No	No	No	380
PP16	No	**Yes**	No	No	No	No	No	408
PP17	No	No	No	No	No	No	No	430
PP18	No	**Yes**	No	No	No	No	No	454
PP19	No	No	No	No	No	No	No	714
PP21	**Yes**	No	No	No	No	No	No	2893
PP22	No	**Yes**	No	No	No	No	No	2932
Good prognosis patients								
GP2	No	No	No	No	No	No	No	1286
GP5	**Yes**	No	No	No	No	No	No	1499
GP7	No	**Yes**	No	No	No	No	No	1913
GP8	No	No	No	No	No	No	No	1929
GP9	**Yes**	No	No	No	No	No	No	2115
GP10	No	**Yes**	No	No	No	No	No	2408
GP11	**Yes**	No	No	No	No	No	No	2764
GP12	**Yes**	No	No	No	No	No	No	2939
GP13	**Yes**	No	No	No	No	No	No	2969
GP14	No	**Yes**	**Yes**	No	No	No	No	2974

GP15	**Yes**	No	No	No	No	No	No	3357
GP17	No	**Yes**	No	No	No	No	No	3528
GP18	No	No	No	No	No	No	No	3650
GP19	**Yes**	No	No	No	No	No	No	3921
GP20	**Yes**	No	No	No	No	No	No	4357

Table S3-3. **Proteotypic peptides in SRM analysis of AJCC stage III melanoma samples**. Lymph node resections from Good (n=16, >4 years survival post-resection) and Poor (n=14, <2 years survival) prognostic groups were analysed by SRM. The target proteins were input to Skyline software 2.0 to pick target peptides and transitions. Transitions were then exported to Analyst software to generate acquisition methods for an AB-SCIEX 5500 QTRAP mass spectrometer.

Protein	Proteotypic peptide	RT (min)	Precursor (m/z)	Fragment (m/z)	CE (eV	DP (eV)
FBRL	DLINLAK	16.7	393.74	558.36	21	59.8
				445.28	21	59.8
				229.12	21	59.8
				218.15	21	59.8
				342.20	21	59.8
	IVALNAHTFLR	17.9	627.87	1042.58	31.5	76.9
				858.46	31.5	76.9
				673.38	31.5	76.9
				744.42	31.5	76.9
				536.32	31.5	76.9
	DHAVVVGVYRPPPK	16.5	511.96	913.53	23.4	68.4
				253.09	23.4	68.4
				324.13	23.4	68.4
				438.27	23.4	68.4
				423.20	23.4	68.4
MYH10	EQADFAVEALAK	17.8	646.33	701.42	33.1	78.2
				630.38	33.1	78.2
				531.31	33.1	78.2
				848.49	33.1	78.2
				402.27	33.1	78.2
	ALELDPNLYR	18.9	602.32	890.47	28.5	75
				777.39	28.5	75
				662.36	28.5	75
				1019.52	28.5	75
				338.18	28.5	75
	DAASLESQLQDTQELLQEETR	22.5	802.05	775.39	40.2	89.6
				662.31	40.2	89.6
				534.25	40.2	89.6
				587.27	40.2	89.6
				1043.50	40.2	89.6
KAPO	GAISAEVYTEEDAASYVR	16.4	965.96	1140.52	42.6	101.5
				910.43	42.6	101.5
				524.28	42.6	101.5
				595.32	42.6	101.5
				437.25	42.6	101.5
	NVLFSHLDDNER	16.53	729.85	1132.50	33.1	84.3
				985.43	33.1	84.3
				898.40	33.1	84.3
				648.26	33.1	84.3

				418.20	33.1	84.3
	LTVADALEPVQFEDGQK	20.7	930.47	1176.55	44.4	98.9
				1047.51	44.4	98.9
				723.33	44.4	98.9
				851.39	44.4	98.9
				813.44	44.4	98.9
CYC	TGPNLHGLFGR	15.6	584.81	686.37	19.8	73.7
				549.31	19.8	73.7
				483.26	19.8	73.7
				799.46	19.8	73.7
				379.21	19.8	73.7
		15.6	390.21	686.37	19.8	73.7
				549.31	19.8	73.7
				379.21	19.8	73.7
				492.29	19.8	73.7
				232.14	19.8	73.7
	TGQAPGYSYTAANK	12.5	714.84	1142.55	35.6	83.2
				1071.51	35.6	83.2
				287.13	35.6	83.2
				974.46	35.6	83.2
				754.37	35.6	83.2
	ADLIAYLK	18.1	453.77	607.38	26.2	64.2
				494.30	26.2	64.2
				423.26	26.2	64.2
				720.47	26.2	64.2
				300.16	26.2	64.2
GLU2B	ILIEDWK	19.6	458.76	690.35	27.4	64.6
				333.19	27.4	64.6
				227.18	27.4	64.6
				577.26	27.4	64.6
				448.22	27.4	64.6
	LWEEQLAAAK	18.1	579.81	859.45	31.7	73.4
				730.41	31.7	73.4
				300.17	31.7	73.4
				360.22	31.7	73.4
				289.19	31.7	73.4
	AQQEQELAADAFK	17.4	724.85	622.32	36	84
				551.28	36	84
				480.25	36	84
				1121.55	36	84
				864.45	36	84
GSTO1	VPSLVGSFIR	20.2	537.82	878.51	27.2	70.3
				678.39	27.2	70.3
				579.32	27.2	70.3
				791.48	27.2	70.3
				522.30	27.2	70.3

	LEEVLTNK	15.4	473.27	703.40	25.9	65.6
				362.20	25.9	65.6
				243.13	25.9	65.6
				574.36	25.9	65.6
				372.18	25.9	65.6
	EDPTVSALLTSEK	16.7	695.36	848.47	34.9	81.8
				761.44	34.9	81.8
				464.24	34.9	81.8
				577.32	34.9	81.8
				363.19	34.9	81.8
ANAX1	GVDEATIIDILTK	21.8	694.39	916.57	34.9	81.7
				815.52	34.9	81.7
				589.36	34.9	81.7
				474.33	34.9	81.7
				1140.61	34.9	81.7
	TPAQFDADELR	15.7	631.80	1064.50	31.6	77.2
				993.46	31.6	77.2
				865.41	31.6	77.2
				603.31	31.6	77.2
				288.20	31.6	77.2
	GTDVNVFNTILTTR	21.3	775.91	1178.65	35.8	87.7
				965.54	35.8	87.7
				818.47	35.8	87.7
				490.30	35.8	87.7
				377.21	35.8	87.7
PRDX3	DLSLDDFK	18.6	476.73	724.35	25	65.9
				294.18	25	65.9
				229.12	25	65.9
				637.32	25	65.9
				524.24	25	65.9
	DYGVLLEGSGLALR	20.7	731.90	1028.61	33.2	84.5
				802.44	33.2	84.5
				673.40	33.2	84.5
				915.53	33.2	84.5
				529.35	33.2	84.5
	HLSVNDLPVGR	15.8	603.83	956.52	30.6	75.1
				541.35	30.6	75.1
				428.26	30.6	75.1
				869.48	30.6	75.1
				770.42	30.6	75.1
MOES	EVWFFGLQYQDTK	23.2	830.90	1099.54	38.8	91.7
				952.47	38.8	91.7
				654.31	38.8	91.7
				782.37	38.8	91.7
				879.44	38.8	91.7
	FYPEDVSEELIQDITQR	24.5	694.67	760.39	36.4	81.8

				632.34	36.4	81.8
				404.23	36.4	81.8
				303.18	36.4	81.8
				1096.45	36.4	81.8
	EDAVLEYLK	17.8	540.28	665.39	30.3	70.5
				552.30	30.3	70.5
				423.26	30.3	70.5
				835.49	30.3	70.5
				764.46	30.3	70.5
TCP4	GISLNPEQWSQLK	19.8	750.40	1129.56	37.9	85.8
				1015.52	37.9	85.8
				475.29	37.9	85.8
				661.37	37.9	85.8
				485.27	37.9	85.8
	EQISDIDDAVR	14.4	630.81	1003.51	31.6	77.1
				890.42	31.6	77.1
				575.28	31.6	77.1
				688.36	31.6	77.1
				460.25	31.6	77.1
SH3L1	DIAANEENR	12.7	516.24	803.36	27.4	68.8
				732.33	27.4	68.8
				229.12	27.4	68.8
				661.29	27.4	68.8
				300.16	27.4	68.8
	GDYDAFFEAR	17.8	595.76	740.37	29.3	74.5
				669.34	29.3	74.5
				522.27	29.3	74.5
				855.40	29.3	74.5
				375.20	29.3	74.5
PTH2	THTDTESEASILGDSGEYK	15.4	1020.46	868.40	43.6	105.5
				755.32	43.6	105.5
				583.27	43.6	105.5
				1139.56	43.6	105.5
				1068.52	43.6	105.5
	THTDTESEASILGDSGEYK	15.4	680.64	868.40	33.6	80.7
				755.32	33.6	80.7
				310.18	33.6	80.7
				698.30	33.6	80.7
				772.31	33.6	80.7
LDHB	SLADELALVDVLEDK	23.9	815.43	1001.55	36.2	90.6
				930.51	36.2	90.6
				718.36	36.2	90.6
				391.18	36.2	90.6
				912.50	36.2	90.6
	FIIPQIVK	19.1	479.31	697.46	25.1	66.1
				584.38	25.1	66.1

				261.16	25.1	66.1
				374.24	25.1	66.1
				811.51	25.1	66.1
	GLTSVINQK	13.5	480.28	789.45	27.4	66.1
				601.37	27.4	66.1
				502.30	27.4	66.1
				688.40	27.4	66.1
				389.21	27.4	66.1
AMPL	GVLFASGQNLAR	15.7	616.84	963.50	33.1	76.1
				816.43	33.1	76.1
				745.40	33.1	76.1
				658.36	33.1	76.1
				473.28	33.1	76.1
	GSDEPPVFLEIHYK	17.7	544.28	689.36	26.2	70.8
				560.32	26.2	70.8
				310.18	26.2	70.8
				949.51	26.2	70.8
				802.45	26.2	70.8
	GSPNANEPPLVFVGK	17.4	763.40	1099.61	34.3	86.8
				549.34	34.3	86.8
				450.27	34.3	86.8
				856.53	34.3	86.8
				670.28	34.3	86.8
SYWC	KPFYLYTGR	14.6	572.81	1016.52	30.5	72.9
				919.47	30.5	72.9
				772.40	30.5	72.9
				609.34	30.5	72.9
				496.25	30.5	72.9
	DLTLDQAYSYAVENAK	19.7	900.94	1044.50	41.3	96.8
				881.44	41.3	96.8
				461.24	41.3	96.8
				794.40	41.3	96.8
				631.34	41.3	96.8
	ALIEVLQPLIAEHQAR	20.4	901.02	1162.63	43.3	96.8
				1034.57	43.3	96.8
				526.32	43.3	96.8
				711.35	43.3	96.8
				640.32	43.3	96.8
		20.4	601.02	1034.57	43.3	74.9
				640.32	43.3	74.9
				427.26	43.3	74.9
				526.32	43.3	74.9
				639.41	43.3	74.9
MYL12A	LNGTDPEDVIR	15.8	614.81	1001.49	33	75.9
				843.42	33	75.9
				728.39	33	75.9

				502.30	33	75.9
				387.27	33	75.9
	FTDEEVDELYR	16.9	708.32	1167.52	33.4	82.8
				923.45	33.4	82.8
				695.34	33.4	82.8
				580.31	33.4	82.8
				338.18	33.4	82.8
	GNFNYIEFTR	18.5	630.80	942.47	30.6	77.1
				665.36	30.6	77.1
				552.28	30.6	77.1
				828.43	30.6	77.1
				423.24	30.6	77.1
TAGL2	ENFQNWLK	20.4	539.77	688.38	28.3	70.5
				560.32	28.3	70.5
				260.20	28.3	70.5
				835.45	28.3	70.5
				446.28	28.3	70.5
	YGINTTDIFQTVDLWEGK	35.1	1050.52	947.48	48.7	107.7
				747.37	48.7	107.7
				519.26	48.7	107.7
				846.44	48.7	107.7
				632.34	48.7	107.7
	YGINTTDIFQTVDLWEGK	35.1	700.68	747.37	33.7	82.2
				632.34	33.7	82.2
				519.26	33.7	82.2
				846.44	33.7	82.2
				878.43	33.7	82.2
	DDGLFSGDPNWFPK	24.6	797.86	1194.56	35.6	89.3
				1047.49	35.6	89.3
				401.17	35.6	89.3
				960.46	35.6	89.3
				391.23	35.6	89.3
GGH	YYIAASYVK	15.7	539.28	751.43	26.3	70.4
				638.35	26.3	70.4
				567.31	26.3	70.4
				496.28	26.3	70.4
				440.22	26.3	70.4
	FFNVLTTNTDGK	17.5	678.84	849.43	31.3	80.6
				736.35	31.3	80.6
				508.26	31.3	80.6
				635.30	31.3	80.6
				621.34	31.3	80.6
PDIA1	SNFAEALAAHK	13.2	579.80	810.45	27.7	73.4
				739.41	27.7	73.4
				349.15	27.7	73.4
				818.46	27.7	73.4

				747.42	27.7	73.4
	HNQLPLVIEFTEQTAPK	20.2	655.69	774.40	33.3	78.9
				244.17	33.3	78.9
				802.46	33.3	78.9
				921.47	33.3	78.9
				315.20	33.3	78.9
	YKPESEELTAER	12.1	726.35	1160.54	36	84.1
				934.45	36	84.1
				292.17	36	84.1
				589.33	36	84.1
				476.25	36	84.1
TCBP	GATQQILDEAER	15.4	665.83	845.44	32.8	79.7
				732.35	32.8	79.7
				619.27	32.8	79.7
				973.49	32.8	79.7
				504.24	32.8	79.7
HNRNPK	ILSISADIETIGEILK	21.9	858.00	1130.63	40.7	93.7
				902.52	40.7	93.7
				559.34	40.7	93.7
				773.48	40.7	93.7
				502.32	40.7	93.7
	GSYGDLGGPIITTQVTIPK	21.5	959.02	1000.60	41.4	101
				887.52	41.4	101
				707.30	41.4	101
				786.47	41.4	101
				1030.52	41.4	101
MDMH	ANTFVAELK	16.7	496.77	706.41	26.7	67.3
				559.34	26.7	67.3
				460.28	26.7	67.3
				389.24	26.7	67.3
				260.20	26.7	67.3
	VNVPVIGGHAGK	15.2	574.33	835.48	28.5	73
				639.36	28.5	73
				526.27	28.5	73
				934.55	28.5	73
				622.39	28.5	73
	VDFPQDQLTALTGR	20.4	780.90	1199.64	39	88
				974.53	39	88
				618.36	39	88
				731.44	39	88
				333.19	39	88
HSP90B1	FAFQAEVNR	15.9	541.27	863.44	29.3	70.6
				716.37	29.3	70.6
				588.31	29.3	70.6
				517.27	29.3	70.6
				388.23	29.3	70.6

	SILFVPTSAPR	17.9	594.34	874.48	29.3	74.4
				727.41	29.3	74.4
				628.34	29.3	74.4
				461.28	29.3	74.4
				560.34	29.3	74.4
	YNDTFWK	17.3	487.22	696.34	28.4	66.6
				581.31	28.4	66.6
				333.19	28.4	66.6
				810.38	28.4	66.6
				278.11	28.4	66.6
GSTP1	EEVVTVETWQEGSLK	17.5	867.43	1176.59	40.1	94.4
				1077.52	40.1	94.4
				948.48	40.1	94.4
				661.35	40.1	94.4
				533.29	40.1	94.4
	YISLIYTNYEAGK	18.4	767.89	1058.52	35.5	87.1
				945.43	35.5	87.1
				590.35	35.5	87.1
				782.37	35.5	87.1
				681.32	35.5	87.1
KPYM	LDIDSPPITAR	15.7	599.33	856.45	28.4	74.8
				741.43	28.4	74.8
				654.39	28.4	74.8
				969.54	28.4	74.8
				347.20	28.4	74.8
	IYVDDGLISLQVK	20.4	731.91	1186.67	35.2	84.5
				1087.60	35.2	84.5
				574.36	35.2	84.5
				857.55	35.2	84.5
				687.44	35.2	84.5
	DPVQEAWAEDVDLR	18.6	821.89	1074.52	37.4	91
				1003.48	37.4	91
				288.20	37.4	91
				746.37	37.4	91
				640.29	37.4	91
ESTD	FAVYLPPK	15.9	467.77	454.30	27.7	65.2
				341.22	27.7	65.2
				219.11	27.7	65.2
				716.43	27.7	65.2
				617.37	27.7	65.2
	AFSGYLGTDQSK	14.2	637.31	1055.50	29.8	77.6
				968.47	29.8	77.6
				748.38	29.8	77.6
				578.28	29.8	77.6
				477.23	29.8	77.6
	SYPGSQLDILIDQGK	19.2	817.43	901.50	36.3	90.7

				560.30	36.3	90.7
				447.22	36.3	90.7
				786.47	36.3	90.7
				1187.63	36.3	90.7
ACTN4	LVSIGAEEIVDGNAK	16.4	757.91	1102.54	36.1	86.4
				974.48	36.1	86.4
				603.31	36.1	86.4
				716.39	36.1	86.4
				504.24	36.1	86.4
	QFASQANVVGPWIQTK	18.1	887.47	1141.64	40.8	95.8
				928.53	40.8	95.8
				829.46	40.8	95.8
				1027.59	40.8	95.8
				772.44	40.8	95.8
	ETTDTDTADQVIASFK	18.2	871.41	1079.57	40.2	94.6
				452.25	40.2	94.6
				381.21	40.2	94.6
				978.53	40.2	94.6
				907.49	40.2	94.6
PGK1	YSLEPVAVELK	19.1	624.35	997.59	33.3	76.6
				755.47	33.3	76.6
				493.23	33.3	76.6
				884.51	33.3	76.6
				389.24	33.3	76.6
	ITLPVDFVTADK	21.5	659.87	1104.59	32.6	792
				991.51	32.6	792
				795.39	32.6	792
				680.36	32.6	792
				434.22	32.6	792
PPIA	FEDENFILK	18.7	577.79	1007.50	31.7	73.2
				878.46	31.7	73.2
				277.12	31.7	73.2
				763.43	31.7	73.2
				1008.47	31.7	73.2
TBCA	LEAAYLDLQR	17.3	596.32	949.51	28.3	74.6
				807.44	28.3	74.6
				644.37	28.3	74.6
				878.47	28.3	74.6
				531.29	28.3	74.6
	DLEEAEEYK	13.7	563.25	897.38	30.1	72.2
				768.34	30.1	72.2
				639.30	30.1	72.2
				439.22	30.1	72.2
				979.39	30.1	72.2
TCPH	IALLNVELELK	21.1	627.89	1070.65	29.5	76.9
				957.56	29.5	76.9

				844.48	29.5	76.9
				730.43	29.5	76.9
				502.32	29.5	76.9
	ALEIIPR	16.3	406.26	627.38	21.5	60.7
				498.34	21.5	60.7
				272.17	21.5	60.7
				385.26	21.5	60.7
				314.17	21.5	60.7
HNRPU	SSGPTSLFAVTVAPPGAR	19.4	857.96	768.44	40.7	93.7
				568.32	40.7	93.7
				497.28	40.7	93.7
				667.39	40.7	93.7
				1147.60	40.7	93.7
	GYFEYIEENK	17.0	646.30	795.39	32.1	78.2
				632.32	32.1	78.2
				519.24	32.1	78.2
				773.35	32.1	78.2
				902.39	32.1	78.2
	NFILDQTNVSAAAQR	16.9	824.43	1160.57	38.5	91.2
				1045.54	38.5	91.2
				603.32	38.5	91.2
				516.29	38.5	91.2
				374.21	38.5	91.2
TENA	LDAPSQIEVK	15.8	550.30	800.45	30.7	71.2
				703.40	30.7	71.2
				246.18	30.7	71.2
				871.49	30.7	71.2
				300.16	30.7	71.2
	ETFTTGLDAPR	13.9	604.30	830.44	29.6	75.2
				729.39	29.6	75.2
				628.34	29.6	75.2
				343.21	29.6	75.2
				272.17	29.6	75.2
	FTTDLDSPR	15.9	526.26	702.34	26.8	69.5
				587.31	26.8	69.5
				359.20	26.8	69.5
				693.31	26.8	69.5

Abbreviations; RT (retention time), CE (collision energy) and DP (declustering potential)

Italicised transitions were excluded from final analysis.

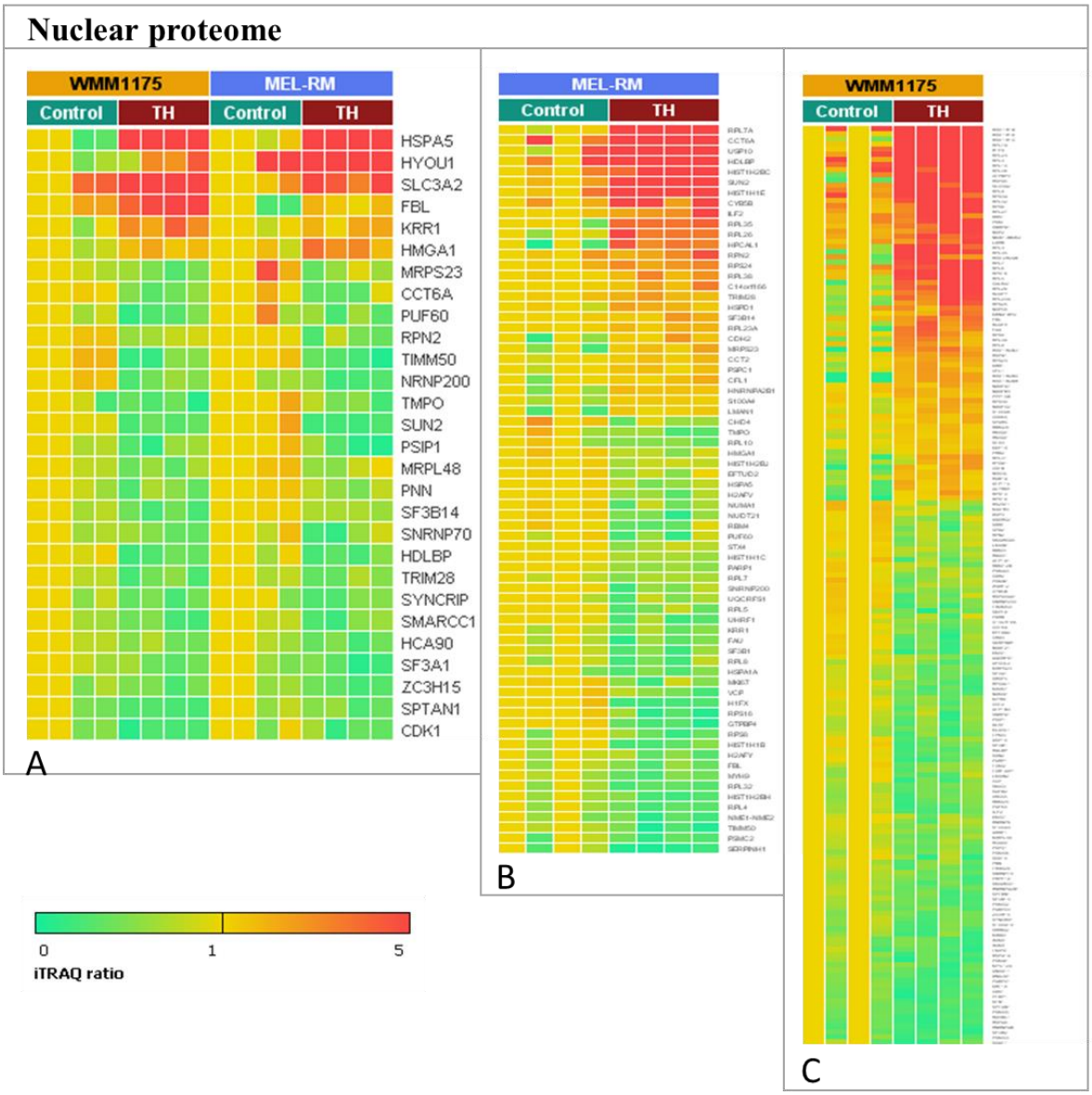

Figure S4-1. Differentially abundant nuclear proteins in Mel-RM and WMM1175 melanoma cell lines with increased ER-stress and activation of the UPR from Chapter 4.

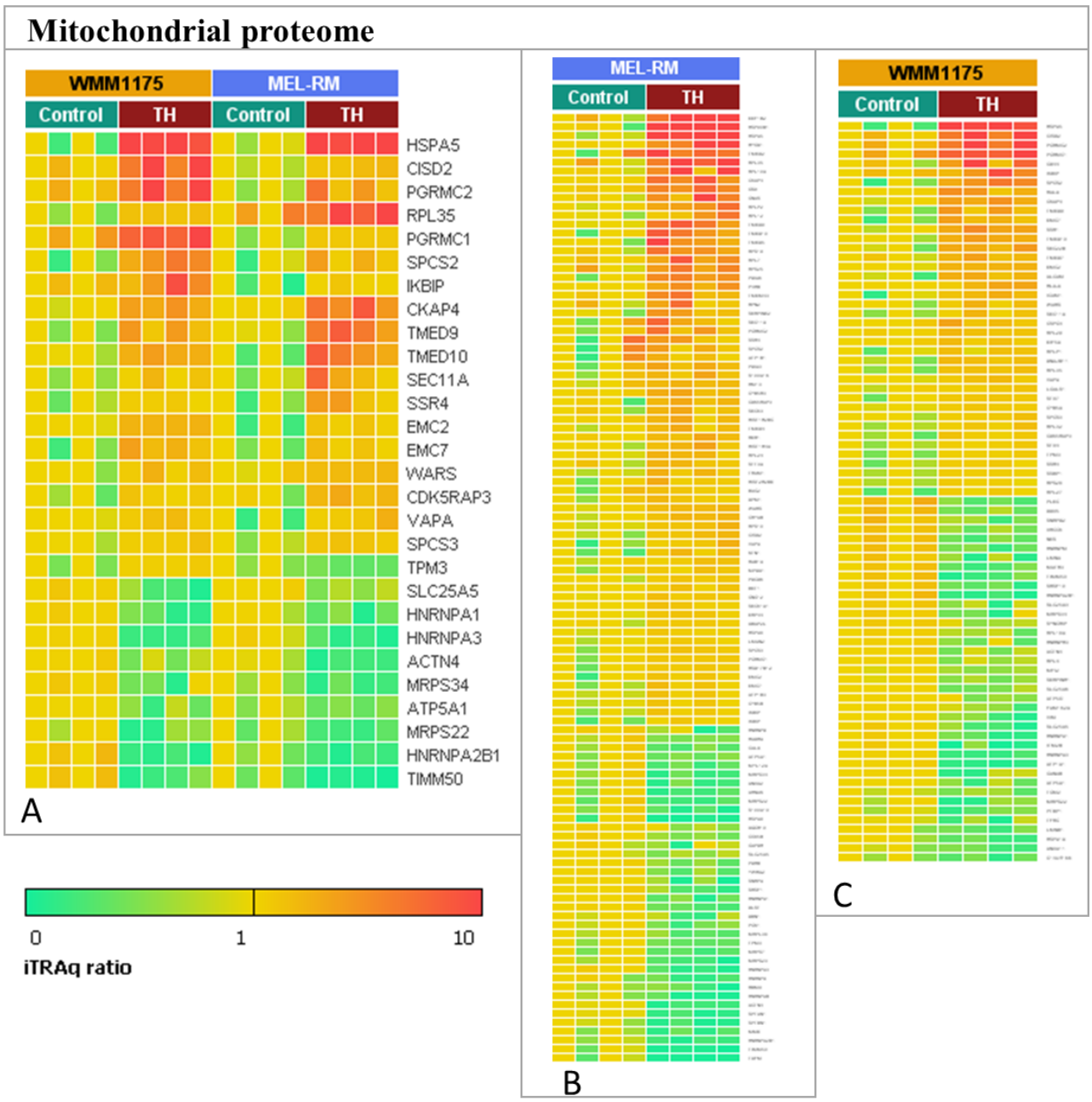

Figure S4-2. Differentially abundant mitochondrial proteins in Mel-RM and WMM1175 melanoma cell lines with increased ER-stress and activation of the UPR from Chapter 4.

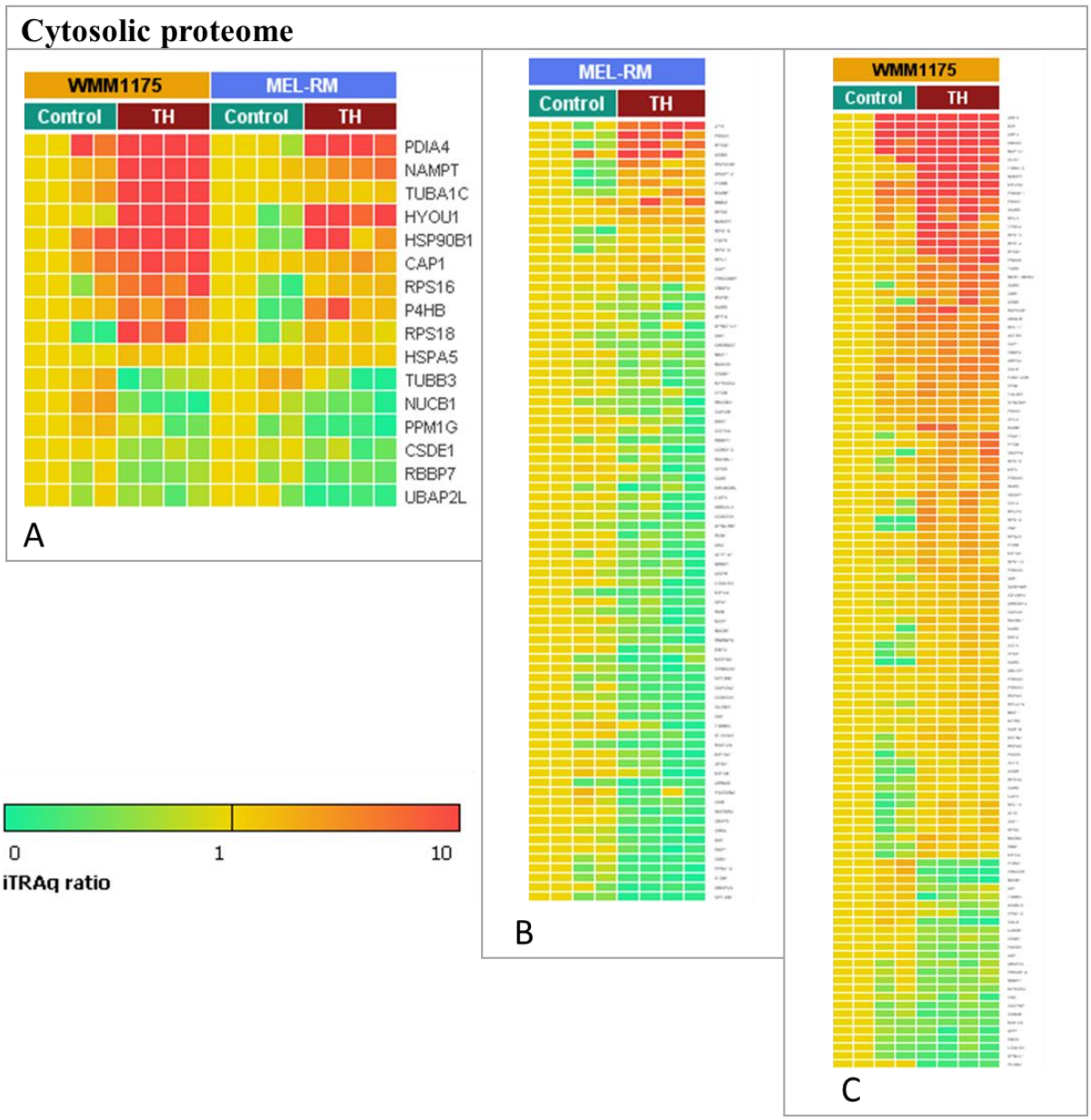

Figure S4-3. Differentially abundant cytosolic proteins in Mel-RM and WMM1175 melanoma cell lines with increased ER-stress and activation of the UPR from Chapter 4.

Table S5-1. Proteotypic peptides selected for SRM analysis in whole cell lysates of 4 melanoma cell lines treated with thapsigargin. The target proteins were input to Skyline software 2.0 to pick target peptides and transitions. Transitions were then exported to Analyst software to generate acquisition methods for an AB-SCIEX 5500 QTRAP mass spectrometer, collision energy (CE) was optimised per precursor, Skyline predicted declustering potential (DP) and scheduled RT with 1 min windows.

Protein target	Peptide target	Standard	Precursor (*m/z*)	Product (m/z)	RT (min)	DP	CE
HYOU1	DAVVYPILVEFTR	light	761.4192	1137.63	26.33	86.6	36.3
HYOU1	DAVVYPILVEFTR	light	761.4192	974.5669	26.33	86.6	36.3
HYOU1	DAVVYPILVEFTR	light	761.4192	385.2082	26.33	86.6	36.3
HYOU1	DAVVYPILVEFTR	heavy	766.4234	1147.639	26.33	86.6	36.3
HYOU1	DAVVYPILVEFTR	heavy	766.4234	984.5752	26.33	86.6	36.3
HYOU1	DAVVYPILVEFTR	heavy	766.4234	385.2082	26.33	86.6	36.3
HYOU1	AEAGPEGVAPAPEGEK	light	754.865	798.3992	12.84	86.1	36
HYOU1	AEAGPEGVAPAPEGEK	light	754.865	727.3621	12.84	86.1	36
HYOU1	AEAGPEGVAPAPEGEK	light	754.865	559.2722	12.84	86.1	36
HYOU1	AEAGPEGVAPAPEGEK	heavy	758.8721	806.4134	12.84	86.1	36
HYOU1	AEAGPEGVAPAPEGEK	heavy	758.8721	735.3763	12.84	86.1	36
HYOU1	AEAGPEGVAPAPEGEK	heavy	758.8721	567.2864	12.84	86.1	36
HYOU1	LYQPEYQEVSTEEQR	light	949.942	1105.512	15.53	100.4	43.1
HYOU1	LYQPEYQEVSTEEQR	light	949.942	977.4534	15.53	100.4	43.1
HYOU1	LYQPEYQEVSTEEQR	light	949.942	1150.542	15.53	100.4	43.1
HYOU1	LYQPEYQEVSTEEQR	heavy	954.9461	1115.52	15.53	100.4	43.1
HYOU1	LYQPEYQEVSTEEQR	heavy	954.9461	987.4617	15.53	100.4	43.1
HYOU1	LYQPEYQEVSTEEQR	heavy	954.9461	1150.542	15.53	100.4	43.1
MANF	DVTFSPATIENELIK	light	838.9407	1127.631	25.18	92.3	39.1
MANF	DVTFSPATIENELIK	light	838.9407	959.5408	25.18	92.3	39.1
MANF	DVTFSPATIENELIK	light	838.9407	932.4724	25.18	92.3	39.1
MANF	DVTFSPATIENELIK	heavy	842.9478	1135.645	25.18	92.3	39.1
MANF	DVTFSPATIENELIK	heavy	842.9478	967.555	25.18	92.3	39.1
MANF	DVTFSPATIENELIK	heavy	842.9478	932.4724	25.18	92.3	39.1
MANF	QIDLSTVDLK	light	566.3164	890.4829	18.42	72.4	29.2
MANF	QIDLSTVDLK	light	566.3164	662.3719	18.42	72.4	29.2
MANF	QIDLSTVDLK	light	566.3164	260.1969	18.42	72.4	29.2
MANF	QIDLSTVDLK	heavy	570.3235	898.4971	18.42	72.4	29.2
MANF	QIDLSTVDLK	heavy	570.3235	670.3861	18.42	72.4	29.2
MANF	QIDLSTVDLK	heavy	570.3235	268.2111	18.42	72.4	29.2
METK2	YLDEDTIYHLQPSGR	light	903.9365	957.4901	17.6	97	41.4
METK2	YLDEDTIYHLQPSGR	light	903.9365	794.4268	17.6	97	41.4
METK2	YLDEDTIYHLQPSGR	light	903.9365	416.2252	17.6	97	41.4
METK2	YLDEDTIYHLQPSGR	heavy	908.9406	967.4984	17.6	97	41.4
METK2	YLDEDTIYHLQPSGR	heavy	908.9406	804.435	17.6	97	41.4
METK2	YLDEDTIYHLQPSGR	heavy	908.9406	426.2335	17.6	97	41.4
METK2	FVIGGPQGDAGLTGR	light	722.8808	1085.533	17.8	83.8	34.9
METK2	FVIGGPQGDAGLTGR	light	722.8808	971.4905	17.8	83.8	34.9
METK2	FVIGGPQGDAGLTGR	light	722.8808	746.3791	17.8	83.8	34.9

METK2	FVIGGPQGDAGLTGR	heavy	727.8849	1095.542	17.8	83.8	34.9
METK2	FVIGGPQGDAGLTGR	heavy	727.8849	981.4988	17.8	83.8	34.9
METK2	FVIGGPQGDAGLTGR	heavy	727.8849	756.3874	17.8	83.8	34.9
NAMPT	VYSYFEC[CAM]R	light	562.2475	861.356	16.44	72.1	29.1
NAMPT	VYSYFEC[CAM]R	light	562.2475	611.2606	16.44	72.1	29.1
NAMPT	VYSYFEC[CAM]R	light	562.2475	263.139	16.44	72.1	29.1
NAMPT	VYSYFEC[CAM]R	heavy	567.2516	871.3642	16.44	72.1	29.1
NAMPT	VYSYFEC[CAM]R	heavy	567.2516	621.2689	16.44	72.1	29.1
NAMPT	VYSYFEC[CAM]R	heavy	567.2516	263.139	16.44	72.1	29.1
NAMPT	EHFQDDVFNEK	light	704.3124	1141.516	15.2	82.5	34.2
NAMPT	EHFQDDVFNEK	light	704.3124	994.4476	15.2	82.5	34.2
NAMPT	EHFQDDVFNEK	light	704.3124	636.3352	15.2	82.5	34.2
NAMPT	EHFQDDVFNEK	heavy	708.3195	1149.53	15.2	82.5	34.2
NAMPT	EHFQDDVFNEK	heavy	708.3195	1002.462	15.2	82.5	34.2
NAMPT	EHFQDDVFNEK	heavy	708.3195	644.3494	15.2	82.5	34.2
NAMPT	GTDTVAGLALIK	light	579.8401	614.4236	17.81	73.4	29.7
NAMPT	GTDTVAGLALIK	light	579.8401	444.318	17.81	73.4	29.7
NAMPT	GTDTVAGLALIK	light	579.8401	474.2195	17.81	73.4	29.7
NAMPT	GTDTVAGLALIK	heavy	583.8472	622.4378	17.81	73.4	29.7
NAMPT	GTDTVAGLALIK	heavy	583.8472	452.3322	17.81	73.4	29.7
NAMPT	GTDTVAGLALIK	heavy	583.8472	474.2195	17.81	73.4	29.7
NUCB1	DLELLIQTATR	light	636.8615	802.4781	23.65	77.5	31.8
NUCB1	DLELLIQTATR	light	636.8615	689.3941	23.65	77.5	31.8
NUCB1	DLELLIQTATR	light	636.8615	576.31	23.65	77.5	31.8
NUCB1	DLELLIQTATR	heavy	641.8657	812.4864	23.65	77.5	31.8
NUCB1	DLELLIQTATR	heavy	641.8657	699.4023	23.65	77.5	31.8
NUCB1	DLELLIQTATR	heavy	641.8657	586.3183	23.65	77.5	31.8
NUCB1	LVTLEEFLASTQR	light	753.9118	675.3784	24.96	86.1	36
NUCB1	LVTLEEFLASTQR	light	753.9118	562.2944	24.96	86.1	36
NUCB1	LVTLEEFLASTQR	light	753.9118	491.2572	24.96	86.1	36
NUCB1	LVTLEEFLASTQR	heavy	758.9159	685.3867	24.96	86.1	36
NUCB1	LVTLEEFLASTQR	heavy	758.9159	572.3026	24.96	86.1	36
NUCB1	LVTLEEFLASTQR	heavy	758.9159	501.2655	24.96	86.1	36
NUCB1	FHPDTDDVPVPAPAGDQK	light	635.9708	979.5207	15.44	77.5	32.2
NUCB1	FHPDTDDVPVPAPAGDQK	light	635.9708	783.3995	15.44	77.5	32.2
NUCB1	FHPDTDDVPVPAPAGDQK	light	635.9708	927.3843	15.44	77.5	32.2
NUCB1	FHPDTDDVPVPAPAGDQK	heavy	638.6422	987.5349	15.44	77.5	32.2
NUCB1	FHPDTDDVPVPAPAGDQK	heavy	638.6422	791.4137	15.44	77.5	32.2
NUCB1	FHPDTDDVPVPAPAGDQK	heavy	638.6422	927.3843	15.44	77.5	32.2
PDIA4	YALPLVGHR	light	513.2982	678.4046	16.65	68.5	27.3
PDIA4	YALPLVGHR	light	513.2982	468.2677	16.65	68.5	27.3
PDIA4	YALPLVGHR	light	513.2982	369.1993	16.65	68.5	27.3
PDIA4	YALPLVGHR	heavy	518.3023	688.4128	16.65	68.5	27.3
PDIA4	YALPLVGHR	heavy	518.3023	478.276	16.65	68.5	27.3
PDIA4	YALPLVGHR	heavy	518.3023	379.2076	16.65	68.5	27.3
PDIA4	VEGFPTIYFAPSGDK	light	814.4038	1195.599	22.06	90.5	38.2

PDIA4	VEGFPTIYFAPSGDK	light	814.4038	884.4149	22.06	90.5	38.2
PDIA4	VEGFPTIYFAPSGDK	light	814.4038	503.246	22.06	90.5	38.2
PDIA4	VEGFPTIYFAPSGDK	heavy	818.4109	1203.614	22.06	90.5	38.2
PDIA4	VEGFPTIYFAPSGDK	heavy	818.4109	892.4291	22.06	90.5	38.2
PDIA4	VEGFPTIYFAPSGDK	heavy	818.4109	511.2602	22.06	90.5	38.2
Q6IB11	DFTPAELR	light	474.7429	686.3832	16.84	65.7	25.9
Q6IB11	DFTPAELR	light	474.7429	585.3355	16.84	65.7	25.9
Q6IB11	DFTPAELR	light	474.7429	288.203	16.84	65.7	25.9
Q6IB11	DFTPAELR	heavy	479.747	696.3914	16.84	65.7	25.9
Q6IB11	DFTPAELR	heavy	479.747	595.3438	16.84	65.7	25.9
Q6IB11	DFTPAELR	heavy	479.747	298.2113	16.84	65.7	25.9
Q6IB11	FDGVQDPR	light	467.2249	671.3471	13.23	65.2	25.7
Q6IB11	FDGVQDPR	light	467.2249	515.2572	13.23	65.2	25.7
Q6IB11	FDGVQDPR	light	467.2249	272.1717	13.23	65.2	25.7
Q6IB11	FDGVQDPR	heavy	472.229	681.3554	13.23	65.2	25.7
Q6IB11	FDGVQDPR	heavy	472.229	525.2655	13.23	65.2	25.7
Q6IB11	FDGVQDPR	heavy	472.229	282.18	13.23	65.2	25.7
Q6IB11	FYGPEGPYGVFAGR	light	758.8646	923.4734	20.54	86.4	36.2
Q6IB11	FYGPEGPYGVFAGR	light	758.8646	866.4519	20.54	86.4	36.2
Q6IB11	FYGPEGPYGVFAGR	light	758.8646	450.2459	20.54	86.4	36.2
Q6IB11	FYGPEGPYGVFAGR	heavy	763.8687	933.4816	20.54	86.4	36.2
Q6IB11	FYGPEGPYGVFAGR	heavy	763.8687	876.4602	20.54	86.4	36.2
Q6IB11	FYGPEGPYGVFAGR	heavy	763.8687	460.2542	20.54	86.4	36.2
PGRC2	GLGAGAGAGEESPATSLPR	light	849.4263	1143.564	15.83	93	39.4
PGRC2	GLGAGAGAGEESPATSLPR	light	849.4263	828.4574	15.83	93	39.4
PGRC2	GLGAGAGAGEESPATSLPR	light	849.4263	741.4254	15.83	93	39.4
PGRC2	GLGAGAGAGEESPATSLPR	heavy	854.4304	1153.572	15.83	93	39.4
PGRC2	GLGAGAGAGEESPATSLPR	heavy	854.4304	838.4657	15.83	93	39.4
PGRC2	GLGAGAGAGEESPATSLPR	heavy	854.4304	751.4336	15.83	93	39.4
PGRC2	DFSLEQLR	light	504.2615	745.4203	19.72	67.9	27
PGRC2	DFSLEQLR	light	504.2615	658.3883	19.72	67.9	27
PGRC2	DFSLEQLR	light	504.2615	545.3042	19.72	67.9	27
PGRC2	DFSLEQLR	heavy	509.2656	755.4285	19.72	67.9	27
PGRC2	DFSLEQLR	heavy	509.2656	668.3965	19.72	67.9	27
PGRC2	DFSLEQLR	heavy	509.2656	555.3125	19.72	67.9	27
PGRC2	FYGPAGPYGIFAGR	light	736.8697	937.489	21.85	84.8	35.4
PGRC2	FYGPAGPYGIFAGR	light	736.8697	880.4676	21.85	84.8	35.4
PGRC2	FYGPAGPYGIFAGR	light	736.8697	450.2459	21.85	84.8	35.4
PGRC2	FYGPAGPYGIFAGR	heavy	741.8738	947.4973	21.85	84.8	35.4
PGRC2	FYGPAGPYGIFAGR	heavy	741.8738	890.4758	21.85	84.8	35.4
PGRC2	FYGPAGPYGIFAGR	heavy	741.8738	460.2542	21.85	84.8	35.4
SET	LNEQASEEILK	light	637.3353	1046.536	15.72	77.6	31.8
SET	LNEQASEEILK	light	637.3353	789.4353	15.72	77.6	31.8
SET	LNEQASEEILK	light	637.3353	718.3981	15.72	77.6	31.8
SET	LNEQASEEILK	heavy	641.3424	1054.551	15.72	77.6	31.8
SET	LNEQASEEILK	heavy	641.3424	797.4495	15.72	77.6	31.8

SET	LNEQASEEILK	heavy	641.3424	726.4123	15.72	77.6	31.8
SET	VEVTEFEDIK	light	604.8059	980.4935	18.29	75.2	30.6
SET	VEVTEFEDIK	light	604.8059	881.4251	18.29	75.2	30.6
SET	VEVTEFEDIK	light	604.8059	229.1183	18.29	75.2	30.6
SET	VEVTEFEDIK	heavy	608.813	988.5077	18.29	75.2	30.6
SET	VEVTEFEDIK	heavy	608.813	889.4393	18.29	75.2	30.6
SET	VEVTEFEDIK	heavy	608.813	229.1183	18.29	75.2	30.6
SET	IDFYFDENPYFENK	light	920.9069	1155.495	23.05	98.3	42
SET	IDFYFDENPYFENK	light	920.9069	797.3828	23.05	98.3	42
SET	IDFYFDENPYFENK	light	920.9069	537.2667	23.05	98.3	42
SET	IDFYFDENPYFENK	heavy	924.914	1163.509	23.05	98.3	42
SET	IDFYFDENPYFENK	heavy	924.914	805.397	23.05	98.3	42
SET	IDFYFDENPYFENK	heavy	924.914	545.2809	23.05	98.3	42
SUN2	LLYWWAGTTWYR	light	808.4064	1040.495	18.91	90	38
SUN2	LLYWWAGTTWYR	light	808.4064	783.3784	18.91	90	38
SUN2	LLYWWAGTTWYR	light	808.4064	833.4345	18.91	90	38
SUN2	LLYWWAGTTWYR	heavy	813.4106	1050.503	18.91	90	38
SUN2	LLYWWAGTTWYR	heavy	813.4106	793.3867	18.91	90	38
SUN2	LLYWWAGTTWYR	heavy	813.4106	833.4345	18.91	90	38
SUN2	LEALAAEFSSNWQK	light	797.399	1096.506	20.98	89.2	37.6
SUN2	LEALAAEFSSNWQK	light	797.399	1025.469	20.98	89.2	37.6
SUN2	LEALAAEFSSNWQK	light	797.399	896.4261	20.98	89.2	37.6
SUN2	LEALAAEFSSNWQK	heavy	801.4061	1104.52	20.98	89.2	37.6
SUN2	LEALAAEFSSNWQK	heavy	801.4061	1033.483	20.98	89.2	37.6
SUN2	LEALAAEFSSNWQK	heavy	801.4061	904.4403	20.98	89.2	37.6
SUN2	IRPTAVTLEHVPK	light	487.6243	244.1656	14.13	66.7	24.1
SUN2	IRPTAVTLEHVPK	light	487.6243	539.33	14.13	66.7	24.1
SUN2	IRPTAVTLEHVPK	light	487.6243	638.3984	14.13	66.7	24.1
SUN2	IRPTAVTLEHVPK	heavy	490.2957	252.1798	14.13	66.7	24.1
SUN2	IRPTAVTLEHVPK	heavy	490.2957	539.33	14.13	66.7	24.1
SUN2	IRPTAVTLEHVPK	heavy	490.2957	638.3984	14.13	66.7	24.1
SPTN1	ALINADELASDVAGAEALLDR	light	709.7025	587.3511	27.35	82.9	36.2
SPTN1	ALINADELASDVAGAEALLDR	light	709.7025	516.314	27.35	82.9	36.2
SPTN1	ALINADELASDVAGAEALLDR	light	709.7025	403.23	27.35	82.9	36.2
SPTN1	ALINADELASDVAGAEALLDR	heavy	713.0385	597.3594	27.35	82.9	36.2
SPTN1	ALINADELASDVAGAEALLDR	heavy	713.0385	526.3223	27.35	82.9	36.2
SPTN1	ALINADELASDVAGAEALLDR	heavy	713.0385	413.2382	27.35	82.9	36.2
SPTN1	EAALTSEEVGADLEQVEVLQK	light	1129.574	1085.62	21.8	113.5	49.5
SPTN1	EAALTSEEVGADLEQVEVLQK	light	1129.574	972.536	21.8	113.5	49.5
SPTN1	EAALTSEEVGADLEQVEVLQK	light	1129.574	843.4934	21.8	113.5	49.5
SPTN1	EAALTSEEVGADLEQVEVLQK	heavy	1133.581	1093.634	21.8	113.5	49.5
SPTN1	EAALTSEEVGADLEQVEVLQK	heavy	1133.581	980.5502	21.8	113.5	49.5
SPTN1	EAALTSEEVGADLEQVEVLQK	heavy	1133.581	851.5076	21.8	113.5	49.5
SPTN1	SQLLGSAHEVQR	light	662.852	996.5221	12.62	79.4	32.7
SPTN1	SQLLGSAHEVQR	light	662.852	883.4381	12.62	79.4	32.7
SPTN1	SQLLGSAHEVQR	light	662.852	329.1819	12.62	79.4	32.7

SPTN1	SQLLGSAHEVQR	heavy	667.8562	1006.53	12.62	79.4	32.7
SPTN1	SQLLGSAHEVQR	heavy	667.8562	893.4463	12.62	79.4	32.7
SPTN1	SQLLGSAHEVQR	heavy	667.8562	329.1819	12.62	79.4	32.7
TBB3	FPGQLNADLR	light	565.8013	886.4741	17.2	72.4	29.2
TBB3	FPGQLNADLR	light	565.8013	701.3941	17.2	72.4	29.2
TBB3	FPGQLNADLR	light	565.8013	288.203	17.2	72.4	29.2
TBB3	FPGQLNADLR	heavy	570.8054	896.4824	17.2	72.4	29.2
TBB3	FPGQLNADLR	heavy	570.8054	711.4023	17.2	72.4	29.2
TBB3	FPGQLNADLR	heavy	570.8054	298.2113	17.2	72.4	29.2
TBB3	LAVNMVPFPR	light	572.3208	860.4447	20.46	72.8	29.5
TBB3	LAVNMVPFPR	light	572.3208	615.3613	20.46	72.8	29.5
TBB3	LAVNMVPFPR	light	572.3208	516.2929	20.46	72.8	29.5
TBB3	LAVNMVPFPR	heavy	577.3249	870.453	20.46	72.8	29.5
TBB3	LAVNMVPFPR	heavy	577.3249	625.3696	20.46	72.8	29.5
TBB3	LAVNMVPFPR	heavy	577.3249	526.3012	20.46	72.8	29.5
UBP2L	IDLAVLLGK	light	471.3051	713.492	23.36	65.5	25.8
UBP2L	IDLAVLLGK	light	471.3051	600.4079	23.36	65.5	25.8
UBP2L	IDLAVLLGK	light	471.3051	529.3708	23.36	65.5	25.8
UBP2L	IDLAVLLGK	heavy	475.3122	721.5062	23.36	65.5	25.8
UBP2L	IDLAVLLGK	heavy	475.3122	608.4221	23.36	65.5	25.8
UBP2L	IDLAVLLGK	heavy	475.3122	537.385	23.36	65.5	25.8
UBP2L	DGSLASNPYSGDLTK	light	762.8625	1152.553	16.56	86.7	36.3
UBP2L	DGSLASNPYSGDLTK	light	762.8625	1081.516	16.56	86.7	36.3
UBP2L	DGSLASNPYSGDLTK	light	762.8625	880.4411	16.56	86.7	36.3
UBP2L	DGSLASNPYSGDLTK	heavy	766.8696	1160.567	16.56	86.7	36.3
UBP2L	DGSLASNPYSGDLTK	heavy	766.8696	1089.53	16.56	86.7	36.3
UBP2L	DGSLASNPYSGDLTK	heavy	766.8696	888.4553	16.56	86.7	36.3
SYWC	KPFYLYTGR	light	572.8111	1016.52	16.35	72.9	29.5
SYWC	KPFYLYTGR	light	572.8111	919.4672	16.35	72.9	29.5
SYWC	KPFYLYTGR	light	572.8111	772.3988	16.35	72.9	29.5
SYWC	KPFYLYTGR	heavy	577.8153	1026.528	16.35	72.9	29.5
SYWC	KPFYLYTGR	heavy	577.8153	929.4755	16.35	72.9	29.5
SYWC	KPFYLYTGR	heavy	577.8153	782.4071	16.35	72.9	29.5
SYWC	DLTLDQAYSYAVENAK	light	900.9362	1044.5	21.98	96.8	41.3
SYWC	DLTLDQAYSYAVENAK	light	900.9362	881.4363	21.98	96.8	41.3
SYWC	DLTLDQAYSYAVENAK	light	900.9362	461.2354	21.98	96.8	41.3
SYWC	DLTLDQAYSYAVENAK	heavy	904.9433	1052.514	21.98	96.8	41.3
SYWC	DLTLDQAYSYAVENAK	heavy	904.9433	889.4505	21.98	96.8	41.3
SYWC	DLTLDQAYSYAVENAK	heavy	904.9433	469.2496	21.98	96.8	41.3
SYWC	ALIEVLQPLIAEHQAR	light	901.0202	1162.633	22.45	96.8	41.3
SYWC	ALIEVLQPLIAEHQAR	light	901.0202	1034.574	22.45	96.8	41.3
SYWC	ALIEVLQPLIAEHQAR	light	901.0202	526.3235	22.45	96.8	41.3
SYWC	ALIEVLQPLIAEHQAR	heavy	906.0243	1172.641	22.45	96.8	41.3
SYWC	ALIEVLQPLIAEHQAR	heavy	906.0243	1044.582	22.45	96.8	41.3
SYWC	ALIEVLQPLIAEHQAR	heavy	906.0243	526.3235	22.45	96.8	41.3
4F2	VILDLTPNYR	light	602.3402	991.5207	19.43	75	30.5

4F2	VILDLTPNYR	light	602.3402	878.4367	19.43	75	30.5
4F2	VILDLTPNYR	light	602.3402	549.278	19.43	75	30.5
4F2	VILDLTPNYR	heavy	607.3444	1001.529	19.43	75	30.5
4F2	VILDLTPNYR	heavy	607.3444	888.4449	19.43	75	30.5
4F2	VILDLTPNYR	heavy	607.3444	559.2862	19.43	75	30.5
4F2	LLTSFLPAQLLR	light	686.4216	1145.668	25.44	81.2	33.6
4F2	LLTSFLPAQLLR	light	686.4216	810.5196	25.44	81.2	33.6
4F2	LLTSFLPAQLLR	light	686.4216	697.4355	25.44	81.2	33.6
4F2	LLTSFLPAQLLR	heavy	691.4257	1155.676	25.44	81.2	33.6
4F2	LLTSFLPAQLLR	heavy	691.4257	820.5279	25.44	81.2	33.6
4F2	LLTSFLPAQLLR	heavy	691.4257	707.4438	25.44	81.2	33.6
4F2	GQSEDPGSLLSLFR	light	753.3834	1104.605	24.6	86	36
4F2	GQSEDPGSLLSLFR	light	753.3834	989.5778	24.6	86	36
4F2	GQSEDPGSLLSLFR	light	753.3834	522.3035	24.6	86	36
4F2	GQSEDPGSLLSLFR	heavy	758.3875	1114.613	24.6	86	36
4F2	GQSEDPGSLLSLFR	heavy	758.3875	999.5861	24.6	86	36
4F2	GQSEDPGSLLSLFR	heavy	758.3875	532.3117	24.6	86	36
ARI1A	LYELGGEPER	light	581.7906	886.4265	15.67	73.5	29.8
ARI1A	LYELGGEPER	light	581.7906	757.3839	15.67	73.5	29.8
ARI1A	LYELGGEPER	light	581.7906	644.2998	15.67	73.5	29.8
ARI1A	LYELGGEPER	heavy	586.7947	896.4348	15.67	73.5	29.8
ARI1A	LYELGGEPER	heavy	586.7947	767.3922	15.67	73.5	29.8
ARI1A	LYELGGEPER	heavy	586.7947	654.3081	15.67	73.5	29.8
ARI1B	DMGAQYAAASPAWAAAQQR	light	655.3075	644.3474	18.42	78.9	33.2
ARI1B	DMGAQYAAASPAWAAAQQR	light	655.3075	502.2732	18.42	78.9	33.2
ARI1B	DMGAQYAAASPAWAAAQQR	light	655.3075	808.3294	18.42	78.9	33.2
ARI1B	DMGAQYAAASPAWAAAQQR	heavy	658.6436	654.3557	18.42	78.9	33.2
ARI1B	DMGAQYAAASPAWAAAQQR	heavy	658.6436	512.2815	18.42	78.9	33.2
ARI1B	DMGAQYAAASPAWAAAQQR	heavy	658.6436	808.3294	18.42	78.9	33.2
COF1	NIILEEGK	light	458.2609	688.3876	16.75	64.5	25.4
COF1	NIILEEGK	light	458.2609	333.1769	16.75	64.5	25.4
COF1	NIILEEGK	light	458.2609	228.1343	16.75	64.5	25.4
COF1	NIILEEGK	heavy	462.268	696.4018	16.75	64.5	25.4
COF1	NIILEEGK	heavy	462.268	341.1911	16.75	64.5	25.4
COF1	NIILEEGK	heavy	462.268	228.1343	16.75	64.5	25.4
COF1	EILVGDVGQTVDDPYATFVK	light	1083.552	1055.504	23.76	110.1	47.9
COF1	EILVGDVGQTVDDPYATFVK	light	1083.552	940.4775	23.76	110.1	47.9
COF1	EILVGDVGQTVDDPYATFVK	light	1083.552	825.4505	23.76	110.1	47.9
COF1	EILVGDVGQTVDDPYATFVK	heavy	1087.559	1063.519	23.76	110.1	47.9
COF1	EILVGDVGQTVDDPYATFVK	heavy	1087.559	948.4917	23.76	110.1	47.9
COF1	EILVGDVGQTVDDPYATFVK	heavy	1087.559	833.4647	23.76	110.1	47.9
COF1	YALYDATYETK	light	669.3166	827.3781	16.24	79.9	33
COF1	YALYDATYETK	light	669.3166	712.3512	16.24	79.9	33
COF1	YALYDATYETK	light	669.3166	641.3141	16.24	79.9	33
COF1	YALYDATYETK	heavy	673.3237	835.3923	16.24	79.9	33
COF1	YALYDATYETK	heavy	673.3237	720.3654	16.24	79.9	33

COF1	YALYDATYETK	heavy	673.3237	649.3283	16.24	79.9	33
REQU	GPGLASGQLYSYPAR	light	768.8939	1141.564	17.2	87.2	36.5
REQU	GPGLASGQLYSYPAR	light	768.8939	1054.532	17.2	87.2	36.5
REQU	GPGLASGQLYSYPAR	light	768.8939	756.3675	17.2	87.2	36.5
REQU	GPGLASGQLYSYPAR	heavy	773.898	1151.572	17.2	87.2	36.5
REQU	GPGLASGQLYSYPAR	heavy	773.898	1064.54	17.2	87.2	36.5
REQU	GPGLASGQLYSYPAR	heavy	773.898	766.3758	17.2	87.2	36.5
REQU	LSFPSIKPDTDQTLK	light	845.4565	1045.552	17.98	92.8	39.3
REQU	LSFPSIKPDTDQTLK	light	845.4565	917.4575	17.98	92.8	39.3
REQU	LSFPSIKPDTDQTLK	light	845.4565	705.3777	17.98	92.8	39.3
REQU	LSFPSIKPDTDQTLK	heavy	849.4636	1053.567	17.98	92.8	39.3
REQU	LSFPSIKPDTDQTLK	heavy	849.4636	925.4717	17.98	92.8	39.3
REQU	LSFPSIKPDTDQTLK	heavy	849.4636	713.3919	17.98	92.8	39.3
REQU	EGLISQDGSSLEALLR	light	844.4467	1188.622	23.57	92.7	39.3
REQU	EGLISQDGSSLEALLR	light	844.4467	1060.563	23.57	92.7	39.3
REQU	EGLISQDGSSLEALLR	light	844.4467	945.5364	23.57	92.7	39.3
REQU	EGLISQDGSSLEALLR	heavy	849.4508	1198.63	23.57	92.7	39.3
REQU	EGLISQDGSSLEALLR	heavy	849.4508	1070.572	23.57	92.7	39.3
REQU	EGLISQDGSSLEALLR	heavy	849.4508	955.5446	23.57	92.7	39.3
ICAM1	TFLTVYWTPER	light	706.8641	502.262	21.27	82.6	34.3
ICAM1	TFLTVYWTPER	light	706.8641	401.2143	21.27	82.6	34.3
ICAM1	TFLTVYWTPER	light	706.8641	911.4662	21.27	82.6	34.3
ICAM1	TFLTVYWTPER	heavy	711.8682	512.2703	21.27	82.6	34.3
ICAM1	TFLTVYWTPER	heavy	711.8682	411.2226	21.27	82.6	34.3
ICAM1	TFLTVYWTPER	heavy	711.8682	911.4662	21.27	82.6	34.3
ICAM1	DGTFPLPIGESVTVTR	light	844.9463	1058.584	22.02	92.7	39.3
ICAM1	DGTFPLPIGESVTVTR	light	844.9463	662.3832	22.02	92.7	39.3
ICAM1	DGTFPLPIGESVTVTR	light	844.9463	631.3086	22.02	92.7	39.3
ICAM1	DGTFPLPIGESVTVTR	heavy	849.9505	1068.592	22.02	92.7	39.3
ICAM1	DGTFPLPIGESVTVTR	heavy	849.9505	672.3914	22.02	92.7	39.3
ICAM1	DGTFPLPIGESVTVTR	heavy	849.9505	631.3086	22.02	92.7	39.3
IKIP	LETNEFQQLQSK	light	732.8701	878.473	16.47	84.5	35.2
IKIP	LETNEFQQLQSK	light	732.8701	603.3461	16.47	84.5	35.2
IKIP	LETNEFQQLQSK	light	732.8701	475.2875	16.47	84.5	35.2
IKIP	LETNEFQQLQSK	heavy	736.8772	886.4872	16.47	84.5	35.2
IKIP	LETNEFQQLQSK	heavy	736.8772	611.3603	16.47	84.5	35.2
IKIP	LETNEFQQLQSK	heavy	736.8772	483.3017	16.47	84.5	35.2
IKIP	ISGLVTDVISLTDSVQELENK	light	1130.6	1162.559	19.18	113.5	49.6
IKIP	ISGLVTDVISLTDSVQELENK	light	1130.6	898.5244	19.18	113.5	49.6
IKIP	ISGLVTDVISLTDSVQELENK	light	1130.6	1098.641	19.18	113.5	49.6
IKIP	ISGLVTDVISLTDSVQELENK	heavy	1134.607	1170.573	19.18	113.5	49.6
IKIP	ISGLVTDVISLTDSVQELENK	heavy	1134.607	898.5244	19.18	113.5	49.6
IKIP	ISGLVTDVISLTDSVQELENK	heavy	1134.607	1098.641	19.18	113.5	49.6
ITB1	LKPEDITQIQPQQLVLR	light	673.7248	981.584	20.44	80.2	34.2
ITB1	LKPEDITQIQPQQLVLR	light	673.7248	853.5254	20.44	80.2	34.2
ITB1	LKPEDITQIQPQQLVLR	light	673.7248	925.4989	20.44	80.2	34.2

ITB1	LKPEDITQIQPQQLVLR	heavy	677.0608	991.5923	20.44	80.2	34.2
ITB1	LKPEDITQIQPQQLVLR	heavy	677.0608	863.5337	20.44	80.2	34.2
ITB1	LKPEDITQIQPQQLVLR	heavy	677.0608	925.4989	20.44	80.2	34.2
ITB1	IGFGSFVEK	light	492.2635	870.4356	19.11	67	26.6
ITB1	IGFGSFVEK	light	492.2635	813.4141	19.11	67	26.6
ITB1	IGFGSFVEK	light	492.2635	666.3457	19.11	67	26.6
ITB1	IGFGSFVEK	heavy	496.2706	878.4498	19.11	67	26.6
ITB1	IGFGSFVEK	heavy	496.2706	821.4283	19.11	67	26.6
ITB1	IGFGSFVEK	heavy	496.2706	674.3599	19.11	67	26.6
ITB1	LSENNIQTIFAVTEEFQPVYK	light	824.0882	1039.509	26.33	91.2	42.4
ITB1	LSENNIQTIFAVTEEFQPVYK	light	824.0882	910.4669	26.33	91.2	42.4
ITB1	LSENNIQTIFAVTEEFQPVYK	light	824.0882	506.2973	26.33	91.2	42.4
ITB1	LSENNIQTIFAVTEEFQPVYK	heavy	826.7596	1047.524	26.33	91.2	42.4
ITB1	LSENNIQTIFAVTEEFQPVYK	heavy	826.7596	918.4811	26.33	91.2	42.4
ITB1	LSENNIQTIFAVTEEFQPVYK	heavy	826.7596	514.3115	26.33	91.2	42.4
KPYM	LDIDSPPITAR	light	599.3273	856.4523	17.09	74.8	30.4
KPYM	LDIDSPPITAR	light	599.3273	741.4254	17.09	74.8	30.4
KPYM	LDIDSPPITAR	light	599.3273	654.3933	17.09	74.8	30.4
KPYM	LDIDSPPITAR	heavy	604.3315	866.4606	17.09	74.8	30.4
KPYM	LDIDSPPITAR	heavy	604.3315	751.4336	17.09	74.8	30.4
KPYM	LDIDSPPITAR	heavy	604.3315	664.4016	17.09	74.8	30.4
KPYM	IYVDDGLISLQVK	light	731.9112	1186.668	21.73	84.5	35.2
KPYM	IYVDDGLISLQVK	light	731.9112	1087.599	21.73	84.5	35.2
KPYM	IYVDDGLISLQVK	light	731.9112	574.3559	21.73	84.5	35.2
KPYM	IYVDDGLISLQVK	heavy	735.9183	1194.682	21.73	84.5	35.2
KPYM	IYVDDGLISLQVK	heavy	735.9183	1095.614	21.73	84.5	35.2
KPYM	IYVDDGLISLQVK	heavy	735.9183	582.3701	21.73	84.5	35.2
KPYM	GVNLPGAAVDLPAVSEK	light	818.9489	1028.562	19.94	90.8	38.3
KPYM	GVNLPGAAVDLPAVSEK	light	818.9489	858.4567	19.94	90.8	38.3
KPYM	GVNLPGAAVDLPAVSEK	light	818.9489	630.3457	19.94	90.8	38.3
KPYM	GVNLPGAAVDLPAVSEK	heavy	822.956	1036.576	19.94	90.8	38.3
KPYM	GVNLPGAAVDLPAVSEK	heavy	822.956	866.4709	19.94	90.8	38.3
KPYM	GVNLPGAAVDLPAVSEK	heavy	822.956	638.3599	19.94	90.8	38.3
LDHB	SLADELALVDVLEDK	light	815.4327	930.5142	26.25	90.6	38.2
LDHB	SLADELALVDVLEDK	light	815.4327	718.3618	26.25	90.6	38.2
LDHB	SLADELALVDVLEDK	light	815.4327	1126.599	26.25	90.6	38.2
LDHB	SLADELALVDVLEDK	heavy	819.4398	938.5284	26.25	90.6	38.2
LDHB	SLADELALVDVLEDK	heavy	819.4398	726.376	26.25	90.6	38.2
LDHB	SLADELALVDVLEDK	heavy	819.4398	1126.599	26.25	90.6	38.2
LDHB	FIIPQIVK	light	479.3102	697.4607	21.09	66.1	26.1
LDHB	FIIPQIVK	light	479.3102	584.3766	21.09	66.1	26.1
LDHB	FIIPQIVK	light	479.3102	261.1598	21.09	66.1	26.1
LDHB	FIIPQIVK	heavy	483.3173	705.4749	21.09	66.1	26.1
LDHB	FIIPQIVK	heavy	483.3173	592.3908	21.09	66.1	26.1
LDHB	FIIPQIVK	heavy	483.3173	261.1598	21.09	66.1	26.1
LDHB	GLTSVINQK	light	480.2796	789.4465	14.97	66.1	26.1

LDHB	GLTSVINQK	light	480.2796	688.3988	14.97	66.1	26.1
LDHB	GLTSVINQK	light	480.2796	502.2984	14.97	66.1	26.1
LDHB	GLTSVINQK	heavy	484.2867	797.4607	14.97	66.1	26.1
LDHB	GLTSVINQK	heavy	484.2867	696.413	14.97	66.1	26.1
LDHB	GLTSVINQK	heavy	484.2867	510.3126	14.97	66.1	26.1
LEG3	GNDVAFHFNPR	light	637.3073	888.4475	15.97	77.6	31.8
LEG3	GNDVAFHFNPR	light	637.3073	817.4104	15.97	77.6	31.8
LEG3	GNDVAFHFNPR	light	637.3073	670.342	15.97	77.6	31.8
LEG3	GNDVAFHFNPR	heavy	642.3114	898.4558	15.97	77.6	31.8
LEG3	GNDVAFHFNPR	heavy	642.3114	827.4187	15.97	77.6	31.8
LEG3	GNDVAFHFNPR	heavy	642.3114	680.3502	15.97	77.6	31.8
LEG3	QSVFPFESGKPFK	light	499.9294	792.425	18.77	67.6	24.8
LEG3	QSVFPFESGKPFK	light	499.9294	663.3824	18.77	67.6	24.8
LEG3	QSVFPFESGKPFK	light	499.9294	391.234	18.77	67.6	24.8
LEG3	QSVFPFESGKPFK	heavy	502.6008	800.4392	18.77	67.6	24.8
LEG3	QSVFPFESGKPFK	heavy	502.6008	671.3966	18.77	67.6	24.8
LEG3	QSVFPFESGKPFK	heavy	502.6008	399.2482	18.77	67.6	24.8
LEG3	IQVLVEPDHFK	light	442.2468	643.3198	17.02	63.4	21.6
LEG3	IQVLVEPDHFK	light	442.2468	341.2183	17.02	63.4	21.6
LEG3	IQVLVEPDHFK	light	442.2468	454.3024	17.02	63.4	21.6
LEG3	IQVLVEPDHFK	heavy	444.9182	651.334	17.02	63.4	21.6
LEG3	IQVLVEPDHFK	heavy	444.9182	341.2183	17.02	63.4	21.6
LEG3	IQVLVEPDHFK	heavy	444.9182	454.3024	17.02	63.4	21.6
PB1	YIEGLSAESNSISK	light	749.3752	1092.553	16.08	85.7	35.8
PB1	YIEGLSAESNSISK	light	749.3752	922.4476	16.08	85.7	35.8
PB1	YIEGLSAESNSISK	light	749.3752	835.4156	16.08	85.7	35.8
PB1	YIEGLSAESNSISK	heavy	753.3823	1100.567	16.08	85.7	35.8
PB1	YIEGLSAESNSISK	heavy	753.3823	930.4618	16.08	85.7	35.8
PB1	YIEGLSAESNSISK	heavy	753.3823	843.4298	16.08	85.7	35.8
PHB2	IGGVQQDTILAEGLHFR	light	618.6671	942.5156	20.49	76.2	31.2
PHB2	IGGVQQDTILAEGLHFR	light	618.6671	829.4315	20.49	76.2	31.2
PHB2	IGGVQQDTILAEGLHFR	light	618.6671	629.3518	20.49	76.2	31.2
PHB2	IGGVQQDTILAEGLHFR	heavy	622.0032	952.5238	20.49	76.2	31.2
PHB2	IGGVQQDTILAEGLHFR	heavy	622.0032	839.4398	20.49	76.2	31.2
PHB2	IGGVQQDTILAEGLHFR	heavy	622.0032	639.3601	20.49	76.2	31.2
PHB2	LGLDYEER	light	497.7456	881.3999	15.81	67.4	26.8
PHB2	LGLDYEER	light	497.7456	711.2944	15.81	67.4	26.8
PHB2	LGLDYEER	light	497.7456	596.2675	15.81	67.4	26.8
PHB2	LGLDYEER	heavy	502.7498	891.4082	15.81	67.4	26.8
PHB2	LGLDYEER	heavy	502.7498	721.3027	15.81	67.4	26.8
PHB2	LGLDYEER	heavy	502.7498	606.2757	15.81	67.4	26.8
PHB2	FNASQLITQR	light	589.3198	916.5211	17.72	74.1	30.1
PHB2	FNASQLITQR	light	589.3198	630.3933	17.72	74.1	30.1
PHB2	FNASQLITQR	light	589.3198	404.2252	17.72	74.1	30.1
PHB2	FNASQLITQR	heavy	594.324	926.5293	17.72	74.1	30.1
PHB2	FNASQLITQR	heavy	594.324	640.4016	17.72	74.1	30.1

PHB2	FNASQLITQR	heavy	594.324	414.2335	17.72	74.1	30.1
RS16	LLEPVLLLGK	light	547.8628	868.5502	23.37	71.1	28.6
RS16	LLEPVLLLGK	light	547.8628	739.5076	23.37	71.1	28.6
RS16	LLEPVLLLGK	light	547.8628	227.1754	23.37	71.1	28.6
RS16	LLEPVLLLGK	heavy	551.8699	876.5644	23.37	71.1	28.6
RS16	LLEPVLLLGK	heavy	551.8699	747.5218	23.37	71.1	28.6
RS16	LLEPVLLLGK	heavy	551.8699	227.1754	23.37	71.1	28.6
RS16	DILIQYDR	light	518.2771	694.3519	17.28	68.9	27.5
RS16	DILIQYDR	light	518.2771	581.2678	17.28	68.9	27.5
RS16	DILIQYDR	light	518.2771	229.1183	17.28	68.9	27.5
RS16	DILIQYDR	heavy	523.2812	704.3601	17.28	68.9	27.5
RS16	DILIQYDR	heavy	523.2812	591.2761	17.28	68.9	27.5
RS16	DILIQYDR	heavy	523.2812	229.1183	17.28	68.9	27.5
RS16	TLLVADPR	light	442.7636	670.3883	15.62	63.4	24.8
RS16	TLLVADPR	light	442.7636	272.1717	15.62	63.4	24.8
RS16	TLLVADPR	light	442.7636	215.139	15.62	63.4	24.8
RS16	TLLVADPR	heavy	447.7678	680.3965	15.62	63.4	24.8
RS16	TLLVADPR	heavy	447.7678	282.18	15.62	63.4	24.8
RS16	TLLVADPR	heavy	447.7678	215.139	15.62	63.4	24.8
S10A6	LQDAEIAR	light	458.2483	674.3468	12.32	64.5	25.4
S10A6	LQDAEIAR	light	458.2483	559.3198	12.32	64.5	25.4
S10A6	LQDAEIAR	light	458.2483	242.1499	12.32	64.5	25.4
S10A6	LQDAEIAR	heavy	463.2525	684.355	12.32	64.5	25.4
S10A6	LQDAEIAR	heavy	463.2525	569.3281	12.32	64.5	25.4
S10A6	LQDAEIAR	heavy	463.2525	242.1499	12.32	64.5	25.4
GDN	DIVTVANAVFVK	light	638.369	948.5513	15.94	77.7	31.8
GDN	DIVTVANAVFVK	light	638.369	748.4352	15.94	77.7	31.8
GDN	DIVTVANAVFVK	light	638.369	677.3981	15.94	77.7	31.8
GDN	DIVTVANAVFVK	heavy	642.3761	956.5655	15.94	77.7	31.8
GDN	DIVTVANAVFVK	heavy	642.3761	756.4494	15.94	77.7	31.8
GDN	DIVTVANAVFVK	heavy	642.3761	685.4123	15.94	77.7	31.8
SMCA2	GIVEDIHC[CAM]GSMK	light	673.3156	719.2963	17.71	80.2	33.1
SMCA2	GIVEDIHC[CAM]GSMK	light	673.3156	582.2374	17.71	80.2	33.1
SMCA2	GIVEDIHC[CAM]GSMK	light	673.3156	764.3937	17.71	80.2	33.1
SMCA2	GIVEDIHC[CAM]GSMK	heavy	677.3227	727.3105	17.71	80.2	33.1
SMCA2	GIVEDIHC[CAM]GSMK	heavy	677.3227	590.2516	17.71	80.2	33.1
SMCA2	GIVEDIHC[CAM]GSMK	heavy	677.3227	764.3937	17.71	80.2	33.1
SMCA5	TEQEEDEELLTESSK	light	883.8944	1150.547	16.01	95.6	40.7
SMCA5	TEQEEDEELLTESSK	light	883.8944	664.3512	16.01	95.6	40.7
SMCA5	TEQEEDEELLTESSK	light	883.8944	551.2671	16.01	95.6	40.7
SMCA5	TEQEEDEELLTESSK	heavy	887.9015	1158.562	16.01	95.6	40.7
SMCA5	TEQEEDEELLTESSK	heavy	887.9015	672.3654	16.01	95.6	40.7
SMCA5	TEQEEDEELLTESSK	heavy	887.9015	559.2813	16.01	95.6	40.7
SMCA5	STLHNWMSEFK	light	690.3243	1078.477	17.45	81.4	33.7
SMCA5	STLHNWMSEFK	light	690.3243	941.4186	17.45	81.4	33.7
SMCA5	STLHNWMSEFK	light	690.3243	510.2558	17.45	81.4	33.7

SMCA5	STLHNWMSEFK	heavy	694.3314	1086.492	17.45	81.4	33.7
SMCA5	STLHNWMSEFK	heavy	694.3314	949.4328	17.45	81.4	33.7
SMCA5	STLHNWMSEFK	heavy	694.3314	518.27	17.45	81.4	33.7
SMCA5	ESEITDEDIDGILER	light	867.4074	1174.559	20.44	94.4	40.1
SMCA5	ESEITDEDIDGILER	light	867.4074	702.3781	20.44	94.4	40.1
SMCA5	ESEITDEDIDGILER	light	867.4074	417.2456	20.44	94.4	40.1
SMCA5	ESEITDEDIDGILER	heavy	872.4116	1184.567	20.44	94.4	40.1
SMCA5	ESEITDEDIDGILER	heavy	872.4116	712.3863	20.44	94.4	40.1
SMCA5	ESEITDEDIDGILER	heavy	872.4116	427.2539	20.44	94.4	40.1
SNF5	DHGYTTLATSVTLLK	light	810.4356	1147.693	19.64	90.2	38
SNF5	DHGYTTLATSVTLLK	light	810.4356	1046.646	19.64	90.2	38
SNF5	DHGYTTLATSVTLLK	light	810.4356	761.4767	19.64	90.2	38
SNF5	DHGYTTLATSVTLLK	heavy	814.4427	1155.707	19.64	90.2	38
SNF5	DHGYTTLATSVTLLK	heavy	814.4427	1054.66	19.64	90.2	38
SNF5	DHGYTTLATSVTLLK	heavy	814.4427	769.4909	19.64	90.2	38
SNF5	QQIESYPTDSILEDQSDQR	light	751.3486	990.4487	17.94	85.9	38.5
SNF5	QQIESYPTDSILEDQSDQR	light	751.3486	877.3646	17.94	85.9	38.5
SNF5	QQIESYPTDSILEDQSDQR	light	751.3486	303.1775	17.94	85.9	38.5
SNF5	QQIESYPTDSILEDQSDQR	heavy	754.6847	1000.457	17.94	85.9	38.5
SNF5	QQIESYPTDSILEDQSDQR	heavy	754.6847	887.3729	17.94	85.9	38.5
SNF5	QQIESYPTDSILEDQSDQR	heavy	754.6847	313.1858	17.94	85.9	38.5
SMRC2	TPQQTSASQQMLNFPDK	light	960.9596	1120.546	20.02	101.2	43.5
SMRC2	TPQQTSASQQMLNFPDK	light	960.9596	864.4284	20.02	101.2	43.5
SMRC2	TPQQTSASQQMLNFPDK	light	960.9596	359.1925	20.02	101.2	43.5
SMRC2	TPQQTSASQQMLNFPDK	heavy	964.9667	1128.56	20.02	101.2	43.5
SMRC2	TPQQTSASQQMLNFPDK	heavy	964.9667	872.4426	20.02	101.2	43.5
SMRC2	TPQQTSASQQMLNFPDK	heavy	964.9667	367.2067	20.02	101.2	43.5
SMRC2	ADPAFGLESSGIAGTTSDEPER	light	1104.009	1062.47	24.23	111.6	48.6
SMRC2	ADPAFGLESSGIAGTTSDEPER	light	1104.009	991.4327	24.23	111.6	48.6
SMRC2	ADPAFGLESSGIAGTTSDEPER	light	1104.009	401.2143	24.23	111.6	48.6
SMRC2	ADPAFGLESSGIAGTTSDEPER	heavy	1109.013	1072.478	24.23	111.6	48.6
SMRC2	ADPAFGLESSGIAGTTSDEPER	heavy	1109.013	1001.441	24.23	111.6	48.6
SMRC2	ADPAFGLESSGIAGTTSDEPER	heavy	1109.013	411.2226	24.23	111.6	48.6
SMRC2	DIGEGNLSTAAAAALAAAAVK	light	943.0049	1186.679	23.93	99.9	42.8
SMRC2	DIGEGNLSTAAAAALAAAAVK	light	943.0049	1099.647	23.93	99.9	42.8
SMRC2	DIGEGNLSTAAAAALAAAAVK	light	943.0049	927.5622	23.93	99.9	42.8
SMRC2	DIGEGNLSTAAAAALAAAAVK	heavy	947.012	1194.693	23.93	99.9	42.8
SMRC2	DIGEGNLSTAAAAALAAAAVK	heavy	947.012	1107.661	23.93	99.9	42.8
SMRC2	DIGEGNLSTAAAAALAAAAVK	heavy	947.012	935.5764	23.93	99.9	42.8
SMRD1	IHETIETINQLK	light	719.8986	1188.647	15.57	83.6	34.8
SMRD1	IHETIETINQLK	light	719.8986	1059.604	15.57	83.6	34.8
SMRD1	IHETIETINQLK	light	719.8986	380.1928	15.57	83.6	34.8
SMRD1	IHETIETINQLK	heavy	723.9057	1196.661	15.57	83.6	34.8
SMRD1	IHETIETINQLK	heavy	723.9057	1067.619	15.57	83.6	34.8
SMRD1	IHETIETINQLK	heavy	723.9057	380.1928	15.57	83.6	34.8
SMRD2	MPTTQETDGFQVK	light	741.3507	923.4469	15.64	85.2	35.5

SMRD2	MPTTQETDGFQVK	light	741.3507	578.3297	15.64	85.2	35.5
SMRD2	MPTTQETDGFQVK	light	741.3507	904.3717	15.64	85.2	35.5
SMRD2	MPTTQETDGFQVK	heavy	745.3578	931.4611	15.64	85.2	35.5
SMRD2	MPTTQETDGFQVK	heavy	745.3578	586.3439	15.64	85.2	35.5
SMRD2	MPTTQETDGFQVK	heavy	745.3578	904.3717	15.64	85.2	35.5
SMRD2	IITDVIGNPEEER	light	742.8832	943.448	17.57	85.3	35.6
SMRD2	IITDVIGNPEEER	light	742.8832	830.3639	17.57	85.3	35.6
SMRD2	IITDVIGNPEEER	light	742.8832	659.2995	17.57	85.3	35.6
SMRD2	IITDVIGNPEEER	heavy	747.8873	953.4562	17.57	85.3	35.6
SMRD2	IITDVIGNPEEER	heavy	747.8873	840.3722	17.57	85.3	35.6
SMRD2	IITDVIGNPEEER	heavy	747.8873	669.3078	17.57	85.3	35.6
SMRD3	DLYGPDNHLVEWHR	light	875.9184	839.4522	17.3	95	40.4
SMRD3	DLYGPDNHLVEWHR	light	875.9184	627.2998	17.3	95	40.4
SMRD3	DLYGPDNHLVEWHR	light	875.9184	498.2572	17.3	95	40.4
SMRD3	DLYGPDNHLVEWHR	heavy	880.9226	849.4605	17.3	95	40.4
SMRD3	DLYGPDNHLVEWHR	heavy	880.9226	637.308	17.3	95	40.4
SMRD3	DLYGPDNHLVEWHR	heavy	880.9226	508.2654	17.3	95	40.4
SMCE1	AEAALEEESR	light	552.762	904.4371	11.95	71.4	28.8
SMCE1	AEAALEEESR	light	552.762	762.3628	11.95	71.4	28.8
SMCE1	AEAALEEESR	light	552.762	649.2788	11.95	71.4	28.8
SMCE1	AEAALEEESR	heavy	557.7662	914.4453	11.95	71.4	28.8
SMCE1	AEAALEEESR	heavy	557.7662	772.3711	11.95	71.4	28.8
SMCE1	AEAALEEESR	heavy	557.7662	659.287	11.95	71.4	28.8
SMCE1	FLESTDSFNNELK	light	772.3674	1154.532	18.18	87.4	36.7
SMCE1	FLESTDSFNNELK	light	772.3674	1067.5	18.18	87.4	36.7
SMCE1	FLESTDSFNNELK	light	772.3674	966.4527	18.18	87.4	36.7
SMCE1	FLESTDSFNNELK	heavy	776.3745	1162.547	18.18	87.4	36.7
SMCE1	FLESTDSFNNELK	heavy	776.3745	1075.515	18.18	87.4	36.7
SMCE1	FLESTDSFNNELK	heavy	776.3745	974.4669	18.18	87.4	36.7
SMCE1	IAAEIAQAEEQAR	light	700.3624	902.4326	15.4	82.2	34.1
SMCE1	IAAEIAQAEEQAR	light	700.3624	831.3955	15.4	82.2	34.1
SMCE1	IAAEIAQAEEQAR	light	700.3624	632.2998	15.4	82.2	34.1
SMCE1	IAAEIAQAEEQAR	heavy	705.3666	912.4409	15.4	82.2	34.1
SMCE1	IAAEIAQAEEQAR	heavy	705.3666	841.4038	15.4	82.2	34.1
SMCE1	IAAEIAQAEEQAR	heavy	705.3666	642.3081	15.4	82.2	34.1
SMCA5	STLHNWMSEFK	light	690.3243	941.4186	17.48	81.4	33.7
SMCA5	STLHNWMSEFK	light	690.3243	827.3756	17.48	81.4	33.7
SMCA5	STLHNWMSEFK	light	690.3243	294.1812	17.48	81.4	33.7
SMCA5	STLHNWMSEFK	heavy	694.3314	949.4328	17.48	81.4	33.7
SMCA5	STLHNWMSEFK	heavy	694.3314	835.3898	17.48	81.4	33.7
SMCA5	STLHNWMSEFK	heavy	694.3314	302.1954	17.48	81.4	33.7
SMCA5	ESEITDEDIDGILER	light	867.4074	1174.559	20.44	94.4	40.1
SMCA5	ESEITDEDIDGILER	light	867.4074	702.3781	20.44	94.4	40.1
SMCA5	ESEITDEDIDGILER	light	867.4074	417.2456	20.44	94.4	40.1
SMCA5	ESEITDEDIDGILER	heavy	872.4116	1184.567	20.44	94.4	40.1
SMCA5	ESEITDEDIDGILER	heavy	872.4116	712.3863	20.44	94.4	40.1

SMCA5	ESEITDEDIDGILER	heavy	872.4116	427.2539	20.44	94.4	40.1
SPRC	NVLVTLYER	light	553.8139	893.5091	19.01	71.5	28.8
SPRC	NVLVTLYER	light	553.8139	780.425	19.01	71.5	28.8
SPRC	NVLVTLYER	light	553.8139	681.3566	19.01	71.5	28.8
SPRC	NVLVTLYER	heavy	558.818	903.5174	19.01	71.5	28.8
SPRC	NVLVTLYER	heavy	558.818	790.4333	19.01	71.5	28.8
SPRC	NVLVTLYER	heavy	558.818	691.3649	19.01	71.5	28.8
SPRC	LEAGDHPVELLAR	light	473.9245	797.488	16.42	65.7	23.4
SPRC	LEAGDHPVELLAR	light	473.9245	601.3668	16.42	65.7	23.4
SPRC	LEAGDHPVELLAR	light	473.9245	243.1339	16.42	65.7	23.4
SPRC	LEAGDHPVELLAR	heavy	477.2606	807.4962	16.42	65.7	23.4
SPRC	LEAGDHPVELLAR	heavy	477.2606	611.3751	16.42	65.7	23.4
SPRC	LEAGDHPVELLAR	heavy	477.2606	243.1339	16.42	65.7	23.4
SPCS2	YVENFGLIDGR	light	641.825	1020.511	19.34	77.9	32
SPCS2	YVENFGLIDGR	light	641.825	891.4683	19.34	77.9	32
SPCS2	YVENFGLIDGR	light	641.825	630.357	19.34	77.9	32
SPCS2	YVENFGLIDGR	heavy	646.8291	1030.519	19.34	77.9	32
SPCS2	YVENFGLIDGR	heavy	646.8291	901.4766	19.34	77.9	32
SPCS2	YVENFGLIDGR	heavy	646.8291	640.3652	19.34	77.9	32
SPCS2	FFDHSGTLVMDAYEPEISR	light	738.6772	893.4363	20.31	85	37.8
SPCS2	FFDHSGTLVMDAYEPEISR	light	738.6772	730.373	20.31	85	37.8
SPCS2	FFDHSGTLVMDAYEPEISR	light	738.6772	601.3304	20.31	85	37.8
SPCS2	FFDHSGTLVMDAYEPEISR	heavy	742.0133	903.4446	20.31	85	37.8
SPCS2	FFDHSGTLVMDAYEPEISR	heavy	742.0133	740.3813	20.31	85	37.8
SPCS2	FFDHSGTLVMDAYEPEISR	heavy	742.0133	611.3387	20.31	85	37.8
SPCS2	LHDSLAIER	light	527.288	803.4258	13.66	69.6	27.8
SPCS2	LHDSLAIER	light	527.288	688.3988	13.66	69.6	27.8
SPCS2	LHDSLAIER	light	527.288	488.2827	13.66	69.6	27.8
SPCS2	LHDSLAIER	heavy	532.2921	813.434	13.66	69.6	27.8
SPCS2	LHDSLAIER	heavy	532.2921	698.4071	13.66	69.6	27.8
SPCS2	LHDSLAIER	heavy	532.2921	498.291	13.66	69.6	27.8
ZC3HF	HALPPGFVLK	light	539.824	870.5448	16.48	70.5	28.3
ZC3HF	HALPPGFVLK	light	539.824	757.4607	16.48	70.5	28.3
ZC3HF	HALPPGFVLK	light	539.824	819.4512	16.48	70.5	28.3
ZC3HF	HALPPGFVLK	heavy	543.8311	878.559	16.48	70.5	28.3
ZC3HF	HALPPGFVLK	heavy	543.8311	765.4749	16.48	70.5	28.3
ZC3HF	HALPPGFVLK	heavy	543.8311	819.4512	16.48	70.5	28.3
ZC3HF	DVDETGITVASLER	light	752.8781	945.5364	18.84	86	36
ZC3HF	DVDETGITVASLER	light	752.8781	775.4308	18.84	86	36
ZC3HF	DVDETGITVASLER	light	752.8781	575.3148	18.84	86	36
ZC3HF	DVDETGITVASLER	heavy	757.8822	955.5446	18.84	86	36
ZC3HF	DVDETGITVASLER	heavy	757.8822	785.4391	18.84	86	36
ZC3HF	DVDETGITVASLER	heavy	757.8822	585.323	18.84	86	36
JAK2	HDFVHGWIK	light	380.1979	503.2976	16.37	58.8	18.3
JAK2	HDFVHGWIK	light	380.1979	400.1615	16.37	58.8	18.3
JAK2	HDFVHGWIK	light	380.1979	499.23	16.37	58.8	18.3

JAK2	HDFVHGWIK	heavy	382.8693	511.3118	16.37	58.8	18.3
JAK2	HDFVHGWIK	heavy	382.8693	400.1615	16.37	58.8	18.3
JAK2	HDFVHGWIK	heavy	382.8693	499.23	16.37	58.8	18.3
JAK2	ENDQTPLAIYNSISYK	light	928.4573	1058.552	21.08	98.8	42.3
JAK2	ENDQTPLAIYNSISYK	light	928.4573	987.5146	21.08	98.8	42.3
JAK2	ENDQTPLAIYNSISYK	light	928.4573	874.4305	21.08	98.8	42.3
JAK2	ENDQTPLAIYNSISYK	heavy	932.4644	1066.566	21.08	98.8	42.3
JAK2	ENDQTPLAIYNSISYK	heavy	932.4644	995.5288	21.08	98.8	42.3
JAK2	ENDQTPLAIYNSISYK	heavy	932.4644	882.4447	21.08	98.8	42.3

Abbreviations; RT (retention time), CE (collision energy) and DP (declustering potential)

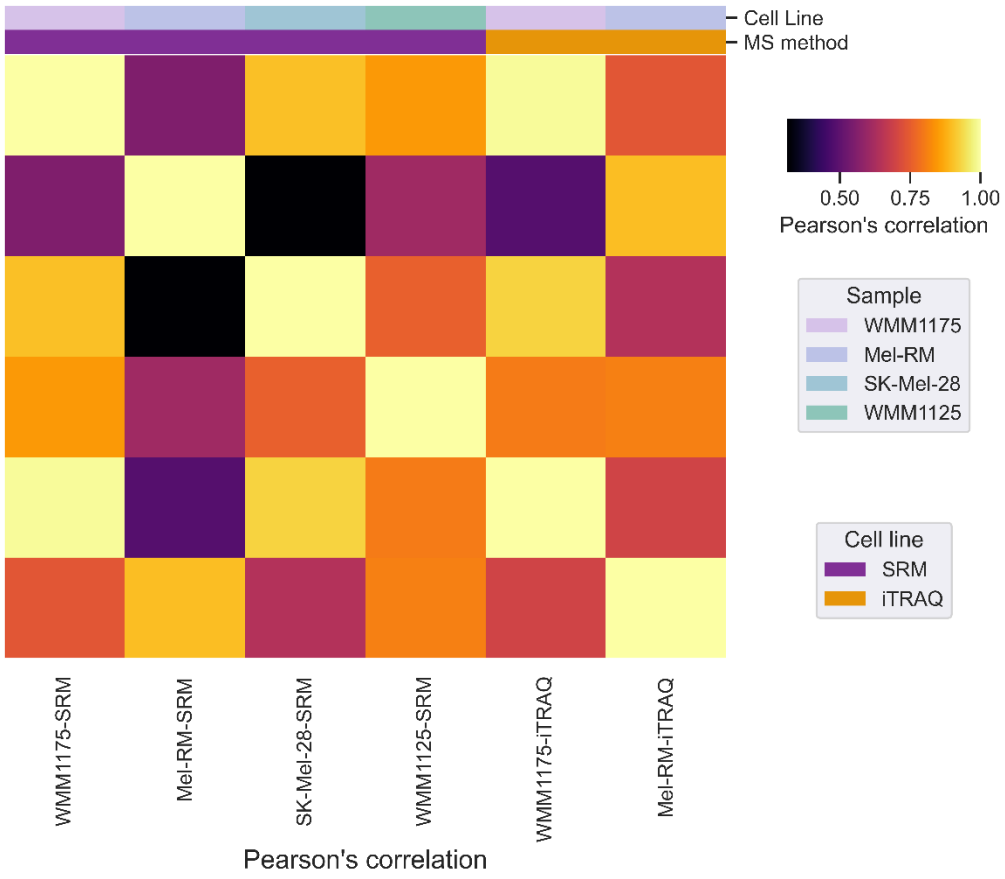

Figure S5-1. Correlation of the eight differentially abundant protein comparing quantitation by iTRAQ and SRM acquisition. Pearson's correlation of the quantitation of the eight UPR-associated proteins when measured by iTRAQ and SRM mass spectrometry methodologies.

Table S6-1. Correlation of differentially abundant protein with increased UPR from iTRAQ analysis and stage III melanoma patient prognosis.

Accession	Gene Name	Name	Major Function	Fold-change with poor prognosis	*p*-value in SWATH	Correlation to poor prognosis
E9PL22	**HYOU1**	Hypoxia up-regulated protein 1	Stress response	2.09	0.366	Yes
P43490	**NAMPT**	Nicotinamide phosphoribosyltransferase	Metabolic	1.73	**0.005**	Yes
P62269	RPS18	40S ribosomal protein S18	RNA biogenesis	1.97	0.483	Yes
P13667	**PDIA4**	Protein disulfide-isomerase A4	Protein processing	2.04	0.704	Yes
P62249	RPS16	40S ribosomal protein S16	RNA biogenesis	1.97	0.510	Yes
P14625	HSP90B1	Endoplasmin	Stress response	2.04	0.528	Yes
Q01518	CAP1	Adenylyl cyclase-associated protein 1	Cytoskeletal	1.98	0.708	Yes
P07237	P4HB	Protein disulfide-isomerase	Protein processing	2.08	0.300	Yes
P11021	**HSPA5**	78 kDa glucose-regulated protein	Stress response	1.99	0.940	Yes
P31153	MAT2A	S-adenosylmethionine synthase isoform type-2	Metabolic	1.95	0.745	No
O15355	PPM1G	Protein phosphatase 1G	Protein processing	1.58	0.642	No
Q13509	TUBB3	Tubulin beta-3 chain	Cytoskeletal	3.75	0.090	No
Q02818	NUCB1	Nucleobindin-1	Stress response	1.81	0.279	No
P22087	FBL	rRNA 2'-O-methyltransferase fibrillarin	rRNA processing	1.85	0.297	Yes
P17096	HMGA1	High mobility group protein HMG-I/HMG-Y	Transcriptional regulation	5.06	0.504	Yes
P04844	RPN2	Dolichyl-diphosphooligosaccharide--protein glycosyltransferase subunit 2	Protein processing	1.88	0.553	No
P08621	SNRNP70	U1 small nuclear ribonucleoprotein 70 kDa	mRNA processing	2.21	0.612	No
Q9H307	PNN	Pinin	Cell adhesion	1.78	0.443	No
Q15459	SF3A1	Splicing factor 3A subunit 1	mRNA processing	1.87	0.510	No
O75475	PSIP1	PC4 and SFRS1-interacting protein	Transcriptional regulation/ stress response	1.95	0.730	No
O60506	SYNCRIP	Heterogeneous nuclear ribonucleoprotein Q	mRNA processing	2.02	0.866	No
P40227	CCT6A	T-complex protein 1 subunit zeta	Stress response	2.03	0.712	No

Q92922	**SMARCC1**	SWI/SNF complex subunit SMARCC1	Transcriptional regulation	2.12	0.718	No
Q13263	TRIM28	Transcription intermediary factor 1-beta	Transcriptional regulation	1.99	0.931	No
O75643	NRNP200	U5 small nuclear ribonucleoprotein 200 kDa helicase	mRNA processing	2.10	0.342	No
Q9Y3B4	SF3B14	Pre-mRNA branch site protein p14 OS=Homo sapiens	mRNA processing	2.04	0.820	No
Q13813	SPTAN1	Spectrin alpha chain, non-erythrocytic 1	Cytoskeletal	2.00	0.980	No
Q9UHX1	PUF60	Poly(U)-binding-splicing factor PUF60	Apoptosis	1.89	0.703	No
Q9UH99	**SUN2**	SUN domain-containing protein 2	Cytoskeletal	2.09	0.809	No
Q00341	HDLBP	Vigilin	Metabolic	2.04	0.809	No
Q8N5K1	CISD2	CDGSH iron-sulfur domain-containing protein 2	Metabolic	2.00	0.998	Yes
O15173	**PGRMC2**	Membrane-associated progesterone receptor component 2	steroid receptor	1.85	0.448	Yes
Q9BVK6	TMED9	Transmembrane emp24 domain-containing protein 9	Transporter	2.33	0.387	Yes
Q07065	CKAP4	Cytoskeleton-associated protein 4	Cytoskeletal	2.22	0.153	Yes
P49755	TMED10	Transmembrane emp24 domain-containing protein 10	Transporter	2.16	0.434	Yes
O00264	PGRMC1	Membrane-associated progesterone receptor component 1	Steriod receptor	2.04	0.849	Yes
Q15006	EMC2	ER membrane protein complex subunit 2	Metabolic	2.32	0.092	Yes
P42766	RPL35	60S ribosomal protein L35	Protein processing	1.78	0.470	Yes
P23381	**WARS**	Tryptophan--tRNA ligase, cytoplasmic	Protein processing\ angiogenic	1.88	0.425	Yes
Q96JB5	CDK5RAP3	CDK5 regulatory subunit-associated protein 3	Cell cycle	1.84	0.212	Yes
P61009	SPCS3	Signal peptidase complex subunit 3	Protein processing	0.52	0.762	No
P51571	SSR4	Translocon-associated protein subunit delta	Transporter	1.87	0.490	Yes
O43707	ACTN4	Alpha-actinin-4	Cytoskeletal	1.91	0.039	No
P25705	ATP5A1	ATP synthase subunit alpha, mitochondrial	Metabolic	1.96	0.472	No
P05141	SLC25A5	ADP/ATP translocase 2	Transporter	2.05	0.864	No
P51991	HNRNPA3	Heterogeneous nuclear ribonucleoprotein A3	mRNA processing	2.00	0.988	No
P22626	HNRNPA2B 1	Heterogeneous nuclear ribonucleoproteins A2/B1	mRNA processing	1.91	0.194	No

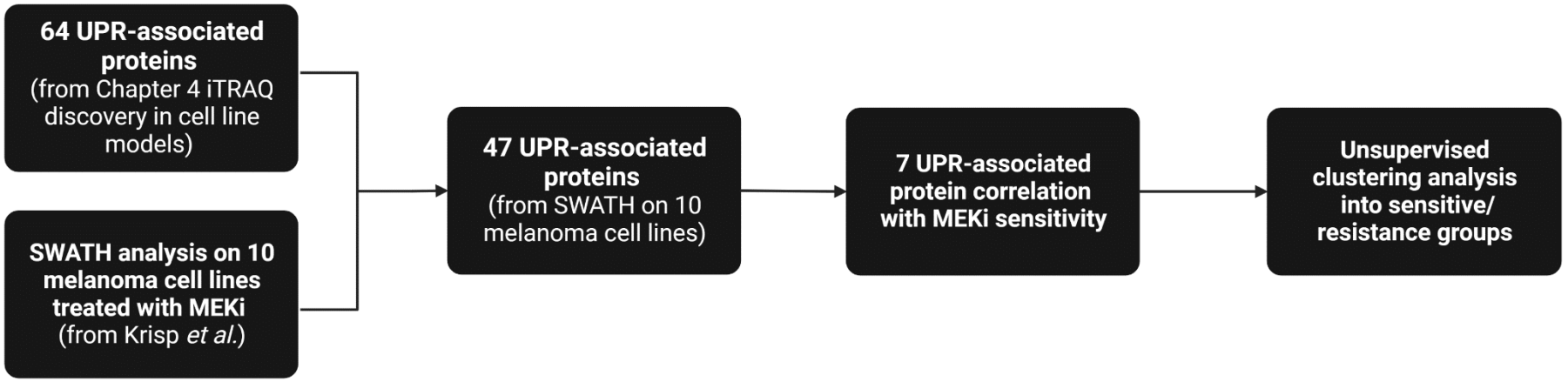

Figure S6-1. Method summary for Chapter 6.2.1. Correlation of UPR-associated proteins with MEK inhibitor (MEKi) resistance in melanoma cell lines. Proteins identified to be differentially abundant with UPR activation in Chapter 4 were examined in publicly available proteomic data of 10 melanoma cell lines treated with MEKi [284]. The abundance of seven proteins was found to be associated with MEKi resistance (Pearson's correlation of >0.5). The heatmap shows the abundance (z-score) of the seven proteins and their association with the MEKi sensitivity of individual cell lines.

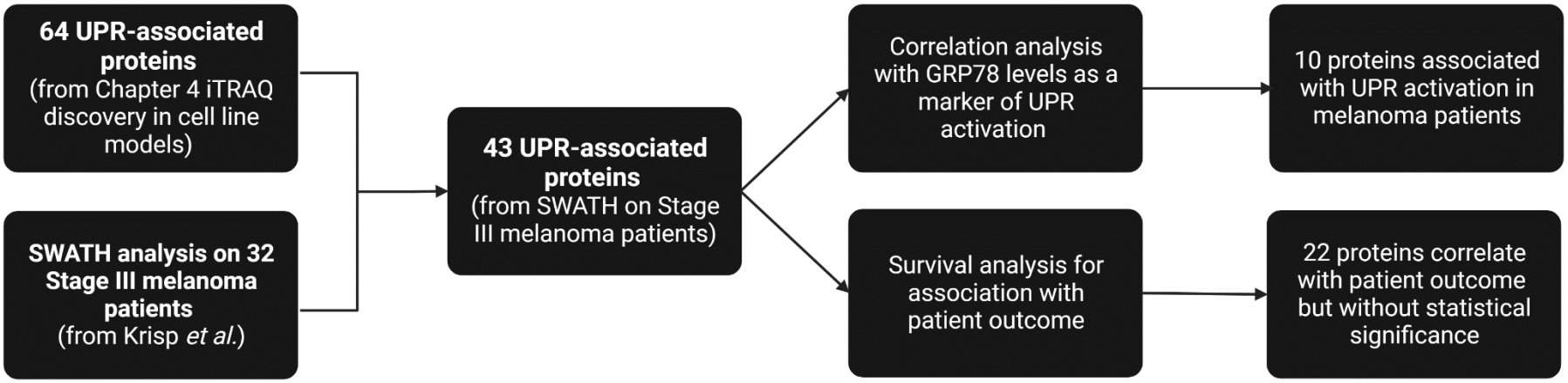

Figure S6-2. Method summary for Chapter 6.2.2. Proteomic data from 32 stage III melanoma patients was taken from publicly available data. Quantitative data from 43 of the 64 UPR-associated proteins found in the melanoma patient data was examined for its correlation to GRP78 levels as a marker of UPR activation. Eleven UPR-associated proteins discovered in Chapter 4 were found to correlate with GRP78 levels in proteomic data of stage III melanoma patients, ten of which with the same trend in abundance. Twenty two of the 64 UPR-associated proteins discovered in melanoma cell line models in Chapter 4 were found to correlate with poor outcome in proteomic data of stage III melanoma patients.

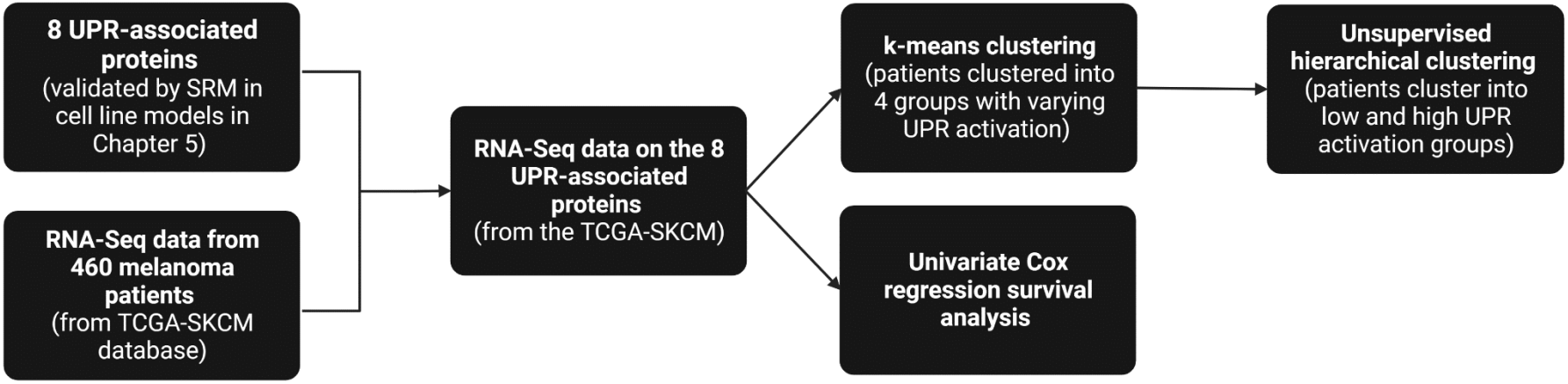

Figure S6-3. Method summary for Chapter 6.2.3. RNA-Seq abundance levels of the eight UPR-associated proteins were analysed from 460 melanoma patients from the TCGA-SKCM cutaneous melanoma dataset. Clustering of the 460 melanoma patients was performed using k-means clustering, fitting the patients into four clusters based upon the abundances of the eight UPR-associated proteins. Abundance levels of the eight UPR-associated proteins in RNA-Seq patient data correlated with the cell lines model of UPR activation discovered in previous chapters. Patients were divided into high and low expression groups with overall survival used as a binary outcome. Univariate Cox proportional hazard testing was performed using RNA-Seq abundance levels of the eight UPR-associated proteins.

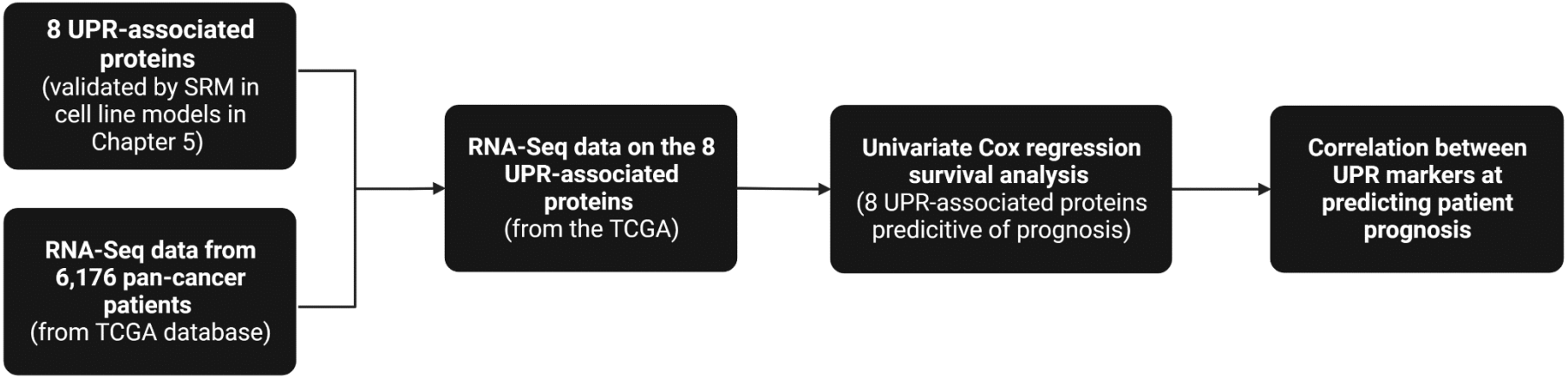

Figure S6-4. Method summary for Chapter 6.2.4. RNA-Seq data from the TCGA for 6,176 patients across 16 solid tumours was analysed. The 8 UPR-associated proteins were analysed using Cox univariate regression analysis and visualised by Kaplan-Meier plots to determine their prognostic value for overall survival in cancer patient**.** UPR-associated proteins were considered prognostic with log rank *p*-values <0.05.

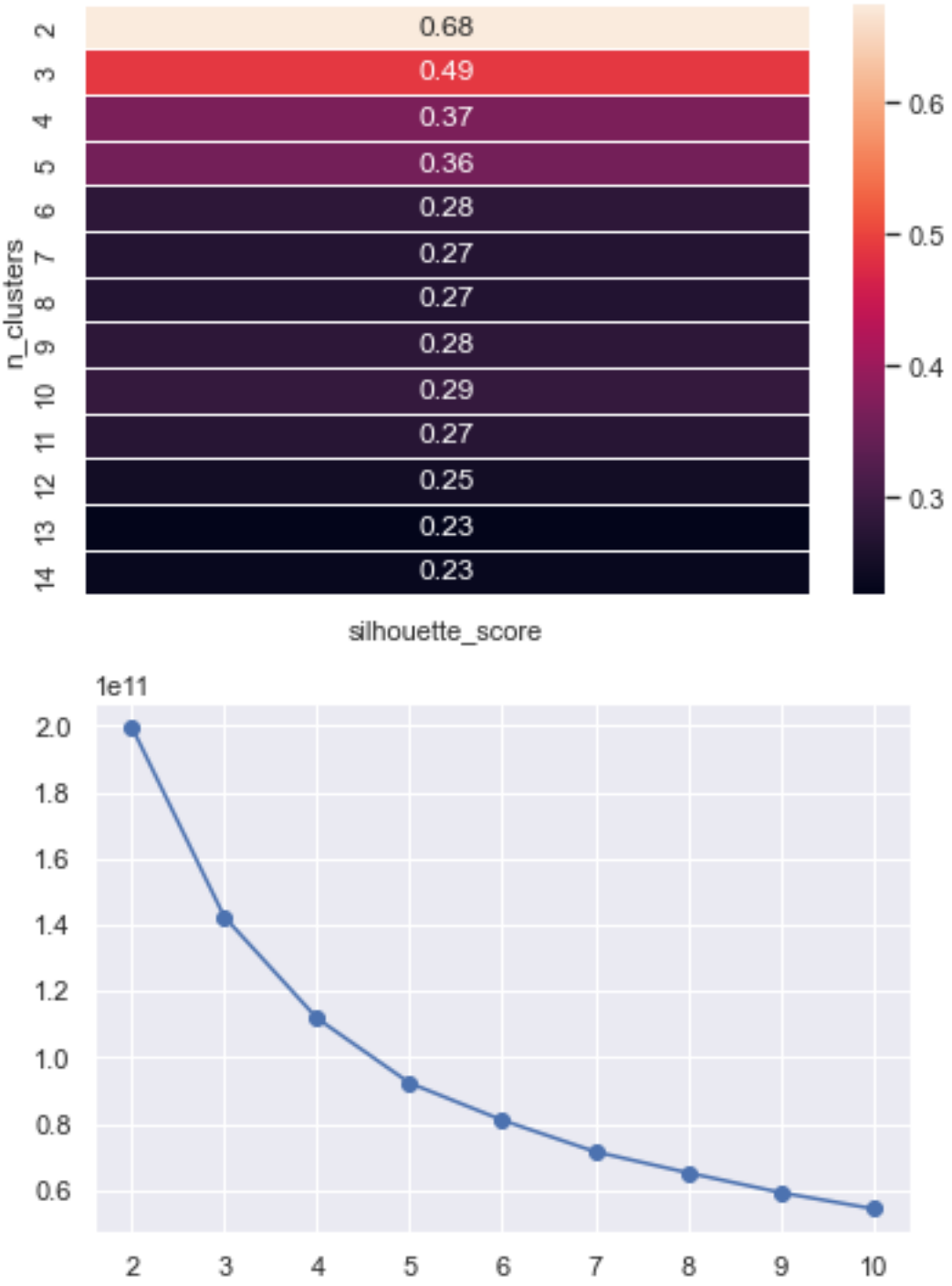

Figure S6-5. Optimal number of clusters for the k-means algorithm in melanoma pateint RNA-Seq data from the TCGA data portal. Silhouette coefficents were calucated from a random subset of data (n=100) using the python package sklearn.

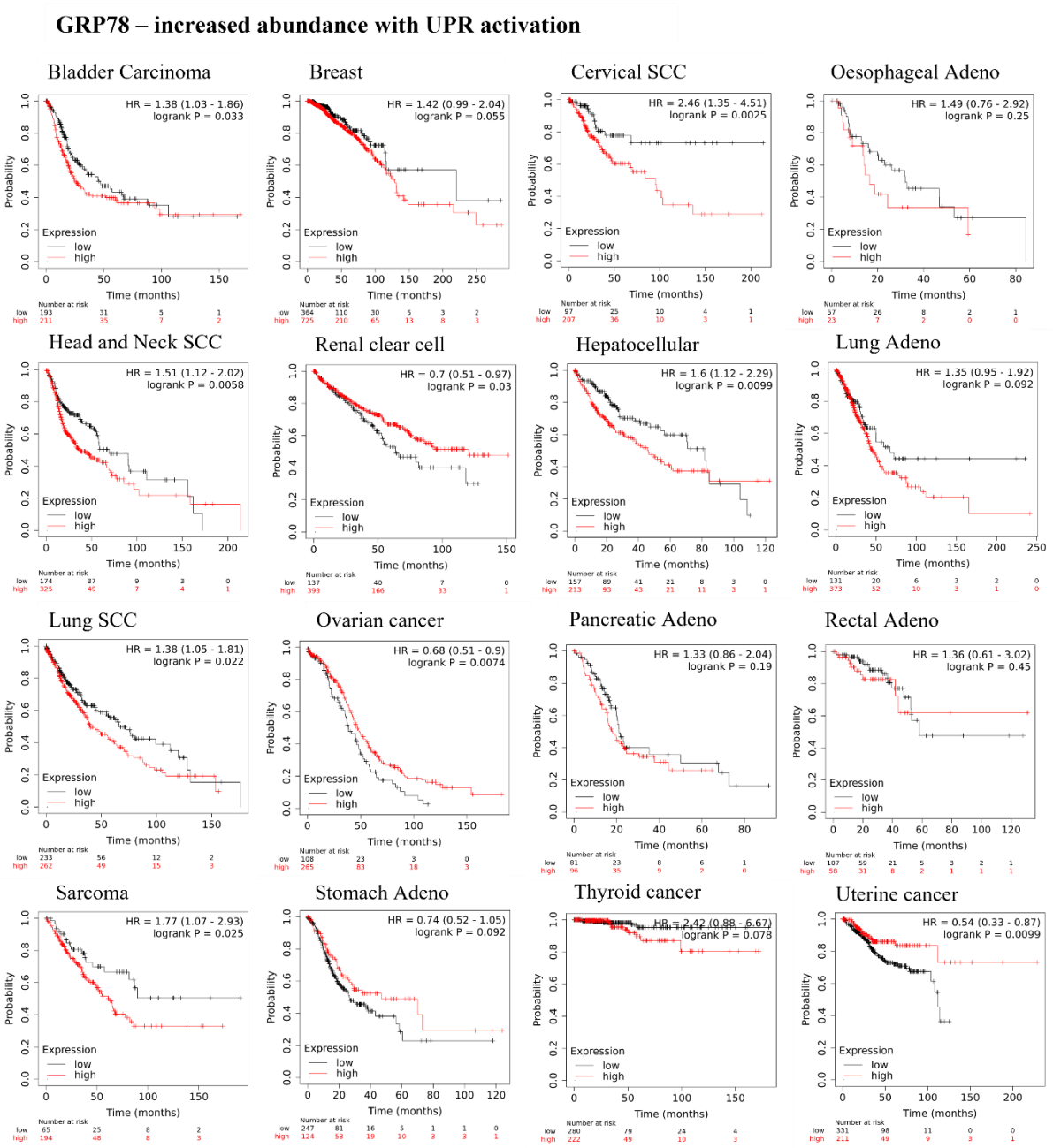

Figure S6-6. **Pan-cancer survival analysis with GRP78 abundance**. GRP78 as a predictor of survival in 16 solid tumours utilising RNA-Seq and patient survival data from the TCGA, GEO and EGA data repositories.

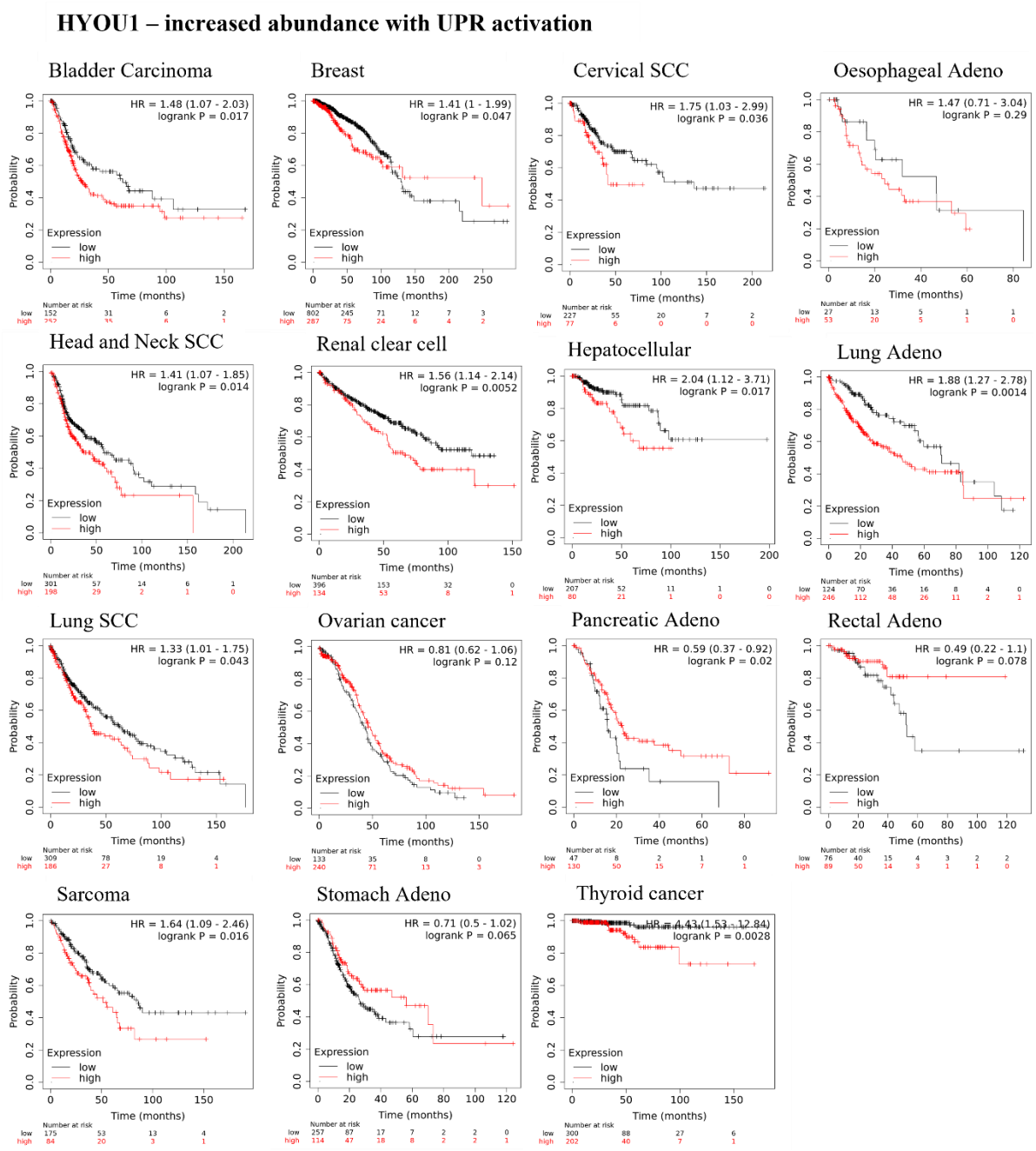

Figure S6-7. **Pan-cancer survival analysis with HYOU1 abundance.** HYOU1 expression as a predictor of survival in 16 solid tumours utilising RNA-Seq and patient survival data from the TCGA, GEO and EGA data repositories.

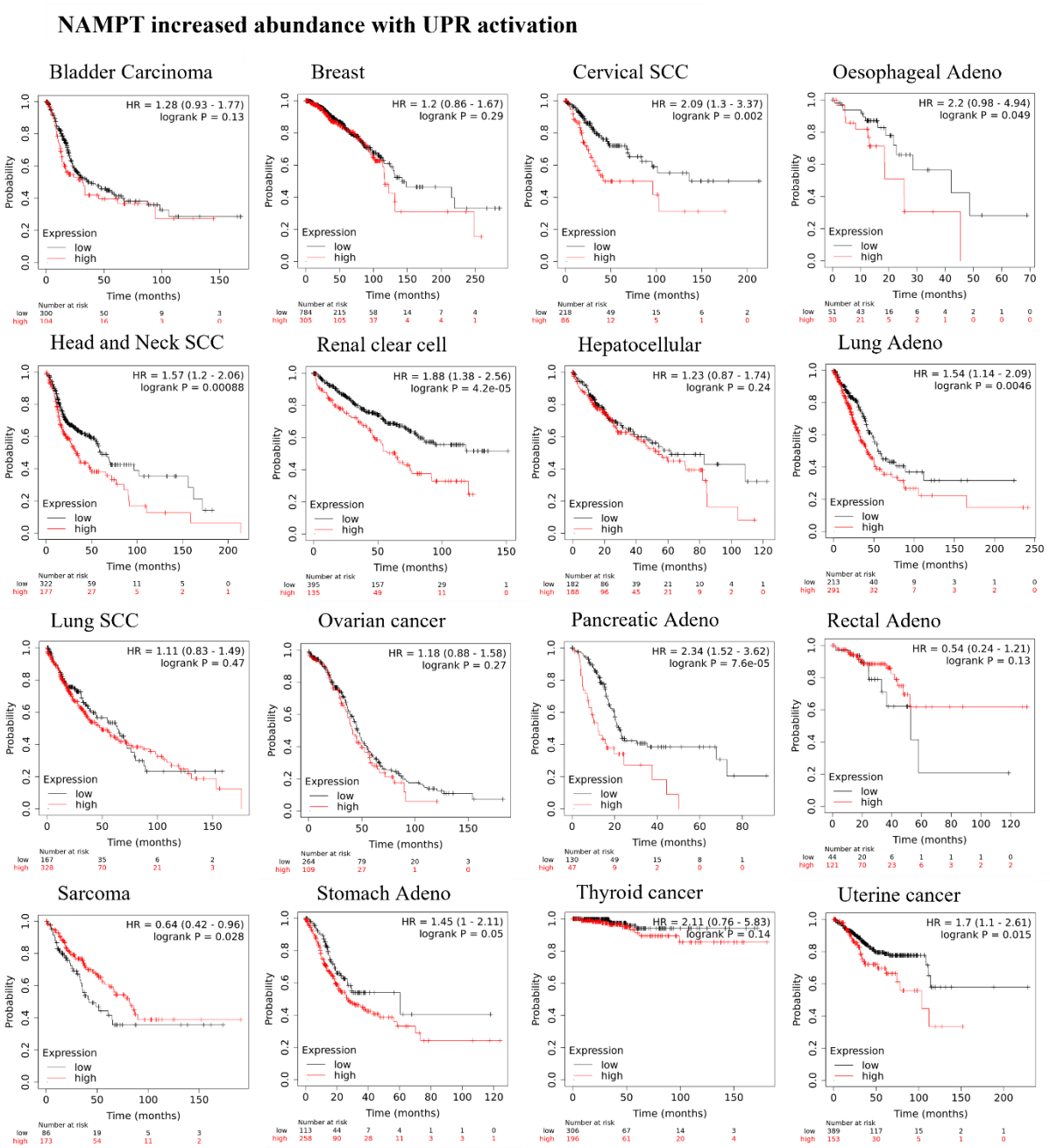

Figure S6-8. **Pan-cancer survival analysis with NAMPT abundance**. NAMPT expression as a predictor of survival in 16 solid tumours utilising RNA-Seq and patient survival data from the TCGA, GEO and EGA data repositories.

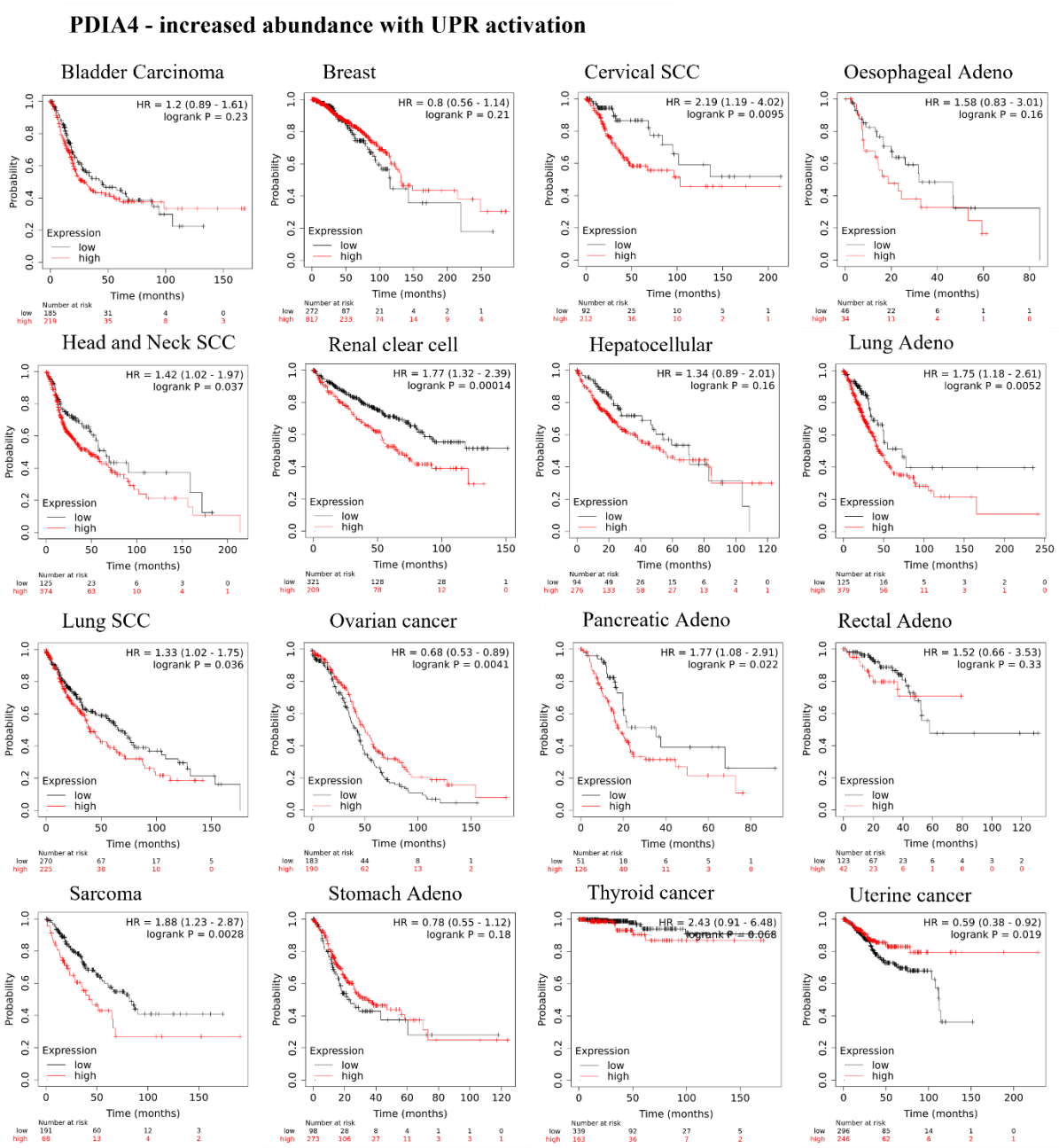

Figure S6-9. **Pan-cancer survival analysis with PDIA4 abundance.** PDIA4 expression as a predictor of survival in 16 solid tumours utilising RNA-Seq and patient survival data from the TCGA, GEO and EGA data repositories.

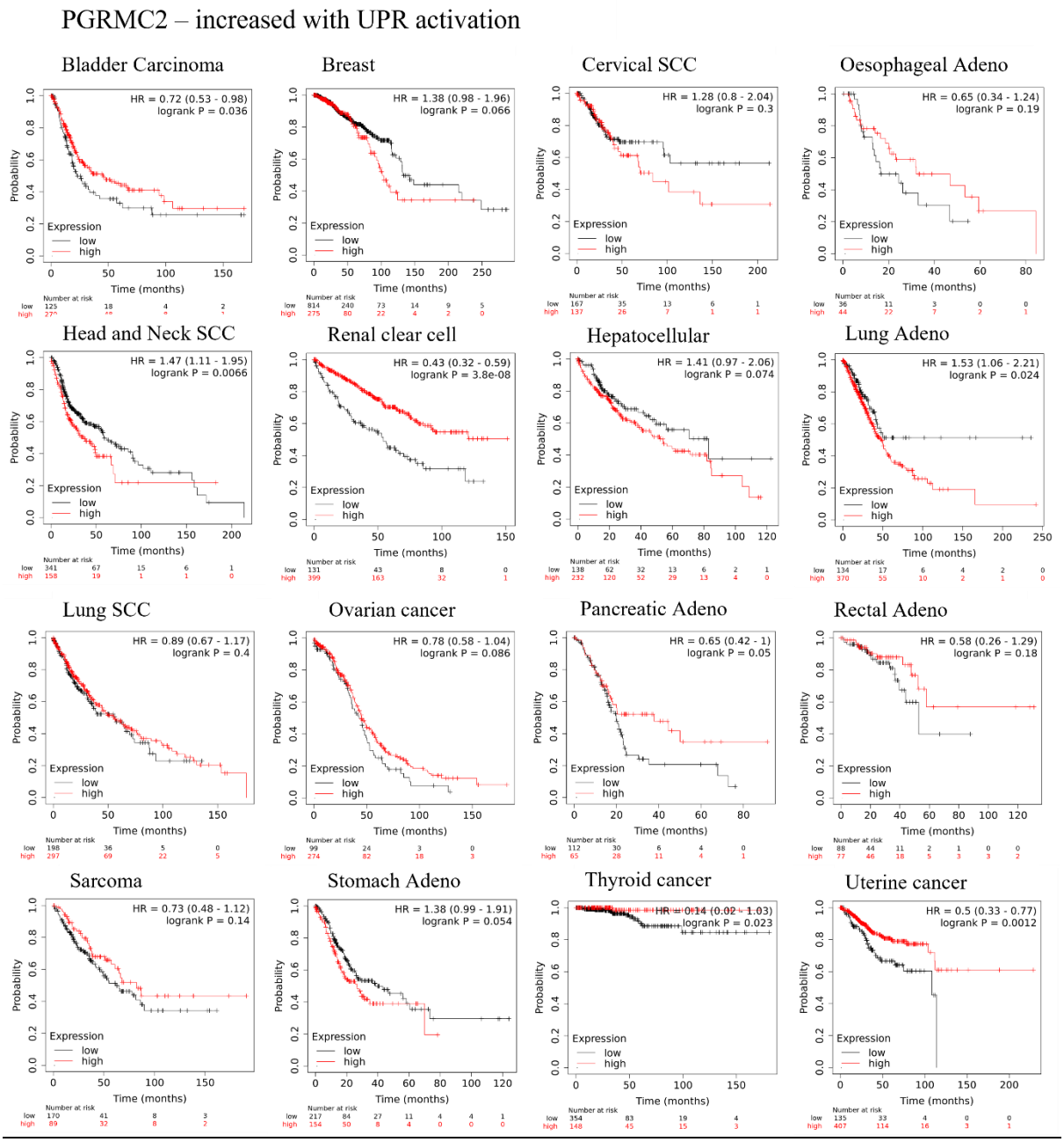

Figure S6-10. **Pan-cancer survival analysis with PGRMC2 abundance.** PGRMC2 expression as a predictor of survival in 16 solid tumours utilising RNA-Seq and patient survival data from the TCGA, GEO and EGA data repositories.

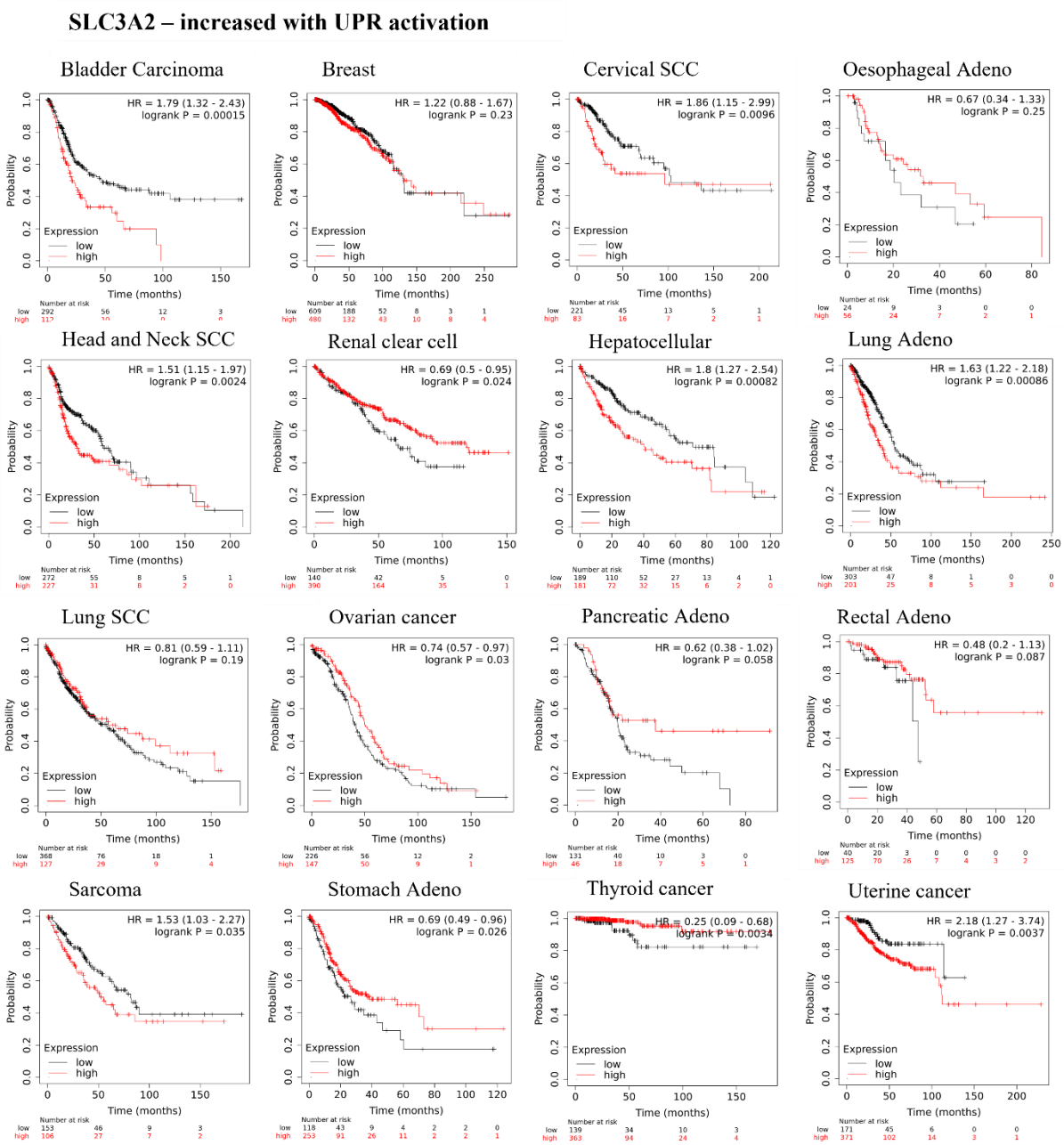

Figure S6-11. **Pan-cancer survival analysis with SLC3A2 abundance.** SLC3A2 expression as a predictor of survival in 16 solid tumours utilising RNA-Seq and patient survival data from the TCGA, GEO and EGA data repositories.

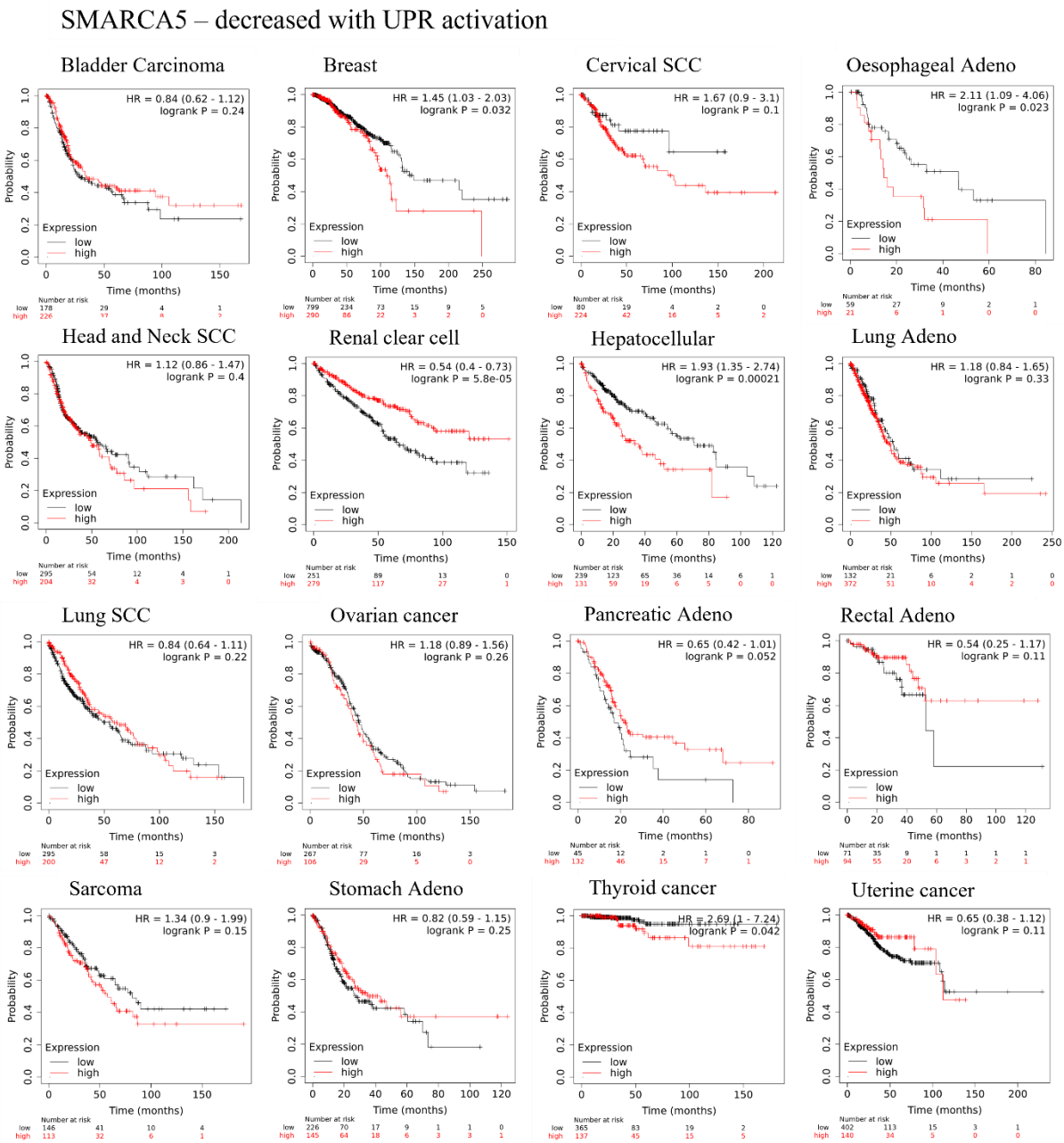

Figure S6-12. Pan-cancer survival analysis with SMARCA5 abundance. SMARCA5 expression as a predictor of survival in 16 solid tumours utilising RNA-Seq and patient survival data from the TCGA, GEO and EGA data repositories.

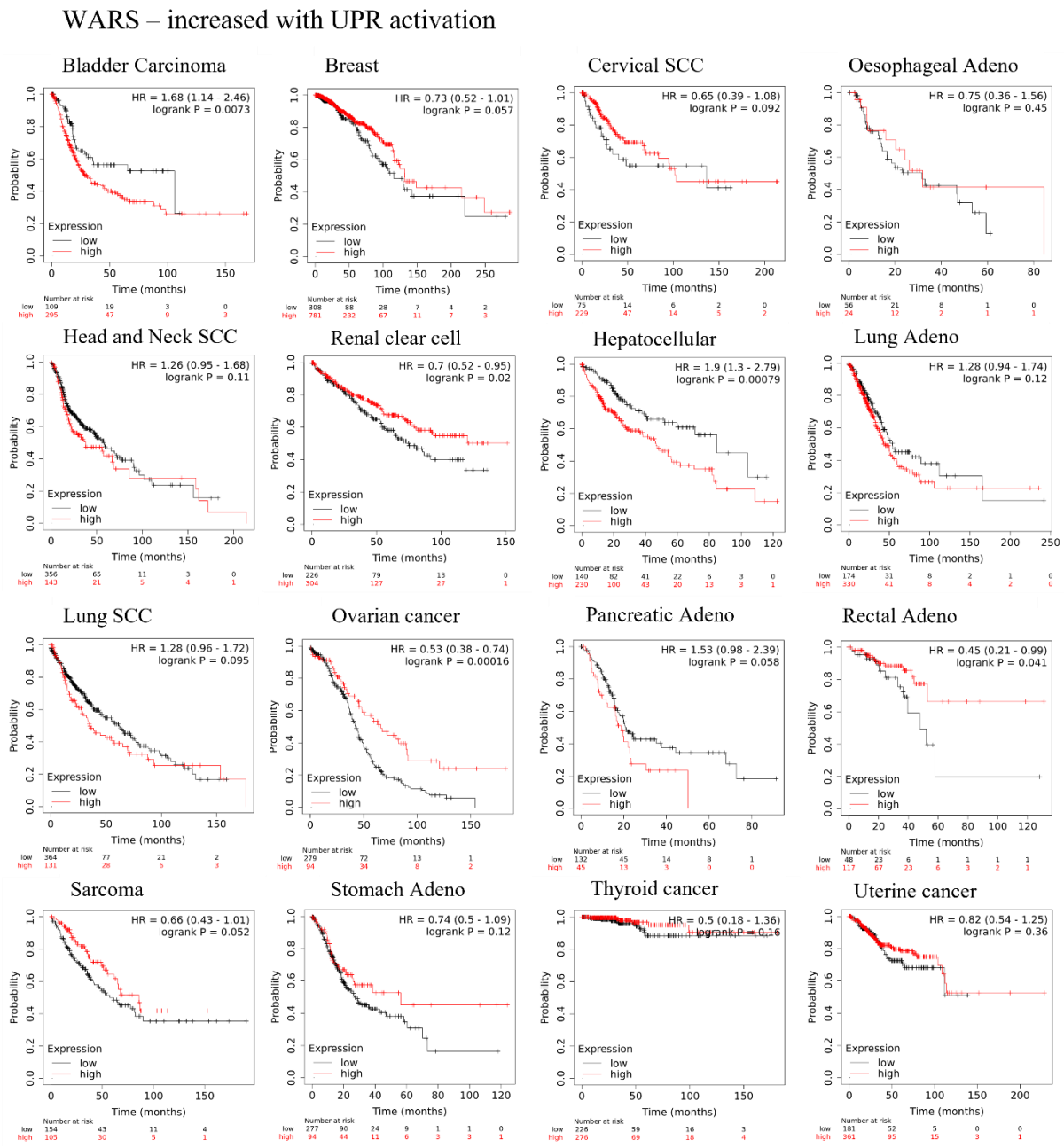

Figure S6-13. **Pan-cancer survival analysis with WARS abundance.** WARS expression as a predictor of survival in 16 solid tumours utilising RNA-Seq and patient survival data from the TCGA, GEO and EGA data repositories.

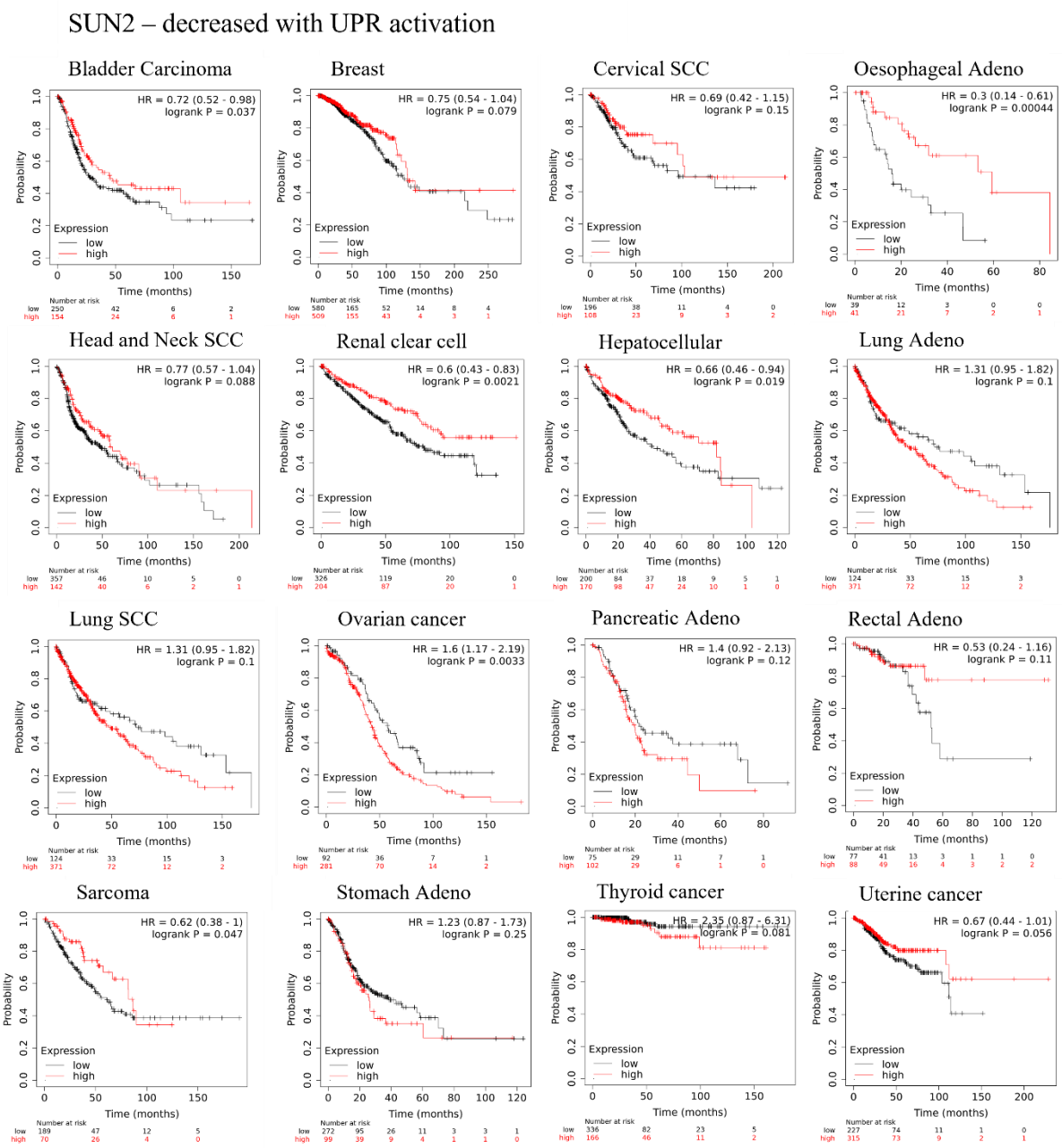

Figure S6-14. Pan-cancer survival analysis with SUN2 abundance. SUN2 expression as a predictor of survival in 16 solid tumours utilising RNA-Seq and patient survival data from the TCGA, GEO and EGA data repositories.